Groundwater and contaminant mass fluxes monitoring in heterogeneous aquifers

by

Pierre JAMIN

Submitted on March 2019
in partial fulfillment of the requirements for the degree of

Doctor in Philosophy

In Applied Sciences at the University of Liège, Belgium

Jury

Toye Dominique (President)	Pr. Dr. Ir., University of Liège
Brouyère Serge (Promotor)	Dr. Ir., University of Liège
Dassarges Alain (Co-promotor)	Pr. Dr. Ir., University of Liège
Nguyen Frédéric	Pr. Dr. Ir., University of Liège
Goderniaux Pascal	Pr. Dr. Ir., University of Mons
Annable Michael	Pr. Dr. Ir., University of Florida
Atteia Olivier	Pr. Dr. Ir., University of Bordeaux

To Suzanne, Léon and Anne-Marie

Abstract

Groundwater is one of the most important natural resources of our planet and it requires appropriate management and protection in order to guarantee its availability for future generations. From a water quality point of view, old industrial activities and modern accidental releases have locally impacted groundwater resource. Management of these contaminated aquifers has historically relied on comparison between measured contaminant concentrations in groundwater and threshold values. This approach is a necessary early characterization step but is totally insufficient to fully investigate the contaminants behavior in groundwater and to quantify the associated risks.

Since the beginning of the years 2000, a consensus has been growing among the scientific, technical and decision makers' community on the fact that management of contaminated aquifers should be performed in terms of contaminant flux metrics. Accordingly, it has become necessary to dispose of techniques able to accurately measure mass fluxes and mass discharges of contaminants in aquifers. Contaminant mass flux usually relies on measurements of both groundwater flux and contaminant concentration in monitoring wells drilled in the aquifer of concern. Research efforts must lead to the proposition of new solutions, methodologies and techniques, in particular for measuring groundwater fluxes. In this work, the Finite Volume Point Dilution Method (FVPDM), is proposed as an innovative single-well method for monitoring groundwater fluxes in aquifers.

Mathematical basis and a first analytical solutions allowing to interpret FVPDM experiments performed in steady state groundwater flow conditions were already developed and validated on a few field applications. In this research, a generalized FVPDM interpretation framework for monitoring groundwater fluxes over time is proposed, based on a new finite difference expression proposed to calculate groundwater fluxes from FVPDM experiments performed in transient groundwater flow fields.

In a first step, the FVPDM technique was successively applied in various laboratory and field experiments allowing to define its accuracy, precision and resolution under transient groundwater flow conditions. A first lab-scale flow tank experiment demonstrated the accuracy of the FVPDM for groundwater fluxes measurements in both steady and transient state flow conditions. Difference between the prescribed water flux in the flow tank and the measured water flux using FVPDM was as low as 0.15 %. In a second experiment the FVPDM was applied to measure groundwater fluxes on several fractured zones of an open well installed in a crystalline rock aquifer. This constitutes the first successful application of the FVPDM technique in a fractured aquifer, using straddle packers. The classical point dilution method (PDM) was also applied during this experiment, under the same groundwater flow conditions to compare the sensitivity and uncertainty of both methods. It demonstrated that FVPDM generally provides a better precision than PDM but it may require longer experimental durations. A third FVPDM experiment undertaken in an alluvial aquifer allowed to validate in the field the method for monitoring rapidly changing groundwater fluxes. This first series of experiment allowed to validate the FVPDM as a fully operational method for measurements of groundwater fluxes for a wide spectrum of experimental and flow conditions.

In a second step, three field-scale applications of the method were performed. The first relates to direct groundwater fluxes measurements in a sub-permafrost aquifer located in the remote territories of northern Quebec. These measurements came in support to a thermo-hydrodynamic model of a watershed where permafrost thaw occurs. This specific application demonstrated the robustness and versatility of the FVPDM. In a second field application, the FVPDM was used to monitor, under controlled conditions a solute mass discharge experiment undertaken in a heterogeneous alluvial aquifer at a series of control planes in order to compare different methods for calculating the total mass discharge based on discrete groundwater fluxes and concentration measurements. In a third application, the FVPDM was successfully used in a groundwater pollution investigation to characterize highly transient groundwater flows and pollutant mass fluxes within a coastal aquifer influenced by marked tides. The results of this experiment allowed to improve and refine the conceptual site model and provided crucial information for optimizing further investigations and risk mitigation measures at this polluted site.

The FVPDM was applied in a wide range of environmental contexts, of application scales, of experimental setups, of aquifer types, of time scales, of groundwater flow conditions, and for both research and consultant-type purposes. The FVPDM was proven to be a robust and versatile method that provides high-quality reliable groundwater flux data for general hydrogeological characterizations and for contaminant mass fluxes monitoring, even under highly transient flow conditions. From a more general perspective, this research demonstrated the great importance and the huge benefits of having direct and reliable in situ measurements of groundwater fluxes for any kind of hydrogeological studies. This research proves once more the value of undertaking mass flux measurements for characterization of contaminated sites, risk assessment and design of risk mitigation measures.

Résumé

Les eaux souterraines comptent parmi les ressources naturelles les plus importantes de notre planète et nécessitent une gestion et une protection appropriées afin de garantir leur disponibilité pour les générations futures. D'un point de vue qualitatif, anciennes activités industrielles et rejets accidentels récents peuvent impacter localement les eaux souterraines. La gestion de ces aquifères contaminés est traditionnellement basée sur la comparaison des concentrations en contaminants dans l'eau souterraine par rapport à des normes. Cette approche constitue une étape de caractérisation préliminaire nécessaire mais reste insuffisante pour étudier de manière approfondie le comportement des contaminants dans les eaux souterraines et pour quantifier les risques associés.

Au début des années 2000, un consensus a vu le jour parmi les différents acteurs du domaine des aquifères contaminés sur le fait que la gestion de ces aquifères devait reposer sur des approches basées sur des flux de contaminants plutôt que sur des concentrations. En conséquence, il est nécessaire de disposer de techniques permettant de mesurer avec précision les flux massiques de contaminants dans les aquifères. Le calcul du flux massique de contaminants repose généralement sur des mesures de flux d'eau souterraine et de la concentration en contaminants effectuées au niveau de différents puits. La recherche doit donc proposer de nouvelles solutions, méthodes et techniques, notamment en ce qui concerne la mesure des flux d'eau souterraine. Dans ce travail de recherche, la méthode "Finite Volume Point Dilution Method" (FVPDM) est proposée comme méthode innovante de monitoring des flux d'eau souterraine.

La base mathématique ainsi qu'une première solution analytique permettant d'interpréter les expériences FVPDM réalisées dans des conditions d'écoulement en régime permanent avaient déjà été développées et validées sur quelques applications de terrain. Dans cette recherche, un nouveau cadre d'interprétation généralisé pour le monitoring au cours du temps des flux d'eau souterraine par la méthode FVPDM est proposé. Il est basé sur une discrétisation par différences finies de l'équation différentielle FVPDM et permet de calculer les flux d'eau souterraine à partir d'expériences réalisées dans des conditions d'écoulements transitoires.

Dans un premier temps, la méthode FVPDM a été appliquée lors de différentes expériences en laboratoire et sur le terrain afin d'en évaluer toutes les spécifications à savoir sa précision, son exactitude et sa résolution dans des conditions d'écoulements transitoires. Une première expérience en laboratoire sur un modèle réduit d'aquifère a démontré l'exactitude de la FVPDM pour la mesure des flux d'eaux souterraines dans des conditions d'écoulement permanent et transitoire. La différence entre le flux d'eau imposé dans le modèle réduit et le flux d'eau mesuré par FVPDM était de 0,15%. Lors d'une seconde expérience, la FVPDM a été appliquée pour mesurer des flux d'eau souterraine à différentes profondeurs dans un puits foré dans un aquifère fracturé. Cette manipulation a été la première application de la FVPDM dans un aquifère fracturé en utilisant un système de double packers. Une méthode classique de dilution ponctuelle (PDM) a également été utilisée, ce qui a permis de comparer la sensibilité et les incertitudes des deux méthodes. Il a été démontré que la FVPDM fourni des résultats plus précis que la PDM mais peut requérir une durée de mesure plus longue. Une troisième expérience réalisée dans un aquifère alluvial a permis de valider sur le terrain le monitoring des flux d'eau souterraine variables dans

un contexte d'écoulement transitoire contrôlé. Cette première série d'expériences a permis de valider la FVPDM en tant que méthode entièrement opérationnelle pour la mesure des flux d'eau souterraine variables.

Dans un second temps, trois applications de la méthode en conditions de terrain réelles ont été effectuées. La première concerne des mesures directes de flux d'eau souterraine dans un aquifère situé dans la zone de pergélisol discontinu au Nunavik, Québec. Ces mesures ont servi de base à un modèle thermo-hydrodynamique d'un bassin affecté d'un phénomène de dégel du pergélisol. Cette application spécifique a démontré la robustesse et la polyvalence de la méthode FVPDM. Lors d'une deuxième application de terrain, la méthode FVPDM a été utilisée dans le cadre de calculs de débits massiques de soluté au sein d'un aquifère alluvial hétérogène dans lequel un soluté a été injecté de façon contrôlée. Différentes méthodes de calcul du débit massique de soluté reposant sur des mesures de flux d'eau souterraine et de concentration en soluté effectuées au niveau de panneaux de contrôles ont été comparées. Dans une troisième expérience, la méthode FVPDM a été utilisée pour la caractérisation d'un aquifère côtier pollué au sein duquel les conditions d'écoulement des eaux souterraines sont fortement transitoires. Les résultats de cette expérience ont permis d'améliorer significativement le modèle conceptuel du site en fournissant des informations cruciales pour l'optimisation des investigations ultérieures et pour la mise en place de mesures d'atténuation des risques.

Au cours de cette thèse, la méthode FVPDM a été appliquée dans un large éventail de conditions : contextes environnementaux différents, setup expérimentaux complexes, milieu poreux et fracturés, puits superficiels et profonds, conditions de laboratoire et de terrain, échelles de temps variables, conditions d'écoulement stationnaires et transitoires. La FVPDM s'est révélée être une méthode robuste et polyvalente qui fournit des données fiables et de haute qualité pour le monitoring des flux d'eau souterraine et de contaminants, même dans des conditions d'écoulements transitoires. D'un point de vue plus général, cette recherche a démontré l'importance de disposer de mesures in situ fiables des flux des eaux souterraines pour tout type d'études hydrogéologiques. Cette recherche prouve une fois de plus l'intérêt de procéder à des mesures de flux massique de contaminants pour la caractérisation des aquifères, pour l'évaluation des risques et pour la conception des mesures visant à réduire ces risques.

Knowledge dissemination

Journal article as first author

Jamin, P., Cochand, M., Dagenais, S., Lemieux, J.-M., Fortier, R., Molson, J., Brouyère, S. (2019). Direct measurement of groundwater flux in aquifers within the discontinuous permafrost zone: an application of the finite volume point dilution method near Umiujaq (Nunavik, Canada). *Hydrogeology Journal*, Topical collection TC04 "Hydrogeology of a cold-region watershed near Umiujaq (Nunavik, Canada)", accepted.

Jamin, P., & Brouyère, S. (2018). Monitoring transient groundwater fluxes using the Finite Volume Point Dilution Method. *Journal of Contaminant Hydrology*, *218*, 10–18. http://doi.org/10.1016/j.jconhyd.2018.07.005

Jamin, P., Goderniaux, P., Bour, O., Le Borgne, T., Englert, A., Longuevergne, L., & Brouyère, S. (2015). Contribution of the finite volume point dilution method for measurement of groundwater fluxes in a fractured aquifer. *Journal of Contaminant Hydrology*, *182*, 244–255. http://doi.org/10.1016/j.jconhyd.2015.09.002

Jamin, P., Dollé, F., Chisala, B., Orban, P., Popescu, I. C., Hérivaux, C., … Brouyère, S. (2012). A regional flux-based risk assessment approach for multiple contaminated sites on groundwater bodies. *Journal of Contaminant Hydrology*, *127*(1–4), 65–75. http://doi.org/10.1016/j.jconhyd.2011.07.001

Under review

Jamin, P., Cosme, F., Briers, P., Orban, P., De Greene, K., & S. Brouyère (2019). Monitoring of contaminant mass fluxes in an aquifer subject to tidal cycles. Submitted to Groundwater Monitoring and Remediation.

Journal article as coauthor

Vera, N. F. De, Beaujean, J., **Jamin, P.**, Caterina, D., Vanclooster, M., Dassargues, A., … Brouyère, S. (2016). Combining cross-hole geophysical and vadose zone monitoring systems for vadose zone characterization at industrial contaminated sites. Hydrological Sciences Journal, (March), 1–18. http://doi.org/10.5194/hess-2016-79

Klepikova, M., Wildemeersch, S., Hermans, T., **Jamin, P.**, Orban, P., Nguyen, F., … Dassargues, A. (2016). Heat tracer test in an alluvial aquifer: Field experiment and inverse modelling. Journal of Hydrology, 540, 812–823. http://doi.org/10.1016/j.jhydrol.2016.06.066

Palau, J., **Jamin, P.**, Badin, A., Vanhecke, N., Haerens, B., Brouyere, S., & Hunkeler, D., (2016). Use of dual carbon e chlorine isotope analysis to assess the degradation pathways of 1,1,1-trichloroethane in groundwater. Water Research, 92, 235–243. http://doi.org/http://dx.doi.org/10.1016/j.watres.2016.01.057

Hermans, T., Wildemeersch, S., **Jamin, P.**, Orban, P., Brouyère, S., Dassargues, A., & Nguyen, F. (2015). Quantitative temperature monitoring of a heat tracing experiment using cross-borehole ERT. Geothermics, 53, 14–26. http://doi.org/10.1016/j.geothermics.2014.03.013

Vera, N. F. De, Beaujean, J., **Jamin, P.**, Hakoun, V., Caterina, D., Dahan, O., … Brouyère, S. (2015). Tracer Experiment in a Brownfield Using Geophysics and a Vadose Zone Monitoring System. Vadoze Zone Journal, 16(1), 1–15. http://doi.org/10.2136/vzj2016.06.0051

Wildemeersch, S., **Jamin, P.**, Orban, P., Hermans, T., Klepikova, M., Nguyen, F., … Dassargues, A. (2014). Coupling heat and chemical tracer experiments for estimating heat transfer parameters in shallow alluvial aquifers. Journal of Contaminant Hydrology, 169, 90–99. http://doi.org/10.1016/j.jconhyd.2014.08.001

Dujardin, J., Anibas, C., Bronders, J., **Jamin, P.**, Hamonts, K., Dejonghe, W., … Batelaan, O. (2014). Combining flux estimation techniques to improve characterization of groundwater–surface-water interaction in the Zenne River, Belgium. Hydrogeology Journal, 22(7), 1657–1668. http://doi.org/10.1007/s10040-014-1159-4

Chapters of collective work

Briers, P., **Jamin, P.**, Ruthy, I., Orban, P., & Brouyère, S. (2016). Hydrogéologie du bassin du Hoyoux. Atlas du Karst Wallon. Bassins versants du Hoyoux et de la Solières. Commission Wallonne d'Etude et de Protection des Sites Souterrains. http://hdl.handle.net/2268/207529

Gesels, J., Goderniaux, P., **Jamin, P.**, Dassargues, A., & Brouyère, S. (2011). Hydrogéologie du bassin du Samson. Atlas du Karst Wallon. Bassins du Bocq et du Samson (pp. 56-65). Commission Wallonne d'Etude et de Protection des Sites Souterrains. http://hdl.handle.net/2268/100288

Published abstracts as co-author

Klepikova, M., **Jamin, P.**, Orban, P., Brouyère, S., & Dassargues, A. (2016). How heterogeneity of the K-field influences a heat plume in a shallow alluvial aquifer: responses from a heat tracer test. Abstract book (pp. 77). http://hdl.handle.net/2268/192394

Wildemeersch, S., Klepikova, M., **Jamin, P.**, Orban, P., Hermans, T., Brouyère, S., & Dassargues, A. (2014). Thermal tracer tests for characterizing a shallow alluvial aquifer. Geophysical Research Abstracts. http://hdl.handle.net/2268/171023

Hermans, T., Wildemeersch, S., **Jamin, P.**, Orban, P., Brouyère, S., Dassargues, A., & Nguyen, F. (2013). A heat injection and pumping experiment in a gravel aquifer monitored with crosshole electrical resistivity tomography. EarthDoc - Near Surface Geosciences 2013 - 19th European Meeting of Environmental and Engineering Geophysics (pp. 2a09). http://hdl.handle.net/2268/155926

Brouyère, S., **Jamin, P.**, Dollé, F., Chisala, B., Orban, P., Popescu, I. C., Hérivaux, C., & Dassargues, A. (2011). A regional flux-based risk assessment approach of contaminated sites on groundwater bodies. In M., Schirmer, E., Hoehn, & T., Vogt (Eds.), Groundwater Quality 2010 : Groundwater Quality Management in a Rapidly Changing World (pp. 159-162). http://hdl.handle.net/2268/57387

Scientific conferences, congresses and symposia as first author or presenter

Jamin, P., & Brouyère, S. (2019, February 2). m-flux : Monitoring des flux de polluants dans les aquifères contaminés. Poster session presented at Department Day Urban and Environmental Engineering, Liège, Belgique.

Brouyère, S., & **Jamin, P.** (2018, September 20). Caractérisation des eaux souterraines par des approches centrées sur les flux : concepts et applications. Oral communication at Formation FedexSol, Château Bayard à Dhuy, Belgique. http://hdl.handle.net/2268/228017

Jamin, P., Orban, P., Verreydt, G., Cosme, F., & Brouyère, S. (2018, September 10). Recent advances for monitoring groundwater and pollutant fluxes using single-well applied tracer techniques. Oral communication at IAH 2018, Daejeon, Corée du sud. http://hdl.handle.net/2268/227969

Jamin, P., Cochand, M., Dagenais, S., Fortier, R., Molson, J., Brouyère, S., & Lemieux, J.-M. (2018, September 10). Direct single well measurement of groundwater flux in permafrost-impacted aquifers in Nunavik, Canada. Poster session presented at IAH 2018, Daejeon, Corée du sud. http://hdl.handle.net/2268/228018

Jamin, P., Dassargues, A., & Brouyère, S. (2017, May 05). MONitOring des flux de POLluants dans les Eaux Souterraines. Poster session presented at Department Day Urban and Environmental Engineering, Liège, Belgique. http://hdl.handle.net/2268/211792

Jamin, P., & Brouyère, S. (2016, July). Continuous monitoring of transient groundwater fluxes using the Finite Volume Point Dilution Method. Oral communication at 9th International Association of Hydrological Sciences (IAHS) Groundwater Quality Conference (GQ16), Shenzhen, China. http://hdl.handle.net/2268/202191

Jamin, P., Goderniaux, P., Bour, O., Le Borgne, T., Englert, A., Longuevergne, L., & Brouyère, S. (2015, September). Contribution of the Finite Volume Point Dilution Method for measurement of groundwater fluxes in a fractured aquifer. Oral communication at AQUA2015, 42nd IAH International Congress, Hydrogeology: back to the future, Rome, Italie. http://hdl.handle.net/2268/183866

Jamin, P., Brouyère, S., Bour, O., LeBorgne, T., & Goderniaux, P. (2013, April 24). Time variyng groundwater flux measurement using a single well tracer technique. Poster session presented at 8th IAHS International Groundwater Quality Conference (GQ13), Gainesville, United States. http://hdl.handle.net/2268/148027

Wildemeersch, S., **Jamin, P.**, Orban, P., Hermans, T., Brouyère, S., & Dassargues, A. (2013, April 22). Coupling heat and salt tracer experiment for the estimation of heat transfer and solute transport parameters. Oral communication at 8th IAHS International Groundwater Quality Conference (GQ13), Gainesville, United States. http://hdl.handle.net/2268/148025

Jamin, P., & Brouyère, S. (2011, May 26). Quantification and monitoring of contaminant mass fluxes in heterogeneous subsurface media. Poster session presented at In-situ Environemental Monitoring and Policy, The Application of Sensors and Passive Samplers, Gand, Belgique. http://hdl.handle.net/2268/148026

Brouyère, S., **Jamin, P.**, Dollé, F., Orban, P., Hérivaux, C., Popescu, I. C., & Dassargues, A. (2010, April 22). A regional flux-based risk assessment approach of contaminated sites on groundwater bodies. Poster session presented at Symposium de la Meuse 2010, Liège, Belgique. http://hdl.handle.net/2268/17035

Scientific conferences, congresses and symposia as co-author

Hoffmann, R., Goderniaux, P., **Jamin, P.**, & Dassargues, A. (2018, September 13). The double porosity of the chalk and its influence on solute and heat transport. Oral communication at 6th International Geologica Belgica Meeting 2018, Leuven, Belgium. http://hdl.handle.net/2268/227892

Robert, T., Hermans, T., Lesparre, N., Nguyen, F., Paulus, C., Bolly, P.-Y., Defourny, A., **Jamin, P.**, Orban, P., Brouyère, S., & Dassargues, A. (2018, September 10). Experimental assessment and prediction of short-term aquifer thermal energy storage for energy demand-side management applications. Oral communication at IAH 2018, Daejeon, Republic of South Korea. http://hdl.handle.net/2268/227899

Nikolenko, O., Orban, P., Jurado, A., Borges, A., Brouyère, S., **Jamin, P.**, Thomas, C., & Morana, C. (2018, April 20). Dynamics of nitrous oxide in groundwater under agricultural areas: insights from multi-isotopic studies (15N, 34S, 18O, 13C, 3H). Oral communication at BASIS Symposium 2018, Liège, Belgium. http://hdl.handle.net/2268/227432

Brouyère, S., **Jamin, P.**, Orban, P., Dassargues, A., & Cosme, F. (2018, April 11). Advanced single-well applied tracer techniques for improving reliability of groundwater and contaminant mass flux monitoring. Oral communication at Conference on Remediation of Chlorinated and Recalcitrant Compounds 2018, Palm Springs, CA. http://hdl.handle.net/2268/222316

Nikolenko, O., Orban, P., **Jamin, P.**, Jurado, A., Borges, A., & Brouyère, S. (2018, April 07). Biogeochemistry of greenhouse gases in groundwater under agricultural area (the Geer catchment, Belgium). Oral communication at EGU GA 2018, Vienna, Austria. http://hdl.handle.net/2268/223849

Nguyen, F., Hermans, T., **Jamin, P.**, wildermmersch, S., Klepikova, M., Orban, P., Brouyère, S., & Dassargues, A. (2016, September 27). Comparison of temperature from DTS and ERT with direct measurements during heat tracer experiments in heterogeneous aquifers. Oral communication at 43rd IAH congress. http://hdl.handle.net/2268/202072

Fernandez de Vera, N., Beaujean, J., **Jamin, P.**, Hakoun, V., Dahan, O., Nguyen, F., & Brouyère, S. (2016, July 26). Monitored tracer experiment using the vadose zone experimental setup (VZES) for studying water and pollutant recharge processes in a brownfield. Oral communication at 9th IAHS Conference on Groundwater Quality GQ2016, Shenzhen, China. http://hdl.handle.net/2268/202419

Klepikova, M., Wildemeersch, S., **Jamin, P.**, Orban, P., Hermans, T., Nguyen, F., Brouyère, S., & Dassargues, A. (2016, April 20). Heat tracer test in an alluvial aquifer: field experiment and inverse modelling. Poster session presented at EGU General Assembly 2016, Vienna, Austria. http://hdl.handle.net/2268/195219

Dassargues, A., Klepikova, M., **Jamin, P.**, Orban, P., & Brouyère, S. (2015, December 18). Heat tracer and solute tests in an alluvial aquifer: field experiment and inverse modelling. Poster session presented at AGU Fall Meeting Session H51F paper 1438, San Francisco, USA. http://hdl.handle.net/2268/193004

Palau, J., **Jamin, P.**, Badin, A., Shouakar-Stash, O., Brouyère, S., & Hunkeler, D. (2015, September 17). Use of dual carbon-chlorine isotope analysis to identify degradation pathways of 1,1,1-trichloroethane in groundwater. Oral communication at AQUA2015, 42nd IAH International Congress, Hydrogeology: back to the future, Rome, Italie. http://hdl.handle.net/2268/188229

Fernandez de Vera, N., Beaujean, J., **Jamin, P.**, Hakoun, V., Vanclooster, M., Dassargues, A., Dahan, O., Nguyen, F., & Brouyère, S. (2015, September). The use of the Vadose Zone Experimental Setup as an innovative in situ characterization method for the vadose zone: a case study at an industrial contaminated site in Belgium. Oral communication at 42nd IAH Congress-AQUA2015, Hydrogeology: back to the future, Rome, Italie. http://hdl.handle.net/2268/183896

Klepikova, M., Wildemeersch, S., **Jamin, P.**, Orban, P., Hermans, T., Nguyen, F., Brouyère, S., & Dassargues, A. (2015, June 05). Use and utility of combined solute and heat tracer tests for characterizing hydrogeothermal properties of an alluvial aquifer. Oral communication at CBH-BCH, Belgian National IAH Chapter Study Day on Geothermy, Mons. http://hdl.handle.net/2268/182626

Klepikova, M., Wildemeersch, S., **Jamin, P.**, Orban, P., Hermans, T., Brouyère, S., & Dassargues, A. (2014, September 22). A heat and dye tracer test for characterizing and modelling heat transfer in an alluvial aquifer. Poster session presented at IAHR 7th International Groundwater Symposium, Perugia, Italy. http://hdl.handle.net/2268/176622

Fernandez de Vera, N., Beaujean, J., **Jamin, P.**, Nguyen, F., Dahan, O., Vanclooster, M., & Brouyère, S. (2014, September 03). Vadose zone studies at an industrial contaminated site: the vadose zone monitoring system and cross-hole geophysics. Oral communication at In Situ Remediation 2014, London, United Kingdom. http://hdl.handle.net/2268/178428

Fernandez de Vera, N., Beaujean, J., **Jamin, P.**, Nguyen, F., Dahan, O., Vancloster, M., & Brouyère, S. (2014, April 29). Vadose zone studies at an industrial contaminated site: the vadose zone monitoring system and cross-hole geophysics. Poster session presented at European Geoscience Union General Assembly 2014. http://hdl.handle.net/2268/170754

Fernandez de Vera, N., Pena Hernandez, J. A., Beaujean, J., **Jamin, P.**, Nguyen, F., Dahan, O., & Brouyère, S. (2014, March 05). Vadose zone studies at an industrial contaminated site: the vadose zone monitoring system and cross-hole geophysics. Oral communication at Envitam PhD Student Day 2014. Universite Catholique de Louvain la Neuve. http://hdl.handle.net/2268/170762

Fernandez de Vera, N., Pena Hernandez, J., Beaujean, J., **Jamin, P.**, Nguyen, F., Dahan, O., & Brouyère, S. (2014, January 15). Vadose zone studies at an industrial contaminated site: the vadose zone monitoring system and cross-hole geophysics. Oral communication at Journée des Doctorants Geosciences. Universite de Liege. http://hdl.handle.net/2268/170761

Dassargues, A., Wildemeersch, S., **Jamin, P.**, Orban, P., Hermans, T., & Brouyère, S. (2013, December 09). Heat transfer characterization using heat and solute tracer tests in a shallow alluvial aquifer. Poster session presented at AGU Fall Meeting 2013, San Francisco, USA. http://hdl.handle.net/2268/161233

Batelaan, O., Dujardin, J., **Jamin, P.**, Bashir, I., Canters, F., Dassargues, A., & Brouyère, S. (2013, September 15). Regional urban groundwater body risk assessment of contaminants using remotely sensed multi-resolution land-cover data. Oral communication at IAH 2013, Solving the Groundwater Challenges of the 21th Century, Perth, Australia. http://hdl.handle.net/2268/161234

Fernandez de Vera, N., Peña Hernandez, J. A., **Jamin, P.**, Vanclooster, M., & Brouyère, S. (2013, April 22). Integrated field assessment of contaminant fate and transport in the unsaturated and saturated zone. Poster session presented at 8th IAHS International Groundwater Quality Conference (GQ13), Gainsville, Florida, Etats-Unis. http://hdl.handle.net/2268/149118

Orban, P., Wildemeersch, S., Gesels, J., **Jamin, P.**, Dassargues, A., & Brouyère, S. (2012, October 10). Modélisation régionale des eaux souterraines dans le cadre de la mise en œuvre de la Directive Cadre sur l'Eau : exemple du projet Synclin'Eau. Oral communication at Ressources en eau souterraine : De la modélisation régionale à la protection des captages, Namur, Belgique. http://hdl.handle.net/2268/132178

Leroy, M., Orban, P., Brouyère, S., Gesels, J., Couturier, J., **Jamin, P.**, Wildemeersch, S., Goderniaux, P., Derouane, J., & Dassargues, A. (2011, May 02). Regional scale flow and transport modelling for the management of groundwater and surface water bodies in the framework of the EU Water Directive. Oral communication at HydroEco'2011, 3rd International Multidisciplinary Conference on Hydrology and Ecology: Ecosystems, Groundwater and Surface Water – Pressures and Options, Vienna, Austria. http://hdl.handle.net/2268/90432

Prizes

Fondation Roi Baudouin, Prix Ernest Dubois [grant no. 2015-F2812650-204355], 20 000 €.

Acknowledgements

Ten years ago, when Pr. Alain Dassargues and Serge Brouyère hired me, I had a clear view of what I wanted. I agreed to work on applied research projects, but at one condition: no PhD thesis! During the first 3 years, I have been working on various projects and tasks: research, teaching, consulting and managing field equipment. All these different tasks made me realized that smarter techniques for aquifer characterization had to be developed, in particular in support to contaminated aquifers management. This is how this PhD started. It is applied and field-oriented. It corresponds me.

This research was supervised by Pr. Alain Dassargues and Serge Brouyère. Dear Professor Dassargues, I sincerely thank you for the time you spend discussing with me. We may have discussed more about the "sides" of the thesis than the actual research. Nevertheless, these discussions were essential to me and your support has always been a great encouragement to finish this PhD. Dear Serge, I dare to say that we did make the FVPDM grow pretty well. From the first equations you wrote to the last field application I performed, the FVPDM can be claimed a mature method. Thank you for all your help, advices and outstanding scientific strength.

I would like to thank Pr. Domique Toye, Pr. Pascal Goderniaux, Pr. Frédéric Ngyuen, Pr. Olivier Atteia and Pr. Michael Annable who devoted some of their precious time to evaluate this PhD thesis. It is a real honor for me to have you all as members of this jury. I also thank Ludo Diels for taking part of the PhD follow-up committee meetings.

Guys from the Hydrogeology and Environmental Geology group, this would not have been possible without you. Thanks to all the colleagues I had/have the pleasure to work with, Philippe the keystone of the group, Ingrid, Pascal, Samuel, Pierre, Joël who's lab remains a bit yellow and pink from the dye tracers I spilled during many years, Caroline, Agathe, Thomas, Vivien, Emilie, Richard, Olha, Julie, Natalia, David, Tanguy. Discussions, field support, field craziness and hard work time with you meant a lot for me. Thank you to Christiane, Martine, Nadia, Leila, Lidja, the secretariat staff for their availability.

I also would like to address my thanks to the team Geosciences Rennes for the good time we shared on Ploemeur test site. Pr. Olivier Bour, Tanguy Le Borgne, Andreas Englert, Pascal Goderniaux and all the team Ploemeur summer '12. Thank you Nicolas for all your advices and teachings about field equipment. Thank you Rebecca for the delicious gingerbreads that kept us motivated during the typical rain of Brittany. Field work was pretty hectic but we also managed to gather around some really nice tables.

I am very grateful to Pr. Jean-Michel Lemieux for the opportunity he gave me to work in Nunavik. This field experience remains one of the most amazing I had. Thanks to all the members of the team Umiujaq '16, Pr. Richard Fortier, Pr. John Molson, Marion, Sophie, Veronik, Marie-Catherine, Jonathan and Renaud. Thanks for integrating me in your team this way, thanks for your help during demanding field works and thanks for the more relax moments including swimming around icebergs, staring at aurora borealis and returns back to base camp in

"commando mode". Special thanks to Jean-Michel, Richard and John for reviewing the article so efficiently. The way you work on manuscripts is truly gold for PhD students.

Of course I don't forget you, team iFLUX. Thank you Goedele, Tim and Filip for letting me work on your sand box, for the good time we shared in the field and for the very interesting conversations we had about mass flux. I'm really looking forward to our future collaborations.

I also address my thanks to Frederic Cosme and people concerned at Golder Associates. Thank you for the opportunity we had to work with you, on what remains the first real scale application of the FVPDM in a context of polluted aquifer. I really appreciated the conversations we had, the critical eye you kept on the technique and all the good advices that came from someone from the environmental consulting sector. I'm also looking forward to our next collaborations.

I am also grateful for all the financial support I have had during my assistantship at the University of Liège. Research grants from the University of Liège [no. FSRC-12/81], from FNRS Belgium [no. 1.5060.12] and from the Fondation Roi Baudouin, Prix Ernest Dubois [no. 2015-F2812650-204355] were the basis of all the field work undertaken during this PhD. This research also benefited from the CLIMAWAT project (Adapting to the Impacts of Climate Change on Groundwater Quantity and Quality – EU-RDF INTERREG IVA program), from the national network of hydrogeological sites H+ and the ANR project CRITEX ANR-11-EQPX-0011, from the Natural Sciences and Engineering Research Council of Canada (NSERC) through the Strategic Project Grant program, from the Centre d'études nordiques (CEN) at Université Laval and from the Inuit community of Umiujaq.

Finally, I would like to express my warmest thanks to my family and friends who have been supporting, encouraging and challenging me during this research time, directly or indirectly. I am somehow back home now.

Table of content

List of symbols and acronyms

A	Cross sectional flow area	L^2
ADV	Acoustic Doppler Velocimeter	
ASL	Above sea level	
bgs	Below ground surface	
C	Solute concentration	$M\ L^3$
CB	Colloidal Borescope	
C_{DL}	Detection limit of the tracer detector	$M\ L^3$
C_{in}	Tracer concentration initially present in the aquifer	$M\ L^3$
C_{inj}	Injected tracer concentration	$M\ L^3$
C_{SL}	Saturation limit of the tracer detector	$M\ L^3$
CSM	Conceptual Site Model	
C_w	Tracer concentration in a well	$M\ L^3$
C_w*	Adimensional tracer concentration	
$C_{w,0}$	Initial tracer concentration in a well	$M\ L^3$
$C_{w,stab}$	Stabilized tracer concentration	$M\ L^3$
e_{scr}	Screen length	L
FVPDM	Finite Volume Point Dilution Method	
G	Forward model describing observations	
HPFM	Heat Pulse Flow Meter	
h_w	Height of groundwater column in a well	L
i	Hydraulic gradient	
i_{max}	Maximum hydraulic gradient	
i_{min}	Minimum hydraulic gradient	
IPFS	Insitu Permeable Flow Sensor	
IPT	Intergral Pumping Test	
IWPVP	In-Well Point Velocity Probe	
J	Mass flux	$M\ L^{-2}\ T^{-1}$
K	Hydraulic conductivity	$M\ T^{-1}$
K_{est}^{min}	Minimum estimated hydraulic conductivity	$M\ T^{-1}$
k_F	Hydraulic conductivity of the filter pack	$M\ T^{-1}$
k_S	Hydraulic conductivity of the well screen	$M\ T^{-1}$
LDV	Laser Doppler Velocimeter	
M	Mass of tracer in a well	M
m	Series of measurements	
M_d	Solute mass discharge	$M\ T^{-1}$
M_{inj}	Injection tracer mass	M

n	Total porosity	
$p(\theta)$	Posterior density function	
PDM	Point Dilution Method	
Pe	Peclet number	
PFM	Passive Flux Meter	
PVCFM	PVC Flow Meter	
PVP	Point Velocity Probe	
q_{app}	In-well apparent Darcy flux	$L\ T^{-1}$
Q_{cr}	Critical flow rate	$L^3\ T^{-1}$
q_D	Groundwater flux or Darcy flux	$L\ T^{-1}$
Q_{in}	Groundwater flow rate entering a well by the screen	$L^3\ T^{-1}$
Q_{inj}	Tracer injection flow rate	$L^3\ T^{-1}$
Q_{mix}	Mixing flow rate of the water column in a monitoring well	$L^3\ T^{-1}$
Q_{out}	Groundwater flow rate exiting a well by the screen	$L^3\ T^{-1}$
Q_{pump}	Pumping flow rate at well	$L^3\ T^{-1}$
Q_t	Groundwater transit flow rate through the screen of a well	$L^3\ T^{-1}$
$Q_{t,prior}$	A priori estimated groundwater transit flow rate	$L^3\ T^{-1}$
$Q_{t,prior}^{max}$	Maximum a priori estimated groundwater transit flow rate	$L^3\ T^{-1}$
$Q_{t,prior}^{min}$	Minimum a priori estimated groundwater transit flow rate	$L^3\ T^{-1}$
R^2	Coefficient of determination	
r_B	Radius of the borehole	L
r_I	Internal radius of the well screen	L
RMS	Root Mean Square Error	
r_O	Outer radius of the filter screen	L
r_w	Radius of a well	L
SSR	Sum of squared residuals	
S_w	Cross sectionnal flow area delineated by a well screen	L^2
t	Time	T
t_0	Initial time	T
t_c	Stabilization time	T
T_{inj}	Tracer inejction time	T
V_{inj}	Injected volume of tracer	L^3
V_w	Water volume in a well	M^3
a_w	Flow distortion coefficient	
$\triangle L$	Characteristic lenght	L
$\triangle t$	Time step	T
θ	Vector of parameters	
$\varkappa$	Thermal diffusivity	$L^2\ T^{-1}$
σ	Standard deviation	

List of figures

List of tables

Introduction

The current challenge of mass flux measurement in contaminated aquifers

Groundwater is present beneath the soil surface in pores and fractures of the geological formations. More than 95% of the fresh water easily accessible on Earth is found underground and provides drinking water to more than 50% of the global population (UNESCO 2015). Groundwater is also used in agriculture, industry, households and eventually feeds surface water and ecosystems. It is one of the most important natural resources of our planet and requires appropriate management and protection in order to guarantee its availability for future generations.

From a water quality point of view, industrial activities of the past century and modern accidental releases impacted locally the groundwater resource both physically and chemically. In Europe, local soil and groundwater contaminations were assessed in 2.8 million potentially contaminated sites in 2011 (Perez and Eugenio 2018). Characterization, risk assessment, remediation design and more generally management of these contaminated aquifers has historically relied on comparison between measured contaminant concentrations in the aquifer and threshold values. This approach is a necessary first step for contaminated aquifers characterization. However, it is totally insufficient to fully investigate the contaminants behavior in groundwater, to quantify the risk and to design efficient remediation measures. Concentration-based approaches do not consider groundwater flows which act as driving force of contaminant mobility in aquifers. For example, the risk posed by a pollutant in an aquifer depends on the actual transfer between the source and the receptor and is thereby a function of the quantity of pollutant that migrates from the source to the receptor. Hence, neglecting groundwater flow in the management of contaminated aquifers has both environmental and financial consequences.

The amount of contaminant that moves through aquifers can be quantified through mass flux or mass discharge measurements. Since the beginning of the years 2000, a consensus has been growing among the scientific, technical and decision makers' community on the fact that characterization and management of contaminated sites

should be performed in terms of contaminant flux metrics (Einarson & Mackay 2001, API 2003, Nichols and Roth 2004, Annable 2008). Flux-based approaches are complementary alternatives to any concentration-based management of contaminated aquifers. They provide more robust results allowing (1) prioritization of contaminated aquifers or zones within a contaminated aquifer, (2) risk assessment of contaminant spreading from sources to potential nearby receptors, even in case of multiple sources with additive effects, (3) design of remediation measures and evaluation of their efficiency, (4) complex hydrogeological modeling, (5) quantification of natural attenuation and (6) quantification of contaminated groundwater discharge in surface water.

Following these findings, mass flux and mass discharge-based regulations started to be developed all over the world (Newell et al. 2011, CRC CARE 2016). To satisfy these new requirements, it is necessary to dispose of techniques able to accurately measure the mass flux and mass discharge of contaminants in aquifers. Contaminant mass flux calculation usually relies on measurements of both groundwater flux and contaminant concentration in any monitoring well drilled in the aquifer of concern. Since the measurement of contaminant concentration in aquifers is already regulated and part of routine characterization studies, the research must propose new solutions, methodologies and techniques to measure groundwater fluxes.

Existing methods for direct or indirect measurements of groundwater fluxes are affected by various intrinsic and extrinsic limitations (Guaraglia and Pousa 2014, Bayless et al. 2011, Wilson et al. 2001). Acoustic and Laser Doppler Flowmeters (Wilson et al. 2001, Momii et al. 1993), Heat Pulse Flow Meter (Bayless et al. 2011) and PVC Flowmeter (Masciopinto and Palmiotta 2013) are usually not suitable for small diameter piezometers due to the size of the needed apparatus. Direct-push methods such as Point Velocity Probes (Labaky et al. 2007) and In Situ Permeable flow sensor (Ballard 1996) are only applicable in unconsolidated porous aquifers. Furthermore, these methods only allow measurement of local groundwater flux (or velocity) on a discrete vertical sampling point of a few centimeter and may not deliver a groundwater flux representative of the entire length of the well-screen in heterogeneous aquifers. Finally, none of the existing techniques allows for a refined and continuous time monitoring of groundwater fluxes (Kempf et al. 2013). However, in many different hydrogeological contexts, groundwater flow is intrinsically transient and assuming steady state flow conditions may not be adequate.

Moreover, regardless of the method, field calculation of contaminant mass discharge is always affected by uncertainties caused by time or spatial variability of contaminant mass fluxes. Mass discharge calculations are usually made from point-type measurements, performed at specific locations of the aquifer. Due to time and budget constraints, the full spatial variation of the contaminant mass flux within the plume is never fully characterized. Accurate direct groundwater flux measurement, in support to mass flux and mass discharge calculations, can help at better identifying zones of high contaminant discharge, at reducing uncertainties on contaminant mass discharge and at improving the general management of contaminated sites.

Among other available direct groundwater fluxes measurement methods, the Finite Volume Point Dilution Method (FVPDM) is a promising candidate. This innovative technique has the potential to be developed for

monitoring variable groundwater fluxes in transient flow conditions and has already been successfully applied in a few different geological settings. However, the full potential of the method is still to be further investigated.

Research objectives

Before the PhD, the FVPDM was only applied on a few cases with simple interpretations. The research aims at validating the use of the FVPDM and at delivering a fully operational method for measurement of groundwater fluxes for a wide spectrum of experimental and groundwater flow conditions.

As for any new developed technique or instrument, the first objective is to evaluate the full specifications of the FVPDM that define its accuracy (i.e., how far the value measured by the method is from the true value?), its precision (i.e., how close consecutive measurements of the same parameter are to each other?) and its resolution (i.e., what is the smallest increment that can be measured?). Limitations of the method in terms of minimum and maximum groundwater fluxes that can be measured will also be specified.

The second main objective is to develop the mathematical framework, methodology and experimental setup to use the FVPDM technique for continuous monitoring of groundwater fluxes in transient state groundwater flow conditions.

Finally, a more implicit objective is to apply the FVPDM on different lab-scale and field-scale experiments in order to define the smartest experimental setups for different field conditions and constraints. Robustness and versatility of the technique in various and even extreme environmental and hydrogeological contexts will also be demonstrated. More generally this work must also show the advantages of having reliable measurements of groundwater fluxes for all domains of hydrogeological studies.

Thesis outline

Beside the present introduction and the final general conclusions and perspectives, this manuscript is organized in four main chapters.

In the first chapter, the general issue of groundwater quality and contaminated aquifers is introduced (sections 1.1, 1.2 and 1.3). Basic concepts underlying the contaminant mass flux calculation in aquifers are exposed (section 1.3). After a review of existing methods and techniques available to measure groundwater fluxes and contaminant mass fluxes, the general challenges of mass discharge calculation are exposed taking into account the spatial and time variability of the contaminant fluxes in aquifers due to subsurface heterogeneity and to the transient nature of groundwater flows (sections 1.6 to 1.8). Finally, the FVPDM is presented as an alternative for measuring and monitoring changing groundwater fluxes.

The second chapter details the mathematical basis of the FVPDM as a generalization of the single-well point dilution methods. The theoretical background already published by Brouyère et al. (2008) is synthetized to ease the comprehension of the FVPDM further developments (sections 2.1, 2.2, 2.3 and 1.6.12). A newly developed mathematical framework allowing monitoring variable groundwater fluxes is then presented (section 2.4). The experimental setup needed to perform such a measurement is detailed and a new general dimensioning flow chart is provided (sections 2.5 and 2.6).

In chapter three, the specifications of the FVPDM for the measurement of groundwater fluxes in both steady and transient state flow conditions are discussed. In the first section the accuracy of the FVPDM is quantified by comparing measured and prescribed water fluxes within a flow through sand tank in laboratory (section 3.1). A second section relates a field experiment aiming simultaneously at (1) testing the FVPDM using an inflatable straddle packer setup for investigation of a discrete vertical part of a fractured aquifer, and (2) quantifying the precision of the FVPDM versus the more traditional point dilution method (section 3.2). In the third section, a field application aiming at quantifying the resolution of the FVPDM when used to monitor variable groundwater fluxes (section 3.3) is presented.

In the fourth chapter, three field applications of the FVPDM are presented. The first field application is performed in the remote territories of Nunavik in northern Quebec (section 4.1). Here, direct groundwater fluxes measurements were undertaken, in support of a thermo-hydrodynamic characterization of a watershed where permafrost thaw occurs. This specific application demonstrates the robustness and versatility of the FVPDM. In the second field application, the control plane approach is tested as solute mass discharge calculation technique in an aquifer where a controlled steady state solute plume is created (section 4.2). Knowing precisely the solute mass discharge prescribed in the aquifer, the mass discharge calculation based on groundwater flux and solute concentration measurements performed at control planes is discussed. The third reported FVPDM application concerns a contaminated costal aquifer (section 4.3). At this site, industrial activities have led to significant groundwater quality deterioration and to high risks for the downgradient exposed receptors. Here, continuous monitoring of groundwater fluxes influenced by tidal effect allows to refine and improve the conceptual site model. Moreover, contaminant mass flux results constitutes high-value information for optimization of further investigations and risk mitigation measures

Finally, after a summary of the main research outcomes, the conclusions of this research work provide clear answers to the questions posed as initial objectives. The Finite Volume Point Dilution Method is indeed a robust and reliable technique for measuring and monitoring groundwater fluxes and offers numerous perspectives of development and application.

Chapter 1

Mass flux as fundamental metric for contaminated aquifers management

Contaminated groundwater is a major environmental issue. Classical methods currently used for characterization of contaminated aquifers are limited for understanding contaminant behavior in saturated zone, for risk assessment and designing and assessing remediation systems performance. Contaminant mass flux-based approaches deliver more adequate information for contaminated aquifers management. The calculation of contaminant mass fluxes require accurate measurements of contaminant concentrations but, as importantly, accurate measurements of groundwater fluxes by techniques able to capture their time variations.

In this first chapter, the general issue of groundwater quality and contaminated aquifers is introduced and the basic concepts underlying the contaminant mass flux calculation in aquifers are exposed. After a detailed review of existing methods available to measure groundwater and contaminant mass fluxes, the challenges of mass discharge calculation are exposed. Finally, the FVPDM is presented as an alternative for measuring and monitoring changing groundwater fluxes.

1.1. The environmental challenge of groundwater resources protection and management

Water is a very abundant natural resource on Earth. The volume of water on our planet is currently evaluated at 1387 km³. More than 97.5% of this volume is saline water contained in oceans, seas and salty lakes (Figure 1). Fresh water represents only 2.5% of the water on Earth, of which most is contained (for the moment) in ice caps and glaciers and characterized as "uneasy to use water". Almost one third of the freshwater resource lays under the earth surface as groundwater. Thereby, groundwater represents 95% of this "easy to use water" and constitutes as the main reservoir of accessible fresh water (Dassargues 2018). Groundwater generally provides water of good chemical quality and of stable physical properties due to the localization of aquifers which, in depth, benefit from the above located terrains acting both as a filter and as a thermal insulator.

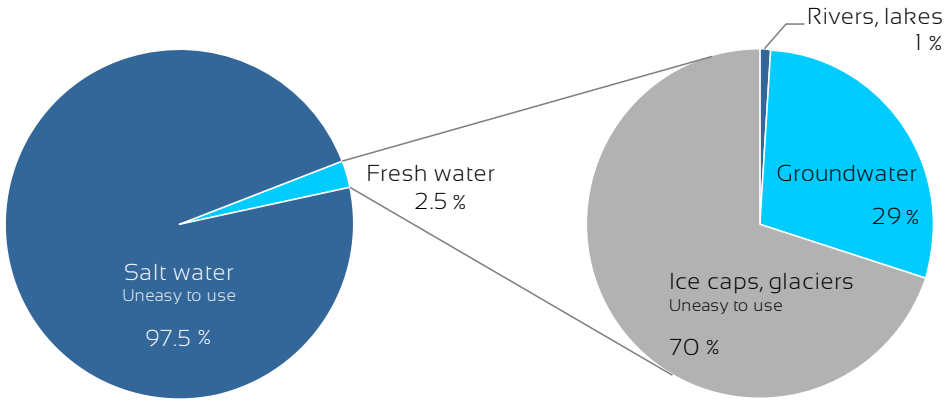

Figure 1: Water distribution on Earth. Fresh water represents only 2.5% of the global water. Groundwater constitutes 95% of the "easy to use water" and is thereby a very important natural resource to preserve.

Groundwater provides drinking water to more than 50% of the global population. Population growth, urbanization, industrialization and increased production and consumption generates an increasing demand for freshwater. With a world's population growing by about 80 million people per year and a global water demands growing by 1% per year, 40% of the global population is projected to face a water deficit by 2050 under the business-as-usual climate scenario (UNESCO 2018).

In Europe, despite relatively comfortable freshwater resources of 3500 m³ per habitant and per year, around one third of the European population was exposed to water scarcity in the summer of 2015. This is due to the uneven continental spread of both the socio economical water demand and the fresh water resource (EEA 2017, EEA 2018). Groundwater is a natural resource requiring a good management and a strict protection in order to guarantee its availability for future generations.

In Wallonia, the freshwater budget is around 13 billions of cubic meters per year, due to abundant precipitations uniformly spread throughout the year. The annual renewable groundwater resource of Wallonia is estimated at 550 million m³ per year of which 370 million m³ are abstracted yearly (SPW 2017a). More than 80% of the groundwater produced is used for public distribution. This use requires water of perfect drinking quality making the protection of the Walloon groundwater resource of great importance. However, more than half of the Walloon groundwater bodies present a "deteriorated chemical" status. The causes of this deterioration come from 4 main drivers: agriculture, industries, collectivities and historical liability (SPW 2017a, 2017b). Apart from agriculture that usually induces diffuse contaminations to soil and groundwater, the rest of the cited driving forces mainly causes point-type contaminations. These contaminations, originally occurring at the surface, accumulate in the soil and later migrate downwards with the infiltration water to reach the saturated zone.

Management and protection of the groundwater resources are thereby current and future major environmental challenges, more specifically regarding to the point type contaminations.

1.2. Contaminated sites in Europe and Wallonia

Soil and groundwater contamination refers to reduced soil or water quality due to the presence of substances resulting from human activity. In Europe, local soil contaminations were assessed in 2.8 million potentially contaminated sites in 2011 (Figure 2). More than 342 000 sites were officially characterized as contaminated and, to date, only 19% of these have been remediated (EEA 2000, Panagos et al. 2013, Perez and Eugenio 2018). 650 000 sites currently in activity are registered as potentially polluting and 19 000 new sites are registered every year.

The budget dedicated to contaminated site management in Europe is evaluated at 15 billion euros for the period 2006-2010 (Ernst & Young 2013). 42% of the expenditure come from public budgets. On average, 85% of this budget is attributed to the remediation actions themselves while only 15% is spent on the site characterization. The mean management cost for a contaminated site in Europe ranges between 50 000 to 500 000 euros while extremely large remediation projects costing more than 5 million euros are rarely reported (EEA 2014).

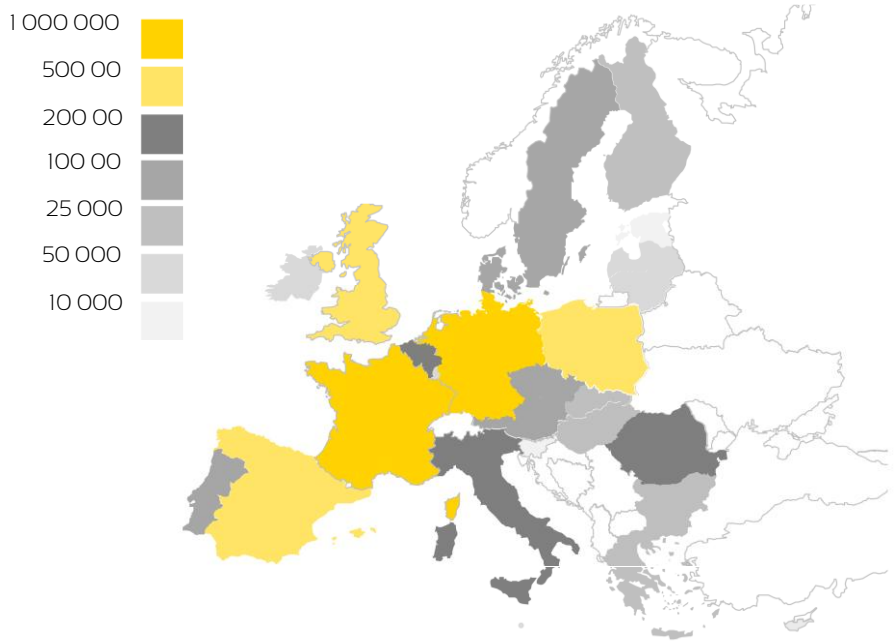

Figure 2: The estimated number of potentially contaminated sites in the largest countries of Europe is in the hundreds of thousands (modified from Ernst & Young 2013). Management of contaminated sites and aquifers remains a major environmental challenge.

Management of contaminated site relies mainly on risk-based approaches (EEA 2000, Anaya-Romero et al. 2016). The actual risk induced by a contamination is the result of a transfer pathway between a contaminant source and a receptor (Figure 3). Concentration-based risk assessment approach is useful for soils management because contaminants in the soil usually show a low mobility and their concentrations remain roughly identical on short time periods. In aquifers, concentration-base approaches are not sufficient to assess the risk since groundwater flow is the main driving force of contaminant mobility by advection and dispersion and therefore of the risk. For contaminated aquifers, groundwater flow data are as important as concentration data for risk assessment.

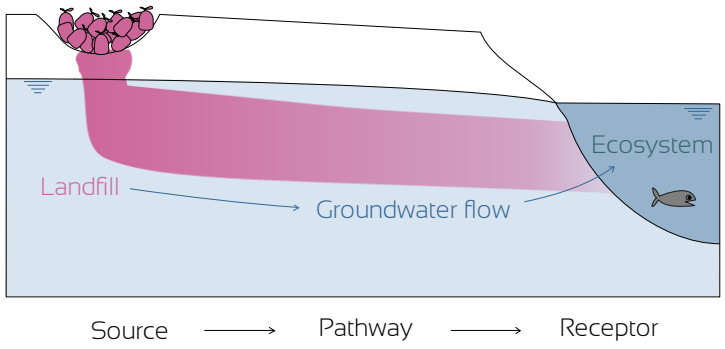

Figure 3: Illustration of a typical SPR schema. The landfill is a source of contamination threatening the ecosystems of the nearby river. Groundwater constitutes the pathway between the source and the receptors. Groundwater flow is the main driving force of contaminant mobility in aquifers and should be quantified accurately in flux-based risk assessment approaches.

The complementary alternative to concentration-based risk assessment is the flux-based risk assessment. Instead of a concentration that only represents the amount of contaminant in a given volume of groundwater, a mass flux measurement delivers the quantity of contaminant that actually travels in the groundwater. Several studies already emphasized the benefit of such flux-based approaches as they focus on the mass of contaminant that migrates downgradient in aquifers and may reach receptors (Einarson and Mackay 2001, Tait et al. 2004, Malina et al. 2006, Jamin et al. 2012, Troldborg 2010, Verreydt et al. 2012).

1.3. Concepts of mass flux and mass discharge

1.3.1. Theoretical background

The mass flux of contaminant in groundwater is defined as the quantity of this contaminant passing through a unitary cross-sectional area over a period of time. This area is positioned orthogonally to the mean groundwater flow direction. Mathematically, mass flux can be expressed as the product between the contaminant concentration (C) [M L^{-3}] and the groundwater flux (or Darcy flux) (q_D) [L T^{-1}] (Equation 1).

$$J = q_D\, C \qquad \textit{Equation 1}$$

The mass flux (J) [M L^{-2} T^{-1}] is thus a vectorial quantity, characterized by an intensity (i.e. the value of the flux) and by an orientation (Figure 4). The unit of mass flux is a mass per area and per time. The measurement of contaminant mass flux often requires an independent measurement of groundwater flux and of aqueous contaminant concentration.

Contaminant mass discharge is the total mass of contaminant travelling in groundwater across a defined area and is thus a scalar quantity (Figure 4). The total mass discharge of a contaminant plume represents the total mass of contaminant migrating per unit time across a given cross-sectional area that encompasses the entire solute plume and is positioned orthogonally to the mean groundwater flow direction. Mass discharge is calculated by integrating the contaminant mass flux over a defined flow cross-sectional area at defined positions along the plume called transects (Equation 2).

$$M_d = \int_A J\, dA \qquad \textit{Equation 2}$$

M_d is the contaminant mass discharge [M T^{-1}] and A is the cross sectional flow area [L^2]. The calculation of mass discharge often requires multiple measurement of contaminant mass flux repeated along the cross sectional flow area of the plume.

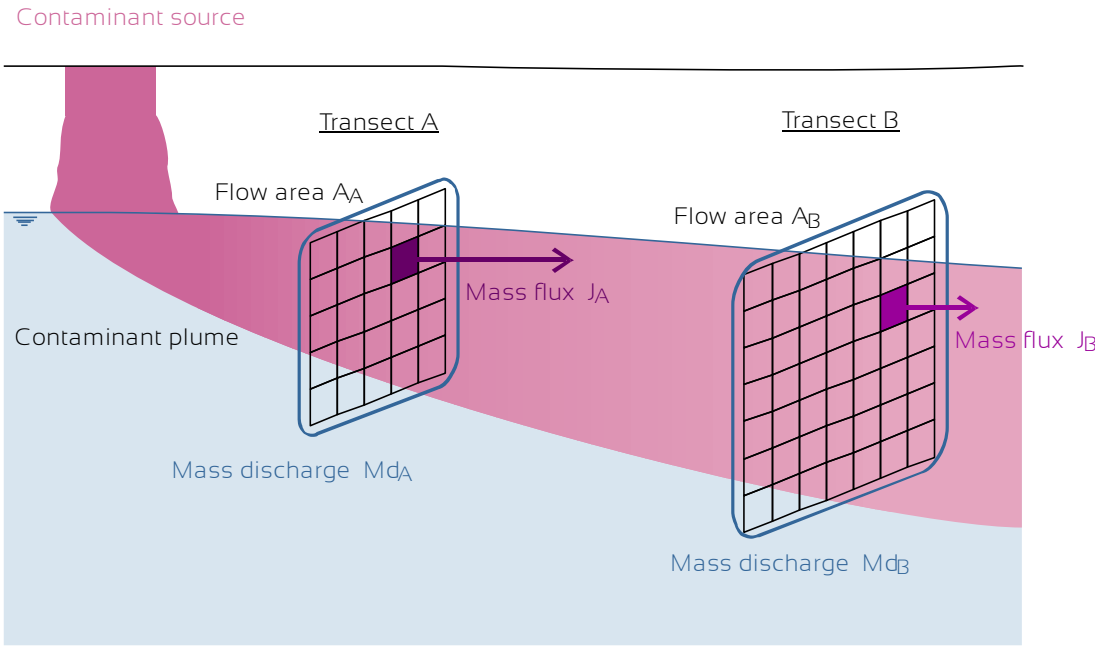

Figure 4: Multiplication of the groundwater flux [L T^{-1}] by the contaminant concentration [M L^{-3}] leads to the contaminant mass flux J [M L^{-2} T^{-1}]. The integration and sum of all the contaminant mass flux measurements on the representative flow section A [L^2] gives the contaminant mass discharge M_d [M T^{-1}] at a given transect (modified from ITRC 2010).

1.3.2. Use and relevance of contaminant mass flux and mass discharge

The interest of mass flux and mass discharge measurements is clearly illustrated in Figure 5. A dual-layer aquifer is contaminated by a same concentration of contaminant in both layers. According to a concentration-based approach, both aquifer layers are managed identically. However, if, in the upper layer, groundwater flows ten times faster than in the lower layer, the upper layer alone carries 91% of the contaminant mass flux that migrates through the aquifer. It becomes obvious that the two layers should not be managed identically.

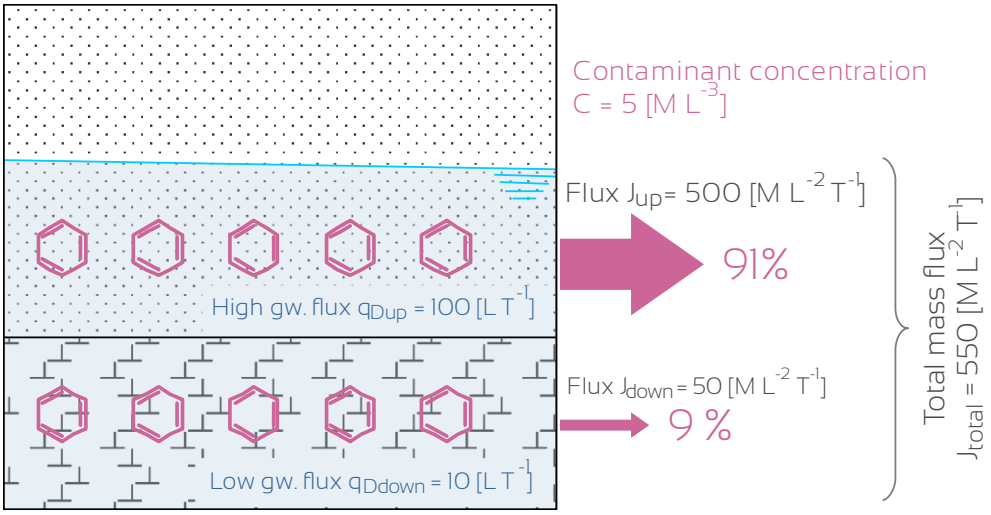

Figure 5: Simplified cross section of a two layers contaminated aquifer. Contaminant concentrations are identical in both layers, leading classically to an identical management of the two layers. However, groundwater flux is ten times higher in the upper aquifer that consequently carries 91% of the contaminant mass flux and constitutes 91% of the risk for a potential downgradient located receptor. The upper layer should thus be treated in priority.

Contaminated aquifer management only based on contaminant concentrations can also lead to contradictory conclusions. Contaminant concentrations measured in an aquifer right beneath a contaminant source can be significantly higher in a low hydraulic conductivity aquifer than in a high hydraulic conductivity aquifer, due to a lower dilution by the groundwater flow (and considering identical hydraulic gradients). It may be concluded that the associated risk, if calculated on concentration data only, is higher for the low hydraulic conductivity aquifer. This is absurd since the volume of aquifer that will be impacted is much lower for the low hydraulic conductivity aquifer and because the transfer of contaminant from the source to a receptor (*i.e.* the risk) will be faster and more important in the high hydraulic conductivity aquifer (Marchal et al. 2018a, 2018b).

When risk-based management is used, the only key question that is addressed is: "How significant are the releases of contaminants in terms of their ability to impact a given receptor?" (Einarson and MacKay 2001). Unlike a traditional concentration-based approach, a mass flux approach combines contaminants concentration and groundwater flow which gives much more information than concentration or flow considered separately (Nichols and Roth 2004, Nichols 2010). Flux-based approaches offers numerous benefits for contaminated aquifer management (Figure 6).

Contaminant risk assessment for a given receptor becomes even more difficult when evaluating the risk posed by multiple sources are involved (Troldborg et al. 2008, Jamin et al. 2012). Additive effects of the multiple sources can not be evaluated on concentration-based approaches but must rather be based on mass flux-based approaches. As it quantifies the contaminant source strength and provides insights on the risk for downgradient receptors, mass fluxes can also be used for site prioritization (Brooks et al. 2008).

Selecting and dimensioning remediation techniques for contaminated aquifers are also more cost effective when based on mass flux and mass discharge measurements. Several studies quantified the benefit of using a flux-based approach for the remediation at more than 30% of the total remediation costs (ITRC 2010). Mass discharge can also be appropriately used for assessment of the remediation efficiency and to calculate contaminant mass removal (Brusseau et al. 2011a, 2011b).

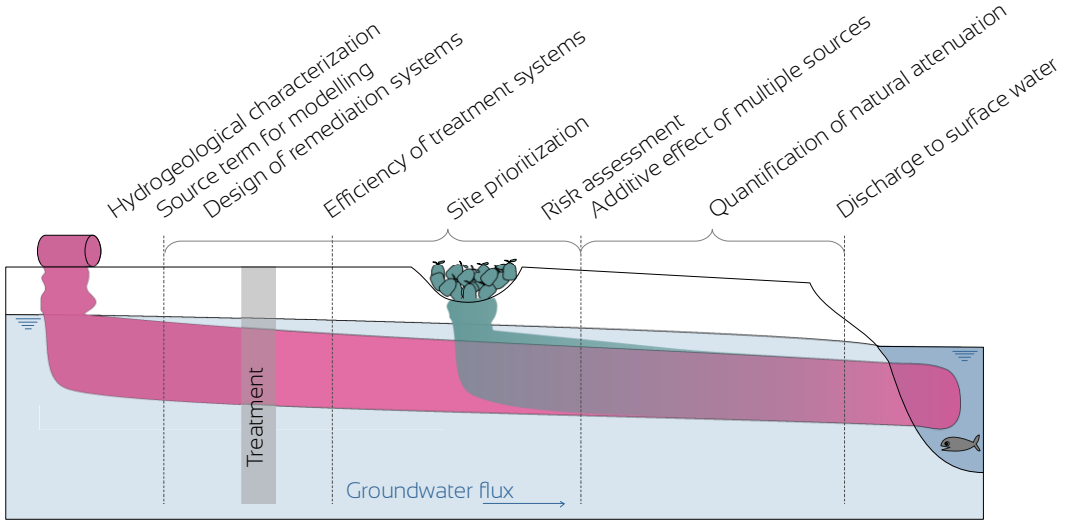

Figure 6: Use and benefits from a mass flux based approach.

Measurement of mass discharge is also acknowledged as the best method to evaluate the natural attenuation of contaminants in aquifer (Bockelmann et al. 2003, Barbaro and Neupane 2006). When the natural attenuation is defined by a reduction of the mass of contaminant (and not only on reduction of concentration due to dilution) (Chiogna et al. 2011), comparing two mass discharge measurement at distant locations of a contaminant plume delivers a precise quantification of the natural attenuation and a robust estimation of decay rates (Devlin et al. 2002, Schirmer et al. 2006, Falta 2008).

Groundwater flow and transport modeling can also benefit from flux measurements. In a recent research, Woodward et al. (2016) emphasized the need for flux constraints in groundwater modeling. These flux data could better tie down the relationship between hydraulic gradient and hydraulic conductivity. Uncertainties of model calibration performed only on piezometric head are often high and would benefit from a more robust parameter such as groundwater flux.

1.3.3. Use of mass flux and mass discharge for regulatory purposes

The concepts of mass flux and mass discharge have gained a large recognition among the different actors of contaminated aquifers. At the last BATTELLE international conference on contaminated soils and aquifers in April 2018, 42 presentations referred to concepts of mass flux and mass discharge. A complete session of 14 talks

was dedicated to applications of mass flux and mass discharge for remedial design and optimization. Finally, on the 18 short courses held at this event, 10 mentioned the use of contaminant mass flux. Despite the general recognition about the usefulness of mass fluxes and mass discharge for management of contaminated aquifers (Basu et al. 2006, Einarson 2017), difficulties are still encountered when trying to gain formal acceptance of mass flux and mass discharge concepts by the regulatory agencies (Hadley and Newell 2012). Very few regulations have formally adopted mass flux approaches. In all countries, regulatory groundwater threshold values are still defined in concentrations.

In the USA, since the publication of the document entitled "Use and Measurement of Mass flux and Mass Discharge" by the ITRC in 2010, the application of mass flux and discharge in regulatory acceptance is evolving slowly. These flux concepts are used more and more for site characterization or remediation performance evaluation but no regulatory compliance has been defined in terms of mass flux or mass discharge yet. The only official mention of mass discharge is a classification of magnitude performed by the USEPA attributing a log scale to mass discharge from <0.001 (magnitude 1) to 100 000 grams per day (magnitude 10) and aiming at prioritize contaminated sites (Newell at al. 2011).

In Europe, countries and regions have their own legislation about contaminated sites, but no legal framework has yet been established at the European level. Austria is currently the more evolved country on mass flux and mass discharge-based regulatory. Since 2002 the mass flux is written in the Austrian legislation for assessment of groundwater contamination. Contaminant mass fluxes are used to identify serious groundwater contaminations and to impose measures when the contaminant mass flux of a plume exceeds the product of the concentration intervention value multiplied by the groundwater flux if it is higher than 500 m^3/d. Mass flux is used to gain further characterization of groundwater plumes involving intensity, extend and temporal trends (*i.e.* stable, extending or shrinking plume). Mass flux can also be used in Austria as the basis of a site specific remediation target value or as a criterion to evaluate the performance of remediation measures (CRC CARE 2016, Müller-Grabherr 2018 personal communication).

OVAM, the environment institute for the Flemish region of Belgium, is currently evaluating the possibility to include mass discharge concepts in official risk assessment guidelines. At the moment, OVAM agrees and encourages contaminant flux measurements for characterization of aquifers and remediation plans but these approaches are not yet included in any regulation (Verreydt 2018, personal communication).

In the Walloon region, the authorities have recently commissioned a revision of the guidelines officially used for risk assessment of contaminated aquifers. In the scope of this revision, a survey carried out to collect expertise from consultant companies and public institutions has revealed that current concentration-based methodology for risk assessment is considered too conservative. A better integration of in situ measurements is also required. To answer these needs, a new flux-based risk assessment framework is currently developed. It will allow for a better integration of contaminants leaching through the vadose zone and spreading within the saturated zone (Marchal

et al. 2018a). Considering these changes, mass flux and mass discharge concepts should be effective in Walloon guidelines in a few months.

Mass flux and mass discharge-based regulations are thus developing all over the World. To satisfy these new requirements, it is necessary to dispose of techniques able to accurately measure contaminants mass flux and calculate mass discharge in aquifers. Little freedom is allowed for the determination of contaminant concentrations that relies on strictly controlled sampling procedures and on analyzes performed in officially certified laboratories. To date, no regulation restricts the choice of method used to measure groundwater flux in aquifer. To better determine contaminant mass flux, research efforts should focus on innovative techniques capable of measuring the groundwater flux since it constitutes the most important driver of contaminants migration through aquifers.

1.4. Methods for contaminant mass discharge calculation

Measurement of mass discharge is possible through a large range of methods. They can be classified according to various criteria: direct/indirect measurement, passive/dynamic tests and sampling, analytical/numerical modeling or performed on a single well or on multiple wells (Yoon 2006, Goltz et al. 2007, 2009). Three of the most commonly used methods are presented in this section.

1.4.1. Well capture method

The easiest way of measuring contaminant mass discharge is directly at the receptor of the contamination when this receptor is a pumping well. The well capture methods has been discussed firstly by Einarson and Mackay (2001). By measuring the contaminant concentration in the water pumped by a well at a specific pumping rate, it is possible to calculate the contaminant mass discharge relative to a specific source (Figure 7, Equation 3). This approach is based on different assumptions: the flow field and the release rate of dissolved contaminant are constant, mass transfer processes are at the equilibrium and there is no loss of dissolved mass by volatilization or transformation, the contaminant sources is the only one located within the capture zone of the well and the entire contaminant plume is captured by the pumping well.

$$M_d = C\ Q_{pump} \qquad \text{Equation 3}$$

where Q_{pump} is the pumping rate [$L^3\ T^{-1}$] at the pumping well.

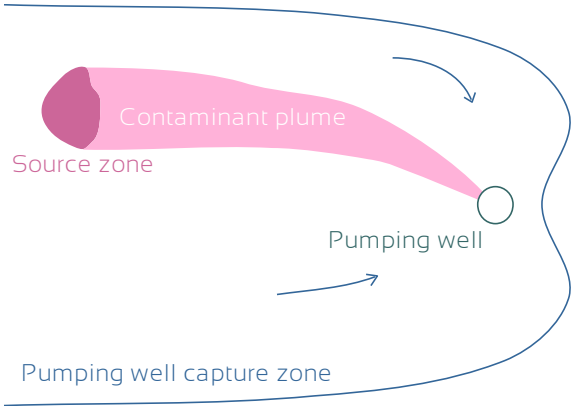

Figure 7: Calculation of mass flux and mass discharge at a pumping well in case of steady state solute plume (modified from ITRC 2010).

This relationship can also be used, if the contaminant mass discharge is already known, to predict the maximum concentration level of contaminant at a pumping well. The well capture method only needs only few data and does not require sophisticated field equipment in addition to the existing pumping equipment but the validation conditions are rarely encountered. Furthermore, a single value of mass discharge is provided for the entire plume and no information about local high discharge zone can be deduced. Finally, the spatial distribution of mass flux is not determined unless multiple pumping wells are used.

1.4.2. Integral Pumping Tests

Integral Pumping Tests (IPT) have been introduced in 1998 by Schwarz et al. and Holder et al. The method consists of one or more pumping wells placed at an imaginary control plane downgradient the contaminant source and operated simultaneously. Pumping rates and well interdistancies are optimized so that the influence radii of the different pumping wells overlap that of the neighbor pumping. This theoretically guarantees the interception of the entire contaminant plume (Figure 8). During the pumping operations, the contaminant concentrations in the abstracted groundwater is monitored and the total mass discharge is determined by an inversion approach of the monitored concentration time series. The interpretation is based on the theory that the concentration time series at the pumping wells provide information on the spatial distribution of the contaminant mass within the capture zone (Ptak et al. 2000, Bauer et al. 2004). IPTs are justified by the fact that it is nearly impossible to know a priori the exact position of the plume hot spot, especially in heterogeneous aquifers (Bockelmann et al. 2001).

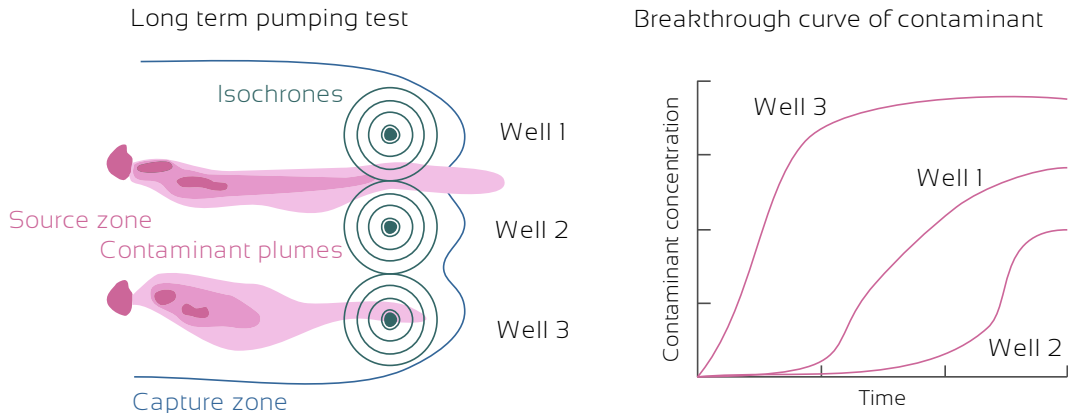

Figure 8: Schematic representation of Integral Pumping Test. The interpretation by inversion of contaminant breakthrough curve at each pumping well allows for determination of the contaminant mass flux and mass discharge and the spatial distribution of the contaminant plume(s) (modified from Bauer et al. *2004).*

The main drawback of the IPT method is the potentially high volumes of abstracted groundwater that have to be treated and the high logistics and energy demands. As every inversion base method, the inversion model does not deliver a unique solution for the contaminant plume spatial distribution, especially when the spatial heterogeneity of the plume is high. Finally, pumping operations can modify the groundwater flow path, hence leading to results biased from the actual contaminant plume shape under natural groundwater flow conditions (Zeru and Schäfer 2005). IPT have been widely tested, used and discussed in recent years (Alberti et al. 2011, Bayer-Raich et al. 2002, 2004, 2006, Béland-Pelletier et al. 2011, Dietze and Dietrich 2011, Herold et al. 2009, Jarsjö et al. 2005, Kalbus et al. 2007, Leschik et al. 2011).

1.4.3. Control panel method

Specific spatial configurations of monitoring wells allow for a direct calculation of the contaminant mass discharge, based on mass fluxes measurements. These configurations consist in arrays of multi-level wells investigating different depth and disposed as control planes that are positioned orthogonally to the main groundwater flow direction (Figure 9). Each monitoring point is considered representative of a sub-area of the control plane where the contaminant mass flux is supposed to be uniform. The mass flux is then integrated over this sub-area to calculate the corresponding mass discharge as in Equation 2. The sum of all discrete mass discharges measured at each location of the sampling array gives the total mass discharge for the whole contaminant plume.

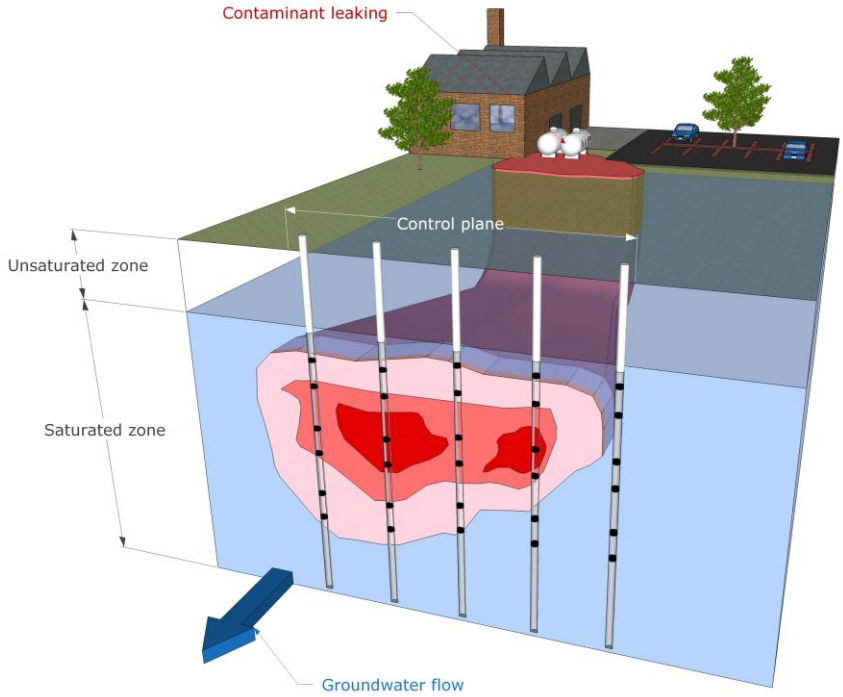

Figure 9: In control planes, multi-level monitoring wells are aligned orthogonally to the main groundwater flow direction and screened at different depths to capture the vertical distribution of groundwater fluxes and contaminant concentrations. The total contaminant mass discharge is calculated by integrating the individual mass fluxes measurements (i.e. measured at each screen) over the whole cross sectional area of the plume intercepted by the control plane.

Contaminant mass discharge calculations based on mass fluxes measured at control plane can be easily justified when the density of measurement points is high and when the investigated aquifer is homogeneous. Practically, homogeneous aquifers are almost non-existent in natural environments (Sudicky 1986) and assuming uniform groundwater flow for heterogeneous aquifer may result in significant inaccuracy in mass discharge quantification (Cai et al. 2011). Such heterogeneity is obvious for fractured aquifers but can also be significant in porous aquifers located in sediment deposited in high energy environments such as alluvial plains or coastal areas (Yang et al. 2012).

In most cases, groundwater flows tend to be focused in high hydraulic conductivity zones, where most of the mass transport occurs (Suthersan et al. 2016). Meanwhile, contaminants often accumulate in low permeability zones made of finer materials (Difilippo et al. 2010). Guilebeaut et al. (2005) have shown that for relatively homogeneous aquifers where hydraulic conductivity varies by only one order of magnitude, the contaminant concentration that can vary by up to four orders of magnitudes over a vertical space between sampling points of 30 cm. For more heterogeneous aquifers, the spatial variability of the permeability field takes on more importance

(Li et al. (2007), and Troldborg et al. (2012) concluded that the uncertainty of mass discharge is strongly dominated by the uncertainty on the distribution of groundwater flow across the control plane.

This high level of heterogeneity requires denser grids of sampling points constituting the control plane in order to improve the accuracy of mass discharge measurements (De Barros and Nowak 2010, Bohling et al. 2012, Chapman et al. 2015). Practically, time, budget, technical or field constrains may limit the sampling density and weaken the trust put in mass discharge approaches despite their undeniable benefits. Several authors proposed geostatistical approaches to evaluate the uncertainties related to estimation of mass discharge in the saturated zone from snapshot concentration and water flux measurements on control planes (Troldborg et al. 2010, 2012, Schwede and Cirpka 2010, Klammler at al. 2012, Cai et al. 2011, Kübert and Finkel 2006, de Barros 2018). These approaches legitimate mass discharge results.

Contaminant mass discharge calculations by the control plane method requires the measurement of contaminant mass flux measured at each sampling point. Contaminant mass fluxes are calculated based on measurements of both the contaminant concentration and the groundwater flux (Equation 1). In the next section three contaminant mass flux measurement methods are presented, two integrated passive methods and a more conventional method based on independent measurements of groundwater flux and contaminant concentration.

1.5. Techniques and methods for contaminant mass flux measurement

1.5.1. Passive Flux Meter

The Passive Flux Meter (PFM) technology was first described by Hatfield et al. (2001) and patented in 2002 in the USA (US6401547 B1). It consists in the deployment of a permeable sorbent pack in the wells of a control plane (Hatfield et al. 2004). PFMs allow for the simultaneous determination of groundwater flux and contaminant concentrations that can be further converted into contaminant mass flux. Flux measurements using this approach are referred to as "passive", in contrast to methods that require pumping of groundwater

PFMs are composed of four vertical segments (Figure 10). The three outermost segments contain a sorbent material which is selected to capture dissolved contaminants in groundwater flowing through the flux meter under natural gradient groundwater flow conditions. The central segment also contains sorbant material but this time pre-saturated with resident tracers. By analyzing the mass of residual tracers and captured contaminants in the four segments of the PFM, it is theoretically possible to estimate the direction of groundwater flow (Klammler et al. 2007) and the contaminant concentration in groundwater. PFMs have been widely used for measurement of chlorinated solvents, metals and oxyanions fluxes in groundwater (Annable et al. 2005, Basu et al. 2006, Campbell et al. 2006, Lee et al. 2007, Verreydt et al. 2013).

Stacks of PFMs in a well screened on the whole thickness of the aquifer allow for the determination of vertical heterogeneity of solute mass discharge (Klammler et al. 2012). As for any passive sampler, PFMs deliver mean values of the contaminant mass flux integrated on the time of exposure and does not capture the time variability of groundwater flows. A specific PFM, the FRPFM, has also been developed for use in uncased wells installed in fractured aquifers (Klammler et al. 2016).

PFMs are commercially available (http://enviroflux.com).

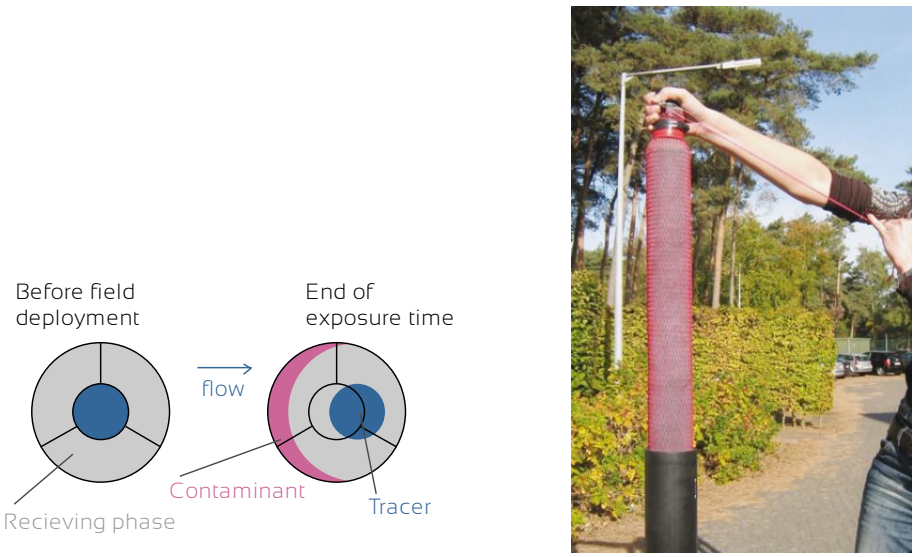

Figure 10: Cross section and picture of a Passive Flux Meter (modified from Verreydt 2012).

1.5.2. iFLUX sampling

The iFLUX system works according to the same passive sampling principle than the PFM and uses at least two cartridges to simultaneously measure groundwater flux and contaminant concentration. The cartridges are fixed on stainless steel rods and lowered in the tested piezometer for a specified period of time depending on the estimated groundwater flux and typically ranging from 1 week to up to 6 months (Figure 11). The standard cartridges are designed to fit perfectly into 2 and 4 inches' wells.

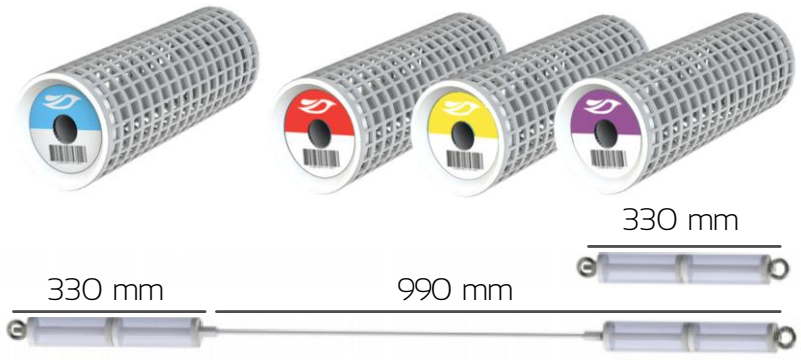

Figure 11: iFLUX cartridges for measurement of groundwater flux and contaminant concentration (modified from www.ifluxsampling.com).

The water flux cartridge contains a set of water soluble tracers. All tracers have different desorption kinetics and independently leach into the groundwater under the effect of groundwater flow that passes through the cartridge. By analyzing the tracer remaining in the cartridges after the exposure time, it is possible to deduce the mean groundwater flux that has passed through the cartridge. The exposure time of the water flux cartridges should be evaluated prior to the field installation according to the assumed groundwater flux. If the exposure time is very long under high groundwater fluxes, the mix of tracers may be completely washed out of the cartridge, making the estimation of groundwater flux impossible.

The "contaminant cartridge" contains a pre-processed sorbent that captures the pollutants of interest. Contaminant fluxes in groundwater are determined through adsorption and recovery processes. Each type of cartridge contains a different type of sorbent. Sampling cartridges for volatile organic compounds (VOCs, BTEX, PAHs…), nutrients (nitrate, phosphate, ammonium…) and heavy metals (nickel, zinc, copper…) are commercially available at the moment. PFAS/PFOS cartridges are currently developed.

iFLUX system is patented (WO2016207769 A1) and commercially available (www.ifluxsampling.com).

1.5.3. Classical point measurement method

The most commonly used method for measuring mass flux simply combines separated measurements of solute concentration and groundwater flux at a sampling point.

Measurement of contaminant concentrations at sampling points of a control plane is performed by traditional pumping of groundwater and later analysis of the collected samples in the laboratory. This method has the advantage of being acknowledged by regulators. Through the extend of the zone influenced by the pumping, active sampling methods deliver groundwater samples that are more spatially integrated than passive measurements that capture very local natural contaminant fluxes.

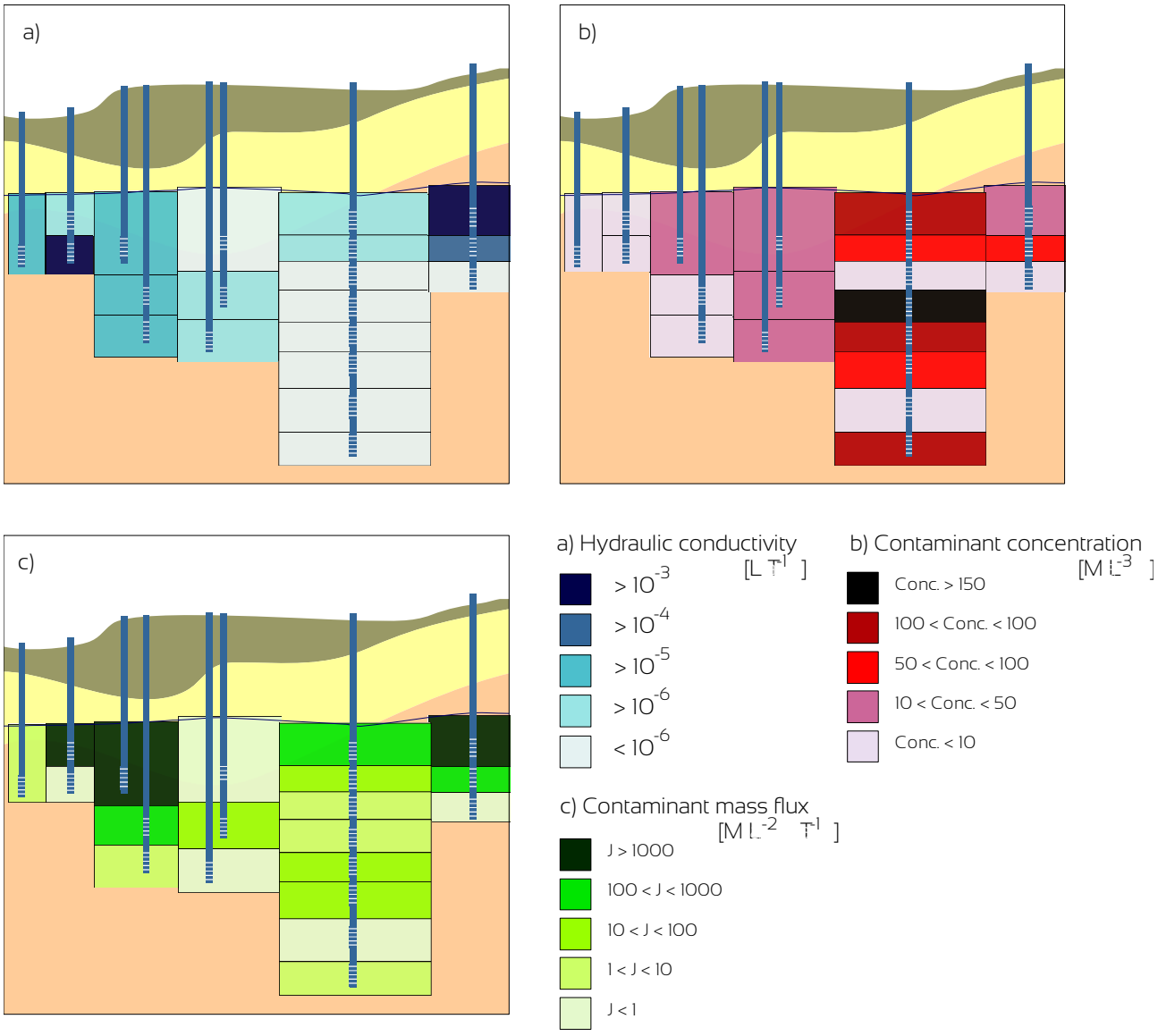

Figure 12: Measurement of mass flux at several monitoring well aligned orthogonally to the groundwater flow direction. The multiplication of hydraulic conductivity (a), hydraulic gradient and contaminant concentration (b) gives the contaminant mass flux (c).

Groundwater flux calculation is traditionally performed using the Darcy's law. First, the hydraulic conductivity of all monitoring wells is estimated using pumping or slug tests. Then the local hydraulic gradient is estimated using piezometric heads measurements carried out in monitoring wells located upgradient and downgradient to the control plane. Other methods can directly measure natural groundwater flow rate that transits through the screen of the well or groundwater flow velocity inside the well (section 1.6). The transit flow rate (Q_t) is directly related to the in-well groundwater velocity or apparent Darcy flux (q_{app}) through the cross-sectional area

S_w [L^2] perpendicular to the groundwater flow (Equation 4). This cross-sectional area can be calculated by multiplying the well screen length (e_{scr}) [L] by the diameter of the well ($2\ r_w$) [L]. As for all other single well groundwater flux measurements, the apparent Darcy flux q_{app} [LT^{-1}], is related to the effective Darcy flux in the aquifer q_D by a flow distortion coefficient a_w that accounts for the convergence or divergence of the flow field in the vicinity of the borehole. A more detailed discussion about the flow distortion around a well is given in section 1.6.12. The apparent Darcy flux q_{app} is given by:

$$q_{app} = \alpha_w\ q_D = \frac{Q_t}{S_w} = \frac{Q_t}{2\ r_w\ e_{scr}} \qquad \text{Equation 4}$$

The currently available methods and techniques to perform such direct groundwater flow measurements are described in the next section.

1.6. Techniques and methods for groundwater fluxes measurement

Estimation of groundwater flux (i.e. groundwater discharge per unit cross sectional area of the porous medium) or groundwater flow velocity (i.e. groundwater linear flow velocity) remains the basis of most hydrogeological studies, from hydraulic characterization to the most advanced reactive transport modeling. Unlike surface water flow, groundwater flow is rather slow. When water flow velocities are smaller than 10^{-3} m/s which is frequently the case for groundwater, conventional spinner or electromagnetic flowmeters cannot be used and alternative methods have to be employed. This section aims at presenting the currently available methods for groundwater flux or groundwater flow velocity measurement.

1.6.1. Classical calculation using the Darcy's law

The most commonly used method for estimation of groundwater fluxes (q_D) [$L\ T^{-1}$] is based on Darcy's law (Darcy 1856) where both the hydraulic conductivity (K) [$L\ T^{-1}$] and hydraulic gradient (i) [$L\ L^{-1}$] are measured independently (Equation 5). Accurate estimates of groundwater fluxes based on Darcy's law hence strongly depend on the quality of hydraulic conductivity estimates and on the accuracy of hydraulic gradients calculated based on piezometric measurements.

$$q_D = K\ i \qquad \text{Equation 5}$$

Pumping tests or slug tests deliver mean hydraulic conductivity values rarely representative of the aquifer the heterogeneity because hydraulic conductivity can vary on several order of magnitudes over short distances (Sudicky 1986). Such spatially averaged values can should not be used for contaminant plume investigations since contaminant plumes do not get homogenized across aquifers but rather move through fine networks of high permeability (Suthersan et al. 2016). Numerous researches aim at improving the representativity of hydraulic conductivity measurement whereas uncertainties associated with the determination of hydraulic gradients are less addressed (Bright et al. 2002, Devlin and McElwee 2007). Hydraulic conductivity is only representative of the close vicinity of the tested well while hydraulic gradient is spatially averaged over the area where piezometric head measurements are performed. Furthermore, hydraulic gradients can be difficult to measure in high hydraulic conductivity aquifers if monitoring wells are located close to each other (Silliman and Mantz 2000). And form a practical point of view, resolution of manual groundwater level measurement using traditional piezometric probe can not be claimed lower than 0.5 cm.

This indirect groundwater flux measurement method can only lead to estimates but rarely provides accurate value of groundwater fluxes. In addition, the groundwater flux estimate is only representative of the time of piezometric head measurements and may not be adequate for transient groundwater flows.

1.6.2. Point Dilution Method

The aim of the Point Dilution Method (PDM) test is to perform a direct measurement of groundwater flux. A tracer is injected at once in a well while the water column within this well is constantly mixed to insure a homogeneous tracer concentration. During the test, the tracer concentration is monitored in the well as it decreases under the influence of the groundwater flow across screens. This exponential decrease is expressed as a function of the groundwater discharge through the screen of the well, called "transit flow rate" (Q_t) [L^3 T^{-1}] (Drost et al. 1968, Hall 1996) (Figure 13, Equation 6). If groundwater flux is high, tracer concentration decreases rapidly. The relationship between observed concentration in the well and groundwater transit flow rate during a PDM is expressed in Equation 4:

$$C_w(t) = C_{w,0}\, e^{-\frac{Q_t}{V_w}(t - t_0)} \qquad \text{Equation 6}$$

where C_w is the tracer concentration [M L^{-3}] at time t [T], $C_{w,0}$ is the tracer concentration [M L^{-3}] at time t = 0 and V_w is the mixing volume [L^3].

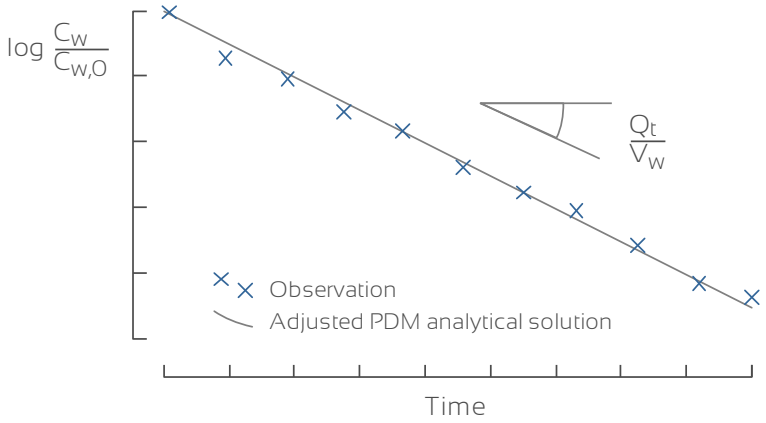

Figure 13: Typical exponential decrease of tracer concentration during a PDM experiment. The slope calculated on the data equals the groundwater transit flow rate (Q_t) divided by the mixing volume (V_w).

Since the first use of PDM in 1916, reported by Halevy et al. (1967), many PDM configurations have been tested, including the experiments by Kaufmann and Todd (1962), Novakowski et al. (1998, 2006) and West and Odling (2007), using inflatable packers to limit the vertical extension of the investigated zone. The tracer can be salts, fluorescent dyes or radio isotopes (Klotz et al., 1979). PDM tests have been widely used for direct measurements of water fluxes in fractured aquifer (Novakowski et al 1998, 2006, Maldaner et al. 2018), for estimation of groundwater velocity in riparian zones (Lamontagne et al. 2002) and to estimate LNAPL flow (Smith et al. 2012, Sale et al. 2007, Mahler et al. 2011).

The main limitation of the PDM concerns the uncertainty affecting the calculation of the transit flow rate Q_t which fully depends on the estimation of the mixing volume V_w (Equation 4, section 3.2.3.2, Jamin et al. 2015). This mixing volume can theoretically be estimated geometrically based on the properties of the tested well and the height of the water column. However, the volume can be difficult to estimate in case of complex experiment configuration when numerous equipments are lowered in the well or when a packer is used. Furthermore, a part of the gravel pack can sometimes be involved in this volume of water that is mixed during the test. Another limitation of the technique is its intrinsic inability at measuring variable groundwater flow.

1.6.3. Colloidal borescope

The colloidal borescope (CB) is an in situ device for the direct observation of the motion of suspended colloidal size particles (1 to 10 µm) and the determination of the groundwater flow velocity and direction in the investigated wellbore (Kearl 1997, James et al. 2006). The probe itself consists of a video camera, an optical magnification lens, an illumination source and a compass, all encased in a water proof housing (Figure 14). It is connected to a computer equipped with a dedicated software that analyses the particles motion. By tracking each particle crossing in the view field of the probe and supposed to travel at the same velocity as groundwater, the

software deduces the mean in-well groundwater flow velocity and the general flow direction. The diameter of the probe that has to be submerged in the tested well is 44 mm making the system fit for common 2 inches' wells. The colloidal borescope is commercially available (www.geotechenv.com).

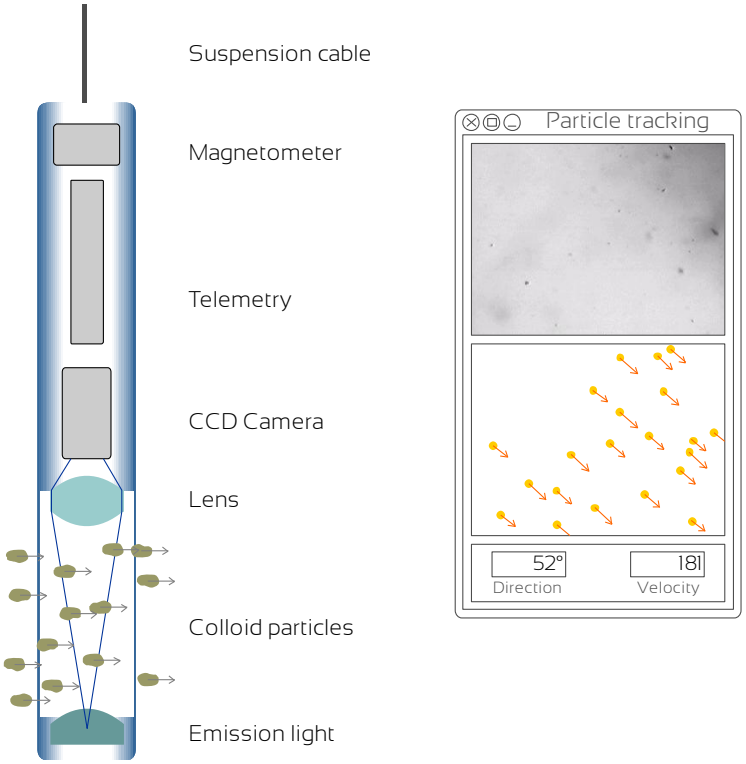

Figure 14: Schematic illustration of the Colloidal Borescope and of the particle tracking software that interpret the movement of particles into groundwater flow velocity and direction (modified from James et al. 2006).

The colloidal borescope has been employed in different studies (Ferry et al. 1995, Kearl et al 1992, 1998, Kearl and Roemer 1998, Narbutovskih et al. 2002, Lengricht and Graw 2002, Beauheim, 2000), allowing to measure in-well groundwater flow velocities from 1.73 to 43.2 m/d. Kearl and Roemer 1998 suggested that the apparatus should run at least 2 hours to obtain reliable measurements.

The limitation of the colloidal borescope arises when groundwater shows important turbidity that makes the particles tracking uneasy. The interpretation software has also been occasionally reported to incorrectly identify different particles in two video frames as the same particle, hence providing erroneous reading of particle velocity and flow direction. However, these erroneous results can be spotted and removed manually.

1.6.4. Point Velocity Probe

The Point Velocity Probe (PVP) has been developed to measure directly groundwater velocity in the aquifer (Labaky et al. 2007, Devlin et al. 2009, Devlin et al. 2012). It consists in a cylinder fitted on its outer face with a tracer release port and one or several tracer detection systems (Figure 15). By timing the tracer between its delivery at the injection port and the detection systems located at different distances from the injection port, both magnitude and direction of the average groundwater flow velocity can be determined. This timing is determined by the interpretation of the tracer breakthrough curve recorded at the detectors resulting from the travel of the tracer around the probe in the aquifer formation.

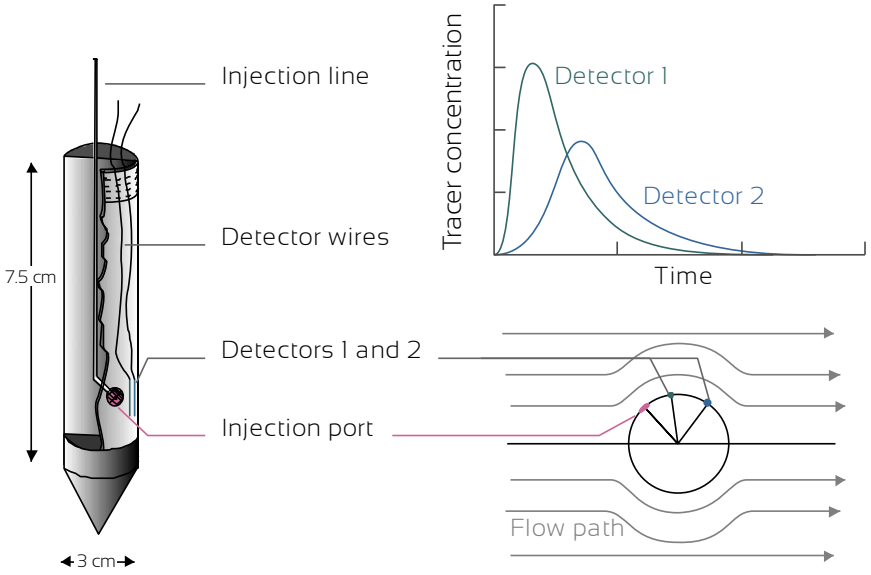

Figure 15: Schematic representation of the Point Velocity Probe. A tracer is injected by a port and is transported by the groundwater flow around the probe to two detectors. The interpretation of the breakthrough curves at the two detectors corrected by the groundwater flow path around the probe gives the groundwater flow velocity and direction (modified from Labaky et al. *2010).*

The system has a 30 mm outer diameter and a 75 mm length and is inserted in the aquifer by direct push. Consequently, the application of the PVP is limited to unconsolidated materials. Furthermore, it requires the use of mechanical force to be pushed in the aquifer and can not be used in existing piezometers. Driving this conical system into the subsurface can compact the sediments locally, leading to reduction of the hydraulic conductivity known as skin effect and to an underestimation of groundwater velocity in the aquifer around the probe. The relatively fast measurement time allows for multiple measurements at increased depths as the probe is driven down in the aquifer. The tracer is usually a saline solution while the detectors measures the water electrical conductivity. The PVP is patented in the United States (US6393925 B1) and in Canada (CA2300794 A1).

The PVP was tested and validated in the lab for measurements of water velocities ranging from 0.05 to 3.5 m/d (Schilling et al. 2016, Walter and Devlin 2017, Gibson and Devlin 2018). It was also compared to other techniques such as the Geoflometer (Guthrie 1986), the Colloidal Borescope and more traditional borehole dilution methods (Labaky et al. 2010). The PVP was also used to measure water velocity in the capillary fringe (Berg and Gillham 2009). Sensitivity analysis of PVP have shown that groundwater velocity can be measured with a precision of ± 15% and flow direction can be measured with a precision ± 15° (Devlin 2016). Nevertheless, Rønde et al. (2017) mentioned that if the injection is oriented incorrectly to the groundwater water flow direction (if the injection port and detectors are positioned downstream of the groundwater flow), the PVP can fail to produce an interpretable breakthrough curve. A specific spreadsheet program was developed for interpretation of the breakthrough curves produced by PVP experiments and to calculate groundwater velocity (Schilling 2012).

1.6.5. In-Well Point Velocity Probe

The In-Well Point Velocity Probe (IWPVP) is an evolution of the aforementioned PVP for use in existing wells (Osorno 2016, Osorno et al. 2018). It consists of a 3D printed plastic flow chamber of 50 mm outer diameter that isolates vertically a portion of the tested well (Figure 16). The device comprises a central chamber were a saline tracer is injected and 4 lateral flow channels equipped with detectors measuring the water electrical conductivity. By tracking the saline tracer through the detectors, it is possible to estimate the groundwater flow velocity through the probe which is considered as proportional to the ambient groundwater flux in the aquifer. Flow direction can also be estimated based on different tracer arrival time at the four detection channels.

Up to now, the IWPVP has only be tested in laboratory on water fluxes prescribed in the tested porous media ranging from 0.48 to 4 m/d. The method returned measurements of groundwater velocity with a precision ranging from ± 40% to ± 10% and precision on the flow direction of ± 15°.

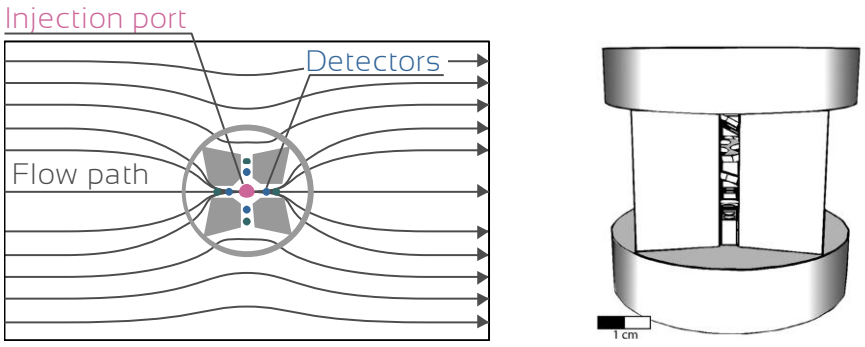

Figure 16: Schematic illustration of the In-Well PVP. The interpretation of the tracer breakthrough curves, from the injection at an injection port to 4 pairs of radially positioned detectors allows for the determination of the groundwater flow velocity and direction (modified from Osorno et al. *2018).*

1.6.6. Acoustic Doppler Velocimeter

The Acoustic Doppler Velocimeter (ADV) is based on conventional acoustic Doppler probes for performing three-dimensional measurements of water flow for oceanic and surface-water applications (Wilson et al. 2001). Three acoustic receivers capture the perturbation of an acoustic wave emitted at the center of the probe. When water flows, acoustic wave frequencies measured by four sensors located around the emitter will differ from the source frequency due to the Doppler effect. Analysis of the perturbation gives the groundwater flow velocity and direction in the tested well. The ADV does not measure fluid velocity directly but tracks the velocity of suspended particles in the water of the tested well.

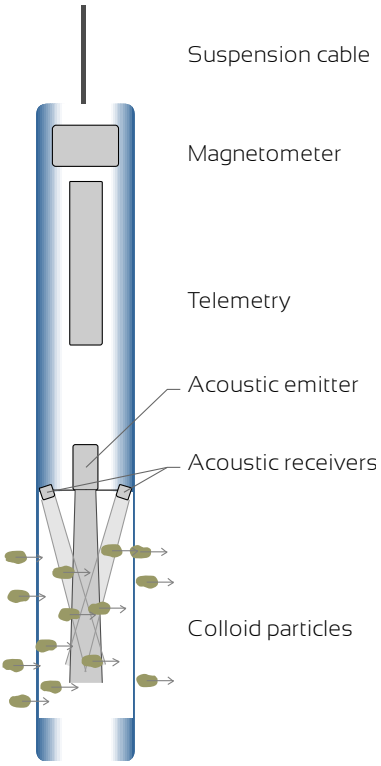

Figure 17: Schematic representation of the Acoustic Doppler Velocimeter. Three acoustic receivers capture the perturbation of an acoustic wave emitted at the center of the probe. Analyze of the perturbation, which is due to moving colloid particles in water, gives the groundwater flow velocity and direction.

The ADV is approximately 4 ft long with a 3-inch outer diameter (Figure 17). The bottom tip of the probe consists of a centrally mounted acoustic emitter and three receivers radially positioned on holding arms. The sample volume of the ADV is roughly cylindrical in shape whose size depends on user-defined parameters of transmitter-pulse length and receiver-window length that are adjusted with the acquisition software. The frequency of

measurement is 25 times per second. The ADV was patented in 1998 (US5796679A) and commercially available (www.sontek.com).

No field application has been found in the groundwater scientific and technical literature. The patent claim that in-well groundwater velocities can be measured with accuracy on a range of 8 m/d to 210 000 m/d.

The patent also mentions that the instrument having a 10 MHz sound source needs 12 h to measure an in-well groundwater velocity of 0.2 m/d with a good precision. This could limit the application of the technique for the measurement of variable groundwater flow. Another limitation of this system is mainly its large diameter of 3 inches which does not fit into most of monitoring wells located in contaminated sites, frequently equipped with 2 inches' wells.

1.6.7. Laser Doppler Velocimeter

The Laser Doppler Velocimeter (LDV) (Momii et al. (1993) is based on the same principle than the ADV but this time the emitted signal is a laser beam instead of an acoustic wave. LDVs have been widely used for measuring fluid speed, from gases to liquids. In a LDV, two coherent laser beams cross in a small investigation volume through which colloid particles are moving, carried by the groundwater flow. The light reflected by these particles is received by a photo detector, and by measuring the Doppler frequency shift of the scattered light it is possible to calculate the velocity of the tracer particles, and hence to estimate the groundwater flow velocity in the tested well.

The LDV allows for measurements of in-well groundwater flow velocity and flow direction of 0.009 to 8.64 m/d with an accuracy of ± 8%. The apparatus to be submerged in the tested well is 10 cm in diameter limiting its use for wells of minimum 4 inches in diameter.

1.6.8. Heat pulse flow meter

The horizontal Heat Pulse (or thermal-pulse) Flow Meter (HPFM) uses heat-pulse and temperature-sensing to measure the direction and velocity of horizontal groundwater flow within a well (Bayless et al. 2011). A pulse of heat is generated in groundwater by a heat resistance located at the center of the probe (Figure 18). Four pairs of temperature sensors are positioned around the heat source in a packer filled with silica beads that surround the heat source and thermistors. The temperature sensors monitor the heat transmission through the silica beads as affected by groundwater flow. The rate at which temperature changes are convected by groundwater flow across the thermistor array allow to determine the groundwater flow velocity in the tested well. The thermistor that measures the largest change in temperature after generation of the heat pulse is considered to be on or near the axis of groundwater flow direction. The reference orientation is given by an integrated compass.

HPFM allows quick, accurate on-site determination of both in-well groundwater flow and direction on a range of 0.06 to 30 m/d with a precision of ± 10% on the flow velocity and ± 5° on the direction. The measurement of the flow and direction at one depth takes less than 10 minutes. The HPFM is commercially available under the name KVA Model 40 GEOFLO and patented in the US (US6227045 B1).

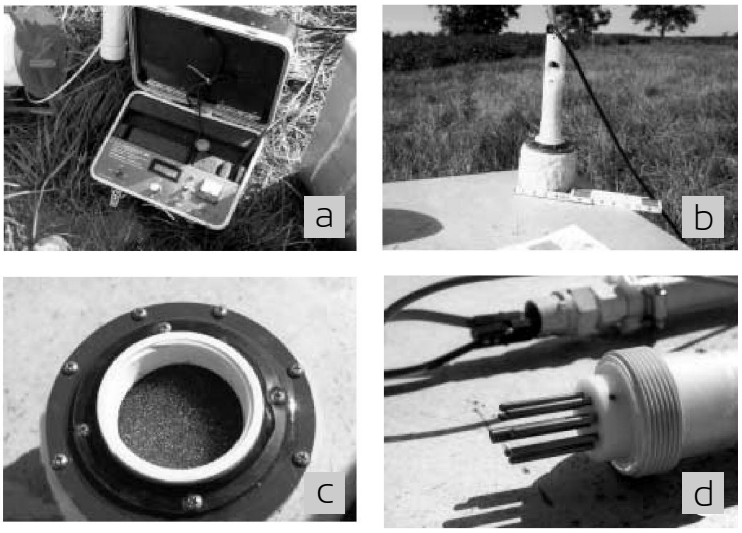

Figure 18: Illustration of the Heat Pulse Flow Meter. (a) Control unit. (b) Probe that is lowered in the tested well. (c) Flow chamber filled with glass beads. (d) Central heat source and the 6 radially disposed heat sensors. Modified from James et al. *2006.*

1.6.9. In situ Permeable Flow Sensor

Another flow meter based on heat transfer is the In situ Permeable Flow Sensor. Unlike the HPFM, the IPFS is buried directly in the aquifer, identically to the PVP. The technology is based on a cylindrical, on the surface of which a heat flux is uniformly distributed, placed in direct contact with the aquifer. The interpretation of the temperature distribution pattern measured across the array of temperatures probes disposed radially and vertically on the cylinder allow to determine the groundwater velocity and both the azimuthal and vertical direction of the groundwater flow (Ballard 1996).

The experimental setup consists of a cylinder of 0.75 m in length and 5 cm in diameter that is pushed directly in contact with the aquifer. This limits the application of this device to shallow and unconsolidated aquifer. An array of 30 carefully calibrated thermistors are connected to a data logger. The technology has been proven suitable for the measurement of groundwater flow velocities in the tested aquifer in the range of approximately 0.004 to 0.864 m/d. The precision achieved on the measurements of the azimuths of net horizontal flow is around 10° (Ballard et al. 1996, Alden and Munster 1997).

The use of IPFS is limited by two factors. The first is relative to all direct push methods that limit application to shallow and unconsolidated aquifers and can cause skin effect affecting groundwater flow measurements. The second is the time required for the experiment to be reliable and the associated low sensitivity and resolution of the system to variation of the groundwater flow. Field experiments of the system allowed to figure out that the thermal lag of the sensor can be estimated to two days.

1.6.10. PVC Flow Meter

More recently, Masciopinto and Palmiotta (2013) presented a new flow meter for the measurement of groundwater velocity in large wells. The PVC Flow Meter (PVCFM) device is made of a PVC tubing 15 cm long and 13 cm in diameter that is lowered in the tested well. The cylinder comprises an injection port through which a saline solution is injected and 5 electrical conductivity sensors. 4 of those are separated from the injection port by a synthetic porous filter. This filter aims at reducing the effect of molecular diffusion that can be relatively high compared to advection processes in case of very low groundwater velocity. The method measures the elapsed time between the injection of the saline solution and its detection by the sensors located downgradient. The PVCFM has been tested in both laboratory and field conditions for in-well groundwater flow velocity ranging from 0.3 to 3.7 m/d.

The large size of the device limits its application to wells of a diameter of minimum 6 inches. Since the device comprises an upgradient and a downgradient side that have to be positioned accordingly in the well, it seems mandatory to have an approximate idea of the groundwater flow direction previously to the measurement. As described in the article, the measurement direction is not very precise, with no further details. The orientation of the device regarding the groundwater flow is only controlled during the installation phase during which the PVCFM is maintained against the wall of the well and slowly lowered into the well to avoid twisting of the suspension cable.

1.6.11. Discussion of the methods

A summary of the properties, scope, size and measurement time of the different methods identified in the literature for direct groundwater flux measurement is given at Table 1.

Some of these methods and devices were reviewed by independent experts and compared under various field and laboratory conditions (Guaraglia and Pousa 2014). Wilson et al. published in 2001 the first evaluation of three borehole flowmeters on real field experiments. Bayless et al. (2011) compared the accuracy of the HPFM, the CB and the ADV on a flow through tank using controlled water fluxes of 1.5 10^{-5} to 5.5 10^{-4} m/s. They concluded that the three systems delivered consistent results but needed improvements in case of low groundwater fluxes. Kempf et al. (2013) evaluated the performance of PVP and HPFM under transient groundwater flow

conditions. They compared the results given by these two methods to more classical single well PDM and found very similar results. Nevertheless, they clearly pointed out the relatively long time needed for these systems to be sensitive to a change in groundwater velocity. As a consequence, they advise the use of these methods for steady state or slowly varying groundwater fluxes only.

*Table 1: Comparison of groundwater flow velocity measurement by single-well methods. * In-well groundwater velocity. ** Groundwater flow velocity in the aquifer formation. *** Groundwater flux in the aquifer formation.*

Method	Implementation	Diameter of the device [mm]	Minimum groundwater flux of velocity [m/s]	Maximum groundwater flux of velocity [m/s]	Time for measurement [h]
Colloidal Borescope*	In-well	45	0	3×10^{-2}	2
Point Velocity Probe**	Direct push	30	6×10^{-7}	4×10^{-5}	1 to 12
In-well point velocity probe***	In-well	50	6×10^{-6}	4.5×10^{-5}	
Acoustic Doppler velocimeter*	In-well	76	9×10^{-5}	2.5	±10
Laser Doppler Velocimeter*	In-well	100	10^{-7}	10^{-4}	
Heat pulse flow meter*	In-well	50 or 100	7×10^{-7}	3.5×10^{-4}	0.1
In situ permeable sensor**	Direct push	50	5×10^{-8}	10^{-5}	24
PVC flowmeter*	In-well	150	3.5×10^{-6}	4.3×10^{-5}	0.25

When used to measure of contaminant mass fluxes, the PVP and IPFS have the same drawback. They deliver a measurement result in terms of groundwater flow velocity in the aquifer. However the contaminant mass flux is based on the groundwater flux or Darcy flux (Equation 1). Groundwater flow velocity can be converted to Darcy flux by a multiplication with the effective porosity (Hall et al. 1991). This means that an additional measurement of the aquifer effective porosity, usually performed by tracer tests, is requested, extending even more the time and the budget needed for the measurement of contaminant fluxes.

Another general disadvantage of these methods is that they have a discrete vertical sampling point, often not larger than a few centimeters. They only allow the measurement of very local flow velocities that can also be highly influenced by intra-borehole vertical flow (Ma et al. 2010). Mass flux calculations based on such local

measurements can lead to inaccurate results if the variation of groundwater fluxes along the vertical axis of the well is not characterized. The measurements should then be repeated along the vertical axis of the well. Each displacement of the probe within the well disturbs the laminar water flow through the well. It is thus necessary to wait for the flow to stabilize after the displacement of the probe. This can lead to unmanageable measurement times.

More recently, Bayer-Raich et al. (2018), using a detailed numerical model, demonstrated that the introduction of a measurement device in a well significantly disturbs the water flow within that well and leading to discrepancies in the measured water velocity up to 20% according to the orientation of the device compared to the water flow direction. Since theses measurement devices perform a very local measurement of water velocity with spatially limited volume of investigation, this local disturbance of the water flow can have a significant impact on the results. Vertically integrative methods such as point dilution methods may be more representative of the global groundwater flow through the whole screen of the tested well.

1.6.12. Influence of the flow field distortion around a monitoring well

In theory, the groundwater flow is higher in a well than in the surrounding aquifer formation and the stream lines tend to converge through the borehole (Wu et al. 2008). This phenomenon has been observed by Drost et al. (1968) (Figure 19) and studied by many authors (Oglivi et al. 1958, Elci et al. 2001, Klammler et al. 2007, Wu et al. 2008, Clemo 2010, Verreydt et al. 2015, Bayer-Raich et al. 2018).

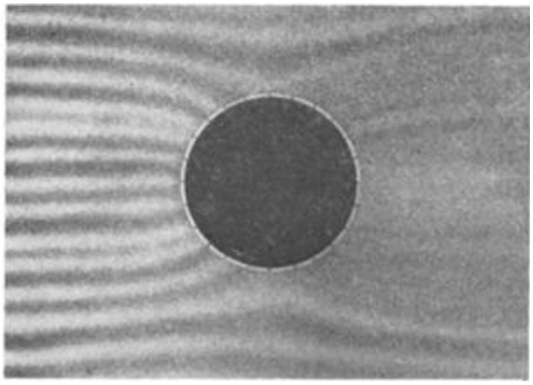

Figure 19: Observation of flow stream line convergence through a wellbore using dye tracer (Drost et al. *1968).*

Well construction and hydraulic properties of the materials used for the well screens and filter packs have a significant influence on the groundwater flow patterns around the wells. While well constructions parameters are most of the time carefully considered for pumping wells for which the hydraulic performances have to be

optimized, the hydraulic properties of monitoring wells traditionally used on contaminated sites are often disregarded (Baptiste and Chapuis 2014). However, monitoring well screens may strongly influence results of hydraulic tests (pumping or slug tests) or natural groundwater flow measurements within the well.

The combined effect of the wellbore opening in the porous media and of the well construction on the groundwater flow around and through the well is commonly considered by a flow distortion coefficient (a_w) which defines the ratio between the flux of water passing through the well (i.e. the apparent water flux (q_{app}) [L T^{-1}]) and the groundwater flux in the aquifer formation (q_D) (Equation 7). This distortion coefficient characterizes the degree of convergence or divergence of the groundwater flow in the vicinity of the monitoring well (Figure 20).

$$\alpha_w = \frac{q_{app}}{q_D} \qquad \text{Equation 7}$$

If the equivalent hydraulic conductivity of the well construction (including its equipment such as screens and filter pack) is higher than the aquifer hydraulic conductivity, the flow lines are converging and the value of a_w is higher than 1. Conversely, if the equivalent hydraulic conductivity of the well construction is lower than the hydraulic conductivity of the aquifer, the groundwater tends to bypass the well, the stream lines are diverging and the flow distortion coefficient is lower than 1. (Figure 20).

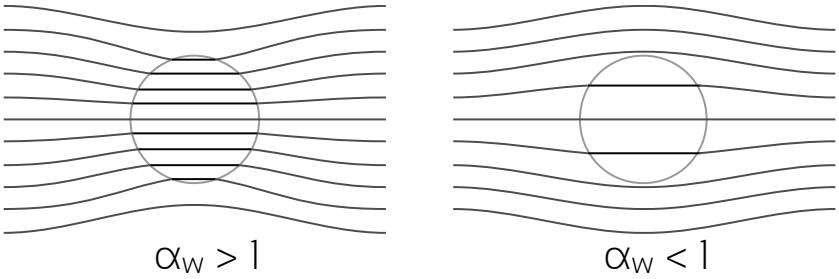

Figure 20: Converging and diverging flow lines in a uniform groundwater flow that are influenced by a well.

For a piezometer constructed with a filter pack, the convergence/divergence factor can be calculated as follow (Drost et al. 1968):

$$\alpha_w = \frac{8}{\left(1+\frac{K}{k_F}\right)\left(\left(1+\left(\frac{r_I}{r_O}\right)^2\right)+\frac{k_F}{k_S}\left(1-\left(\frac{r_S}{r_B}\right)^2\right)\right)+\left(1-\frac{K}{k_F}\right)\left(\left(\frac{r_I}{r_B}\right)^2+\left(\frac{r_O}{r_B}\right)^2\right)+\left(\frac{k_F}{k_S}\right)\left(\left(\frac{r_I}{r_B}\right)^2-\left(\frac{r_O}{r_B}\right)^2\right)} \qquad \text{Equation 8}$$

where K is the hydraulic conductivity of the aquifer, k_F the hydraulic conductivity of the filter pack, k_S the hydraulic conductivity of the well screen. r_I is the internal radius of the well screen, r_O is the outer radius of the filter screen and r_B is the radius of the borehole (Figure 21).

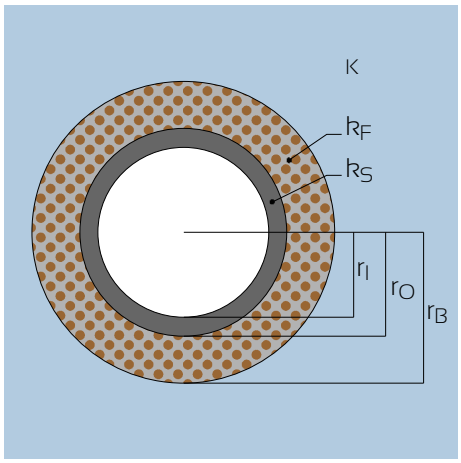

Figure 21: A monitoring well construction contains two concentric filter separating the open wellbore from the aquifer formation, the well screen and the gravel or sand filter pack.

Most uncertain parameters in the calculation of the a_w factor are the hydraulic conductivities of the filter pack and of the well screen. Both are sensitive to the well field construction such as proper centering or appropriate development and can be influenced by long term phenomenon such as clogging or fouling. This emphasizes the importance of a perfect well construction that has to be realized carefully if water fluxes measurements are planned in the well.

Recently, Bayer-Raich et al. (2018) investigated the water flow through well screens by mean of a detailed numerical model. This kind of sophisticated model are relevant to compare and validate techniques such as the Colloidal Borescope, the Heat Pulse Flowmeter or the Laser/Acoustic Doppler Velocimeter that measures very locally the groundwater velocity in the well. For more integrative point dilution methods, the Drost solution (Equation 8) delivered the same result as the numerical model for determination of a_w and can reasonably be used to relate q_{app} to q_D. a_w values for commonly used screens and filter packs vary between 2 to 4. Wu et al. 2008 found that for high apparent Darcy flux (>2×10^{-3} m/s) a_w remains between 3 and 5 for commonly used screens.

1.7. Time variability of groundwater flow and consequences on mass flux measurements

In many different hydrogeological contexts, groundwater flow is intrinsically transient and assuming steady state conditions may not be adequate. This is the case for groundwater-surface water interactions (Dujardin et al. 2014, Battle-Aguilar et al. 2014) or tidal effects (Ataie-Ashitani et al 2001, Chen and Pinder 2011, Post et al. 2018), where variations in surface water levels often induce rapid and significant changes in hydraulic gradients and groundwater fluxes. This can also occur in sectors of groundwater catchments characterized by preferential pathways, where intense rainfall events lead to fast recharge mechanisms and accelerated groundwater flow (Lubczynskia and Gurwinb 2005). Changes in groundwater flow can also be caused by human activities related to groundwater abstraction well operations (Jamin et al. 2015) or overly intense irrigation. Such groundwater flow variations may be characterized by very different time scales, from short tidal or daily barometric to longer seasonal and annual variations (Dentz and Carrera 2005, Yang et al. 2012).

Kempf et al. (2013) applied the PDM, the HPFM and the PVP different techniques for measuring transient groundwater flows in an aquifer influenced by tidal variations. These techniques sometimes require hours to hours to quantify the groundwater flux because they rely on concentration decline interpretation of a solute or heat tracer. On the time scale of contaminated aquifer management, such measurements can be considered as snapshot groundwater flux measurements, only representative of the groundwater flow conditions in the aquifer at a given time (Figure 22). On the other side of the time scale, passive and cumulative measurement techniques have been developed to obtain measurements representative of a more time integrated period of time (Verreydt et al. 2010). While such passive samplers provide robust estimates of mean contaminant mass fluxes, they only deliver a cumulative value of this contaminant mass flux smoothed over the time of exposure and does not capture the temporal dynamic of the contaminant plume (Figure 22). These methods must be undertaken sequentially to obtain successive, yet temporally time-averaged, estimates of groundwater flux (Schilling et al. 2011).

Transient groundwater flow conditions influence contaminant mass flux estimates Rein et al. (2009) and have a major effect on contaminant degradation Rolle et al. (2009). Seasonal or tidal variability of groundwater flow generally enhances contaminants degradation by mixing at the plume edges and by bringing more electron donors or acceptors (Prommer et al. 2002, Batlle-Aguilar et al. 2014). Transient flows can also have an effect on vertical and horizontal dispersion of the contaminant plume in the saturated zone. Groundwater flow both in terms of quantity and direction may considerably vary with time and cover several orders of magnitude of Darcy flux values. Changes in groundwater levels may also contribute to local mobilization of contaminants residually retained in the vadose zone. This can create further inputs in the saturated zone and produce variations of contaminant concentrations and mass fluxes (Zosseder et al. 2009).

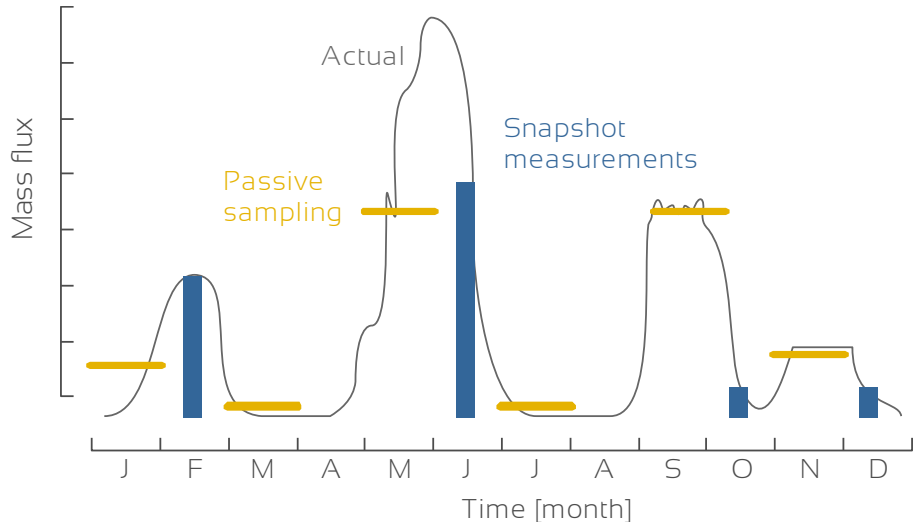

Figure 22: Comparison between point and passive sampling measurements of mass flux. Passive samplers provide a cumulative value of this contaminant mass flux smoothed over the time of exposure and does not capture the temporal dynamic of the contaminant plume.

The lack of techniques and methodologies allowing to visualize and communicate on transient processes is also cited as a cause for neglecting these transient processes. Improving visualization of transient groundwater flow and associated communications would also improve the general perception of the variation of groundwater fluxes and the awareness of problems related to transient contaminant mass fluxes in aquifers (Seidel et al. 2014).

1.8. Conclusion

All these contexts, descriptions and examples illustrate how important is a reliable measurement of groundwater flux and a detailed understanding of its time dynamics for mass flux and mass discharge calculation but also for hydrogeological characterization in general. Even if some groundwater flux measurement methods are currently available, they still are limited in their abilities to perform groundwater flux measurements that are representative of the entire well screen and to capture the dynamics of transient groundwater flows.

A recent groundwater flux measurement method proposed by Brouyère et al. (2008) seems to correspond to the aforementioned needs. The Finite Volume Point Dilution Method (FVPDM, section 2) is a promising candidate since it has a potential to be developed for the monitoring of transient groundwater flows and it has been successfully applied in a variety of geological settings. In this PhD research, the Finite Volume Point Dilution Method is presented as a robust, sensitive and accurate method for the measurement and monitoring of both steady state and transient state groundwater fluxes, in support of general hydrogeological characterization and of contaminant mass fluxes and mass discharge measurements.

Chapter 2

The Finite Volume Point Dilution Method: theoretical concepts and developments

The classical Point Dilution Method (PDM) is known since more than 100 years and frequently used for groundwater flux measurements. This method is relatively fast to apply and simple to interpret. However, its precision is limited by experimental setup constrains and does not allow for the measurement of variable groundwater fluxes.

Ten years ago a new tracer technique based on single-well dilution has been published. The so-called Finite Volume Point Dilution Method (FVPDM) is a generalization of the PDM. It differs from the traditional PDM by the continuous tracer injection in the well rather than a pulse type injection. This method is more precise than the PDM and allows for the monitoring of transient groundwater fluxes.

In this chapter, the FVPDM theoretical framework and experimental setup are synthetized. The mathematical basis and a first analytical solution allowing to interpret FVPDM experiments performed in steady state groundwater flow conditions already existed prior to this PhD. In this work a new solution for interpreting FVPDM undertaken for monitoring variable groundwater fluxes in transient flow conditions is proposed. A new general flow chart for the dimensioning of FVPDM experiments is also provided.

2.1. Origin and fundamental principles of the FVPDM.

Measurement of groundwater fluxes is useful for any hydrogeological study, from early hydraulic characterization to most advanced flow and transport modeling. Convinced that the control of the tracer input function in the tested aquifer plays a major role in the interpretation of a tracer test, Brouyère (2003) developed a new physically-based approaches that accurately models the tracer injection in a well. This new model and the analytical solution developed to facilitate its application for steady state groundwater flow measurements (Brouyère et al. 2005) are the basis of the Finite Volume Point Dilution Method (FVPDM) (Brouyère et al. 2008).

The Finite Volume Point Dilution Method (FVPDM) is a generalization of the PDM technique that aims to perform a direct measurement of groundwater flux. It differs from the classical PDM by its continuous low-flow injection of tracer into the tested well at a controlled rate. The tracer concentration within the tested well is constantly monitored and the quantification of the groundwater flux is based on the interpretation of the evolution of this tracer concentration. If the groundwater flow rate through the well screen due to natural water motion in aquifer is high, the tracer injected in the well will be strongly diluted and the tracer concentrations measured in the well will be low. Conversely, if the groundwater flow rate is low, the measured tracer concentration will be high due to less tracer dilution by the water passing through the well screen.

As for other single-well tracer dilution techniques, the FVPDM allows the measurement of a flow rate of groundwater across the well screen that can be converted into a groundwater flux or Darcy flux (q_D) [LT^{-1}] (Equation 4).

2.2. Mathematical basis for the FVPDM

The FVPDM model is based on mass balance equations applied to water and tracer in the tested well and integrated over the volume of water present in the well, known as the mixing volume (V_w) [L^3]. The water mass balance depends on the various flow rates entering and exiting the well (Figure 23, Equation 9).

$$\frac{\partial V_w}{\partial t} = Q_{inj}(t) + Q_{in}(t) - Q_{out}(t) \qquad \text{Equation 9}$$

Q_{inj} [LT^{-3}] is the tracer injection flow rate and Q_{in} [LT^{-3}] and Q_{out} [LT^{-3}] are respectively the groundwater flow rate entering and exiting the well by the screen. The volume of water in the well V_w [L^3] can be calculated using geometric properties of the well (i.e. radius (r_w) [L]) and the height of the water column (h_w) [L] as follows (Equation 10):

$$V_w = \pi r_w^2 h_w$$ *Equation 10*

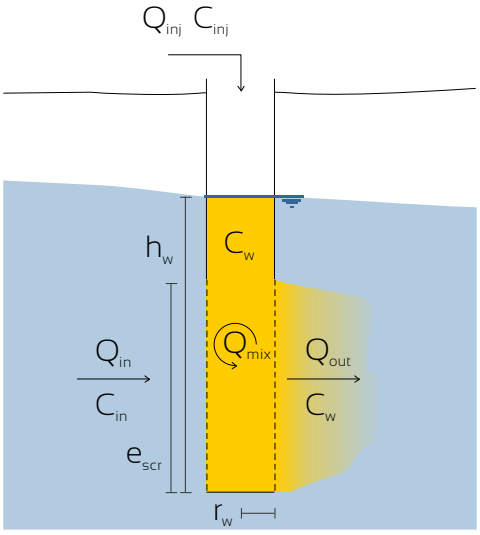

Figure 23: Schematic representation of the well-aquifer system and exchanged water and tracer fluxes. During an FVPDM experiment a tracer is continuously injected into a well at a controlled low flow rate while the water column of the well is constantly mixed to ensure a homogeneous distribution of the tracer. By measuring the tracer dilution induced by the groundwater transit flow rate through the well screen, it is possible to calculate the groundwater flux in the aquifer.

The transit flow rate (Q_t) which represents the flow rate of groundwater that passes through the screen of the well (Q_{in}) depends on the injection flow rate (Q_{inj}). When $Q_{inj} = 0$, the groundwater flow rate that enters the well equals the water flow rate exiting the well (Figure 23a), as it would happen by natural motion of groundwater through the aquifer. As Q_{inj} increases, Q_{in} decreases (Figure 24b) until a critical value called the critical flow rate ($Q_{cr} = \pi Q_t$) at which the transit flow rate is cancelled ($Q_t = 0$ and $Q_{out} = Q_{inj}$) (Figure 24c). Above the critical value, Q_{in} is so high that a radial diverging flow is creates around the well. (Figure 24d). The continuous variation of Q_{in} as a function of Q_{inj} has been formulated by Brouyère (2003) as:

$$Q_{in} = Q_t \sin\left(arcos\left(\frac{Q_{inj}}{\pi Q_t}\right)\right) - \frac{Q_{inj}}{\pi} arcos\left(\frac{Q_{inj}}{\pi Q_t}\right)$$ *Equation 11*

Equation 11 assumes that locally all those water fluxes reach equilibrium instantaneously. In order to measure groundwater flux using the FVPDM, Q_{inj} must be maintained below Q_{cr}. If not, the tracer concentration in the well will eventually reach the tracer injection concentration when all the water of the well will be replaced by the injected tracer solution.

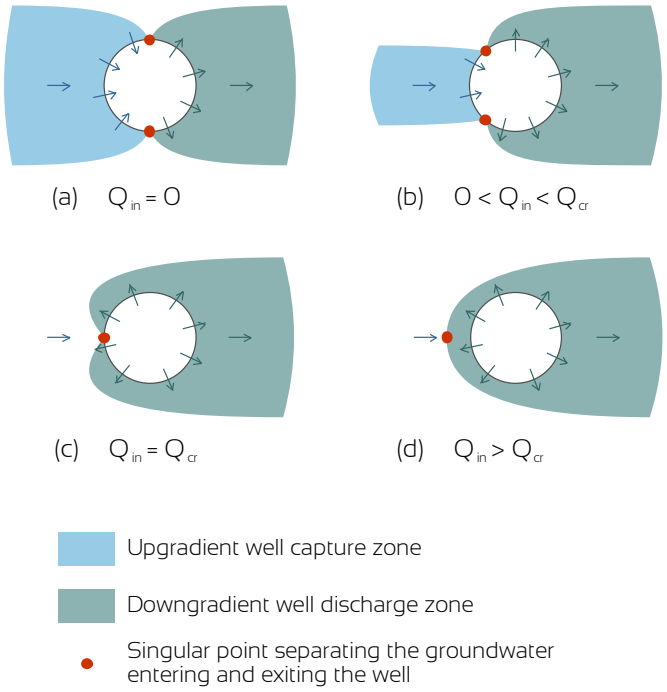

Figure 24: Influence of the injection flow rate on the flow around a well. As the injection flow rate increases, (a) to (d), the groundwater flow rate entering the well decreases to the point of becoming null. When the injection flow rate reaches this critical value, the flow around the well is fully diverging. In order to measure groundwater flow using the FVPDM, the injection flow rate must be kept under this critical flow rate (modified from Brouyère 2003).

If a perfect mixing of the water column is performed in the tested well and if the tracer injection flow rate is lower than the critical flow rate, the tracer mass balance equation is (Equation 12):

$$\frac{\partial M(t)}{\partial t} = \frac{\partial (V_w C_w)}{\partial t} = \left(C_w \frac{\partial V_w}{\partial t} + V_w \frac{\partial C_w}{\partial t} \right) = Q_{inj}\, C_{inj} + Q_{in}\, C_{in} - Q_{out}\, C_w \qquad \text{Equation 12}$$

where M [M] is the mass of tracer in the well, C_w [ML^{-3}] the tracer concentration in the water of the well and in the water leaving the well, C_{inj} [ML^{-3}] the injected tracer concentration and C_{in} [ML^{-3}] the tracer concentration initially present in the aquifer and that enters the well. This equation represents the fundamental principles of the FVPDM which consists of exchanges between a tracer injected into a well and its dilution by the groundwater flow rate passing through the well screen.

2.3. Analytical solution for FVPDM interpretation in steady state groundwater flow

Equation 12 was been derived into a more useful analytical solution expression, based on a series of assumptions (Brouyère et al. 2008). First, the groundwater flow in the tested aquifer is steady state. In this case, both the height of the water column in the well (h_w) and the mixing volume (V_w) are constant. Secondly, no tracer is initially present in the groundwater or at negligible concentration. Equation 13 expresses the variation of tracer concentration with time ($C_w(t)$) for an FVPDM experiment performed in steady state groundwater flow conditions.

$$C_w(t) = \frac{Q_{inj}C_{inj} - \left(Q_{inj}C_{inj} - \left(Q_{inj} + Q_{in}\right)C_{w,0}\right)e^{-\frac{Q_{inj}+Q_{in}}{V_w}(t-t_0)}}{Q_{inj} + Q_{in}} \qquad \text{Equation 13}$$

$C_{w,0}$ is the initial tracer concentration at time t_0. Provided that the tracer injection is long enough, the tracer concentration in the well will stabilize at a value $C_{w,stab}$ [ML^{-3}], calculated at the limit of Equation 13 for an infinite time:

$$C_{w,stab} = \frac{Q_{inj}C_{inj}}{Q_{inj} + Q_{in}} \qquad \text{Equation 14}$$

From Equation 14, it can be noted that once $C_{w,stab}$ is reached, the calculation of the transit flow rate does not depend on the mixing volume anymore. $C_{w,stab}$ depends only on C_{inj}, Q_{inj} and Q_{out}. This can be considered as the first advantage of the FVPDM over a standard PDM and will be discussed later in section 3.2.

A typical FVPDM experiment can be divided into three phases (Figure 25). At the beginning of the experiment, the tracer concentration in the well C_w, until equilibrium is reached between the different groundwater and tracer fluxes. The duration of this first phase depends on the renewing of V_w by Q_{out}. $C_{w,stab}$ is reached faster if V_w is low and Q_{out} is high (Figure 26). The time to reach $C_{w,stab}$ is estimated as a critical time t_c [T] fixed to the time necessary to reach 99% of the FVPDM steady state tracer concentration (Equation 15). At the end of the experiment, the injection of tracer is stopped and this last phase corresponds to a classical dilution.

$$t_c = -\frac{\ln(0.01)\ V_w}{Q_{out}} \qquad \text{Equation 15}$$

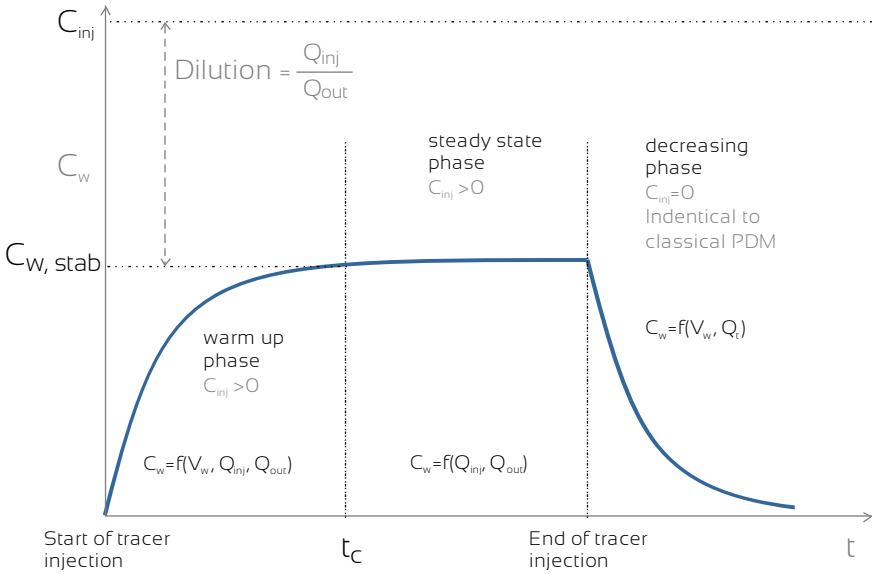

Figure 25: Evolution of tracer concentrations (C_w) in a well where a FVPDM is performed. After a warm-up phase which duration depends on the mixing volume (V_w) and on the groundwater transit flow rate (Q_t), a stabilized tracer concentration ($C_{w,stab}$) is reached when the mass flux of tracer injected in the well equilibrates the mass flux of tracer flushed out of the well by the groundwater flow that transits by the well screen. The experiment ends as a classical PDM when the injection of tracer is stopped.

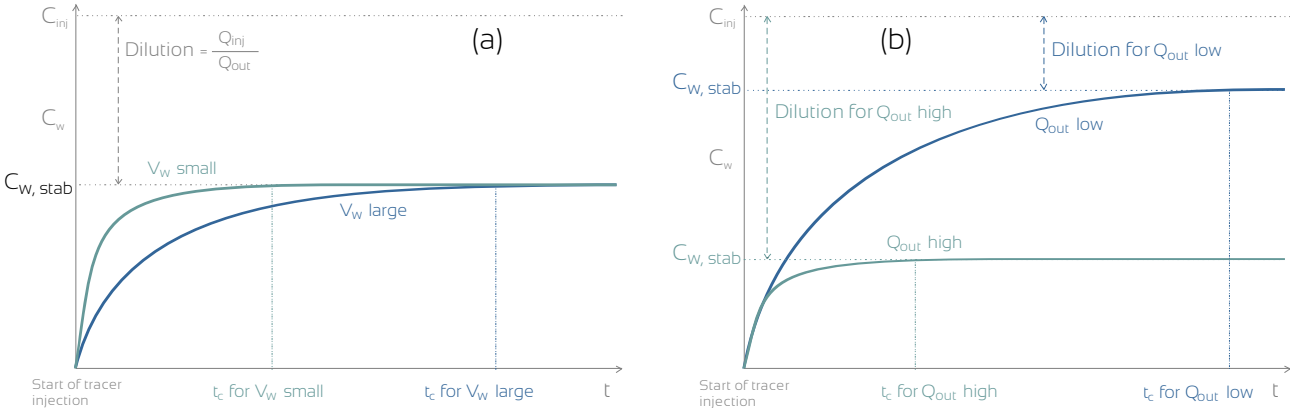

Figure 26: (a) The tracer concentration reaches a stabilized value sooner when the mixing volume is small. The stabilized concentration value remains identical as long as the groundwater transit flow rate is not changed. (b) In case of different groundwater transit flow rate, the stabilized concentration is higher and is reached later for low transit flow rate than for high transit flow rate due to slower renewing of the mixing volume and lower dilution.

The interpretation of a FVPDM test using the analytical solution consists in: (1) calculating the transit flow rate from the stabilized tracer concentration ($C_{w,stab}$), (2) adjusting the mixing volume (V_w) to fit the transient phase of the experiment. Allowing the system to reach this stabilized tracer concentration strongly decreases the uncertainties on the FVPDM interpretation because the two unknown parameters of the FVPDM equation (V_w

and Q_{in}) can be determined on different parts of the experimental curve. Finally, the natural groundwater transit flow rate can be calculated using Equation 11 and the Darcy flux in the aquifer is calculated using Equation 4.

2.4. Generalization of the FVPDM to transient state groundwater flow

This section is based on the following publication:

Jamin, P., & Brouyère, S. (2018). Monitoring transient groundwater fluxes using the Finite Volume Point Dilution Method. Journal of Contaminant Hydrology, 218(July), 10–18. http://doi.org/10.1016/j.jconhyd.2018.07.005

The first applications of the FVPDM highlighted the sensitivity of the technique to variable groundwater flow (Brouyère et al. 2008, Goderniaux et al. 2010). However, in these studies, the variations of groundwater flux were sequential and long enough to allow a stabilization of the tracer concentration. Hence the response of the FVPDM to the variation of the groundwater flux were only interpreted as a succession of steady state steps, on which the analytical solution of Brouyère et al. (2008) could be applied. However, in many hydrogeological environments, transient groundwater flow conditions may induce variations in groundwater fluxes over a shorter time span than the duration required for the FVPDM to stabilize. In these cases, the steady state FVPDM interpretation is no longer applicable.

If the groundwater flow is transient, the tracer concentration in the tested well (C_w) during an FVPDM experiment is also transient (Figure 27, blue line). When the groundwater flow increases in the aquifer, the tracer dilution in the well increases, and the measured concentration decreases. Conversely, when the groundwater flow decreases, the tracer dilution in the well decreases, and the measured concentration increases.

The aim of the following section is to present the development of the interpretation framework needed for monitoring groundwater fluxes over time using the FVPDM. The methodology is developed as a generalization of the FVPDM to transient groundwater flow fields. A mathematical formalism is proposed to calculate variable groundwater fluxes as a function of monitored concentrations in a tested well. This formalism is based on a finite difference expression of the FVPDM mass balance differential equation (Equation 12).

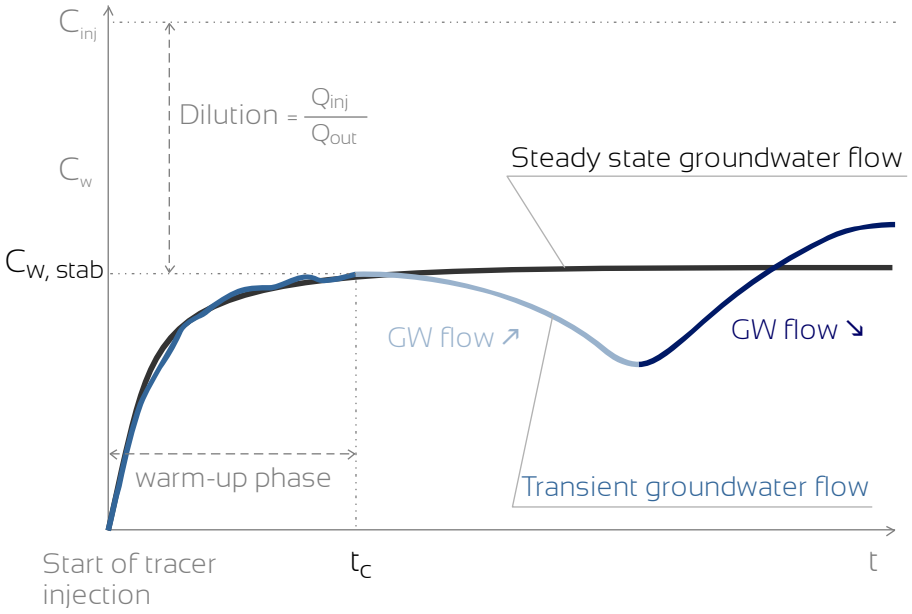

Figure 27: Typical temporal evolution of tracer concentration in a well tested by FVPDM. The black curve corresponds to steady state groundwater flow conditions with a stabilization of tracer concentration at $C_{w,stab}$. The blue curve corresponds to transient state groundwater flow conditions. If groundwater flow decreases (dark blue), the tracer is less diluted in the well, and its concentration increases. If the groundwater flow increases (light blue), the tracer is more diluted in the well, and its concentration decreases.

All the variables of Equation 12 are time dependent in case of transient groundwater flow. Nevertheless, the tracer injection flow rate and concentration (Q_{inj} and C_{inj}) are always known because they are part of the experimental configuration. The water column h_w can also be known independently of the FVPDM experiment if monitored with time (e.g. using a piezometric level sensor) in order to calculate changes in the mixing volume V_w.

Assuming no tracer is present initially in groundwater, C_{in} is equal to zero and the term $Q_{in}\ C_{in}$ simplifies. The term $C_w\ \frac{\partial V_w}{\partial t}$ can be expressed based on Equation 9 and introduced in Equation 12.

$$C_w\ Q_{inj} + C_w\ Q_{in} - C_w\ Q_{out} + V_w\ \frac{\partial C_w}{\partial t} = Q_{inj}\ C_{inj} - Q_{out}\ C_w \qquad \textit{Equation 16}$$

The two terms $Q_{out}\ C_w$ simplify and Equation 16 leads to:

$$V_w\ \frac{\partial C_w}{\partial t} = Q_{inj} C_{inj} - Q_{inj}\ C_w - Q_{in}\ C_w \qquad \textit{Equation 17}$$

Equation 17 can be solved using an implicit finite difference scheme over the time step $\Delta t = t_{n+1} - t_n$. Other types of finite difference schemes (e.g. explicit or central) could of course be considered. All time-variable terms Q_{in}, h_w and C_w are thus expressed at time t_{n+1}, i.e. $Q_{in}(t_{n+1})$, $h_w(t_{n+1})$ and $C_w(t_{n+1})$ respectively; $\frac{\partial C_w}{\partial t}$ is approximated over the time step as $\frac{C_w(t_{n+1}) - C_w(t_n)}{\Delta t}$.

A generalization to transient groundwater flow of the analytical solution established by Brouyère et al. (2008) is given with:

$$h_w(t_{n+1})\,\pi\,{r_w}^2\,\frac{C_{w\,n+1} - C_{w\,n}}{\Delta t} = Q_{inj}\,C_{inj} - Q_{inj}\,C_w(t_{n+1}) - Q_{in}(t_{n+1})\,C_w(t_{n+1}) \qquad \textit{Equation 18}$$

The evolution with time of tracer concentration in the well is given by:

$$C_w(t_{n+1}) = \left(Q_{inj}\,C_{inj} + \frac{\pi\,r^2\,h_w(t_{n+1})}{\Delta t}C_w(t_n)\right) \Big/ \left(\frac{\pi\,r^2\,h_w(t_{n+1})}{\Delta t} + Q_{inj} + Q_{in}(t_{n+1})\right) \qquad \textit{Equation 19}$$

Finally, the flow rate Q_{in} can be calculated at each time step as follows:

$$Q_{in}(t_{n+1}) = \left(Q_{inj}\left(C_{inj} - C_w(t_{n+1})\right) - h_w(t_{n+1})\,\pi\,{r_w}^2\,\frac{C_w(t_{n+1}) - C_w(t_n)}{\Delta t}\right) / C_w(t_{n+1}) \qquad \textit{Equation 20}$$

Under steady state groundwater flow conditions, h_w and C_w are constant. In this case, the concentration C_w in the tested well should stabilizes and Equation 20 can be expressed as follows:

$$C_{w,stab} = C_{inj}\frac{Q_{inj}}{Q_{inj} + Q_{in}} \qquad \textit{Equation 21}$$

Equation 21 is equivalent to Equation 14.

2.5. General experimental setup

Technically, the FVPDM setup requires two pumps (Figure 28). The first pump is used to inject the tracer fluid at a controlled low-flow rate (Q_{inj}). The second pump is used to mix the water column and ensure a homogeneous tracer distribution within the well. Monitoring tracer concentration within the well (C_w) can be achieved using a measurement unit placed directly into the well or inline the circulation loop. Groundwater samples can also be collected during the experiment for later tracer concentration measurements in the lab.

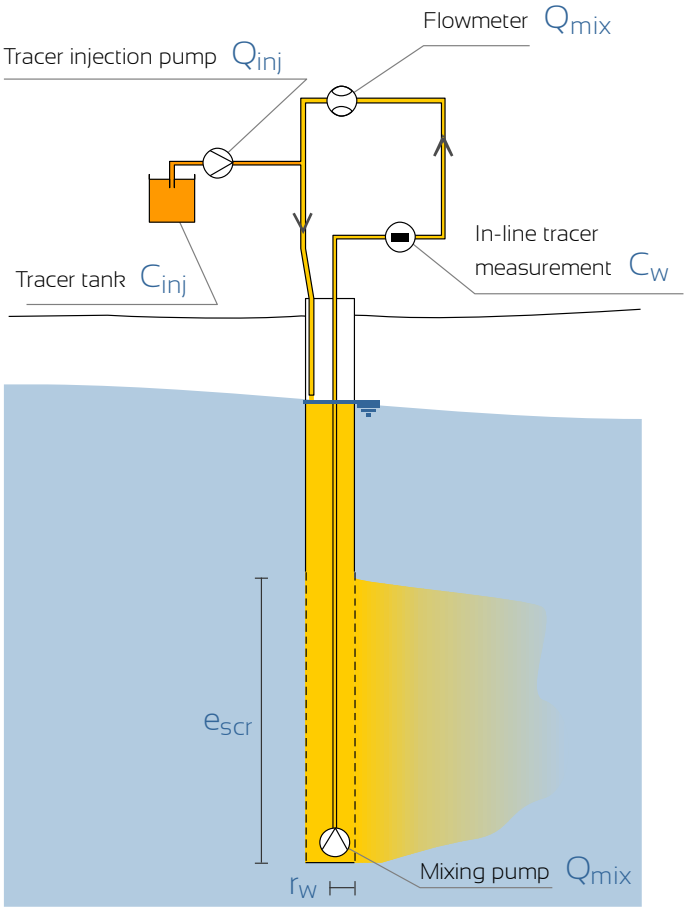

Figure 28: FVPDM experimental configuration. The water volume within the well is constantly mixed using a pump and circulated to the surface, where tracer is injected using a dosing pump. Concentration of tracer is monitored using measurement unit placed in the line or directly into the well.

As described by Equation 15, the time needed for the tracer concentration to stabilize when measuring steady state groundwater flow depends on the mixing volume and on the groundwater flow rate. In well equipped with small screens and where the water column is high, the time to reach a stabilized tracer concentration might

be long. When the water column is high comparing to the transit flow rate, the time to reach the stabilized tracer concentration might become difficult to manage for field experiments (Figure 29). For example, tracer concentrations during an FVPDM experiment performed in a monitoring well of 2 inches in diameter, with a screen length of 1 m, a flow distortion coefficient of 1, Q_{inj} = 0.5 Q_{cr}, a 10 m water column and a constant groundwater flux in the aquifer of 1 m/d require up to 23 hours to stabilize. In this case, the use of a device such as an inflatable packer isolating only the water column corresponding to zone in front of the well screen reduces the needed stabilization time down to 2 hours. When measuring groundwater fluxes in transient flow conditions, it is preferable to start the interpretation of the experimental FVPDM tracer curve after a time corresponding to t_c. This allows for a first approximation of the groundwater flux using the analytical solution and serves as initial groundwater flux value for interpretation in transient flow.

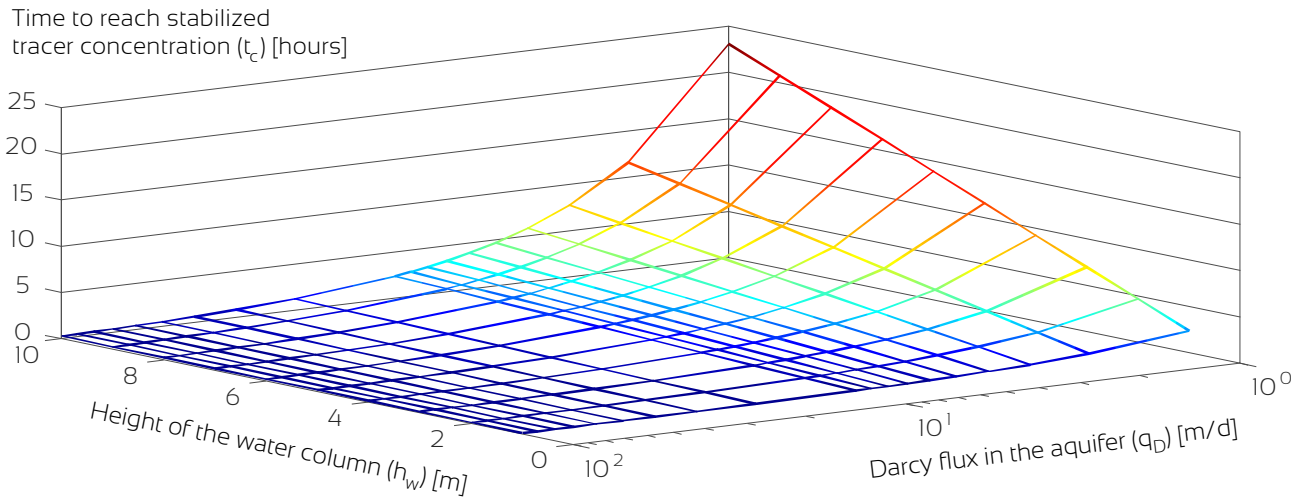

Figure 29: Time needed for the FVPDM to reach a stabilized tracer concentration calculated with Equation 15 and considering a monitoring well of 2 inches in diameter, a screen length of 1 m, a flow distortion coefficient of 1, Q_{inj} = 0.5 Q_{cr} and for different groundwater fluxes (a) and heights of water column (b).

2.6. Dimensioning flow chart for FVPDM experiments

This section is based on the following publication:

Jamin, P., & Brouyère, S. (2018). Monitoring transient groundwater fluxes using the Finite Volume Point Dilution Method. Journal of Contaminant Hydrology, 218(July), 10–18. http://doi.org/10.1016/j.jconhyd.2018.07.005

In Brouyère et al. (2008), a general flowchart was proposed for dimensioning a FVPDM experiment undertaken in a steady state groundwater flow field. This flowchart has to be adapted to the case of transient

groundwater flow conditions. The critical point in dimensioning the FVPDM is still to maintain the injection flow rate (Q_{inj}) below the critical flow rate (Q_{cr}), as well as to keep the tracer concentration in the tested well (C_w) within the detection range of the detector. When groundwater fluxes decrease in the aquifer, Q_t decreases in the well, and Q_{cr} also decreases. Thereby, Q_{inj} should be dimensioned according to a minimum estimate of transit groundwater flow across the screens ($Q_{t,prior}^{min}$). In contrast, when groundwater fluxes in the aquifer increase, Q_t also increases, and a stronger tracer dilution occurs in the tested well. In the case of very strong groundwater flows, the tracer concentration may decrease below the detection limit (C_{DL}).

Considering all these aspects, the design of an FVPDM field experiment for transient groundwater flux monitoring can be established in six steps (Figure 30):

(1) A priori estimation of the transit flow rate ($Q_{t, prior}$): this is obtained using estimates of the hydraulic conductivity (K) of the tested aquifer and of the hydraulic gradient (i) multiplied by the flow section (S_w) perpendicular to groundwater flow (Equation 4). Minimum ($Q_{t,prior}^{min}$) and maximum ($Q_{t,prior}^{max}$) expected transit flow rates can be calculated considering maximum and minimum estimates of hydraulic gradient (i_{min}) and (i_{max}).

(2) Estimation of the critical injection flow rate (Q_{cr}) based on the minimal expected transit flow rate $Q_{cr} = \pi Q_{t,prior}^{min}$ (see Brouyère et al. 2008 for details on the relationship).

(3) Definition of the injection flow rate Q_{inj} as a fraction of Q_{cr} (e.g., $Q_{inj} = 0.1\ Q_{cr}$) with a safe conservative choice with respect to the a priori estimate of Q_{cr}.

(4) Definition of the experiment duration (T_{inj}): this depends upon the characteristic time of the transient process driving changes in groundwater fluxes. For example, it is recommended to measure the tidal effect over 24 or 48 hours to capture 2 or 4 tidal cycles. The tracer injection duration should be at least as long as the characteristic time.

(5) Definition of the volume of tracer fluid (V_{inj}) calculated based on Q_{inj} and T_{inj} ($V_{inj} = Q_{inj}\ T_{inj}$).

(6) Definition of the mass of tracer (M_{inj}) to be diluted in V_{inj} to obtain a tracer concentration (C_{inj}) so that C_w remains between the detection limit (C_{DL}) and saturation limit (C_{SL}) of the detector used to monitor the evolution of concentration in the tested well, taking into account the minimal and maximal dilutions expected in the tested well.

The use of this flowchart is illustrated using the dimensioning data of an actual FVPDM experiment in section 3.3.3.

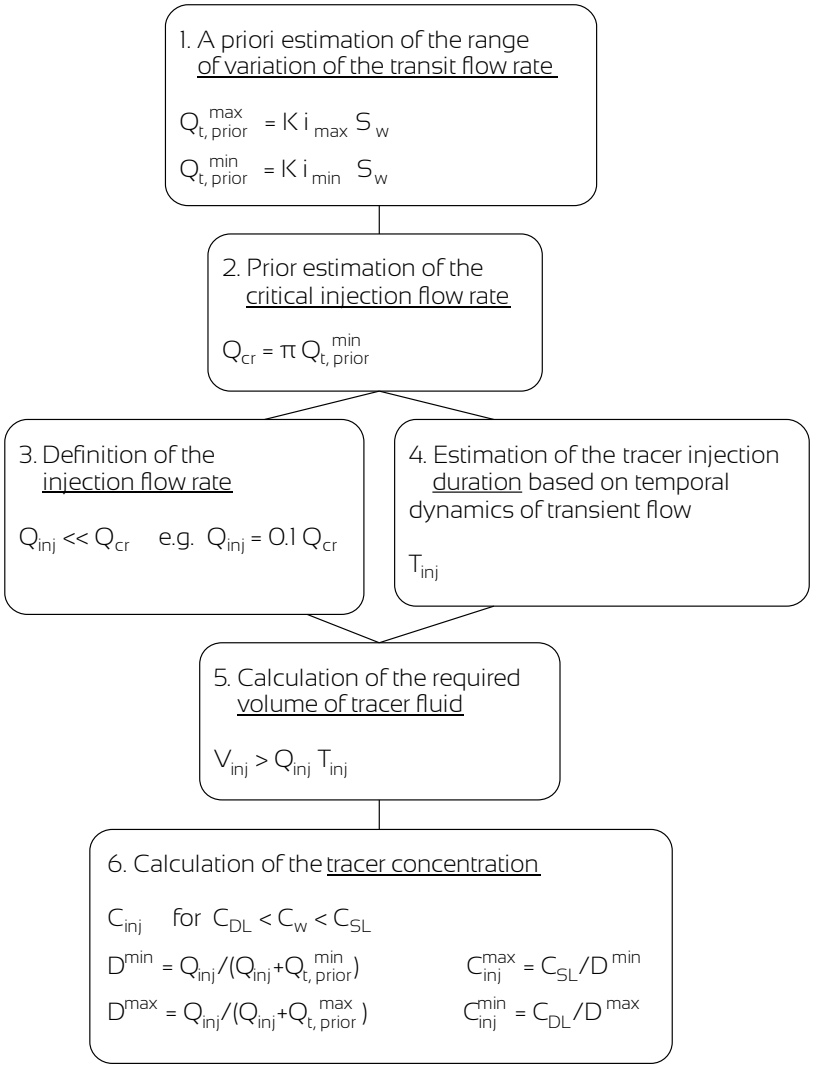

Figure 30: Flow chart of the dimensioning of the optimal FVPDM experimental configuration for continuous monitoring of transient groundwater flux.

Chapter 3

Study of the accuracy, of the precision and of the resolution of the FVPDM

The first field applications of the FVPDM proved the aptitude of the method for measuring groundwater flux and suggested its potential for monitoring transient groundwater flow. However, the methods had never been evaluated regarding to its precision, accuracy and sensitivity to groundwater flow variation on a controlled case.

In the first section of this chapter (section 3.1) the results of a laboratory experiment that aimed at validating the accuracy of groundwater flux measurements in a sand flow through tank are presented. Optimization of the FVPDM experimental setup for better precision and accuracy is also discussed.

In a first experimental field campaign (section 3.2), the FVPDM is compared with classical PDM on the same experimental site, hydraulic conditions and experimental setup. Relative precision of both techniques on groundwater flux measurements is investigated. The specific hydrogeological properties of the experimental test site located in a crystalline fractured aquifer also allow testing a new FVPDM experimental setup between packers for groundwater flux measurements linked to specific fractures in depth.

Thirdly, resolution of the FVPDM for monitoring of variable groundwater fluxes in transient flow conditions is evaluated at an experimental test site. To do so, FVPDM experiments are ran continuously at two piezometers installed in an alluvial aquifer while variable pumping was applied at a nearby well, generating controlled transient flow within the aquifer (section 3.3).

3.1. Laboratory validation of the FVPDM for measuring horizontal flows

3.1.1. Introduction

In order to fully validate the FVPDM as a reliable mean of measuring in-situ groundwater fluxes, the accuracy of the method needs to be evaluated. Quantifying the accuracy of a measurement method requires comparison of the measurements results to the actual value of the measured parameter. For environmental processes occurring in the nature, this tends to be complex because of the difficulty of knowing a priori the actual value of the result. For groundwater flux in particular, there is currently no way of knowing for sure the value of groundwater flux in an aquifer. The valisation of a groundwater flux measurement technique must be undertaken under strictly controlled water fluxes created in laboratory conditions.

"Sand tanks" have extensively been used as physical scale down models of aquifers for both teaching (Gleeson et al. 2012, Rodhe 2012, Hakoun et al. 2013) and research purposes from general water flow studies to more complex NAPL behavior characterization (Kang et al. 2018, Zhou and Cardiff 2017) or quantification of contaminant degradation (Sentenac et al. 2015, Mazy et al. 2016). The simple sand tank design allows for an accurate control of water flow and solute mass balance within the constructed the porous or fractured media and for direct visualization of flow and transport phenomenon if made of transparent casing.

All the existing methods developed for the measurement of groundwater fluxes and velocities were previously tested on laboratory sand tanks to assess their reliability and accuracy: Point Velocity Probe (Labaky et al. 2007), in-Well Point Velocity Probe (Osorno 2016), Colloidal Borescope (Kearl 1997, Bayless et al. 2011), Passive flux meter (Verreydt et al. 2015), Lasert Doppler Velocimeter (Momii et al. 1993), Accoustic Doppler Velocimeter (Bayless et al. 2011), Heat Pulse Flow meter (Bayless et al. 2011). Since the well construction is likely to have a significant influence on in-well groundwater flow measurements, Wu et al. (2008) studied this influence on sand tank experiments.

The aim of this experiment is to assess the accuracy of the FVPDM for the measurement of groundwater fluxes artificially created within a fully controlled laboratory model of aquifer where water fluxes are prescribed.

3.1.2. Experimental setup

3.1.2.1. Flow through sand tank

The experiment took place in a lab scale flow through tank of the Ecosystem Management Research Group (ecobe) of the University of Antwerp. The experimental setup of the tank is described in details in Verreydt et al. (2015).

The tank was used to undertake FVPDM experiments under strictly controlled water flow conditions. It measures 87 cm in length, 72 cm in width and 62 cm in height. The size of the tank was initially designed to be at least 10 times the diameter of a two inches well in order to minimize boundary effects. The tank was filled under water saturated condition with a homogeneous fine silica sand (Sibelco M30) which physical and hydraulic properties are summarized in Table 2. The hydraulic conductivity of the saturated sand is 3.7×10^{-4} m/s and the total porosity is 36%. The sand is separated from the lateral water reservoirs by a screened baffle plate. The water flux through the sand is obtained by imposing a hydraulic gradient between the upgradient and the downgradient lateral water reservoirs. The water heads in the reservoir are controlled by small external water reservoirs designed to maintain a constant head by overflow (Figure 31).

Table 2: Properties of the Sibelco M30 sand filling the flow through tank.

Hydraulic conductivity	3.7×10^{-4}	m/s
Total porosity	36.42	%
Mean grain size	0.32	mm
Bulk density	1.7	kg/l

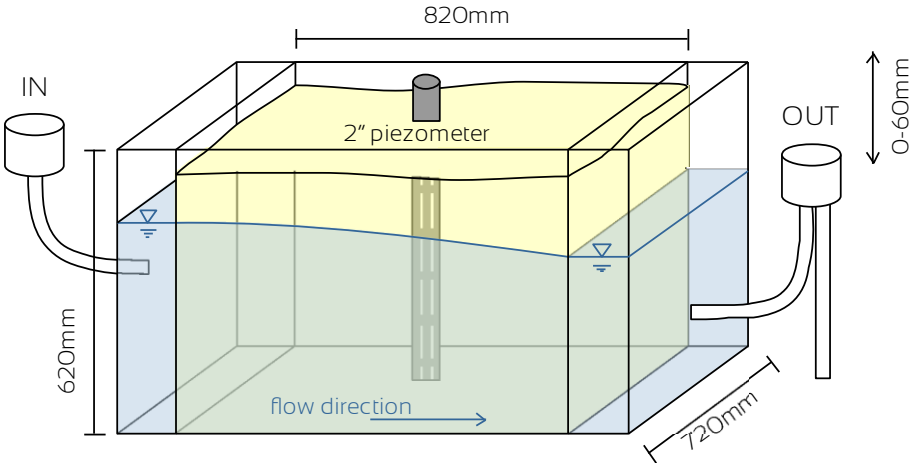

Figure 31: Laboratory sand flow through tank.

3.1.2.2. Experimental methodology and FVPDM setup

A polypropylene screened tube was installed at a central position in the sand tank to serve as a monitoring well. The tube has and external diameter of 65 mm and an internal diameter of 50.8 mm. The screen is made of 1 mm slots and has a hydraulic conductivity of 0.3 m/s (data from the provider). The tube is screened from the bottom of the tank to the surface of the sand. With a water column of 0.49 m, the volume of water contained in this monitoring well is 0,993 L. No gravel filter pack is installed around the well to separate it from the sand. A flow distortion coefficient of 2.45 was calculated for this well using the Drost et al. method (1968).

The FVPDM experimental setup used for these experiments was the basic setup described in chapter 2. A peristaltic pump (Waston-Marlow 520SN-REL) was used to mix the water column within the well with a mixing flow rate of 2.45 L/min. The pump used to inject the tracer was a peristaltic pump Watson-Marlow QDos60. The injected tracer, Uranine (CAS no. 518-47-8), was used at an initial concentration (C_{inj}) of 150 ppb. The tracer concentration in the tested well (C_w) was monitored by a Schnegg GGUN-FL30 fluorometer coupled to a Tetraedre TRMC-5 data logger with a measurement time step of one minute. The fluorometer was placed in line on the circulation loop. The total mixing volume (V_w) was 1.268 L.

During all the experiment, the upgradient reservoir was maintained at a constant level and the downgradient lateral reservoir was moved up and down in order to create several different hydraulic gradient and water fluxes, from long steps to reach quasi steady states to very short time steps to obtain almost fully transient flow conditions in the sand tank. In this way, the accuracy of the FVPDM can be tested on both steady state and transient water fluxes. The different water fluxes prescribed in the sand tank were calculated by application of Darcy's law based on the hydraulic conductivity of the sand, on the geometric parameters and on the prescribed hydraulic gradient. The water flux was also episodically verified by measuring the flow discharging from the tank.

The first experiment consisted in a single measurement of a steady state water flux. The outflow reservoir was placed vertically to create a hydraulic gradient of 0.032 m/m. The tracer injection for the FVPDM experiment was started 15 minutes after the establishment of the hydraulic gradient in order to let the water flux stabilizes in the sand tank. The tracer injection was maintained during 120 minutes and the tracer concentration was monitored during 137 minutes. The decreasing of tracer concentrations was thus observed during 17 minutes. This first FVPDM experiment was interpreted using the analytical solution of Brouyère et al. (2008).

A second FVPDM experiment was run under variable water flow conditions. The downgradient lateral reservoir is placed to create an initial hydraulic gradient of 0.027 m/m. During the 20 hours FVPDM monitoring experiment, the downgradient lateral reservoir was moved vertically to create variable water fluxes in the sand tank, with time steps decreasing from 90 to 5 minutes. The resulting variable water fluxes started thus with a succession of steady state water flow conditions whose duration shortened down to create fully transient flow at the end. The second FVPDM experiment was interpreted using two different methods. The FVPDM steady state analytical

solution (Brouyère et al. (2008) was used when water fluxes in the sand tank could be considered as a succession of steady state water flow conditions, namely when the change of hydraulic gradient were made after 90, 60 or 30 minutes. The transient state interpretation developed in section 2.4 was used to interpret the whole FVPDM experiment, namely when the changes of hydraulic gradient were made after 90, 60, 30 and 5 minutes.

The complete experimental setup for the FVPDM is detailed in Table 3.

Table 3: Experimental setup of the FVPDM and prescribed water flux in the tank and corresponding groundwater fluxes as measured with the FVPDM.

FVPDM experiment	Q_{mix} [L/min]	Q_{inj} [mL/min]	C_{inj} [ppb]	Time step duration [min]	Prescribed q_D [m/s]	Measured q_D [m/s]
1	2.45	35.82	299	120	1.18×10^{-5}	1.18×10^{-5}
2	2.45	35.82	299	90	8.90×10^{-6}	8.85×10^{-6}
				90	9.99×10^{-6}	9.80×10^{-6}
				60	1.25×10^{-5}	1.20×10^{-5}
				60	9.99×10^{-6}	1.00×10^{-5}
				60	8.08×10^{-6}	8.07×10^{-6}
				60	1.11×10^{-5}	1.11×10^{-5}
				30	1.02×10^{-5}	1.05×10^{-5}
				30	9.99×10^{-6}	9.93×10^{-6}
				30	9.36×10^{-6}	9.21×10^{-6}
				30	8.51×10^{-6}	8.72×10^{-6}
				30	7.23×10^{-6}	7.94×10^{-6}
				30	7.66×10^{-6}	7.44×10^{-6}
				30	6.80×10^{-6}	6.81×10^{-6}
				30	5.95×10^{-6}	6.28×10^{-6}
				30	4.68×10^{-6}	5.56×10^{-6}
				30		3.65×10^{-6}
	2.45	40.02	149	5 (assumed fully transient)	Variable from 1.46×10^{-6} to 1.255×10^{-5}	Variable from 3×10^{-6} to 1.45×10^{-5}

3.1.3. Results

3.1.3.1. Single water flux measurement under steady state water flow conditions

The result of the single measurement of a constant water flux, interpreted with the FVPDM steady state analytical solution (Equation 13) is show at Figure 32. The calculated evolution of the tracer concentration fits almost perfectly the observed data. The adjusted water flux considering the flow distortion coefficient of 2.45 is $1.180\times10^{-5} \pm 0.002\times10^{-5}$ m/s. The uncertainties over the adjusted water flux was calculated with the same procedure as described in section 3.2.2.4. The difference between the water flux measured with the FVPDM and the water flux prescribed in the sand tank is 0.15%.

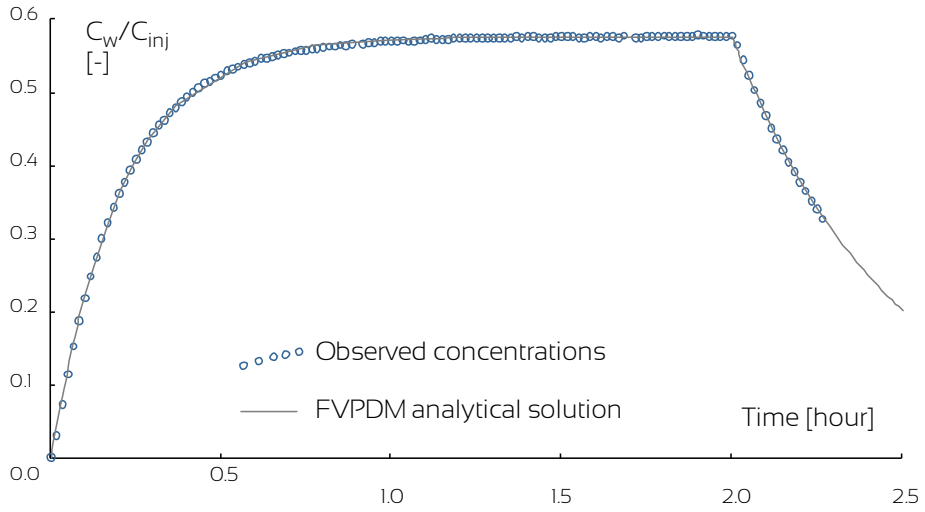

Figure 32: Relative tracer concentrations observed in the observation well, and calculated with the FVPDM analytical solution. The adjusted water flux of $1.180\times10^{-5} \pm 0.002\times10^{-5}$ m/s differs from the flux prescribed in the sand tank by only 0.15%.

3.1.3.2. Monitoring of water fluxes under transient state water flow conditions

The FVPDM experiment performed under variable water flux was interpreted using both the FVPDM analytical solution (Equation 13) and the transient solution (Equation 20) (Table 3 and Figure 33). The analytical solution was used only up to 12 hours into the experiment, as long as the time steps of the water flux variations were long enough for considering a succession of steady state flow regimes. For the 5 min time steps, the water fluxes were assumed to be fully transient and could not be interpreted using the analytical solution. The transient solution has been used to interpret the whole test.

The adjustment of the FVPDM analytical solution shows a nearly perfect fit on the observed data (Figure 33). The water fluxes calculated with the FVPDM transient solution are also in good agreement with the water

fluxes prescribed in the sand tank. Small oscillations due to a combination of measurement noises coming from the pressure sensor used to measure the water height and from the fluorometer used to quantify tracer concentrations can be noticed. These oscillations can be filtered by simple smoothing functions such as moving average.

The last 30 min experimental step when a minimal water flux was prescribed and the three first steps of 5 minutes where a maximal flux was prescribed can not be used to judge the accuracy of the method. The reason is that the change between the consecutive values water flux was so abrupt that the groundwater flow conditions prevailing within the tank took time to equilibrate. As a consequence, the prescribed hydraulic gradient between the two external reservoirs can not be considered representative of the hydraulic gradient within the sand tank.

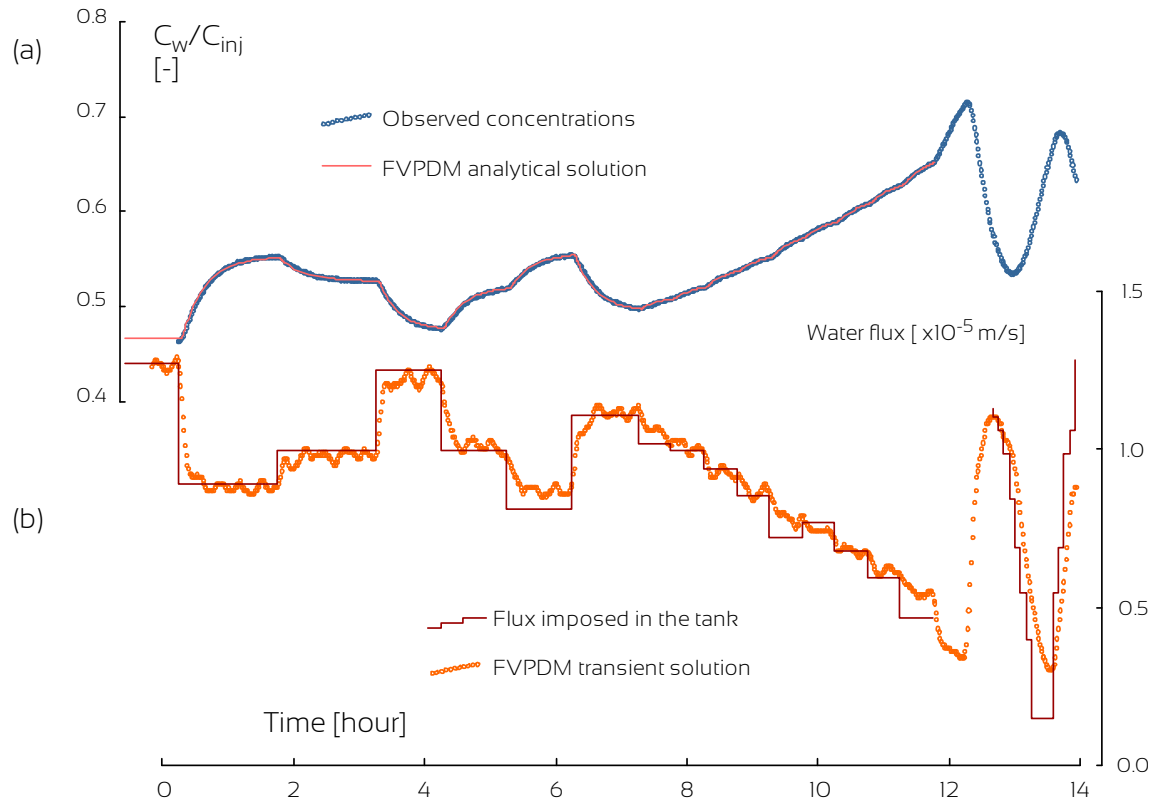

Figure 33: (a) The tracer concentration calculated with the FVPDM analytical solution fit almost perfectly on the observed tracer concentrations. (b) The water fluxes calculated with the FVPDM transient solution are in accordance with the fluxes prescribed in the tank. No comparison is possible for the last 30 min step and for the three first steps of 5 minutes. The reason is that the change between consecutive values of prescribed water flux was so abrupt that the hydraulic gradient measured between the external reservoirs can not be considered representative of the hydraulic gradient within the sand tank.

Figure 34 shows the water flux calculated with the analytical solution for each prescribed water flux in the sand tank. The coefficient of determination between the water fluxes prescribed in the tank and the fluxes

calculated by the transient interpretation of the FVPDM experiment is 96%. Figure 35 shows the water flux calculated with the transient solution. The coefficient of determination between the water fluxes prescribed in the tank and the fluxes calculated by the transient interpretation of the FVPDM experiment is 95%.

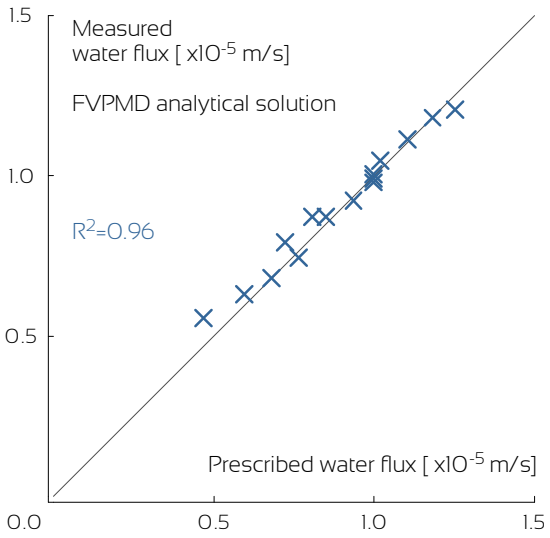

Figure 34: The coefficient of determination between the water fluxes measured with the FVPDM interpreted using the analytical solution and the water fluxes prescribed in the sand tank is 96%.

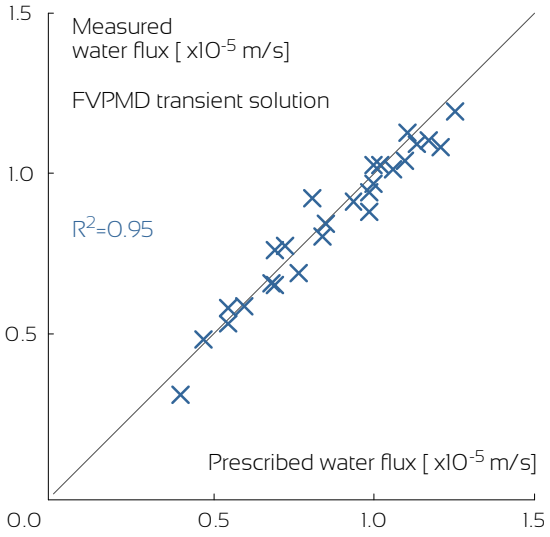

Figure 35: The coefficient of determination between the water fluxes measured by the FVPDM interpreted using the transient solution and the water fluxes prescribed in the sand tank is 95%.

3.1.4. Measurement of groundwater flow direction with the FVPDM by means of a rotating window

The aptitude of the FVPDM to monitor changes in water flux opens additional perspectives. Among them is the possibility to investigate the water flow direction of water. A tube with an external diameter slightly lower than the internal diameter of the tested piezometer, and equipped with two vertical aligned slots can be inserted in the piezometer and lowered down at the depth of the piezometer screen (Figure 36). When the slots are positioned parallel to the water flow direction, the water flux measured by the FVPDM should be maximum (Figure 36 dark blue arrow) and the tracer concentration measured during the test should be lower due to higher dilution. Conversely, when the slots are aligned perpendicularly to the water flow direction, the water flux measured by the FVPDM should be minimum (Figure 36 light blue arrow) and the tracer concentration maximum. Hence, a directional FVPDM experiment should produce a sinusoidal evolution of the tracer concentration while rotating the inner tube on 180°.

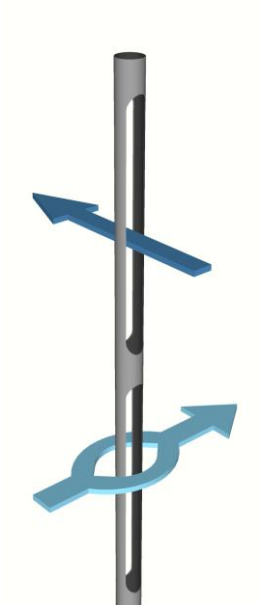

Figure 36: Slotted rotating tube for determination of water flow direction using FVPDM. Tracer dilution should be minimum when the slots are oriented perpendicularly to the groundwater flow direction and maximum when oriented parallel.

For this setup, it is not necessary to fully characterize the FVPDM experimental parameters such as injection flow rate, injected tracer concentration and mixing volume in order to interpret the tracer concentration results. The only evolution of tracer concentration during the test must be measured and plotted against the orientation of the slotted tube. Three conditions must be fulfilled to perform the estimation of groundwater flow by FVPDM. (1) As for any FVPDM experiment, the tracer injection flow rate should never exceed the critical flow rate (see

section 2.2 for more details). (2) The screen of the tested piezometer must be made of slots disposed evenly across the whole circumference of the tube. Screen types such as vertical slots, continuous-slot wire-warp screens or bridge slotted screen are ideal. On the opposite, piezometer with horizontal screen slots or louvered screens can not be investigated for water flow direction since a vertical plain wall sits along the tube (Sterrett 2007). (3) The groundwater flux in the tested aquifer must remain constant during all the experiment.

For this experiment, an inner tube of an external diameter of 50 mm was inserted into the piezometer of the sand tank. This internal tube is equipped with two vertical slots of 20 mm wide and 500 mm height (Figure 36). The FVPDM was started with the slot aligned on the presumed water flow direction to obtain the highest possible water flux through the piezometer and accelerate the stabilization of the tracer concentration. When the tracer concentration was stabilized in the piezometer, the inner tube was rotated by steps of 22.5° every 5 minutes.

Figure 37 shows the results of the FVPDM directional monitoring. The relative tracer concentration is presented as the mean value of the five concentration measurement taken for each corresponding rotation angle of the inner tube. The curve shows the expected sinusoidal evolution. The maximum tracer concentration corresponding to the lowest dilution of tracer by the water flux was observed when the slots were oriented at 90° of the main water flow direction. Inversely, the lowest tracer concentrations are measured when the slots were aligned parallel to the water flow direction and the dilution of the injected tracer by the water flux is maximum. The precision of such a water flux direction measurement depends on the size of the incremental orientation steps considered.

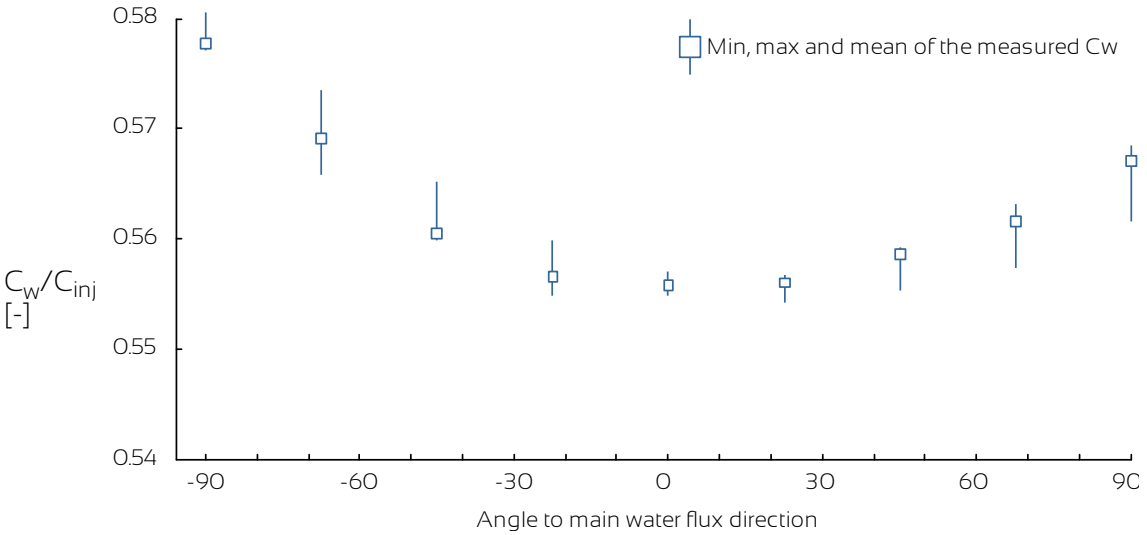

Figure 37: Evolution of the tracer concentration during a FVPDM experiment performed with a rotating slotted tube. The lowest tracer concentrations are observed when the slots are positioned parallel to the main water flow direction due to maximum dilution of the tracer.

3.1.5. Conclusions

This series of FVPDM laboratory experiments under controlled water fluxes allowed to validate the FVPDM for water fluxes measurements and to evaluate the additional possibility of water flow direction identification.

Difference between the water flux prescribed in the sand tank and the water flux measured by FVPDM was as low as 0.15%. Coefficient of determination between the fluxes prescribed and measured by FVPDM was at least 95% for water fluxes ranging from 4.5×10^{-6} to 1.25×10^{-5} m/s. The range of application of the FVPDM is not limited to this interval since measuring lower or higher fluxes only requires an adaptation of the experimental setup by adjusting either the injected tracer concentration or the tracer injection flow rate accordingly.

Several points of the experimental setup should be considered to guarantee the most accurate result possible. The parameters that have to be fully controlled for an FVPDM experiment are the tracer injection flow rate, the height of the water column within the tested well and its variation, the injected tracer concentration and the tracer concentration in the well during the experiment. Only robust field equipment able to deliver stable and precise inputs or readings should be used for field scale applications.

3.2. Evaluation of the precision of the FVPDM versus PDM in a fractured aquifer

This section is based on the following publication:

Jamin, P., Goderniaux, P., Bour, O., Le Borgne, T., Englert, A., Longuevergne, L., & Brouyère, S. (2015). Contribution of the finite volume point dilution method for measurement of groundwater fluxes in a fractured aquifer. Journal of Contaminant Hydrology, 182, 244–255. http://doi.org/10.1016/j.jconhyd.2015.09.002

3.2.1. Introduction

Estimation of groundwater fluxes in fractured aquifers is a challenge given the heterogeneity that is induced by discrete fractures (Novakowski 2006). The characterization of fracture flow based on hydraulic pressure measurements can actually lead to misinterpretation about the role of the fracture in terms of flow path and solute transport. For example, a dead-end fracture subjected to pumping will react in terms of hydraulic pressure variations even if no groundwater flow is occurring. Zha et al. (2014) recently emphasized that flux data used in hydraulic characterization of fractured media improve estimation of fracture patterns and hydraulic conductivity fields.

Therefore, tracer tests become essential tools because they allow studying the actual displacement of water. Classical tracer tests provide averaged information between two injection and recovery points. Alternative methods, such as point dilution tracer tests are promising to obtain a direct measurement of local groundwater fluxes or Darcy fluxes (q_D) (Halevy et al. 1967, Klotz et al. 1979, Zlotnik and Zurbuchen 2003, Brainerd and Robbins 2004, Hatfield et al. 2004, Huang and Goltz 2005, Pitark et al. 2007, West and Odling 2007, Sale et al. 2007). Novakowski et al. (1995 and 2006) performed classical dilution tests between packers and pointed out two major issues. The first issue is related to the estimation of the actual mixing volume (V_w), which has to be accurately known to interpret the dilution test. This mixing volume is difficult to calculate in case of dilution test performed between the packers because the test space is full of equipment (hoses, probes, mixing propellers …) and may include zone of immobile water. Furthermore, the open borehole geometry in front of the tested zone may not be perfectly cylindrical and part of the adjacent fractured medium may also be involved in the mixing processes. The second issue is that groundwater velocity changed during their experiments and disturbed the recording. The point dilution method (PDM) is actually a short time experiment that is constrained by both the maximum concentration that can be injected and the minimum concentration that can be measured in the well. The experiment stops when all the tracer has been eluted from the well, precluding continuous monitoring of groundwater fluxes.

The Finite Volume Point Dilution Method (FVPDM) (Brouyère 2003, Brouyère et al. 2008) allows overcoming those two issues and provides a quantification by a simultaneous and independent estimation of the mixing volume (V_w) and Darcy flux (q_D) on experimental data. The duration of the test is not limited and can last as long as the experiment is maintained active by injecting tracer and monitoring its concentrations in the mixed

water volume. Measurements of groundwater flux at a local scale, as achieved with this method, are complementary with more regional and indirect estimations from Darcy's law.

In this context, the objectives of this research are twofold: (1) test the method in a fractured geological context; and (2) compare the FVPDM with classical Point Dilution Methods (PDM) on the same experimental site, hydraulic conditions, and experimental setup. The comparison investigates the relative precision of the two techniques on the measurement of groundwater fluxes and it provides guidelines for dilution experiments in fractured media. The contribution of the FVPDM for groundwater fluxes measurement in fractured aquifer is also discussed in terms of experimental setup.

A series of tracer dilution experiments were performed in the Ploemeur test site (Britany, France) on several fractured zones of an open well. For the first time, the FVPDM was used between a double packer system to investigate localized groundwater flows in discrete fractures. Successive experiments were carried out with different pumping rates applied at a nearby well, to investigate the largest range of possible groundwater flux measurements, and to study the consistency of results over this range. Classical PDM were also performed following each FVPDM experiment to compare the sensitivity and uncertainties of both methods. After a description of the methodology and the experimental setup, the results of the groundwater flux measurements are discussed along with uncertainties on the interpretation of the FVPDM and PDM.

3.2.2. Methodology

3.2.2.1. Point dilution techniques

The aim of a single borehole dilution test is to perform a direct measurement of groundwater fluxes. PDM relate the concentration evolution of a tracer previously injected in a borehole as a function of the intensity of groundwater flow through the screen of the borehole. The result of such test is a groundwater flux, which depends on the hydraulic conditions within the geological formation and in the vicinity of the tested borehole (Drost et al. 1968, Hall 1996).

Considering Equation 13, the classical PDM (Equation 6) is only a specific case of the FVPDM, for $Q_{in} = 0$ and $C_{w,0} > 0$. C_w is related to the ratio of the transit flow rate on the mixing volume, in an exponential decay relation. This implies that the precision of the calculation of the transit flow rate (Q_t) fully relies on an accurate external estimation of the mixing volume (V_w).

Considering the assumptions that are inherent to the classical PDM and FVPDM, both methods are affected by *a priori* limits. Classical PDM requires (1) steady state of the aquifer groundwater flow during a time sufficient for estimating Q_t, (2) a homogeneous mixing of a large amount of the tracer in the water column instantaneous at the beginning and continuously during the experiment and (3) the accurate and precise knowledge of the mixing

volume. The quality of FVPDM relies on the duration of the experiment. In case of large mixing volume and/or limited groundwater flux, the FVPDM may require a long time to reach the steady state phase.

3.2.2.2. Experimental test site

The Stang Er Brune experimental test site is located at Ploemeur on the south coast of Brittany (France), in a crystalline rock aquifer constituted of micashists and granites (Figure 38a). This site belongs to the H+ observatory (http://hplus.ore.fr/en/) which is a national network of highly instrumented research sites in subsurface hydrology. The site is equipped with three uncased, 0.12m diameter wells of 80 to 100 m depth (B1, B2 and B3) and separated by less than 10 m and arranged in a triangular shape (Figure 38b). At this location the contact between the micashists and the underlying granite is observed at about 40 m below ground surface. The mean transmissivity obtained by various hydraulic tests in all the wells is around 10^{-3} m²/s (Le Borgne et al. 2006a and b). For the experiments described in this paper, two of the open boreholes (B1 and B2) were used. Wells B1 and B2 are intersected by 4 and 5 fracture zones, respectively, which are designated B1-1 to B1-4 and B2-1 to B2-5 (Figure 38b).

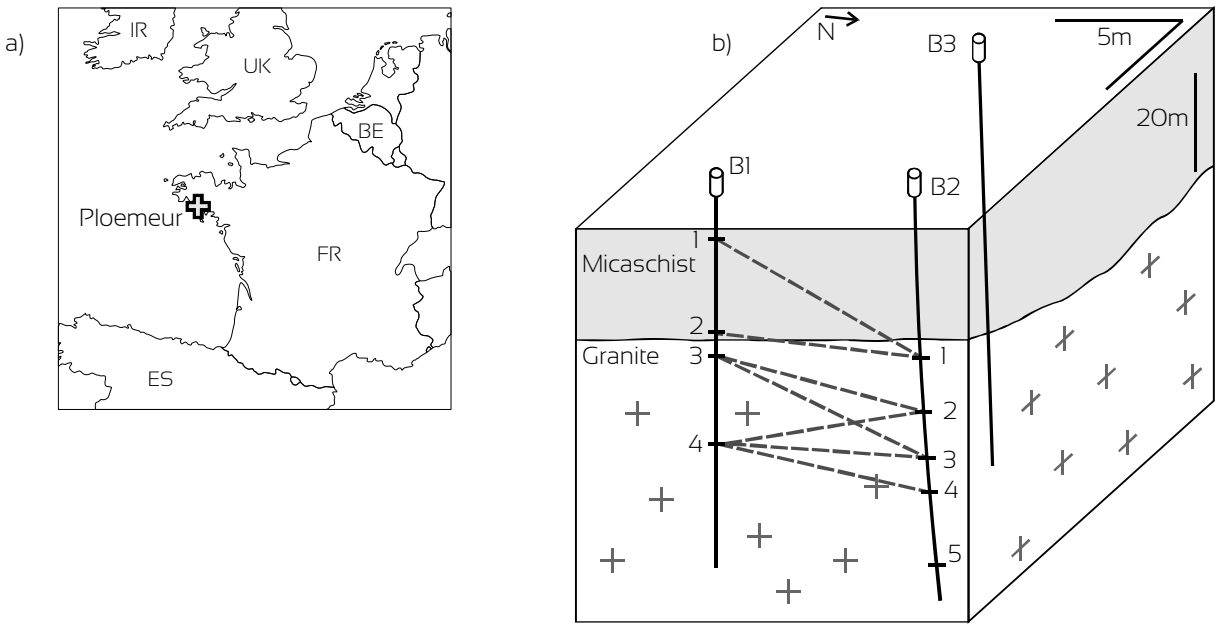

Figure 38: a) Location of the Ploemeur test site. b) Configuration of the three 90 meters deep wells (B1, B2, B3), and the fracture network. Dashed lines represents the hydraulic connections by group of fractures between B1 and B2 identified by tracer tests (Le Borgne et al. *2007, Dorn* et al. *2012).*

This site offers several advantages. (1) The fractured aquifer has already been characterized by geophysical, thermal, hydraulic and tracer tests (Le Borgne et al. 2007, Dorn et al. 2012, Read et al. 2013). (2) Open boreholes without any casing are suitable for instrumentation with packers. (3) The small distances between the wells ensures a hydraulic connection that can be exploited for the purposes of the FVPDM experiments, i.e., to modify the transit flow rate Q_t in a given fracture set in the test well by pumping one of the other wells.

3.2.2.3. Double packer experimental setup

The experiments were performed in the deepest fracture zone identified in the well B1 (B1-4), where optical imagery showed two open fractures of 3 cm aperture in total at 78.7 m below the surface. The transmissivity of this fracture zone was estimated at 1.6×10^{-4} m²/s (Klepikova et al., 2014). The flow section A [L^2] perpendicular to the direction of the groundwater flow is then 0.0036 m².

The experimental setup is designed to support FVPDM testing between a double packer system, which isolates the fracture zone (Figure 39). Vertical borehole flows are prevented and the dilution experiment is carried out within the delineated space. The length of the test chamber between the upper and lower inflatable packer was 1.2 m. Pressure sensors were used to monitor piezometric head below, between and above the double packer in order to detect any leaky seals. A submersible pump was connected above the upper packer and linked to the test chamber to create a water circulation loop between the packers and the ground surface, where the loop was connected to a field fluorometer, a pressure gauge, a water meter (to monitor flow rate of circulated water) and an electromagnetic pump for the low flow rate tracer injection. From the surface, the loop was completed at a connection allowing tracer injection at the bottom of the double packer test chamber (Figure 39). The B2 well, located 6 m away from B1, was equipped with a submersible pump to impose the groundwater fluxes around B2 and in all the surrounding fractures, including the fractured zone identified in B1-4. The FVPDM-PDM experiments were performed for different pumping rates in well B2 in order to investigate the ability and limitations of the two dilution methods to measure different groundwater fluxes. B2 pumping rates ranged from 0 and 2.4×10^{-3} m³/s (0 to 144 L/min). Groundwater levels are also monitored in B2 and B3 wells using STS pressure sensors.

FVPDM experiments were performed under specified pumping flow rates in well B2. When the conditions have stabilized in the vicinity of wells (no pressure variations greater than 1 cm in 5 min), the tracer injection was started and the tracer concentration was monitored in the test chamber (thanks to the circulation loop). The circulation flow rate was precisely maintained at 4.2×10^{-5} m³/s (2.52 L/min) and the tracer injection at 3.5×10^{-7} m³/s (0.02 L/min) with a concentration of 207 ppb of fluorescein (CAS no. 518-47-8). In total, a succession of 10 FVPDM (F1 to F10) and 8 classical PDM (P1 to P8) experiments were performed iteratively (Table 4). Mixing volume V_w and transit flow rate Q_t were then adjusted on the experimental data for each test separately. For the PDM experiments, an external estimations of V_w was used (*i.e.* independent of the interpretation

of the exponential decay of tracer concentration observed during the PDM experiment). Uncertainties around adjusted values were estimated, and the results obtained for PDM and FVPDM compared and discussed.

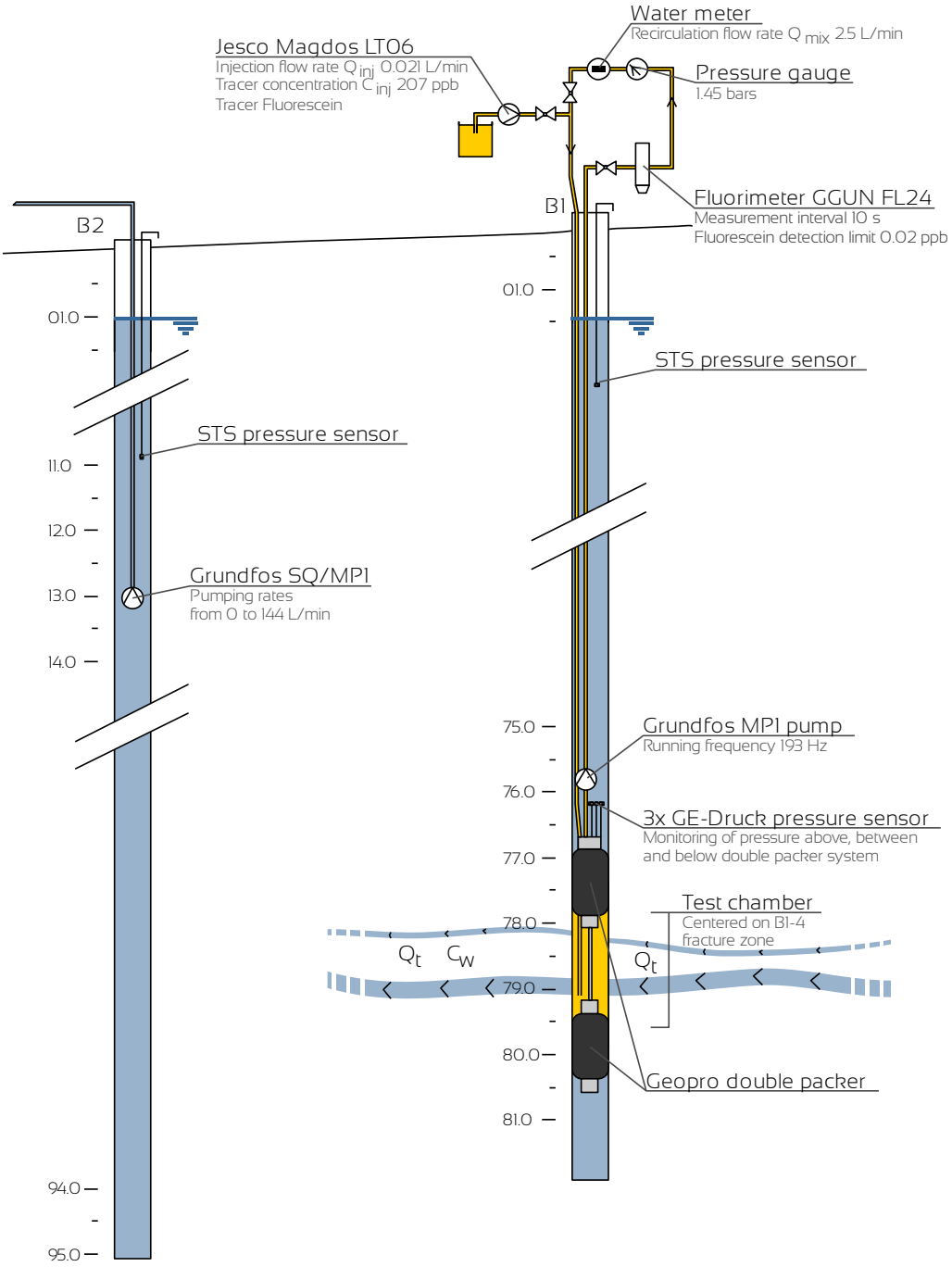

Figure 39: Experimental setup limiting vertically the investigated fracture zone with double packers. The dilution tests are performed within this 1.2 m delineated test chamber. The corresponding volume of groundwater is mixed using a pump and circulated to the surface, where tracer is injected using a dosing pump. Concentration of tracer in the loop is monitored using a field fluorometer placed in line. An immersed pump placed in the nearby well B2 allows the modification of the groundwater fluxes in the fracture B1-4. The aperture of the fractures are not at scale.

Table 4: Characteristics and sequence of tracer injections for FVPDM and PDM experiments on well B1-4. $C_{w,0}$ is the initial tracer concentration in well B1-4 at the beginning of the experiment. Q_{pump} corresponds to the pumping rate at well B2 and Q_{inj} to the tracer injection flow rate at a concentration C_{in} of 207 ppb.

Id	Duration [h]	$C_{w,0}$ in B1-4 [ppb]	Q_{in} in B1-4 [$\times 10^{-7}$ m^3/s]	Q_{pump} in B2 [$\times 10^{-3}$ m^3/s]
FVPDM 1	4.02	0	3.5	2.39
PDM 1	0.88	5	0	2.39
FVPDM 2	2.35	0.2	3.5	1.86
PDM 2	2.28	6.1	0	1.86
FVPDM 3	6.70	0.3	3.5	1.46
PDM 3	1.67	9.2	0	1.46
FVPDM 4	3.39	1.4	3.5	1.00
FVPDM 5	2.83	12.5	3.5	0
PDM 4	1.88	31.4	0	0
PDM 5	2.24	30.3	0	1.00
FVPDM 6	3.15	10.2	3.5	1.00
FVPDM 7	8.67	14.1	3.5	0.63
FVPDM 8	7.84	23.2	3.5	0
PDM 6	5.93	68.0	0	0
PDM 7	2.45	64.9	0	0.63
FVPDM 9	28.01	2.4	3.5	0.31
FVPDM 10	8.72	45.1	3.5	0.62
PDM 8	2.10	23.5	0	0.29

3.2.2.4. Uncertainties estimation using a Bayesian approach

An adequate management of uncertainties is a critical issue in experimentation, and more generally in model calibration. Various sources of uncertainties co-exist (observations, experiment set up, simplified interpretation model) and might affect the parameter inference process. The Bayesian approach is a preferred method to perform inversion of nonlinear problems and has been widely used to invert geophysical or hydrogeological data (e.g. Tarantola and Valette, 1982, Ghorbani et al., 2007, Fasbender et al. 2008). This approach consists in propagating the knowledge provided by measurements m through a known and supposed to be exact forward model G (here the dilution Equation 6 and Equation 13), and to combine with an a-priori knowledge of model parameters (here, mixing volume V_w and transit flow rate Q_t). Here, we will use a simplified definition of the posterior density function $p(\theta)$ for the parameter vector θ (Tarantola and Valette (1982). It can be calculated from the a-priori probability density function $\mu(\theta)$ (here taken as uniform), the sum of squared residuals (SSR) between the model

with parameter θ and observations m, as $SSR = \sum(m - G(\theta))^2$ and the standard deviation of measured data σ as:

$$p(\theta) = \mu(\theta) \times e^{-\left(\frac{\sqrt{SSR(\theta)}}{2\sigma}\right)} \qquad \text{Equation 22}$$

Parameter uncertainties are finally computed as marginal probability density function.

3.2.3. Results

Figure 40 shows the experimental data of the succession of FVPDM-PDM tests conducted within the fracture B1-4 under different pumping rates in the nearby well B2. PDM experiments correspond to the periods when the tracer injection flow rate is null (Figure 40b). The cumulated measurement time exceeds 100 hours. As explained in previous sections, it is observed that the time to reach the steady state regime of FVPDM is longer when the pumping rate in B2, and thus the transit flow rates in fractures, decreases. The steady state concentration C_w^{stab} is also higher in this case, due to less important dilution effects.

Each phase of the experiment, corresponding to a specific pumping rate in the well B2 and to the PDM or FVPDM configuration, was interpreted separately. The adjustment of V_w and Q_f were performed by evaluating the RMS error between the experimental C_w values and the C_w values simulated using the analytical solutions of the PDM (Equation 6) and FVPDM (Equation 13).

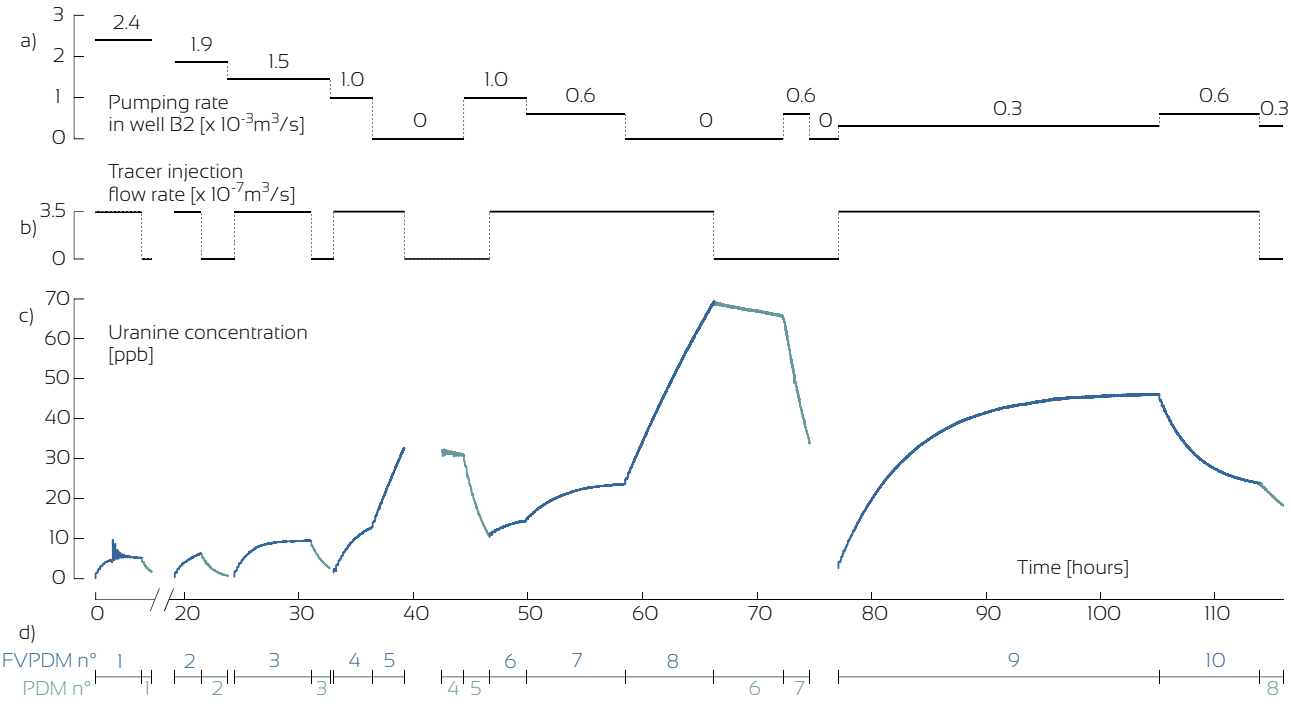

Figure 40: Evolution of tracer concentration (c) during the measurement of groundwater flow by FVPDM and PDM in the B1-4 fracture. The distinction between natural and forced hydraulic conditions is represented by the pumping rate applied in the well B2 (a). The distinction between FVPDM and PDM experiments is figured by the tracer injection flow rate (b), PDM being performed when Q_{in} is null. Discontinuity in the measurement of tracer concentration is due to stops of the fluorometer during equipment manipulations. Spike of tracer concentration during FVPDM no.1 is due to a technical problem but does not prevent the interpretation of the test. The id of the FVPDM and PDM successive experiment are named at the bottom of the figure.

3.2.3.1. Interpretation of a selected FVPDM and PDM experiment

Figure 41 shows the results for the FVPDM and PDM experiments no. 3 (FVPDM 3 and PDM 3, see Table 4 for experimental setup parameters) for a specific pumping rate (Q_{pump}) of 1.5×10^{-3} m³/s (90 L/min) in well B2. Figure 41a shows the FVPDM experimental and simulated curves, which present the typical evolution of the tracer concentration with a transient phase at the beginning of the experiment and a steady state at the end of the test when the system has reached equilibrium. Figure 41c is the RMS error plot between experimental data (FVPDM 3) and the simulated curves, obtained for different values of V_w and Q_t. The graph shows that a minimum RMS value is relatively well identified, corresponding to a unique (V_w, Q_t) pair that best fits the experimental data (Figure 41a). These values are V_w equal to 35.6 L and Q_t equal to 7.43×10^{-6} m³/s.

Figure 41b and d are similar but correspond to the PDM experiment no.3. The experimental curve (Figure 41b) shows the expected exponential decrease of the concentrations with time. However, with this method, it is rather difficult to adjust V_w and Q_t independently. A ratio Q_t/V_w of 2.12×10^{-4} s^{-1} can be fitted on experimental results and, theoretically, a large range of couples (V_w, Q_t) are possible. Accordingly, the RMS error obtained for

the adjustment of V_w and Q_t (Figure 41d) shows that a minimum RMS value can not be identified and that the solution is not unique. Consequently, the mixing volume has to be precisely known to constrain the PDM model and to estimate the transit flow rate correctly.

Note that the values in the RMS plots depend on the data and duration of the experiments, but the shape of these plots will generally remain similar for longer experimental time.

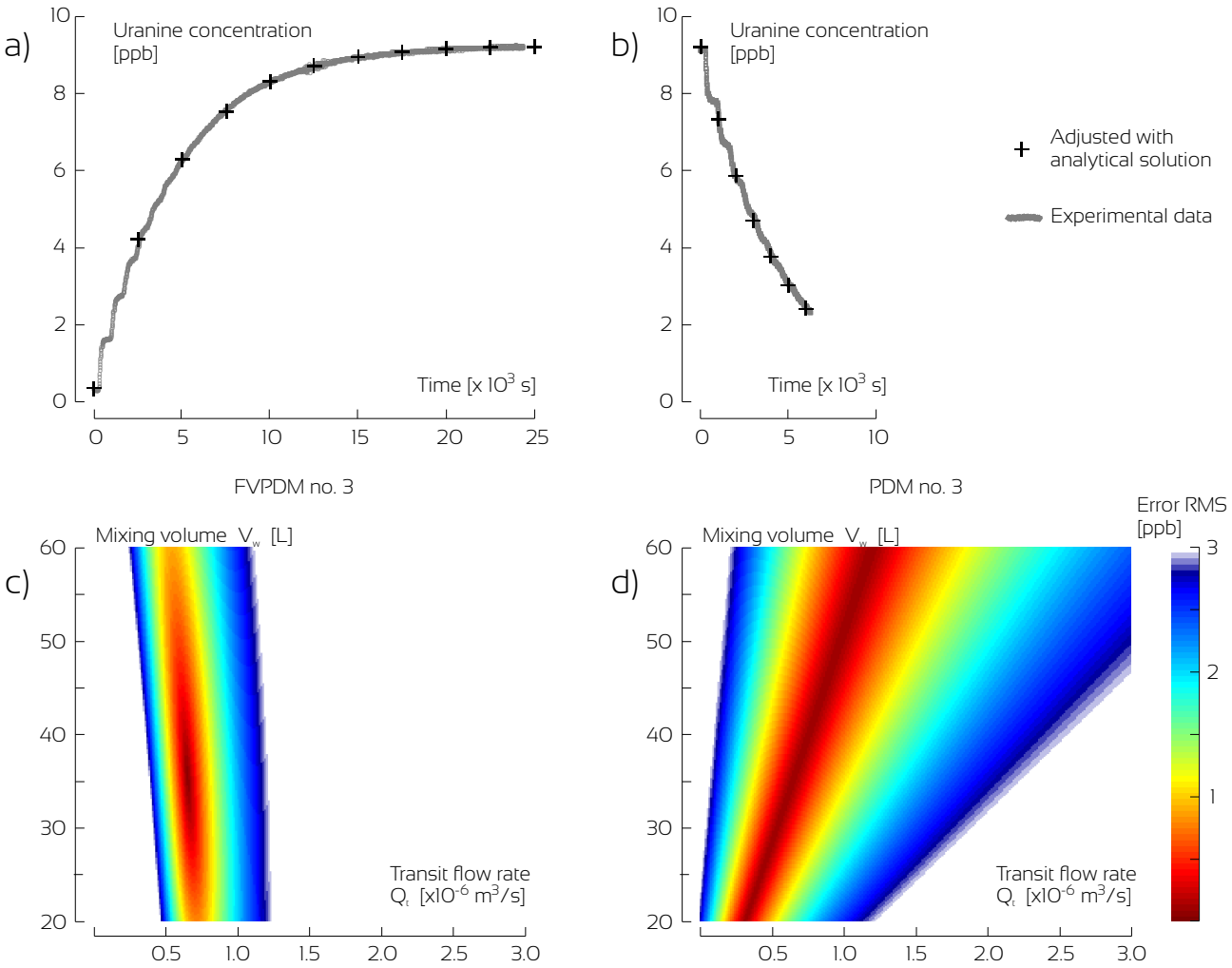

Figure 41 : Experimental data (grey points) and adjusted analytical solutions (black crosses) of FVPDM no.3 (a) and PDM no.3 (b) experiments corresponding to a pumping rate of 1.5×10^{-3} m³/s (90 L/min) in the B2 well. (c) and (d) are the RMS error plot for the FVPDM and PDM experiments for the adjustment of the mixing volume and the groundwater transit flow rate. A unique pair of Q_t/V_w value fits the FVPDM equation (V_w=35.6 L, Q_t =7.43×10^{-6} m³/s). On the contrary, a wide range of Q_t/V_w pairs that satisfies the PDM equation without being able to determine a most probable one ($Q_t/V_w=2.12\times10^{-4}$ s^{-1}). Note the oscillations of tracer concentration in the well (sequential plateaus) at the beginning of FVPDM and PDM experiment.

3.2.3.2. External estimations of Vw for PDM interpretation

Estimating the actual mixing volume based on the characteristics of the experimental setup is difficult, mainly because of the geometry of the well, the use of the double packer system, the presence of equipment in the test chamber, and the use of circulation loop. It has been estimated to approximately 29 L, but the uncertainty on this value is unknown because the estimation was only based on the length and radius of the circulation pipes and on the dimension of the test chamber (radius of the well and distance between upper and lower packer when they are inflated) without taking into account the various equipment present within this delineated space. In this study, the actual mixing volume has been estimated using an alternative method based on an experimental artifact. At Figure 41, PDM and FVPDM curves show oscillations (sequential plateaus) at the beginning of the experiment that attenuate with time. This artifact is due to a non-instantaneous mixing of tracer in the whole recirculated water volume. At the beginning or stopping of the tracer injection, a front of high or low concentration develops when the tracer injection is started or stopped. The mean wavelength of these oscillations has been estimated using Fourier transformations for all the dilution experiments and is equal to 762 s ±119 s (95% confidence interval). It actually corresponds to the time necessary for the water to travel the entire water circulation loop. Considering a circulation flow rate (Q_t) of 0.042 L/s, V_w equals 32±5 L.

Using this value, the transit flow Q_t rate can be calculated from PDM experiments. For PDM no.3 experiment, it is equal to 6.82×10^{-6} m³/s. Both values for V_w (32 L) and Q_t (6.82×10^{-6} m³/s) agree with FVPDM estimates (V_w = 35.6 L and Q_t = 7.43×10^{-6} m³/s) within 10% of error.

3.2.3.3. Evaluation of uncertainties on the adjustment of Vw and Qt for a selected FVPDM and PDM test

Both FVPDM and PDM can be used to estimate groundwater fluxes within the B1-4 fracture zone. However, the two methods are different and the confidence to be attributed to the results has to be determined. The uncertainties on calculated fluxes are related to the adjustment of the analytical solutions on experimental data and to the confidence on the V_w value, in the case of the PDM. The analysis of uncertainties is based on the exploration of Q_t and V_w values between specified intervals, using Equation 6 and Equation 13. The RMS errors between the experimental and simulated C_w values have been converted into probabilities according to Equation 22.

The probabilities are calculated for the FVPDM and PDM experiments no.3. They are multiplied with the normal distribution related to the estimation of V_w, equal to 32 L ± 5 L, to draw the probability plots presented in Figure 42. These plots are further used to calculate the most probable value for V_w and Q_t and the 95% confidence intervals (Table 5), for both PDM and FVPDM. Considering the results related to the experiments no.3, the 95% confidence interval on the calculated transit flow rate is more than five times smaller for the FVPDM than for the

PDM. These methodology and results are also dependent on the respective durations of the experiments, which are not equivalent in this case. To conclude about the general performances of both methods, the issues related to the duration of the different experiments are further discussed in the next section.

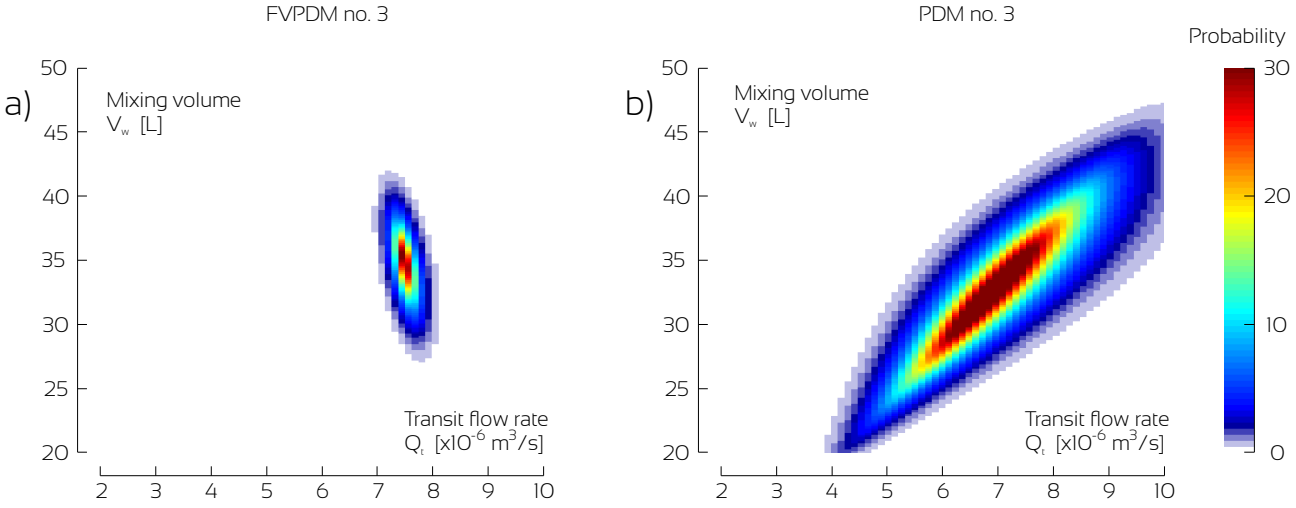

Figure 42: Adjustment of V_w and Q_t for the experiments n°3 (with pumping at 1.5×10^{-3} m^3/h in B2) considering an a priori known V_w of 32±5 L.

Table 5: Results of the adjustment of the parameters Q_t and V_w considering a probability density function on V_w of 32± 5 L for PDM and FVPDM experiment no.3.

	Q_t [×10^{-6} m^3/s]				V_w [L]			
	Adjusted	P05	P95	P95-P05	Adjusted	P05	P95	P95-P05
FVPDM 3	7.55	7.19	7.89	0.70	34.0	29.2	38.0	8.8
PDM 3	6.82	5.11	9.12	4.01	32.2	25.3	41.2	15.9

3.2.3.4. Influence of the duration of the experiment

The accuracy of the adjusted values for the PDM and FVPDM increases with the duration of the experiment. Concerning the FVPDM, this accuracy reaches a maximum value when the tracer concentration has stabilized in the injection well (Equation 14). The time to reach this steady state increases as the mixing volume increases and the transit flow rate decreases. To compare the FVPDM and PDM including the 'time' issue, uncertainties on the adjusted Q_t are investigated as a function of a normalized experiment duration. A normalized time t^* independent of V_w and Q_t is used and is obtained by dividing the mixing volume V_w by the critical injection flow rate Q_{cr} (Equation 23).

$$t^* = \frac{V_w}{Q_{cr}} = \frac{V_w}{\pi\, Q_t} \qquad \text{Equation 23}$$

The uncertainty around Q_t has been calculated for the FVPDM and PDM experiments no.3, but by artificially considering on specific fractions of the available experimental data, corresponding to specific numbers of t^* (Figure 43). Considering Equation 15, the critical time t_c, necessary to reach 99% of the steady state concentration, is reached after 13.9 t^*. If Q_{in} is small enough and neglected in comparison to Q_t, this critical time tends to 14.5 t^*. This is in accordance with the results shown in Figure 43. The total duration of the FVPDM no.3 is 16.8 t^*. The corresponding non dimensional time for the PDM no.3 allowed only a duration of 4.5t^*.

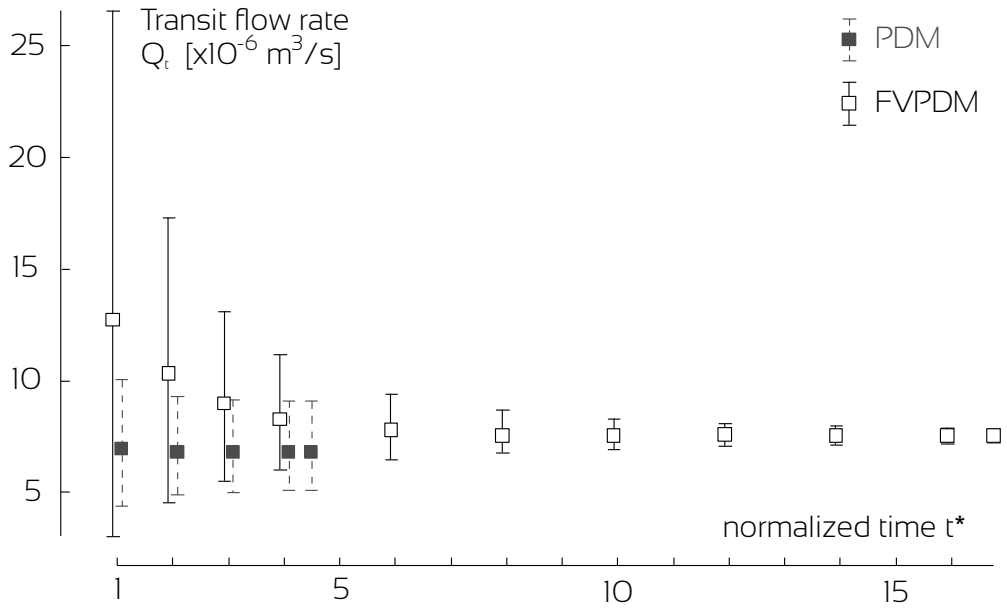

Figure 43: Evolution of the calculated Q_t and the 95% confidence intervals, as a function of the duration of the experiment for FVPDM no.3 (hollow circles) and PDM no.3 (grey squares) (pumping rate of 1.5×10^{-3} m^3/s in B2). t^* corresponds to a normalized time allowing the comparison between dilution experiments with different transit flow rates.

The uncertainty (P05-P95) around the calculated transit flow rate Q_t decreases significantly with time for the FVDPM. The FVPDM is less precise for the determination of Q_t for short experiment durations (t lower that approximately 4 t^* or 0.29 t_c) and clearly overestimates the value of Q_t. In this field campaign, this is partly explained by the non-uniform mixing of tracer in the circulated volume, which disturbed the increase of tracer concentration at the beginning of the experiment. It also comes from the time required for a good estimate. But for long

experiment, the accuracy of measurements becomes very good, with an uncertainty less than 10% of Q_t, for duration higher than 10 t^* or 0.72 t_c. Concerning the classical PDM, the uncertainty also decreases with time due to the attenuation of oscillations in tracer concentration at the beginning of the dilution and but seems to stay relatively high, around 25% of Q_t. But this uncertainty is only dependent on the precision of the externally estimated V_w (see previous sections). Although the uncertainty is relatively high, the mean estimates are acceptable for all times including short times.

Whatever the duration of the PDM test, a complete FVPDM (*i.e.* a FVPDM that reaches the steady state) is more precise. The 'threshold time', when the FVPDM becomes more precise than the PDM is in this case equal to 0.29 t_c, but it depends on the precision of the externally estimated V_w used in the PDM experiments, and increases as V_w is more accurately estimated.

3.2.3.5. Comparison of results for different fracture flow rates

All the dilution experiments have been interpreted separately, considering an a priori estimated mixing volume of 32±5 liters and an unknown transit flow rate. Results are presented in Table 6 and in Figure 44. The critical time t_c corresponds to the time necessary to reach 99% of the FVPDM steady state tracer concentration. It is estimated from Equation 13 considering that the initial tracer concentration is zero. This critical time can be compared to the actual duration of each experiment to estimate if steady state has been reached.

The relationship between the transit flow rate in the fracture B1-4 determined by both FVPDM and PDM and the pumping rate applied in B2 (Figure 44) appears to be linear. A slight deviation may be observed for the highest pumping rates, but this is difficult to confirm, given the calculated uncertainties (see discussion below). However, the relationship between the drawdown and the pumping rate in B2 (data Table 6) also presents a slight deviation from the linear behavior, suggesting that flow in the system may not be fully Darcyan.

The adjusted transit flow rates for all the dilution experiments are always higher for the FVPDM (hollow circles) than for the PDM (grey squares), but the confidence intervals are intersecting. Concerning the PDM, the information on the mixing volume is only provided externally (in this case, thanks to the oscillations artifacts), and it impacts the estimation of the transit flow rate. The bias between FVPDM and PDM results (Figure 44 and Table 6) can be explained by underestimation of this mixing volume. This volume was estimated to 29 L based on geometric characteristics, to 32±5 L based the oscillations in the experimental curves, and a bit higher for the most accurate FVPDM experiments (FVPDM 3 and FVPDM 9 in Table 6). If the PDM is interpreted using a higher value for V_w, as suggested by the most accurate FVPDM tests, the adjusted Q_t converge for the FVPDM and PDM tests. This is indeed logical since the PDM is only the last part of a full FVPDM experiment. This also illustrates the need for precise external estimation of V_w, if using PDM experiments only. This level of precision is however not always possible.

Table 6: Result of the dilution experiments carried out on B1-4. Uncertainties on V_w and Q_t correspond to the calculated confidence interval at 95%. t_c is the critical time necessary to reach 99% of the steady state concentration (not interpretable).*

	Data					Results		
Id	Duration [h]	Q_{pump} in B2 [$\times 10^{-3}$ m^3/s]	Drawdown B2 [m]	Drawdown B1 [m]	Duration/t_c [-]	Q_t [$\times 10^{-6}$ m^3/s]	V_w [L]	q_D [$\times 10^{-3}$ m/s]
FVPDM 1	4.02	2.39	1.89	0.88	1.35	13.80±1.21	32.9±5.5	38.33±3.36
PDM 1	0.88	2.39	1.89	0.88		10.69±3.66	32.5±7.9	29.69±10.17
FVPDM 2	2.35	1.86	1.30	0.60	0.64	11.6±1.80	34.5±6.5	32.22±5
PDM 2	2.28	1.86	1.30	0.60		8.56±2.63	32.4±7.9	23.78±7.31
FVPDM 3	6.7	1.46	0.98	0.44	1.22	7.55±0.35	34.0±4.4	20.97±0.97
PDM 3	1.67	1.46	0.98	0.44		6.82±2.00	32.2±7.9	18.94±5.56
FVPDM 4	3.39	1.00	0.62	0.31	0.48	4.83±0.83	28.8±5.4	13.42±2.31
PDM 5	2.24	1.00	0.68	0.37		4.25±1.16	32.4±7.9	11.81±3.22
FVPDM 6	3.15	1.00	0.68	0.37	0.43	4.60±0.23	28.2±6.4	12.78±0.64
FVPDM 7	8.67	0.63	0.36	0.17	0.67	2.78±0.08	31.7±4.4	7.72±0.22
PDM 7	2.45	0.63	0.41	0.21		2.33±0.66	32.5±7.9	6.47±1.83
FVPDM 10	8.72	0.62	0.38	0.17	0.64	2.93±0.17	34.8±6.0	8.14±0.47
FVPDM 9	28.01	0.31	0.13	0.03	1.09	1.32±0.04	33.5±2.5	3.67±0.11
PDM 8	2.1	0.29	0.17	0.06		1.20±0.32	32.7±7.9	3.33±0.89
FVPDM 5	2.83	0	0.04	0.02	0.03	*	27.0	*
PDM 4	1.88	0	0.04	0.02		0.22±0.09	32.5±10.2	0.61±0.25
FVPDM 8	7.84	0	0.06	0.02	0.07	*	32.0	*
PDM 6	5.93	0	0.06	0.02		0.07±0.02	32.7±7.9	0.19±0.06

The FVPDM generally presents a better precision with smaller confidence intervals, which increase with the calculated transit flow rate and pumping flow rate in well B2 (Figure 44). The differences are due to a higher sensitivity of the FVPDM to the experimental data, and because the FVPDM is also able to provide an independent information on both transit flow rate and mixing volume. In this case, the results of Table 6 show that the adjusted V_w varies for the different FVPDM experiments. These variations of adjusted V_w can be due to the oscillations of tracer concentrations that disturb the rising part of the FVPDM curve and observation errors. This is precisely the part of the curve which is used to adjust the value of the mixing volume. This is particularly the case when the duration of the FVPDM experiment that has not last enough to reach the steady state and therefore limit the precision of the adjustments of V_w and Q_t, as explained in previous sections.

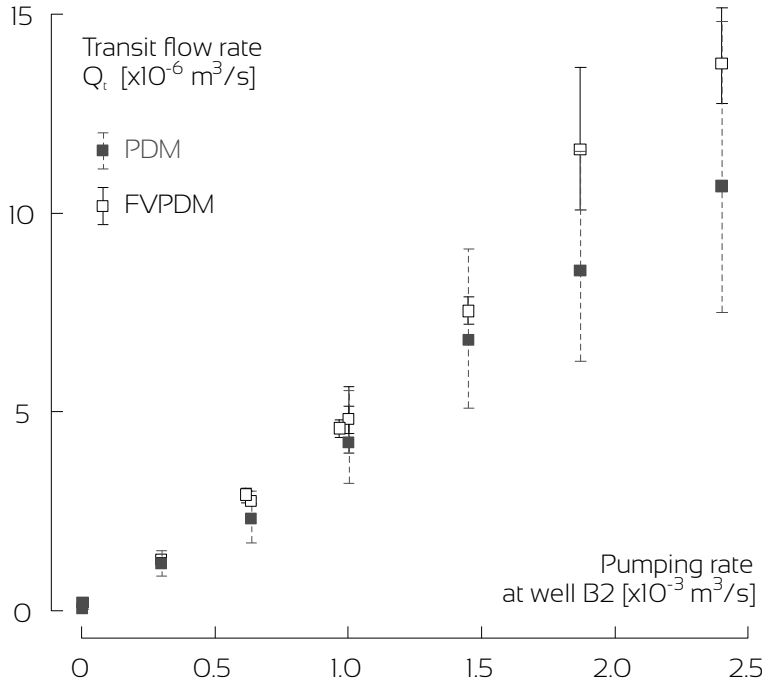

Figure 44: A linear relation is observed between the pumping rate applied in the well B2 and the groundwater flow rate observed in the fracture B1-4. The transit flow rate (Q_t) adjusted for all the dilution experiments are always higher for the FVPDM (hollow circles) than for the PDM (grey squares) due to difference of adjusted V_w and 95% confidence intervals are always shorter for FVPDM than PDM.

The transit flow rate estimated for the FVPDM no. 2 carried out with a pumping rate of 1.86×10^{-3} m³/s at well B2 presents a more important uncertainty and appears to deviate, compared to the other FVPDM experiments. This can be explained by a short experiment duration (Table 6) of only 0.64 t_c, leading to more uncertainty and potential errors. Note that the results of FVPDM no. 1 are also affected by some 'noise' in the experimental data (see Figure 40), due to a technical problem, leading to more uncertainty.

No transit flow rate could be calculated for the FVPDM no.5 and no.8 performed with no pumping at the well B2 (*i.e.* under natural ambient groundwater flow in the aquifer). Under these slow groundwater flow conditions, the critical flow rate determined by the PDM no. 4 and 6 is around 2×10^{-7} m³/s. The injection of tracer at a rate of 3.5×10^{-7} m³/s (the lowest that can be achieved with the available equipment) exceeds thus the critical injection rate Q_{cr} making the experiment invalid as explained in section 2.2. With the available tracer injection pump and an injection flow rate Q_{in} of 6×10^{-8} m³/s, t_c would have been around 10 days.

3.2.4. Discussion

A comparison of the present results with the experiments of Novakovski (2006) that performed PDM between packer shows that the FVPDM experimental setup used during this field campaign can investigate a range of Darcy fluxes transit flow rate higher than Novakowski's PDM. Nevertheless, the FVPDM offers a distinct estimation of V_w that is unavailable with the PDM. The measurement of fracture flow velocities of Novakowski ranges from 1.2×10^{-5} to 4.5×10^{-3} m/s, the present FVPDM performed at Ploemeur measured fractures flow from 3.1×10^{-3} to 3.8×10^{-2} m/s.

Considering these experimental data for dilution experiment no.3, the FVPDM becomes more precise than the PDM from a time corresponding to approximately 4 t^* or 0.29 t_c. This result is consistent with the initial recommendation of Brouyère et al (2008) that recommended an experiment duration of 5 to 7 times t^* to ensure reaching the steady state of the FVPDM. The same calculation has been carried out for all the dilution tests and shows identical trends with the precision on the adjusted Q_t increasing with time for FVPDM. This precision remains high for PDM, whatever the duration of the experiment, but mainly depends on the accuracy of the external estimation of V_w. As a conclusion, classical PDM seems to be a technique suitable for rapid results, including a large range of groundwater fluxes. However, this study has highlighted the crucial need for accuracy regarding the a priori knowledge of V_w when accuracy using PDM experiments. This accuracy actually directly affects the performance and possible bias of PDM results. At the contrary, the FVPDM is more precise, even without estimation of V_w, but may require long experiment durations under specific conditions. In case of very slow groundwater flow and large mixing volume, the time required to reach steady state may actually become very long and unmanageable. For example, if the transit flow rate Q_t is lower than 10^{-7} m³/s and the mixing volume is higher than 10 L simultaneously, the time to reach the critical time t_c (or 5 t^*) exceeds 48 hours. Furthermore, the estimation of the mixing volume V_w by the FVPDM is more robust than simply by using the geometry of the well. Vw determined by FVPDM is an apparent value that takes into account all the water that participates to the mixing of tracer. For example, it can integrate an unknown dead-end fracture that would not be considered with a classic PDM and bias the result of the transit flow rate.

Considering the results of Table 6, the ratio between the transit flow rate calculated with FVPDM and the pumping flow rate in B2, ranges between 170 and 230, approximately. If the fluxes are assumed uniformly distributed around B2, this ratio should be equal to 754. This last value is obtained by considering the following values. The distance between B1 and B2 is equal to 6 m. Calculated flow rates correspond to a 0.1 m section (the diameter of B1) of the circle intercepting B1, and having B2 as a center. Finally, only 50% the total pumping flow rate in B2 is coming from the B1-4 fracture. This was evidenced by Read et al. (2013) using heat tracer tests. The lower experimental ratio, compared to the theoretical ratio, highlights the fact that fluxes are more probably non-uniform within the fractures, for example with some possible channelization.

From a practical point of view, an improvement of the experimental setup could be to get rid of the circulation loop by placing all the surface equipment (tracer injection pump, fluorometer and mixing propeller) into the test chamber. In this case, the water present in the loop represents 25% of the total mixing volume. Such a reduction of V_w would significantly decrease the time to reach a steady state for the FVPDM and avoid the oscillatory effect of the circulation of tracer along the loop. The use of a dosing pump with smaller minimum tracer injection rate would also allowed for determination of smaller transit flow rate such as in natural flow conditions. Moreover, an inflatable double packer of this size (more than 4 meters) is not easy to use in the field and requires heavy equipment to be installed in the well. The development of a specific probe gathering all the required equipment into a compact size device will also improve the practicality of the method.

The FVPDM no. 4 and 5; 6, 7 and 8; and 9 and 10 were performed consecutively by maintaining the injection of tracer and changing the pumping rate at the nearby well. The changes in the groundwater flow velocity were recorded by those continuous FVPDM experiments. This highlights that the FVPDM is capable of monitoring temporal changes of groundwater flow. On the contrary, a variable groundwater flux precludes the interpretation of classical PDM because this method is based on the hypothesis that the groundwater flux is constant. Development of the FVPDM for long term monitoring of transient groundwater flow constitutes the most interesting perspective. For that, the experimental setup has to be optimized by reducing the tracer injection flow rate to avoid frequent refill of the tracer solution tank. And finally a mathematical model has to be developed to interpret the FVPDM experiment in case of transient groundwater flow.

3.2.5. Conclusions

The Finite Volume Point Dilution Method has been applied to measure groundwater fluxes within a local fracture zone of the crystalline aquifer of Ploemeur, France. This manipulation is the first successful application of the FVPDM technique in a fractured aquifer and using a double packer system. Experiments have been carried out for variable groundwater flow, induced by pumping in a well located close to the tested well. In total, 10 FVPDM and 8 classical PDM were performed to compare the two methods.

Measurements of groundwater fluxes by classical PDM provide good estimates, even for short times experiments, if V_w can be precisely estimated. With this method, the precision on the calculated groundwater flux fully depends on the precision of the estimation of the water circulation volume. On the contrary, the FVPDM allows for an independent estimation of both groundwater flow rate Qt and water mixing volume V_w. The best precision is obtained when steady state conditions are reached for tracer concentration in the tested well, which may require long experimental durations. Classical PDM seems to be more accurate than FVPDM for short experiments provided the mixing volume is precisely known. FVPDM generally provides a better precision but requires longer experiment durations. The 'threshold' after which FVPDM becomes more precise than PDM depends on the precision reached in the external estimation of the mixing volume.

The present experiments also highlight the ability of the FVPDM to continuously monitor continuous transient groundwater fluxes. Two short term perspectives could be (1) to develop a mathematical model to interpret a fully transient FVPDM test and (2) to follow a multiple stages pumping test performed at a well with FVPDM monitoring at some nearby piezometer to investigate the benefits of groundwater fluxes information in the interpretation of pumping tests.

In conclusion, both methods are complementary and can investigate the same range of groundwater fluxes. The classical PDM should be used for rapid estimation of steady state groundwater flux. The FVPDM is a more precise method but requires longer duration experiment to achieve a good precision if the investigated groundwater fluxes are low and/or if the mixing volume is large, and has a strong development potential for monitoring of transient groundwater fluxes.

3.3. Field monitoring of a controlled transient groundwater flux using the FVPDM

This section is based on the following publication:

Jamin, P., & Brouyère, S. (2018). Monitoring transient groundwater fluxes using the Finite Volume Point Dilution Method. Journal of Contaminant Hydrology, 218(July), 10–18. http://doi.org/10.1016/j.jconhyd.2018.07.005

3.3.1. Introduction

In many different hydrogeological contexts, groundwater flow is intrinsically transient and assuming steady state conditions may not be adequate. Such groundwater flow variations may be characterized by very different time scales, from short tidal or daily barometric to longer seasonal and annual variations (Dujardin et al. 2014, Battle-Aguilar et al. 2014, Ataie-Ashitani et al 2001, Chen and Pinder 2011, Post et al. 2018, Lubczynskia & Gurwinb 2005, Dentz & Carrera 2005, Yang et al. 2012, Kempf et al. 2013). Available methods described in the first section of this manuscript for the direct measurement of groundwater flow are not able to perform a comprehensive and continuous monitoring of these transient groundwater fluxes. In previous sections (3.2 and 3.1), we highlighted the sensitivity of the FVPDM technique to transient groundwater flow. In section 3.1, the sensitivity of the FVPDM to small and rapid changes in groundwater fluxes has been demonstrated but only on lab experiments. To fully validate the FVPDM as a powerful tool able to accurately and precisely monitor transient groundwater fluxes, a real scale field experiment is requested.

In this section, the methodology developed in section 2.4 is tested based on a field experiment under controlled conditions. The experiment consists of monitoring transient groundwater fluxes using FVPDM experiments performed in piezometers located near a pumping well, in which multiple steps pumping tests are performed to generate transient groundwater flow conditions in an alluvial aquifer. After providing a description of the methodology and experimental configuration, the groundwater flux monitoring results are discussed.

3.3.2. Hermalle-sous-Argenteau experimental test site

A detailed description of the experimental site can be found in Wildemeersch et al. (2014). The site is in the village of Hermalle-sous-Argenteau, which is 13 km northeast of the city of Liège in Belgium. The topography of the site is a vast meadow, which lies upon the Meuse River alluvial plain and is nearly flat. The alluvial deposits can be described as follows (Figure 45). The upper soil layer consists of 1 to 1.5 m of loam with clay lenses. The second layer consists of sandy loam with millimetric gravels, which proportionally increase to a depth of 3 m. From 3 to 10 m below ground surface, the third layer mainly consists of alluvial sand and gravels. The gravel to sand ratio increases progressively with depth and reaches a zone of clean pebbles, which are frequently more than 20 cm in diameter and located at the bottom of the alluvial aquifer. This causes a vertical heterogeneity of the alluvial

sediments and related hydraulic properties of the presumably assumed homogenous alluvial aquifer. Below the alluvial deposits, low permeability carboniferous shale and sandstone formations constitute the basement of the alluvial aquifer.

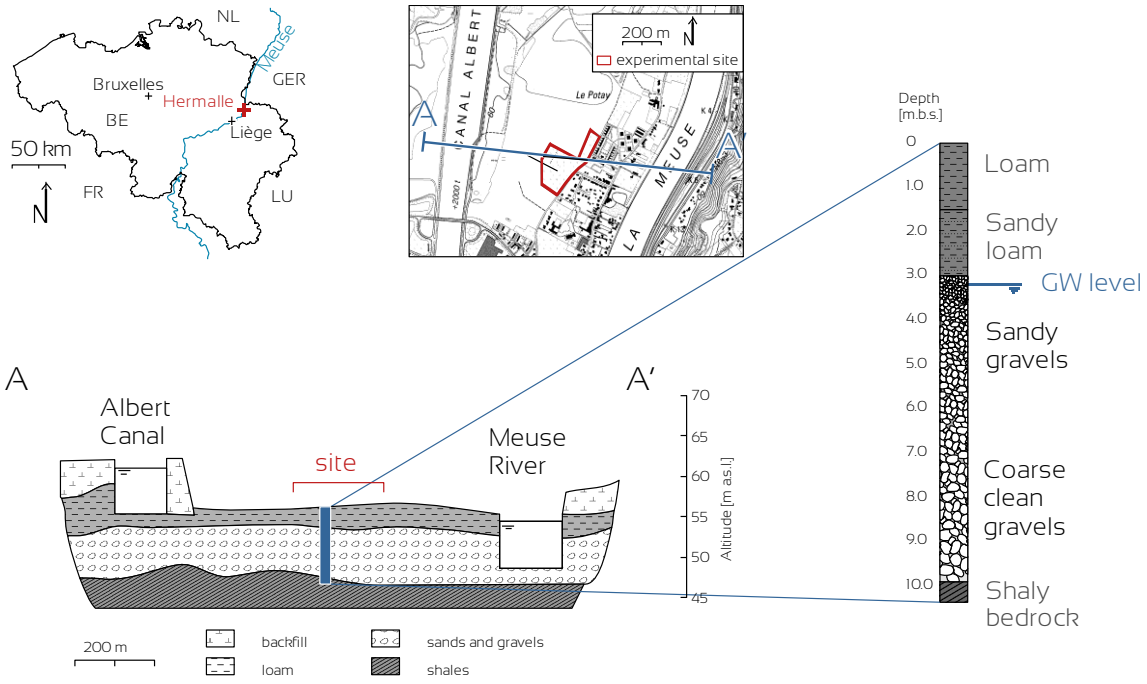

Figure 45: The test site is located on the alluvial plain of the River Meuse, which is 13 km northeast of Liège, Belgium in Western Europe. The aquifer is composed of sandy gravels that becomes coarser to the base. Hydraulic conductivity is approximately 5×10^{-2} m/s (Brouyère, 2001).

The test site is located between the Albert Canal and Meuse River, which controls the piezometric levels in the alluvial aquifer. The groundwater table is located approximately 3.2 m below ground surface and the piezometric gradient in the alluvial aquifer is on the order of 0.6% and directed northeast toward the Meuse River. The site is equipped with one large diameter pumping well, 9 single screened piezometers and 9 double-screened piezometers (including Pz19, which was used afterwards for the FVPDM experiments) (Figure 46). Pumping tests and tracer tests performed at the site (Brouyère, 2001) allowed for estimating the mean hydraulic conductivity values ranging from 2×10^{-2} to 7×10^{-2} m/s, longitudinal dispersivity values ranging from 0.4 to 5 m and effective transport porosity values from 3.7 to 8.5% in the alluvial aquifer. Using Darcy's law with these values of hydraulic gradient and K values, ambient Darcy fluxes in this alluvial aquifer can be estimated in a range between 40 m/d and 800 m/d. Such high values can be explained by the very high hydraulic conductivity of the lower part of the alluvial aquifer constituted by clean large pebbles and by the high hydraulic gradient prescribed by the Canal and

the River. Groundwater modeling of this alluvial aquifer was carried out by Brouyère (2001) and by Klepikova et al. (2016) and support these values.

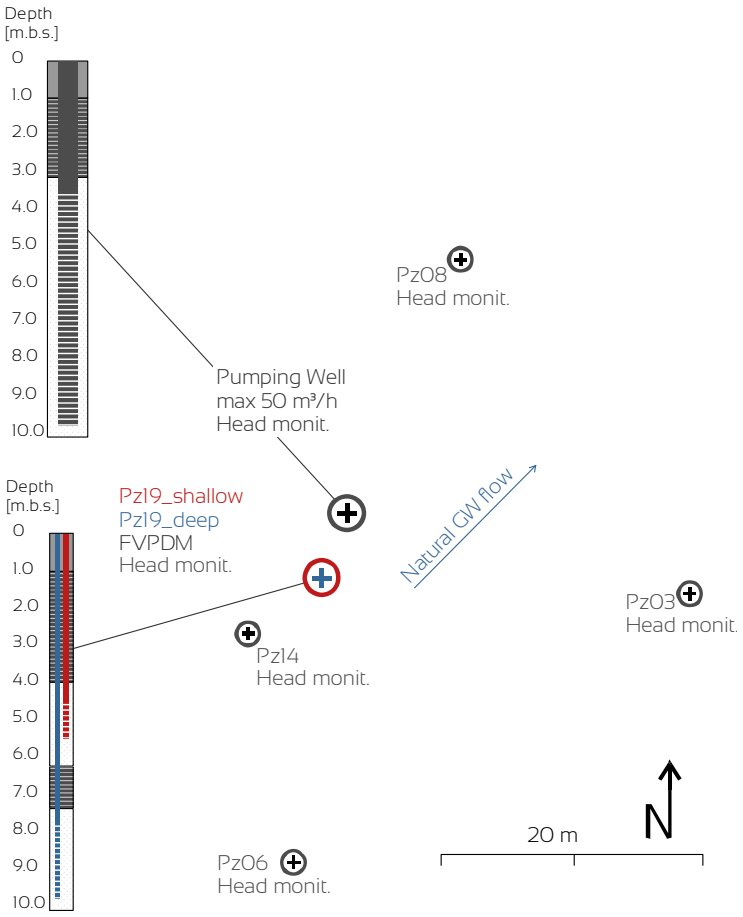

Figure 46: The experimental configuration consists of a typical pumping test arrangement with piezometric head monitoring at 6 piezometers around the pumping well. The originality of the experiment involved performing the FVPDM continuously during the whole pumping test at two piezometers, which were located 5 m up gradient from the pumping well. These two piezometers are either screened in the upper, finer part of the aquifer or in the lower, coarser part of the aquifer.

The existence of a well or piezometer induces a local distortion of the groundwater flow field (Drost et al. 1968, Verreydt et al. 2015). The difference between the effective groundwater flux occurring in the aquifer and the apparent water flux measured in the tested well is taken into account through the flow distortion or convergence/divergence factor (a_w) which characterizes the degree of convergence or divergence of groundwater flow in the vicinity of the monitoring well. In this section, the presented groundwater fluxes resulting from the FVPDM experiment are apparent Darcy fluxes and are not corrected using the convergence/divergence factor.

For a piezometer of the present experimental test site, the convergence/divergence factor was calculated using Equation 8. The properties of the monitoring wells of the Hermalle-sous-Argenteau test site are given in Table 7. The hydraulic properties of the gravel filter pack and of the well screen were provided by the manufacturer. Using these properties in Equation 8 give a convergence factor of 2.87.

Table 7: Geometric and hydraulic parameters of the tested well Pz19 used to calculate the flow distortion coefficient (α_w) of 2.87.

Radius of the borehole	r_B	0.09	m
Inner radius of the well screen	r_I	0.025	m
Outer radius of the well screen	r_O	0.03	m
Hydraulic conductivity of the aquifer	K	3.26×10^{-2}	m/s
Hydraulic conductivity of the filter	k_F	3.97×10^{-1}	m/s
Hydraulic conductivity of the well	k_S	2.90×10^{-1}	m/s

3.3.3. Experimental methodology and technical setup

Variable groundwater flow conditions were produced in the alluvial aquifer by pumping at different rates in the pumping well (Figure 46). Two FVPDM experiments were performed simultaneously in piezometer Pz19_shallow and Pz19_deep. Piezometer Pz19 is to be equipped with two internal tubes inserted in the same borehole: one with a 1 m screen in the upper part of the aquifer where sediments are finer, and one with a 2 m screen in the lower, coarser part of the aquifer. Pz19 is located 5 meters upgradient from the pumping well (6 inches internal diameter), which is where a submersible pump (50 m³/h of maximum flow rate) and AquaTROLL level logger are installed. Schlumberger Diver and AquaTROLL level pressiometric loggers were also installed in 6 piezometers (2 inches inner diameter): Pz03, Pz06, Pz08, Pz14, Pz19_shallow and Pz19_deep, which are 27, 46, 52, 12 and 5 m distance from the pumping well, respectively.

The two FVPDM tests lasted for 3 days continuously. In both cases, the FVPDM experimental configuration is as follows. A Grundfos MP1 pump is placed at the bottom of the piezometer and connected to the surface with a circulation loop made of 10/13 mm of nylon tubing. At the land surface, the circulation loop is connected to a GGUN FL30 fluorometer, which is placed in line to monitor the tracer concentration (C_w) evolution in the tested piezometer. A Jesco Magdos electromagnetic dosing pump is also connected to the loop to inject the tracer solution. Uranine (CAS n° 518-47-8) and Sulforhodamine B (CAS n° 3520-42-1) are used as the fluorescent tracers. Finally, the circulation loop in the piezometer returns down to the groundwater table to simultaneously ensure constant mixing and homogenous concentration of the water volume (V_w) in the well bore.

The experimental parameters and hydraulic properties used for dimensioning the FVPDM experiments according to the flow chart presented in Figure 30 are summarized at Table 8 and Figure 47. Previous classical hydrogeological investigations allowed to measure a minimum hydraulic conductivity of the tested alluvial aquifer (K_{est}^{min}) on the order of 2×10^{-2} m/s and a minimum hydraulic gradient (i_{min}) of 0.5%. According to the well characteristics, the screen flowing section (S_w) is equal to 0.091 m²is which gives an a priori minimum transit flow rate ($Q_{t,\ prior}^{min}$) of 9.2×10^{-6} m³/s (0.55 L/min). This is used to calculate a critical flow rate (Q_{cr}) of 2.9×10^{-5} m³/s (1.72 L/min) and a tracer injection flow rate (Q_{inj}) of 2.9×10^{-6} m³/s (0.17 L/min). The expected time of the experiment (T_{inj}) is here of 48 hours which leads to a total injection volume of tracer fluid (V_{inj}) of approximately 0.5 m³. The tracer solution concentration (C_{inj}) is defined to prevent the saturation of the signal of the field fluorometer (corresponding to a tracer concentration of 300 ppb) while remaining higher than the detection limit (10 ppb). The dilution of the tracer solution depends on the ratio Q_{inj} / $(Q_t + Q_{inj})$ ranging from 0.24 to 0.07 when considering respectively the minimum or maximum transit flow rate. Theoretically, the concentration of the injected tracer C_{inj} should be set between 144 and 1255 ppb to guarantee that the measured tracer concentration in the well C_w remains within the detection limits of the field fluorometer. The final dimensioning of both Pz19_shallow and Pz19_deep is presented in Table 9.

Table 8: Available experimental data of the tested well and known parameters of the alluvial aquifer used for the dimensioning of the FVPMD experiment on Pz19_deep.

Depth of water level	h_{piezo}	3	m
Depth of the tested well	W_{bottom}	10	m
Well radius	r_w	0.025	m
Screen length	e_{scr}	1.8	m
Volume of water in the tested well	V_w	0.014	m³
Surface of flow	S_w	0.091	m²
Temporal dynamic of the transient flow	T_{inj}	48	hours
Minimum hydraulic conductivity	K_{est}^{min}	2×10^{-2}	m/s
Minimum hydraulic gradient	dh/L^{min}	0.5	%
Maximum hydraulic conductivity	K_{est}^{min}	7×10^{-2}	m/s
Maximum hydraulic gradient	i_{min}	0.6	%
Tracer detector saturation limit	C_{SL}	300	ppb
Tracer detector detection limit	C_{DL}	10	ppb

Table 9: Parameters of the experimental configuration used for FVPDM test at piezometers Pz19_shallow and Pz19_deep.

	Q_{inj} [m³/s]	M_{inj} [g]	C_{inj} [ppb]	Tracer
Pz19_shallow	5.17×10^{-7}	0.089	500	Sulforhodamine B
Pz19_deep	3.23×10^{-6}	0.558	250	Uranine

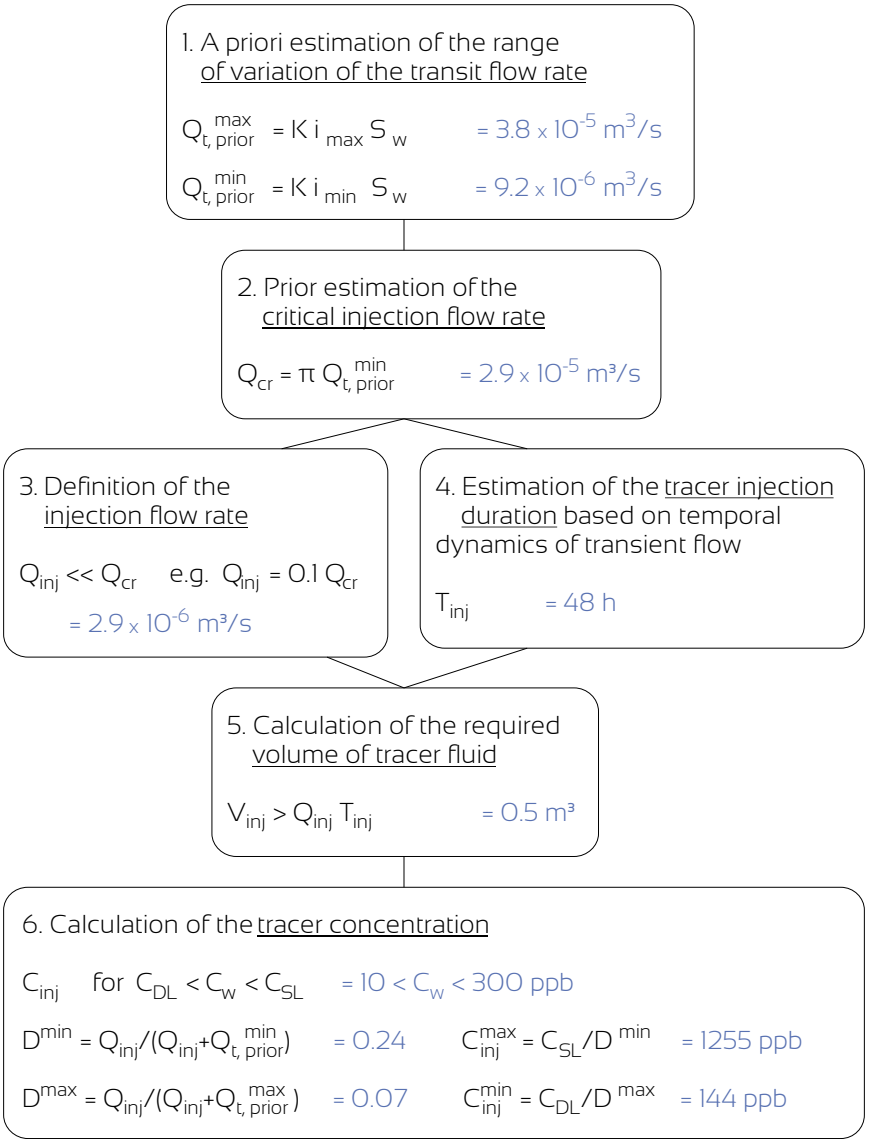

Figure 47: Flow chart of the dimensioning of the FVPDM experimental configuration for continuous monitoring of transient groundwater flux undertaken at piezometer Pz19_deep considering data summarized in Table 9.

The FVPDM monitoring experiment can be divided into 4 phases (Figure 48). The first, which corresponds to the first 12 hours of the experiment, is considered a "warm-up" phase, during which groundwater flow and the two FVPDM injections equilibrate with the pumping conditions generated in the aquifer. The resulting relatively stable tracer concentration reached at the end of this phase is used to calculate an initial groundwater flux value based on the steady state analytical solution from Brouyère et al. (2008). The next three phases (2, 3 and 4) are based on different transient pumping regimes, which are used to evaluate the ability of the transient FVPDM approach, as well as its sensitivity to changes in groundwater fluxes. Phase 2 consisted of 30 minutes of pumping steps with successive pumping rates of 50, 45, 40, 30, 20, 10, 30, 40, and 50 m^3/h. During phase 3, pumping steps were reduced to 5 minutes with a step-by-step 1.1 m^3/h incremental decrease in the pumping rate from 50 to 7.1 m^3/h. This third phase aimed at approaching fully transient groundwater flow conditions in the aquifer to evaluate the FVPDM sensitivity to small and rapid changes in groundwater flow. The fourth and final phase consisted of a multiple step pumping test application with 5 steps of 2 hours each, from 10 to 50 m^3/h and followed by a recovery period. The objective of this last phase was to compare the results and interpretation of this pumping test to the corresponding changes in piezometric head and groundwater fluxes.

3.3.4. Results and discussion

The FVPDM experimental results from Pz19_shallow and Pz19_deep, which were completed during the pumping test, are presented in Figure 6. During the first phase of the experiment, when the pumping rate is maintained at a stable 50 m^3/h at the pumping well (Figure 48a), the tracer concentrations in the two tested piezometers are constant (Figure 48b and d). In Pz19_shallow, the tracer concentration stabilizes 2 hours after beginning the tracer injection at a relative concentration C_w/C_{inj} of 0.12. In Pz19_deep, tracer concentration stabilization occurred more quickly, after less than 15 minutes at a relative concentration of 0.01. These observations (i.e., shorter time to reach a stabilized concentration and higher tracer dilution at Pz19_deep) reflect the occurrence of larger groundwater fluxes in the deeper part of the alluvial aquifer.

During the phases 2 through 4, the results clearly show that the FVPDM is sensitive to changes in groundwater fluxes. Each change in the pumping rate results in a tracer concentration change in the tested piezometers. When the pumping rate decreases, groundwater fluxes in the aquifer are reduced and tracer concentrations in the tested wells increase due to less dilution. Conversely, each increase in pumping rate induces a decrease in the tracer concentrations in the tested piezometers. When pumping rate variations of 10 m^3/h are commenced every 30 or 120 minutes, the monitored tracer concentration at Pz19_shallow does not stabilize between pumping steps. At Pz19_deep, stabilization of the tracer concentration is reached faster because of larger groundwater flux occurrences in the deeper part of the alluvial aquifer. During phase 3, when the pumping rate decreases 1.1 m^3/h every 5 minutes, the two tested piezometers react progressively without showing any tracer concentration stabilization. Then, groundwater fluxes in the alluvial aquifer can be considered as fully transient.

This statement is supported by the monitored piezometric head at the Pz19_deep and Pz19_shallow showing that changes in drawdown takes more than 15 minutes to stabilize to any change of pumping rate (Figure 49).

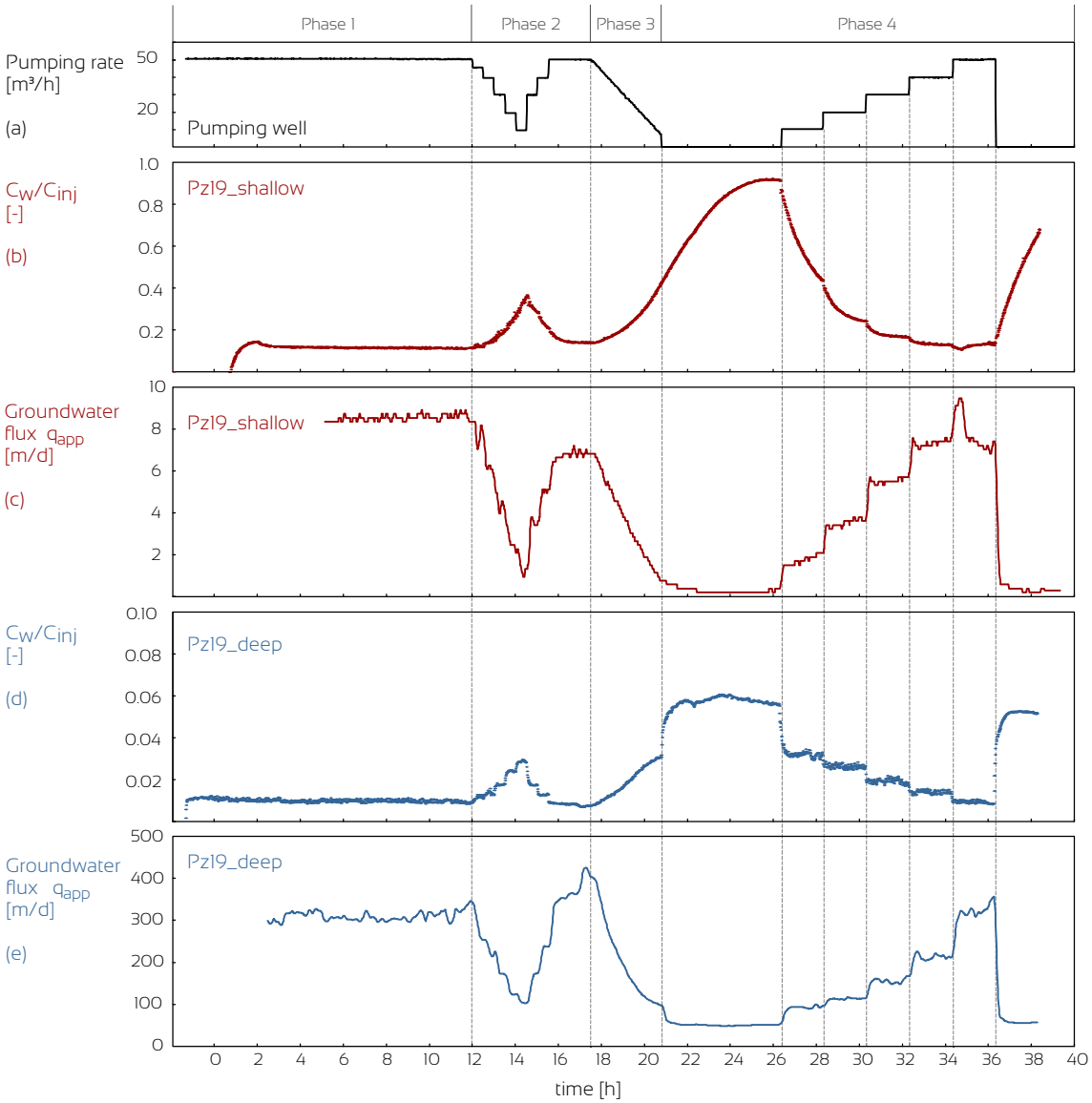

Figure 48: Graph (a) shows the pumping rate schema applied at the well. Graphs (b) and (c) respectively represent the tracer concentration evolution, and the interpretation of the FVPDM into Darcy fluxes for piezometer Pz19_shallow. Graphs (d) and (e) show tracer concentration and groundwater flux for Pz19_deep. These interpretations show that the groundwater flux is higher in the lower part of the aquifer and that the FVPDM can monitor changes in groundwater fluxes. Please note that the maximum ordinate scales for Pz19_shallow and Pz19_deep differs of one order of magnitude for the relative concentration and is 50 times higher for the interpreted groundwater flux.

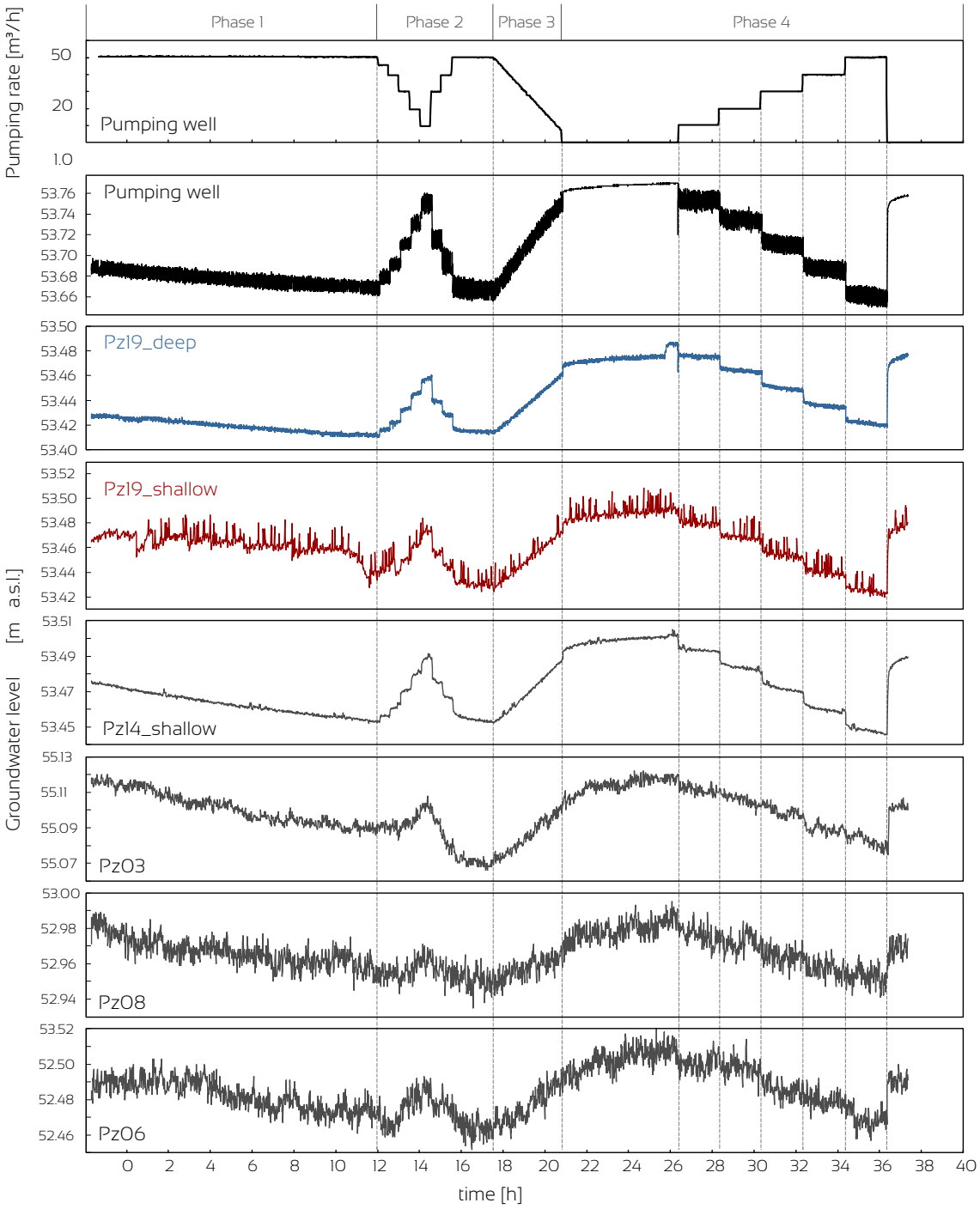

Figure 49: Monitoring of the groundwater levels at Pumping Well, Pz19_deep, Pz19_shallow, Pz14_shallow, Pz03, Pz08 and Pz06 during the whole time of the pumping test and FVPDM experiments.

The FVPDM experimental interpretations in terms of groundwater fluxes was performed using Equation 20 (Figure 48c and e). Darcy fluxes calculated with Equation 20 can also be compared with manual adjustments of the analytical steady state solution (Equation 13) during specific experimental periods, when the groundwater flows are considered steady state. During step 1 and step 4, the pumping steps were long enough to reach tracer concentration stabilization. Groundwater fluxes calculated by the steady state analytical solution and by the finite difference transient solution are in excellent agreement (Figure 50). This confirms that Equation 20 is an accurate approximation that can be used for the interpretation of FVPDM experiments.

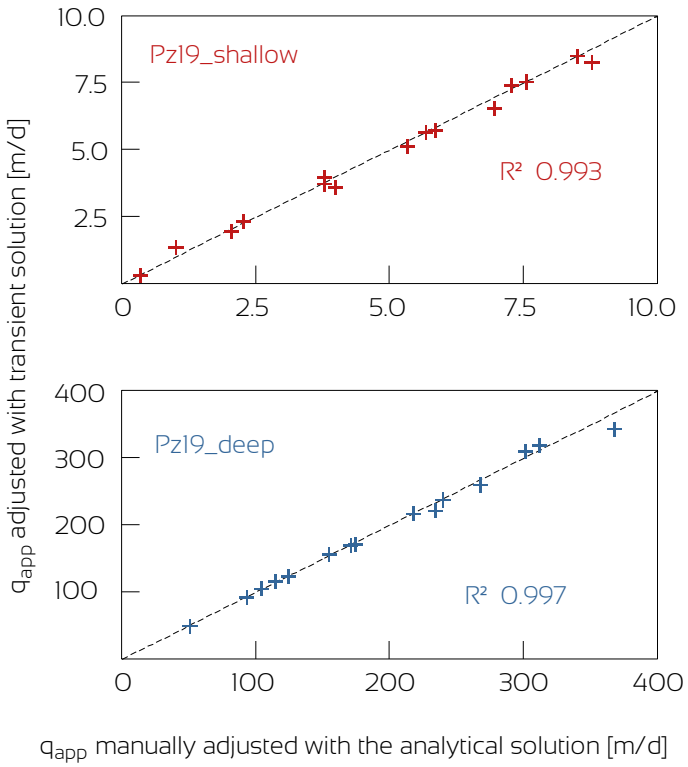

Figure 50: The groundwater fluxes calculated with the new transient solution agree well with the values that have been manually adjusted on the same experimental result using the Brouyère et al. *(2008) analytical solution.*

During the first phase of the experiment, when groundwater flows are assumed to be steady state, oscillations in the calculated groundwater fluxes are observed. These oscillations are due to noise in the concentration data measured by the field fluorometer. In piezometer Pz19_shallow, calculated apparent groundwater fluxes vary between 0.35 m/d when no pumping is applied and 9.64 m/d when pumping at 50 m³/h. In piezometer Pz19_deep, apparent groundwater fluxes are higher, ranging between 52 m/d when no pumping is applied and 321 m/d when pumping at 50 m³/h. During phase 3, apparent transient groundwater fluxes vary approximately 0.15 m/d at Pz19_shallow and 10 m/d at Pz19_deep for each decrease of 1.1 m³/h in the pumping rate.

The phase 4 multiple step pumping test results are presented in Figure 51, which shows the drawdown measured at the pumping well and monitored piezometers. Each 10 m³/h increase in pumping rate leads to an additional stabilized drawdown of 2 cm at the pumping well and a maximum measured drawdown of 0.11 m at 50 m³/h. Noise in the recorded groundwater levels is due to submersible pump turbulence in the well. In piezometers Pz19_shallow and Pz19_deep, the monitored drawdown curves are nearly identical with a maximal cumulative drawdown of 7 cm observed at 50 m³/h and stabilized additive drawdowns of 1.4 cm for each 10 m³/h increase in the pumping rate. Observing similar drawdowns in both piezometer is obvious because they are collocated and screened at two different depths of the same aquifer. The pumping test interpretation using the Dupuit method (1863) and measured drawdown at all 6 monitored piezometers gives a mean hydraulic conductivity of 3.26×10^{-2} m/s (Figure 52). This similar behavior in the two piezometers, which are screened at different depths in the same aquifer, suggests an identical hydraulic response to pumping in both the upper and lower parts of the aquifer. Nevertheless, the FVPDM measurements indicate that groundwater fluxes are stronger in the lower part than in the upper part of the aquifer, with a difference of almost 2 orders of magnitude (Figure 48). This indicates that the FVPDM technique allows for a more precise characterization of groundwater flux variability compared to the pumping test, which only provides a mean estimate.

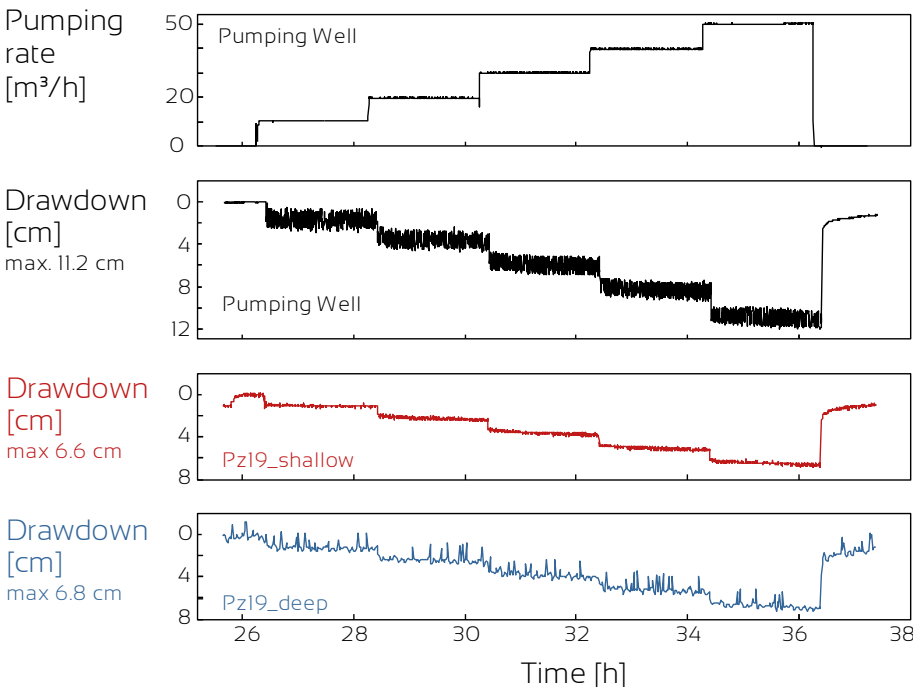

Figure 51: The drawdown measured at the two Pz19 piezometers, up and low, are identical suggesting an identical reaction of the upper and lower zones of the aquifer to pumping. The interpretation of this pumping test using the Dupuit method gives a hydraulic conductivity of 3.26×10^{-2} m/s.

The pumping steps applied between 25 and 38 hours into the test can be interpreted like a conventional pumping test to estimate the hydraulic conductivity near the pumping well. The piezometric drawdown has been recorded at 5 piezometers located around the well. For each pumping rate the drawdowns at the piezometers are plotted as a function of their distance to the pumping well as recommended by the Dupuit method (Dupuit 1863). The fact that the calculated values of H^2-h^2 (at the pumping well and at the different monitored piezometers) align perfectly indicates that the Dupuit hypothesis are respected and so justifies the use of the Dupuit method. The hydraulic conductivity is calculated from the slope of the linear regression adjusted for each pumping rate. The mean hydraulic conductivity for the tested alluvial aquifer is 0.0326 m/s.

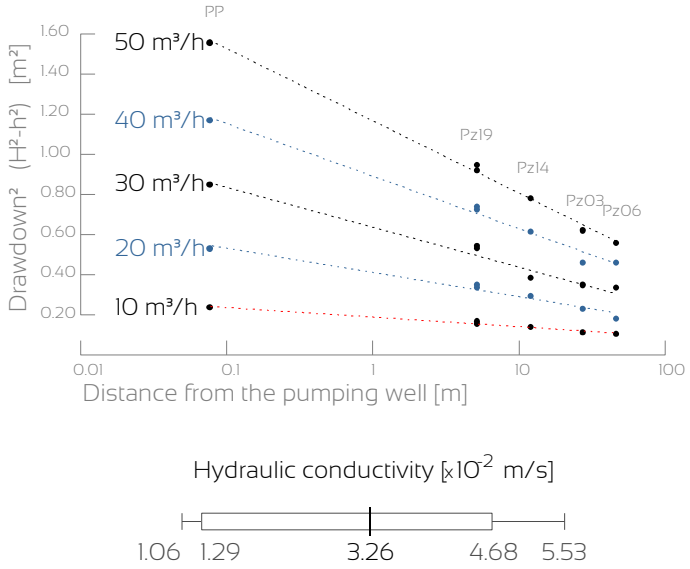

Figure 52: Interpretation of the pumping test using the Dupuis method. The mean hydraulic conductivity is 0.0326 m/s.

In addition, measured groundwater fluxes in Pz19_shallow show a linear increase with an increased pumping rate, and each 10 m³/h increment at the pumping well corresponds to an increment of 1.9 m/d in the measured apparent groundwater flux. At Pz19_deep, measured apparent groundwater fluxes do not vary linearly with an increased pumping rate, but rather, the fluxes follow an exponential increase (Figure 53). The probable explanation is related to the ratio between the groundwater transit flow rate that passes through the well screen and the mixing flow rate used to homogenize the tracer mass on the water column and circulate the water up to the surface to measure the tracer concentration. When pumping at 50 m³/h at the pumping well, the groundwater transit flow rate in Pz19_deep is 27 L/min. The maximum mixing flow rate achieved with the mixing pump is 12 L/min. Consequently, a significant amount of tracer is carried out of the well before reaching the bottom of the well where the mixing pump circulates it to the surface to be measured by the detector. This results in an underestimated tracer concentration and thus an overestimated groundwater flux. For each increase of the pumping rate at the pumping well, the groundwater flux in the aquifer increases and the overestimation of this groundwater flux increases likewise, amplifying the groundwater flux overestimation and the leading to a nonlinear evolution of the

groundwater flux with the pumping rate. To prevent this, the mixing flow rate should always be significantly higher than the groundwater transit flow rate.

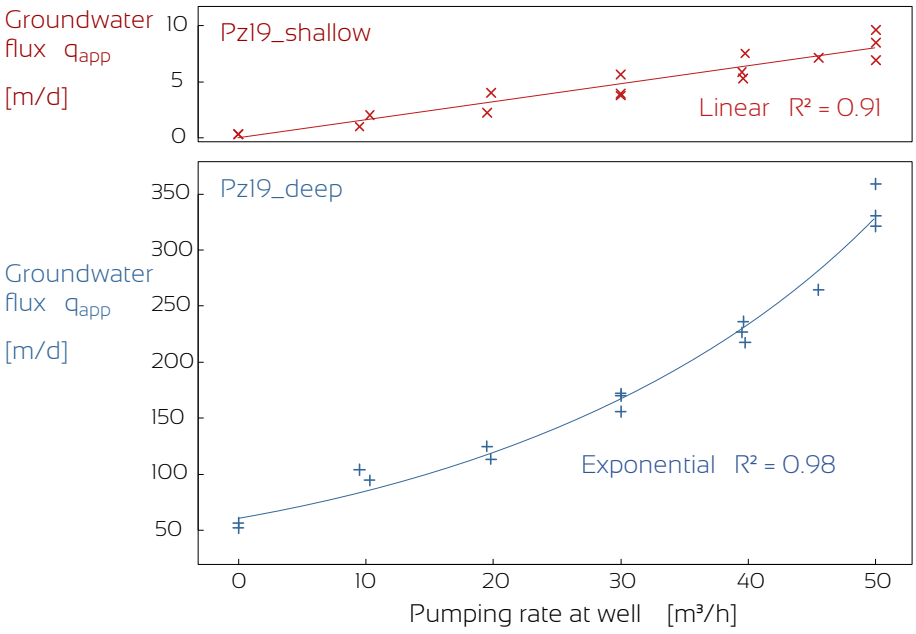

Figure 53: The groundwater flux evolution with pumping is exponential when measured at Pz19_deep, but it remains linear at Pz19_shallow.

3.3.5. Conclusions

From an operational standpoint, the main result of this research is the generalization of the FVPDM technique for monitoring transient groundwater fluxes. The results have shown that the technique is suitable for this purpose due to a high sensitivity to groundwater flux changes. A finite difference solution has been proposed to fit tracer concentration evolutions monitored in the field during transient FVPDM experiments, as well as to calculate corresponding transient groundwater fluxes. An updated flow chart has also been proposed to dimension transient flux FVPDM experiments.

In previous FVPDM studies, Jamin et al. (2015) measured ranges of groundwater fluxes between 260 and 3300 m/d in a fractured aquifer, and Brouyère et al. (2008) measured groundwater fluxes between 0.8 and 3.5 m/d in a chalk aquifer and between 0.26 and 27 m/d in an alluvial aquifer. Here, the investigated groundwater fluxes ranged between 0.35 and 380 m/d. Groundwater fluxes across three orders of magnitude were monitored and quantified using an identical experimental configuration, which demonstrates the versatility of the FVPDM in measuring a wide range of groundwater fluxes. Theoretically, there is no minimal or maximal range limit in

groundwater fluxes that can be measured using the FVPDM technique, because the experimental configuration can be optimized using either the mixing flow rate, the tracer injection flow rate or the injected tracer concentration. However, measuring groundwater fluxes lower than 0.1 m/d using the FVPDM technique may be challenging because of the time required for the tracer concentration to stabilize in the well. This does not constitute a limitation of the FVPDM technique from a physical or technical point of view, but only from an operational point of view due to the required time. In addition, the first part of the evolution of the tracer concentration can still be modelled considering a superposition of two transient effects, i.e. the stabilization of the FVPDM signal and the transient groundwater flow in the aquifer, which might complicate slightly the interpretation.

Two limitations of using the FVPDM for continuous groundwater flow monitoring can be identified. Selected equipment must withstand the stress of a continuous run for days, while remaining calibrated and accurate. Tracer fluid and energy supplies for the equipment can also be challenging at sites with limited access. Continuous monitoring of groundwater level variations in the tested well also become mandatory. The second limitation is inherent to the FVPDM technique. The experiment is a priori dimensioned for an expected range of groundwater fluxes. A significant decrease in groundwater flux during the test may lead to an injection flow rate that becomes higher than the critical transit flow rate (Q_{cr}). In this specific case, the FVPDM test is no longer valid for that low-flow rate period because radially diverging flow conditions develop around the tested well (Brouyère et al. 2008). Monitoring transient groundwater fluxes using the FVPDM technique thus requires regular real time monitoring during the experiment to adapt the injection flow rate (Q_{in}) when required.

In this study, the importance of comparing direct groundwater flux measurements against mean estimates obtained using Darcy's law with mean hydraulic conductivity and hydraulic gradient values has also been demonstrated. The hydraulic conductivity, as estimated based on pumping test results, is a general parameter suitable for evaluating the productivity of the aquifer, but it is not adapted to accurately calculate local groundwater fluxes and associated groundwater flow velocities. The transient FVPDM technique may be applicable to studies in contaminant hydrogeology, where aquifer management is based mainly on the risk of contaminant dispersion. Since groundwater flow is the driving force of contaminant transport and dispersion in the subsurface, having reliable and detailed flux estimates could lead to more accurate pollutant dispersion risk assessment, and ultimately, to optimized management and remediation procedures.

Chapter 4

Field scale applications of the FVPDM

In this chapter, three field-scale applications of the FVPDM are presented.

For the first application (section 4.1), the FVPDM is used to measure in-situ groundwater fluxes in two sandy aquifers within a small watershed in the discontinuous permafrost zone in Nunavik (Quebec). In this context, groundwater flux measurements come in support of a general thermo-hydro-dynamic model of the watershed where permafrost thaw related to global warming occurs. Since heat can be carried by the groundwater flowing in the aquifer laying under the permafrost, the direct and precise measurement of groundwater fluxes within this aquifer is of great importance. This application also shows the versatility of the FVPDM and its robustness at being applied in harsh and remote environments.

The second application of the FVPDM is at an experimental test site where a steady state solute plume was created in an alluvial aquifer between an injection piezometer and a pumping well located 20 m downgradient. Solute mass flux and mass discharge was measured at three control planes made of multi-level piezometers in order to test the representativity of control plane measurements of solute mass discharge (section 4.2).

Finally, the third application relates to contaminant mass flux monitoring in a costal aquifer lying under an industrial complex (section 4.3). The processes of the industrial site released significant amounts of heavy metals in the aquifer which is hydraulically connected to an estuary where tides occur. This transient context leads to very difficult hydrodynamic characterization of the contaminated aquifer by means of traditional methods. FVPDM comes in support for this characterization by monitoring the variations of groundwater fluxes during several tide events and provide a better understanding of the groundwater-surface water interactions at this site. Furthermore, the simultaneous measurements of dissolved heavy metals concentration allows to apply a mass flux characterization approaches that spotted a specific zone where heavy metal mass fluxes were very important and must thereby be treated in priority. This application of contaminant flux based management proves once more the benefits of mass flux approaches.

4.1. Groundwater flux measurement in aquifers of the discontinuous permafrost zone

This section is based on the following publication:

Jamin, P., Cochand, M., Dagenais, S., Lemieux, J.M., Fortier, R., Molson, J. & Brouyère, S. (2019). Direct measurement of groundwater flux in aquifers within the discontinuous permafrost zone: an application of the finite volume point dilution method near Umiujaq (Nunavik, Canada). Hydrogeology Journal, topical Collection TC-03, Hydrogeology of a cold-region watershed near Umiujaq (Nunavik, Canada), accepted for publication.

4.1.1. Introduction

Permafrost in the northern hemisphere covers an area of approximately 2.3×10^7 km², which represents more than two times the area of countries like Canada or United States, and is likely to decrease by 30 to 75% over the next century due to climate change (Grosse et al. 2011, Slater and Lawrence 2013). Onshore and offshore effects of permafrost degradation have already been observed in Alaska (USA), northern Canada, Sweden, Siberia and Tibet since the early 1990s (Romanovsky et al. 2010). Although increasing atmospheric temperatures is the known cause, permafrost thaw is difficult to predict since it is a very complex process resulting from the non-linear interaction between the atmosphere and ground surface including soils, snow cover, vegetation, surface water and groundwater.

Prior to about 2010, only heat conduction had been taken into account in most of the numerical models used for simulating permafrost dynamics and to forecast permafrost degradation. Numerous authors have shown, however, that groundwater flow and heat transport by advection through subsurface flow systems should be considered in order to better understand and predict permafrost dynamics (e.g. Wright et al. 2009, Rowland et al. 2011, de Granpré et al. 2012, McKenzie and Voss 2013, Frampton and Destouni 2015, Kurylyk et al. 2016).

Validation of these models is fundamental since the accuracy of their predictions can be compromised by non-linear coupling and feedback loops. For instance, since thermal conductivity increases with soil water content, groundwater flow through an initially unsaturated porous medium will promote heat transport and permafrost thaw. Thawing permafrost also releases water, which in turn promotes heat transport, creating a positive feedback loop (Wright et al. 2009). Permafrost thaw also increases the hydraulic conductivity and effective porosity of the soil, allowing groundwater flow and groundwater recharge through an active flow layer (Briggs et al. 2014). Although this effect was shown in numerous field and numerical studies (Walvoord and Strieg 2007, St Jacques and Sauchyn 2009, Lyon and Destouni 2010, Ge et al. 2011, O'Donnell et al. 2012), the consequences of this enhanced recharge and groundwater flow on permafrost thaw itself have rarely been examined. The heat carried by groundwater advection is thus likely to increase the rate of permafrost thaw leading to additional feedback processes.

Although groundwater flow and advective heat transport has been found to be important for understanding permafrost dynamics, there is a lack of groundwater tracer data and direct measurements of groundwater parameters such as hydraulic head and hydraulic conductivity for determining flow patterns and groundwater fluxes in permafrost environments (Bense et al. 2012). The challenge to find suitable permafrost sites which are suitably instrumented with groundwater monitoring wells, difficulties in accessing these sites, as well as high costs for field work in northern regions are the main factors which limit the availability of field observations. Existing monitoring wells are often insufficient to allow the assessment of representative hydraulic gradients and realistic groundwater flow rates (Ireson et al. (2013).

In most hydrogeological studies, groundwater (Darcy) fluxes are usually calculated indirectly using Darcy's law which requires access to a network of groundwater monitoring wells sufficiently dense to provide acceptable measurements of the hydraulic gradient and hydraulic conductivity, the latter usually obtained from a pumping test or slug test. Although quite simple, this approach only provides a mean Darcy flux (on the scale of the well spacing) and can yield fluxes with significant margins of error due to uncertainties in the hydraulic gradient and hydraulic conductivity (Bright et al. 2002, Devlin and McElwee 2007).

A crucial need thus exists for more reliable and direct methods to measure groundwater fluxes in the north, and using single-well techniques where possible. Available single-well techniques include both passive and direct measurements. For example, passive methods for measuring groundwater flux include passive flux meters (PFMs, ex. Hatfield et al. 2004) and the iFLUX sampler (www.ifluxsampling.com). However, passive cartridges applied with these methods have only been developed for 2 and 4 inch wells and could not be easily adapted for this specific field site which uses 1.5 inch wells.

Direct measurement methods such as the Colloidal Borescope (Kearl 1997), Acoustic Doppler Flowmeter (Wilson et al. 2001) and In-Well PVP (Osorno et al. 2018) have discrete vertical sampling points that allow measuring local flow velocities which can be significantly different than the average water flux along the entire length of the well-screen. Furthermore, the three cited systems have respective diameters of 1.7, 3 and 2 inches, which prevent their use in 1.5 inch wells. Among the other available methods of direct measurement of groundwater fluxes, the Finite Volume Point Dilution Method (FVPDM, Brouyère et al. 2008) is a promising candidate since it is not limited by the diameter of the piezometer and it has been successfully applied in a variety of geological settings (Goderniaux et al. 2010, Jamin et al. 2015).

In Nunavik (Quebec, Canada), which lies north of the 55° parallel within the province of Quebec, permafrost thaw and groundwater availability are critical issues (Fortier et al. 2011, Lemieux et al. 2016) (Figure 54). Buteau et al. (2010) studied a typical permafrost mound located in a small watershed near the Inuit community of Umiujaq in Nunavik using a heat conduction model. However, they were only able to reproduce observed temperatures within the permafrost by applying an unreasonable geothermal heat flux twice the value expected in this study area.

Recent investigations at the Umiujaq site (Lemieux et al. 2016, Fortier et al. 2019, Lemieux et al. 2019) have shown that an aquifer is located below the permafrost mounds in the lower part of the watershed, in which groundwater flow could be inducing significant advective heat transport and thus could be contributing to permafrost thaw. To help better understand the controlling parameters on permafrost dynamics in this type of periglacial environment, numerical models of groundwater flow and advective-conductive heat transport, accounting for freezing and thawing, have been developed (Dagenais et al. 2017, Dagenais et al. 2019, Parhizkar et al. 2017). A critical component of these models is the groundwater flow rate (Darcy flux) in the aquifer below the permafrost mounds. Indeed, supported by long-term records of temperature within one of these permafrost mounds, the modeling results suggest that advective heat transport is an important mechanism driving permafrost dynamics (Dagenais et al. 2017, Dagenais et al. 2019).

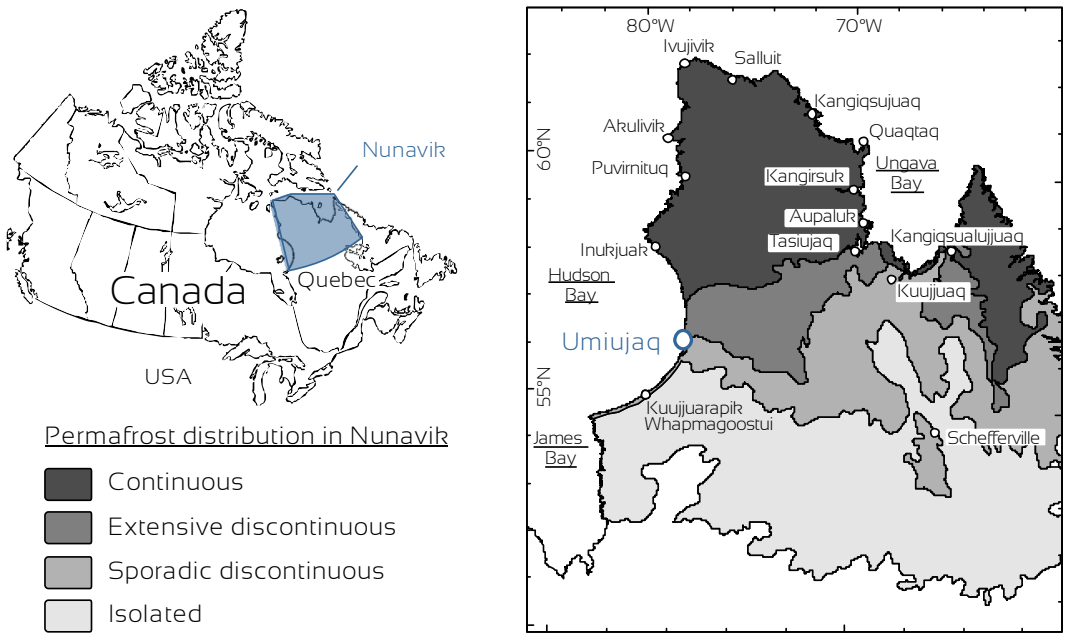

Figure 54: Maps of Canada and permafrost extent and types in Nunavik (Quebec, Allard and Lemay 2012). The experiments were carried out at Umiujaq, an Inuit community located on the east coast of Hudson Bay, in the discontinuous permafrost zone, in Nunavik (Quebec), Canada. The studied 2 km² watershed is located near Umiujaq at the northern end of Lake Tasiujaq, into which it drains.

Since this studied watershed only hosts a few piezometers which are not ideal for determining representative hydraulic gradients, a direct method for determining groundwater fluxes was needed. The aims of this study were therefore: (1) to provide a direct measurement of the in-situ groundwater Darcy flux using the Finite Volume Point Dilution Method (FVPDM) in four piezometers within the studied watershed in the discontinuous permafrost zone of Nunavik (Quebec), Canada, and (2) to evaluate the application of the FVPDM in harsh conditions with

limited accessibility and on-site resources. To the authors' knowledge, this is the first application of this technique in a northern environment, in particular within a sub-permafrost aquifer. Moreover, the measured groundwater fluxes within the sub-permafrost aquifer in this watershed are used to constrain numerical modeling of advective-conductive heat transfer and to assess the impacts of groundwater flow on permafrost dynamics (Dagenais et al. 2019).

After a brief description of the environmental context, the experimental setup adopted for the FVPDM experiments is detailed. The results are then presented and discussed. Finally, a series of recommendations are formulated for the optimization of FVPDM measurements in remote environments.

4.1.2. Study area

4.1.2.1. Environmental context

Located along the eastern shore of Hudson Bay, the Inuit community of Umiujaq lies within the discontinuous permafrost zone in Nunavik (Quebec) (Figure 54). The study site is within a 2 km² watershed located in the Tasiapik Valley, between the village of Umiujaq and the northern end of Lake Tasiujaq, into which it drains. Within this valley, two aquifers, one surficial and one deep, lie above the bedrock (Fortier et al. 2019, Figure 55 and Figure 56).

The thin and unconfined surficial aquifer is found in a Quaternary unit of littoral and intertidal sands which overlies a unit of silty marine sediments deposited during the postglacial marine transgression of the Tyrell Sea. The thickness of the surficial sand unit is greatest in the upper part of the valley where it can be 10 m thick, but this unit is very thin in the lower part of the valley. The silty marine sediments vary in thickness from 10 m in the central part of the valley up to 20 m in the eastern downgradient part of the valley. Being frost-susceptible, the freezing of silty sediments under cold-climate conditions forms ice-rich permafrost mounds which are scattered across the valley (Figure 55 and Figure 56). These raised periglacial landforms due to the localized frost heaving have an approximate diameter of a few tens of meters and a maximum thickness of around 25 m.

The deep aquifer is found in the coarse-grained fluvioglacial/moraine sediments unit overlying the bedrock (Fortier et al. 2019). While unsaturated in the upper part of the valley, this unit becomes saturated in the lower part of the valley. This aquifer is also unconfined in the upper part of the valley, and becomes confined below the layer of frozen silts in the lowermost part of the valley, where artesian conditions may occur in late fall and early winter. The hydraulic conductivity of this aquifer is relatively high and can reach 1 m/d (1.2×10^{-5} m/s) (Lemieux et al. 2016).

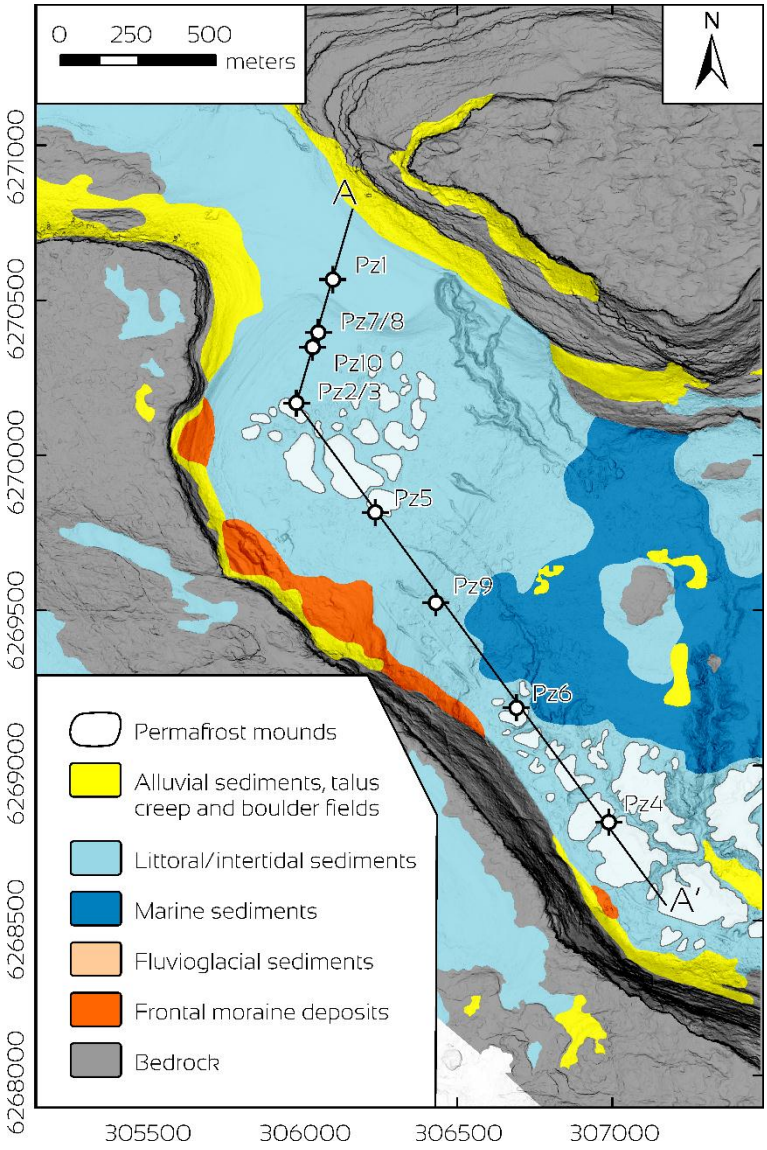

Figure 55: Map of the Quaternary deposits in the Tasiapik Valley. Location of the piezometers and cross-section in the Tasiapik Valley. Projected coordinate system: NAD 1983 MTM Zone 9.

The Tasiapik Valley hosts the Immatsiak sub-network which is part of the provincial network of groundwater monitoring wells commissioned by the Government of Quebec to assess the impacts of climate change on groundwater resources (Réseau de suivi des eaux souterraines du Québec: Gouvernement du Québec 2018). The Immatsiak sub-network is composed of several shallow and deep piezometers installed at seven monitoring sites during the summer of 2012 (Figure 55). The piezometers are oriented along a transect parallel to the axis of the valley from north-west to south-east (Figure 55 and Figure 56).

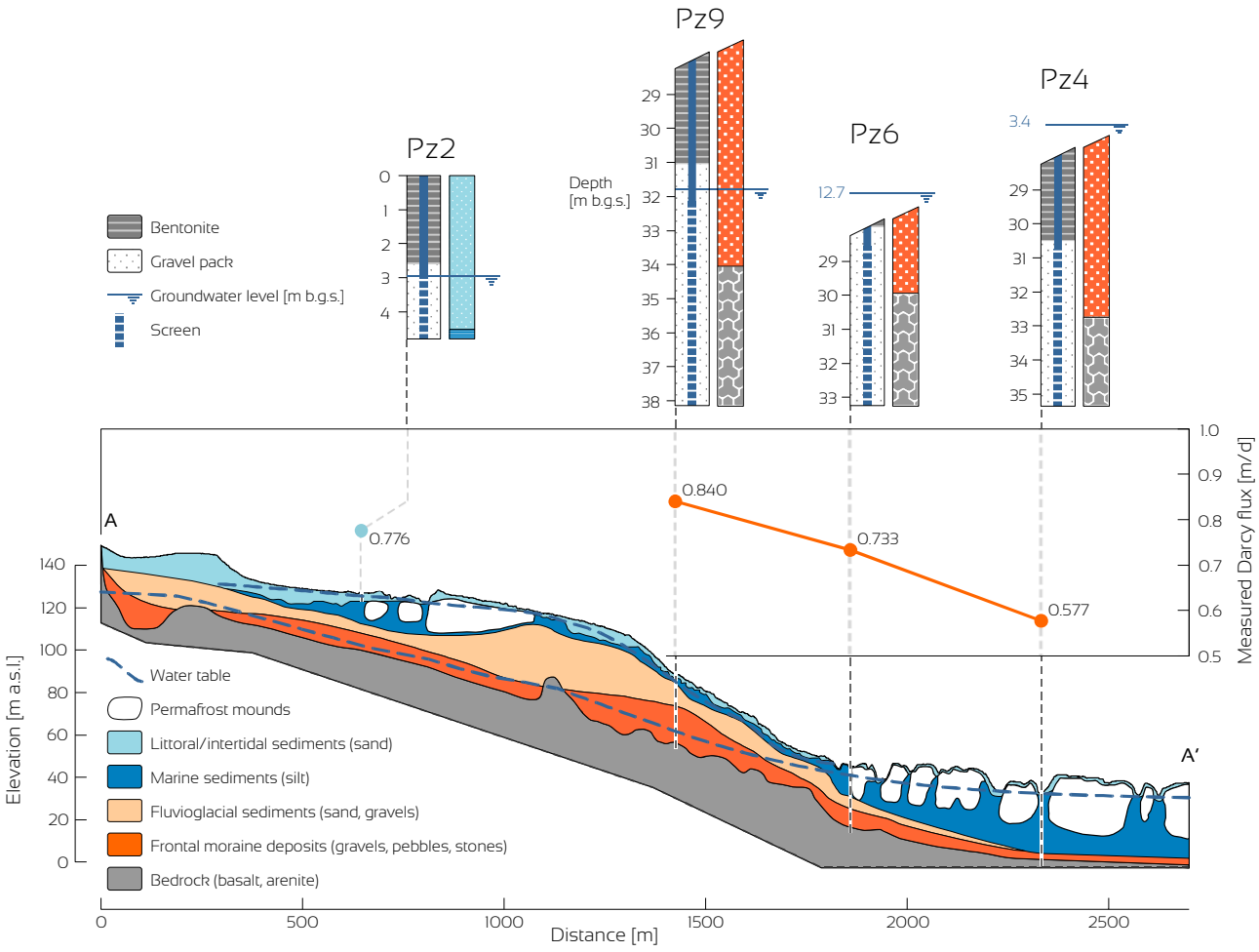

Figure 56: Cross-section of Quaternary deposits in the Tasiapik Valley (see Figure 55 for location). The upper sediment layers are composed of littoral sands and marine silts invaded by permafrost. The uppermost sand layer contains an unconfined perched aquifer. A deep aquifer is found in the coarse-grained fluvioglacial sediments at depth overlying the bedrock. Among the four tested piezometers, three are located in the deep aquifer while one is in the surficial aquifer. Note: for piezometers Pz4, Pz6, and Pz9, only the part of each screen that is located in the deep aquifer is considered representative of the flow system for the calculation of groundwater fluxes. The Darcy fluxes measured within the piezometers installed in the fluvioglacial sediments decrease along the flow direction of the Tasiapik Valley toward Lake Tasiujaq.

4.1.2.2. Piezometer details

Direct groundwater flux measurements were performed in four piezometers in the Tasiapik Valley watershed: three in the deep aquifer (piezometers Pz4, Pz6, and Pz9), and one in the shallow aquifer (piezometer Pz2) (Figure 55 and Figure 56). All piezometers are made of PVC tubing with inside diameters of 1.5 inches (3.8 cm) (Table 10). The deep aquifer piezometers were installed by first drilling down to the contact between the glacial deposits and bedrock, then drilling continued from 2 to 3 m into the bedrock to confirm the bedrock contact (Fortier et al. 2013). The piezometer screen was then installed from the bottom of the drill hole in the bedrock up

to a height of 5 m which implies that only about half of the piezometer screen was in contact with the fluvioglacial sediments aquifer. Two tested piezometers in the deep aquifer, Pz4 and Pz6, are located in the lower part of the valley while piezometer Pz9 is located in the steepest part of the valley where higher groundwater fluxes are expected (Figure 56). The deep aquifer piezometers Pz4, Pz6, and Pz9 were drilled to depths of 33.3, 35.4 and 38.3 m, respectively (Figure 56, Table 10). For these three piezometers, the depth to the water table relative to ground surface at the moment of the direct groundwater flux measurements in summer 2016 was 3.4, 12.7, and 31.78 m, respectively (Figure 56, Table 10). Finally, one measurement was carried out in the piezometer Pz2 which is located in the shallow aquifer in the upper part of the valley (Figure 55 and Figure 56). The depth of this piezometer is 4.65 m and the water table was 2.95 m below ground surface during the experiments (Table 10). This last piezometer was selected because advective heat transport within perched aquifers or shallow flow zones can also have an important effect on the dynamics of the underlying permafrost (Dagenais et al. 2019, Evans and Ge 2017, Frampton et al. 2013, Jiang et al. 2012).

For the piezometers used in this study, only limited information was available on the hydraulic conductivity of the piezometer screen and of the sand filter pack. Consequently, the authors did not attempt to calculate what a dubious a_w estimate would be. At best, and with reasonable assumptions, α_w can be considered to be in the range of 1.8 to 2.4. Hereafter, the term Darcy flux will refer implicitly to the apparent Darcy flux.

4.1.3. Methodology

4.1.3.1. Experimental setup

The general setup for a FVPDM experiment consists of two pumps and one detector (Figure 57). One pump, which can be a submersible pump or a surface pump depending on the depth to the water table, is used to mix the water column in the well, while the second pump is used to inject the tracer fluid into the well at a controlled low flow rate. Good accuracy and precision on the tracer injection flow rate is important since it controls the accuracy of the groundwater flux estimate. A detector is used to quantify the tracer concentration, preferably installed in the well or at the surface, and in-line with the circulation loop to monitor the evolution of tracer concentration over time.

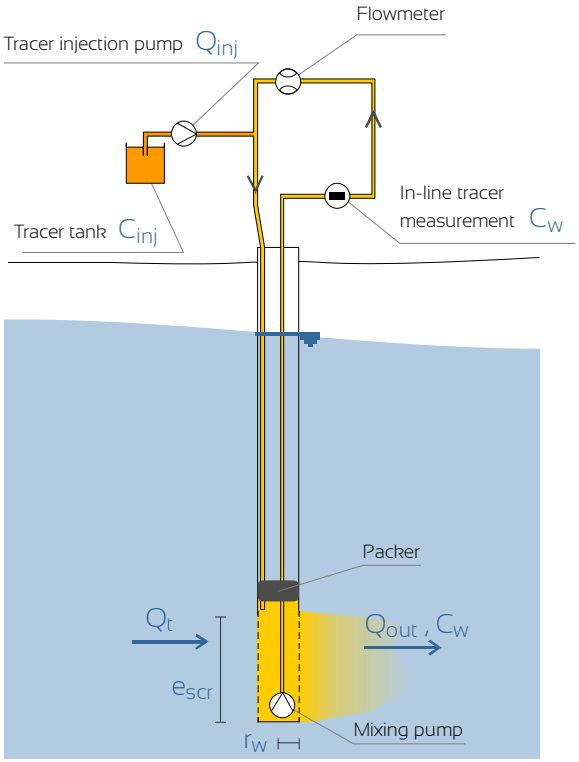

Figure 57: Experimental setup of the FVPDM. The water volume within the well is constantly mixed using a pump and circulated to the surface, where a tracer is injected using a dosing pump. Tracer concentration in the loop is monitored using a field fluorometer placed in-line. A packer was installed in piezometers Pz4 and Pz6 to limit the mixing volume, hence shortening the time required for the FVPDM experiment.

Three types of pumps were tested in the piezometers of the studied watershed to mix the water column: a submersible pump (Supernova 36 SDEC France), a peristaltic pump (Waston Marlow 520 SN-REL) and a bladder pump (Solinst 407 Integra 1"). The circulation loops were made of either 10/13 mm or 4/6 mm nylon tubing. At the surface, a GGUN FL30 fluorometer was connected in line with the circulation loop to monitor the evolution of tracer concentrations (C_w) in the tested piezometer. An electromagnetic dosing pump (Magdos LT, Lutz-Jesco, GmbH) was connected to the loop to inject a fluorescent dye tracer (Uranine CAS n° 518-47-8). Finally, the circulation loop was returned down into the piezometer as far as the top of the groundwater level for experiments carried out on Pz2 and Pz9, or at the top of the water column when limited by a packer at Pz4 and Pz6. Groundwater levels were manually monitored during each experiment. Details of the experimental setup applied for each experiment are given in Table 10.

4.1.3.2. Interpretation of dilution tests

The results of the PDM experiments were interpreted using the exponential decrease of the tracer concentration (Equation 6), the calculation of a linear regression of the logarithm of the tracer concentration data

as a function of time provided the slope of the relationship between these variables equal to the ratio Q_t / V_w. The corresponding apparent Darcy flux was then calculated using Equation 4.

The effective length of the piezometer screen (e_{scr}) used to determine the cross-sectional flow area (S_w) is defined as the portion of the screen exposed within the glacial deposits. The part of the screen in contact with the bedrock underlying the glacial deposits was assumed to have no influence on groundwater flow through the test well.

For the FVPDM test, the groundwater fluxes were calculated by using a least square optimization to fit the analytical solution (Equation 13) to the experimental data. The accuracy of the fit of the analytical solution to the experimental data was evaluated by a Bayesian approach proposed in Equation 22. A set of 500 groundwater flux values (q_D) and mixing volumes (V_w) are first defined between realistic minimum and maximum limits. Each pair of q_D and V_w values was then used in Equation 1 with the corresponding parameters of the experimental setup to model the evolution of tracer concentration versus time. The sum of the residuals between the model and the observations was used to compute a probability density function. From each probability density function, the uncertainty of the fit of the Darcy flux was then defined by the confidence intervals of 5 and 95%.

4.1.3.3. Operational challenges

The FVPDM experiment offers a direct measurement of groundwater flux, independent of any measurement of aquifer parameters such as hydraulic conductivity or water levels. Nevertheless, the design of an FVPDM experiment requires an *a priori* estimate of the groundwater flux to optimize the tracer injection flow rate and injected tracer concentration (Brouyère et al. 2008). For the experiments in the piezometers of the Tasiapik Valley watershed, the first challenge was that the Darcy flux estimates in the aquifer were highly uncertain because of the limited number of piezometers where measurements of hydraulic conductivity had been performed, and because of the irregular spatial distribution of piezometric head measurements. The results of the *a priori* estimate of the Darcy flux in the vicinity of the tested piezometers, based on hydraulic gradients and hydraulic conductivity measured with slug tests (Fortier et al. 2014), are given in Table 11. At piezometer Pz2 in the shallow aquifer, the mean Darcy flux was estimated to be about 0.07 m/d using groundwater levels measured in four nearby piezometers in July 2014, 2015 and 2016. For piezometers Pz4 and Pz9 in the deeper aquifer, the estimated mean Darcy fluxes were 0.008 and 0.017 m/d, respectively. At piezometer Pz6 (also in the deeper aquifer), the estimated Darcy flux is one order of magnitude higher (0.49 m/d) compared to the other piezometers located in the same fluvioglacial aquifer. However, the difference could be due to an over-estimation of the hydraulic conductivity following the slug tests performed in 2014 (Fortier et al. 2014).

As detailed in Brouyère et al. (2008), increasing the tracer injection flow rate (Q_{inj}) close to the critical flow rate (Q_{cr}) decreases the time needed to reach the stabilized concentration plateau, insuring better accuracy of the experiment. A two-step procedure was thus used to conduct a FVPDM test with the optimal injection parameters,

i.e. with an optimized tracer injection flow rate as close as possible to the critical injection flow rate (Q_{cr}) and injected tracer concentration. The first step consisted of a classical PDM test, which was designed using the estimated Darcy flux from the observed heads and hydraulic conductivity. For this first PDM, the mixing volume was calculated based on the geometry of the piezometer (diameter and height of the water column) and on the diameter and length of the circulation loop tubing. The PDM-based estimate of the groundwater flux around the tested piezometer was then used to optimize the full FVPDM test.

The second challenge was related to the geometry of piezometers Pz4, Pz6 and Pz9, which had short screen lengths (4.58 - 6.09 m) located at the bottom of deep boreholes (33.27 - 38.30 m deep). The shallow water levels in these piezometers implied that the water columns were very high relative to length of the screens. The mixing volume (V_w) was thus large, relative to the estimated groundwater flux across the small screens, leading to very long stabilization times for the FVPDM test. To illustrate the order of magnitude of the stabilization time, the dimensioning of a classical FVPDM test in piezometer Pz4 using the available data (V_w = 40 l, q_D = 0.008 m/d, S_w = 0.074 m²) led to estimated test durations of 90 days. Such a long test would have been impossible given the limited availability of a continuous power supply for the pumps, and the high cost of conducting a very long test in a remote area such as Umiujaq. In order to reduce the mixing volume, a custom-made double-flexible joint packer was built for isolating the screened section of the piezometers. This packer was installed in piezometer Pz4 at the top of the piezometer screen, reducing the mixing volume by 80% and thus reducing the estimated stabilization time to less than 12 days. In piezometer Pz6, the packer reduced the mixing volume by 58%. In piezometers Pz2 and Pz9, no packers were required for the FVPDM tests since the groundwater levels at these two piezometers were close to the top of the screen.

The last field-related challenges of performing FVPDM experiments at this test site were the difficult accessibility to the piezometers and the lack of a permanent power supply. Each FVPDM experiment had to run on a light portable electric generator for at least 24 hours. This limitation was overcome by using low electrical consumption pumps and by adaptation of an external fuel tank to the generator, increasing its autonomous operational range from 3 to 22 hours. The experiment could thus run autonomously and only needed manual filling of the fuel tank once or twice a day.

4.1.4. Results

The results of the point dilution experiment carried out in the four piezometers are presented in Figure 58 to Figure 61, with the parameters of the PDM/FVPDM experimental setup provided in Table 10 and Table 11. For piezometers Pz2, Pz4, and Pz6, the results of the classical PDM test are first presented which are then followed by results from the FVPDM experiments. For piezometer Pz9, only a PDM experiment was performed due to the limited available time.

*Table 10: Details of the experimental setup for the PDM and FVPDM experiments at Umiujaq. n.r. = not reached. n.n. = not needed. n.a. = not applicable. *Effective screen length is the part of the piezometer screen within the fluvioglacial sediments aquifer.*

Piezometer	Type of dilution	Tubing radius	Tubing depth	Bedrock depth	Screen length	Effective screen length*	Water level depth	Packer depth	Circulation loop length	Circulation loop radius	Theoretical mixing volume	Mixing pump	Q_{mix}	Injection pump	Q_{inj}	C_{inj}	S_w
		[m]	[m]	[m]	[m]	[m]	[m]	[m]	[m]	[m]	[l]		[l/min]		[ml/min]	[ppb]	[m^2]
Pz2	PDM	0.019	4.57	n.r.	1.52	1.52	2.955	n.n.	80	0.005	0.008	Peristaltic	3.500	Electromagnetic	n.a.	188.0	0.058
	FVPDM	0.019	4.57	n.r.	1.52	1.52	2.955	n.n.	80	0.005	0.008	Peristaltic	3.500	Electromagnetic	47	1627.7	0.058
Pz4	PDM	0.019	35.36	32.72	4.58	1.94	3.400	29.59	80	0.005	0.012	Peristaltic	2.015	Electromagnetic	n.a.	1627.7	0.074
	FVPDM	0.019	35.36	32.72	4.58	1.94	3.400	29.59	80	0.005	0.012	Peristaltic	2.015	Electromagnetic	45	1736.7	0.074
Pz6	PDM	0.019	33.27	29.90	4.64	1.27	12.690	27.74	80	0.005	0.012	Submersible	5.400	Electromagnetic	n.a.	195.4	0.048
	FVPDM	0.019	33.27	29.90	4.64	1.27	12.690	27.74	80	0.005	0.012	Submersible	5.400	Electromagnetic	50 / 29.9	195.4	0.048
Pz9	PDM	0.019	38.30	34.09	6.09	1.88	31.785	n.n.	80	0.002	0.008	Bladder	0.258	Electromagnetic	n.a.	188.0	0.072

Table 11: Estimates of the groundwater flux based on Darcy's law using hydraulic conductivity and hydraulic gradient. Hydraulic conductivity was measured using slug tests (Fortier et al. *2014). Results of the PDM and FVPDM measurements show an apparent Darcy flux much higher than expected.*

Piezometer	Hydraulic conductivity calculated from slug tests	Estimated Darcy flux based on hydraulic gradient and hydraulic conductivity				Measurements based on PDM experiments			Measurements based on FVPDM experiments			
		2014	2015	2016	2017	Theoretical V_w	Estimated Q_t	Estimated q_D	Adjusted V_w	Adjusted Q_t	Adjusted q_{app}	Uncertainty on q_{app}
	[m/d]	[m/d]	[m/d]	[m/d]	[m/d]	[l]	[l/min]	[m/d]	[l]	[l/min]	[m/d]	[m/d]
Pz2	4.25	0.066	0.075	0.070	0.070	7.90	0.017	0.415	9.41	0.031	0.776	±0.012
Pz4	0.85	0.007	0.008	0.009	0.008	11.88	0.037	0.716	8.51	0.030	0.577	±0.006
Pz6	13.82	0.500	0.487	0.486	0.506	11.68	0.058	1.719	9.63	0.025	0.733	±0.003
Pz9	0.27	0.018	0.017	0.016	0.017	7.56	0.042	0.840				

4.1.4.1. Piezometer Pz2

A classical point dilution experiment was first performed in piezometer Pz2 to quickly estimate the transit groundwater flow rate through the piezometer screen and to optimize the dimensions of the full FVPDM experiment. After a brief injection of Uranine, the tracer concentration was monitored in the tested piezometer for 5 hours (Figure 58a). Considering a theoretical mixing volume of 7.9 l calculated from the diameter and height of the water column and from the diameter and length of the circulation loop tubing, the estimated groundwater flow rate through the piezometer screen was 16.6 ml/min, which corresponds to a Darcy flux of 0.415 m/d.

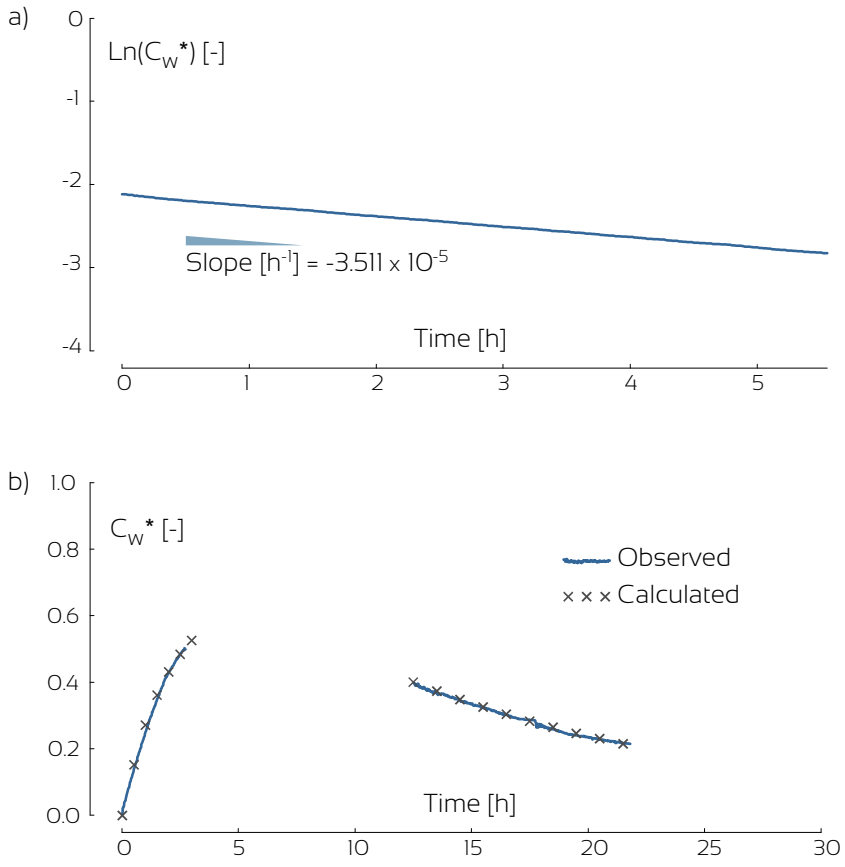

Figure 58: Experimental results in piezometer Pz2 (see Figures 2 and 3 for location). (a) The first PDM dilution experiment provided a groundwater transit flow rate estimate of 15.2 ml/min passing through the piezometer screen. (b) The estimated groundwater flux is 0.78 m/d. A failure of the mixing pump prevented the measurement and stabilization of the tracer concentration during the FVPDM experiment. (C_w = normalized Uranine tracer concentration C_w/C_{inj})*

The full FVPDM experiment was then performed over a period of 22 hours (Figure 58b). Unfortunately, the pump used for mixing the water column in the piezometer overheated and failed 3 hours after the beginning

of the tracer injection, preventing stabilization of the tracer concentration. The experimental setup was only repaired 12 hours later, which at least allowed monitoring the decrease in tracer concentrations. Notwithstanding these difficulties, the test results could be processed and interpreted, yielding an adjusted mixing volume of 9.41 l and an estimated Darcy flux of 0.776 ± 0.012 m/d.

4.1.4.2. Piezometer Pz4

A dilution experiment was performed in piezometer Pz4 over a period of 5.5 hours (Figure 59a). Considering a theoretical mixing volume of 12.9 l, the estimated groundwater flow rate through the well screen was 36.7 ml/min, which corresponds to a Darcy flux of 0.720 m/d. The mixing volume was limited by a packer installed at a depth of approximately 30.5 m.

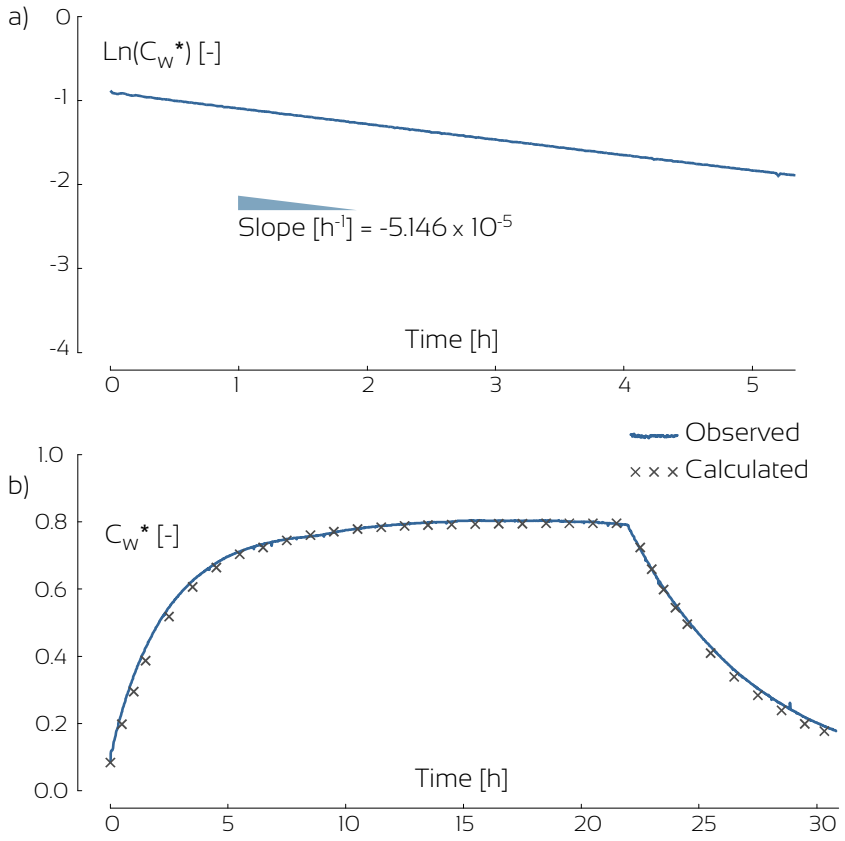

Figure 59: Experimental results in piezometer Pz4 (see Figures 2 and 3 for location). (a) The first dilution experiment provided a groundwater transit flow rate estimate of 36.7 ml/min passing through the piezometer screen. (b) The measured groundwater flux is 0.58 m/d. (C_w = normalized Uranine tracer concentration C_w/C_{inj})*

The results of the full 30-hours FVPDM experiment, including a tracer injection period of 21 hours, are shown in Figure 59b. No problems were encountered during this experiment. Based on the interpretation, a mixing volume of 8.51 l and a Darcy flux of 0.577 ± 0.006 m/d were derived for piezometer Pz4.

4.1.4.3. Piezometer Pz6

The dilution experiment in piezometer Pz6 lasted for 5.2 hours. Considering a theoretical mixing volume of 12.6 l, a volumetric groundwater flow rate of 57.7 ml/min was determined (Figure 60a) which corresponds to a Darcy flux of 1.74 m/d. The mixing volume was limited by a packer installed approximately at 28.5 m deep.

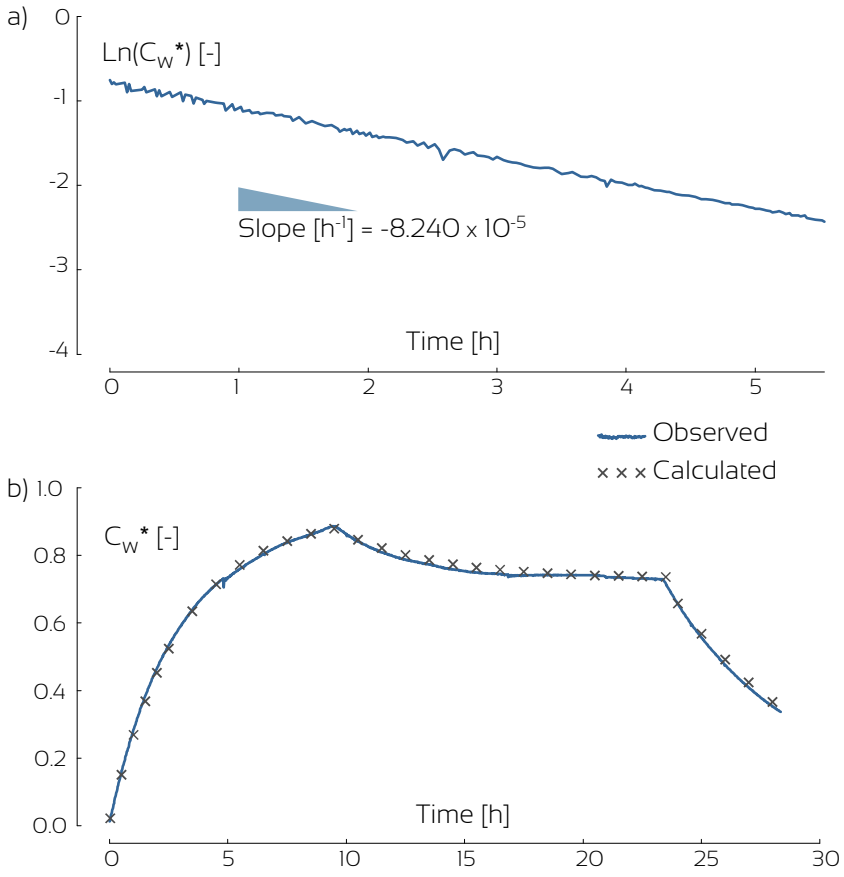

Figure 60: Experimental results in piezometer Pz6 (see Figures 2 and 3 for location). (a) The first dilution experiment provided a groundwater transit flow rate estimate of 57.5 ml/min passing through the piezometer screen. (b) The measured groundwater flux is 0.73 m/d. (C_w = normalized Uranine tracer concentration C_w/C_{inj})*

The transit flow rate determined by the PDM test in this piezometer was slightly higher than in the other piezometers, allowing for a faster stabilization of the concentration during the FVPDM experiment. It was thus

decided to apply two consecutive tracer injection flow rates for the FVPDM experimental setup in order to observe two stabilized tracer plateaus for a better accuracy on the interpreted Darcy flux (Figure 60b). The full FVPDM experiment was conducted flawlessly over a period of 28 hours. The calculated Darcy flux in piezometer Pz6 is 0.733 ± 0.003 m/d and the adjusted mixing volume is 9.63 l.

4.1.4.4. Piezometer Pz9

Due to the piezometer setup, limited available time, and available pumps, only a PDM experiment was performed in the piezometer Pz9. Indeed, only a bladder pump and a peristaltic pump were available for this last experiment. After a brief injection of Uranine lasting for 20 minutes, the decrease in Uranine concentration was monitored over a period of 3 hours (Figure 61). The mixing volume was estimated at 7.56 l and the calculated Darcy flux in the piezometer Pz9 was 0.840 m/d. No uncertainty analysis was possible since only a PDM experiment was performed in this piezometer.

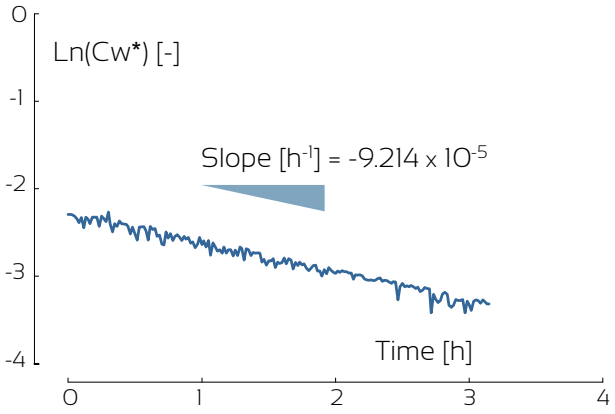

Figure 61: Experimental results in piezometer Pz9 (see Figures 2 and 3 for location). The dilution experiment provided a groundwater flux estimate of 0.84 m/d. (C_w = normalized Uranine tracer concentration C_w/C_{inj})*

4.1.5. Discussion

Based on the FVPDM experiments performed in four piezometers in the Tasiapik Valley watershed, groundwater fluxes vary from 0.58 to 0.84 m/d which are significantly higher than initial estimates based on Darcy's law of 0.01 to 0.49 m/d using monitored water levels from previous years. It is also important to note that the Darcy fluxes measured by dilution tests in the piezometers are apparent Darcy fluxes which might overestimate the actual Darcy flux in the aquifer by a factor 1.8 to 2.4 according to the estimated flow field distortion coefficient. The Darcy flux for each tested piezometer was also estimated using groundwater levels measured at the time of

the FVPDM experiments (Table 11). In piezometer Pz2, the Darcy flux calculated using Darcy's law and water levels from July 2017 is 11 times lower than the flux measured in the FVPDM experiment. In piezometers Pz4 and Pz9, the same estimates are respectively 72 and 48 times lower than the Darcy flux measured by the FVPDM experiments. On the other hand, the Darcy law-estimated groundwater flux in piezometer Pz6 is very close to the flux calculated from the FVPDM experiment. However, these results based on a simple application of Darcy's law are questionable due to the abnormally high value of hydraulic conductivity found at this location. These significant differences highlight the benefits of direct groundwater flux measurements. In this case, the number of available piezometers and their spatial distribution only provided a rough under-estimate of the hydraulic gradient for calculating fluxes based on Darcy's law. An explanation of this underestimation could be that the piezometers used to estimate the Darcy flux based on hydraulic gradients are not aligned along the main groundwater flow direction. Inaccurate hydraulic conductivity values determined from the slug tests could also explain the underestimation of the groundwater flux.

Groundwater fluxes within the deep aquifer decrease along the flow direction from piezometer Pz9 to Pz4, toward Lake Tasiujaq. This distribution of groundwater fluxes is consistent with the hydrogeological setting. The groundwater fluxes are higher near piezometer Pz9 where the deep aquifer is inclined with a steep water table, while they are lower near piezometer Pz4, where the water table is much flatter. In piezometer Pz6, the Darcy flux has an intermediate value of 0.733 m/d.

The Darcy flux in the unconfined perched aquifer in the upper part of the valley in piezometer Pz2 is relatively high (0.776 m/d) with regard to the overall topography of this upland area. This could be explained by the fact that this piezometer is located beside a permafrost mound that forms a local topographical high, about 2-3 m above the surrounding land elevation. Due to the dome shape of the mound, groundwater flows radially away from the mound which likely induces a higher than expected groundwater flux.

The maximum error in the calculated Darcy flux is about ±1%. This high accuracy is due to the good experimental data, very low noise levels in the tracer concentration measurements and careful and frequent calibration of the fluorometer and tracer injection pumps. The duration of all FVPDM experiments was around 20 hours, which is relatively long for a single groundwater flux measurement. As mentioned in Jamin and Brouyère (2018), measuring groundwater fluxes lower than 0.1 m/d using the FVPDM technique may be challenging due to the long test duration required. However, in this study, a long-duration experiment allowed a long stabilized tracer concentration plateau, which significantly increased the accuracy of the results.

Several issues can be noted regarding the interpretation of the tests. First, the mixing volume adjusted by the interpretation of the FVPDM experiment is different from the theoretical mixing volume calculated based on the geometric properties of the well and of the circulation loop. For instance, for piezometer Pz2, the adjusted mixing volume is 20% greater than the theoretical mixing volume. This difference could arise since some of the water present in the filter pack around the internal tubing of the piezometer is likely involved in the mixing volume.

For piezometers Pz4 and Pz6, the adjusted mixing volume is 28 and 17% less than the theoretical mixing volume. Packers were used in both of these piezometers for reducing the mixing volume. This volume might have been underestimated due to inaccuracy in the installation depth of the packers (1.1 l per meter depth error), and due to the volume of the submersible pump used to mix the water (approximately 0.4 l), which was not taken into account, and which would therefore reduce the current mixing volume.

Furthermore, at each tested piezometer, the Darcy fluxes determined from the PDM experiments differ from those determined from the FVPDM experiments. This difference in fluxes between the two methods is likely due to the difference in mixing volumes considered in both cases. The PDM results were interpreted using a geometrically based theoretical mixing volume, while the Darcy fluxes assessed from the FVPDM experiments are independent of the mixing volume estimation. If the PDM-based Darcy fluxes had been calculated using the actual mixing volume adjusted for the interpretation of the FVPDM experiments, the results would have been closer to the FVPDM-based Darcy fluxes. An accurate estimation of the mixing volume is therefore critical for the interpretation of a PDM experiment.

Even if the accuracy of the groundwater fluxes depends on the accuracy of the fluorescent dye tracer concentrations, the piezometer setup also induces some uncertainties. These uncertainties originate from the installation depths of piezometers Pz4, Pz6, and Pz9 which are screened about half in the bedrock and half in the moraine sediments, each characterized by different hydraulic properties. For the interpretation of the dilution experiments, it was assumed that groundwater is only flowing within the moraine sediments and the flow cross-section area (S_w) thus only corresponds to the length of the piezometer's screen in the moraine sediments. This hypothesis was supported by a visual inspection of the rock cores sampled during drilling, which revealed massive structure with only few fractures. However, groundwater flow might also occur within these fractures. Because the flow cross-section has a direct impact on the groundwater flux assessment, choosing a flow section twice the actual value would have reduced the calculated flux by one-half. Since all piezometers in the deep aquifer have about the same configuration, the relative differences between the fluxes would have remained the same, but the absolute value would have changed. For piezometer Pz2, this is not an issue since this piezometer is only screened in the sandy sediments.

The equipment failure during the FVPDM experiment performed in piezometer Pz2 provided new insights for carrying out further FVPDM experiments. As a long-duration measurement, the FVPDM experiment requires flawless operation of all equipment, including the power generator, mixing pump, injection pump and tracer detector. Another aspect to consider is the power supply which should be able to run autonomously and flawlessly during the entire experiment, and be able to withstand the energy consumption of the pumps. The third critical point of the setup is the choice of robust and reliable pumps, particularly in such harsh and remote environments. In this study, the only available pump for mixing the water column was a peristaltic sampling pump, which is not designed to run continuously for several hours. Finally, the setup in the field should be secured against any disturbance either due to weather conditions (e.g. wind, rain or freezing temperatures in the tracer injection tank),

animals or vandalism. The experimental setup could also be improved by integrating the equipment (pumps, detectors, hoses and connections) into a single portable unit, easily handled during transport and field operations. Nevertheless, the dilution experiment in piezometer Pz9 showed that even with limited equipment and time, it is possible to perform a valuable and accurate direct measurement of groundwater flux.

It is acknowledged that groundwater fluxes measured with the PDM and FVPDM experiments are only representative for the specific period of measurement in the field, while the magnitude of these fluxes may change throughout the year, especially in this type of environment where the ground is frozen almost seven months per year. As an example, water level variations up to 12 m were observed in piezometer Pz6 over a single year (2012-2013, Lemieux et al. 2019). Such transient changes in the flow system could be followed by repeating the FVPDM experiments over the different seasons.

The groundwater fluxes obtained from the FVPDM tests are critical independent data for constraining groundwater flow and heat transport models, and for estimating general thermal balances at the Umiujaq site. They can be used, for example, to estimate the relative contribution of convective heat transfer in the confined aquifer to heat transfer by conduction alone. One measure of this contribution is the Peclet number, defined as $Pe = \Delta L\ q_D\ n\ /\ \varkappa$, where ΔL is a characteristic length (m), q_D is the Darcy flux (m/s), n is the porosity and $\varkappa$ is the thermal diffusivity (m^2/s). The Peclet number is a dimensionless ratio between the heat transport by convection and by conduction. Assuming ΔL corresponds to the depth of the confined aquifer below the permafrost (~20 m), a porosity of 0.35, a thermal diffusivity of $8x10^{-7}$ m^2/s (Dagenais et al, 2019), and using the observed mean Darcy flux of $3.3x10^{-6}$ m/s ($qD = q_{app} / a_w = 0{,}6/0{,}21$ = 0.29 m/d), the Peclet number is about Pe = 29, which indicates a heat convection-dominated system. The important role of convective heat transport on permafrost degradation was confirmed in the numerical model of Dagenais et al (2019).

4.1.6. Conclusions

The use of the FVPDM has provided reliable estimates of groundwater fluxes in a shallow supra-permafrost aquifer and in a deep sub-permafrost aquifer beside and below permafrost mounds in the discontinuous permafrost zone in Nunavik (Quebec), Canada. Measured apparent groundwater fluxes range from 0.577 to 0.840 m/d with respective accuracies varying from ±0.003 to ±0.012 m/d, which are consistent with the hydrogeological settings. These data are important since no groundwater fluxes are currently available in this type of periglacial environment. Moreover, these data are essential for constraining numerical models of advective-conductive heat transfer to better understand permafrost dynamics (see Dagenais et al. 2019).

During the PDM and FVPDM experiments carried out in four piezometers within the Tasiapik Valley watershed at Umiujaq, several major challenges were encountered such as small screen/borehole length ratios, small borehole diameters and harsh conditions in a remote environment. Nevertheless, all challenges were overcome, proving the versatility of the method. A key component of the successful application of these point

dilution methods was the use of borehole packers for isolating the piezometer screen, which significantly reduced the duration of the experiments. Based on the experience gained from these experiments, robust equipment should be used and commercially available groundwater sampling pumps should be avoided.

Although the point dilution methods used in this study were useful to assess groundwater flux, the direction of groundwater flow remains unknown. Groundwater flow direction is valuable information for study sites such as the Tasiapik Valley watershed at Umiujaq where only a few boreholes are available and which are not optimally configured for standard application of Darcy's law. Ongoing development of the point dilution method should resolve this aspect in the near future.

4.2. Field scale mass discharge measurement from a controlled solute plume

4.2.1. Introduction

Control planes are currently the most frequently used methods to calculate contaminant mass discharge in aquifers. In homogeneous aquifers they can provide reliable mass discharge results. In heterogeneous aquifers, the representativity of mass discharges calculated by the integration of discrete mass fluxes measurements over the area of the control plane is not guaranteed. Risk assessment of contaminated aquifers requires estimates of mass discharge which must include a quantification of uncertainties in order to establish its credibility (Schwede and Cirpka 2010). The last decade, most studies addressed the evaluation of mass discharge from point measurements by numerical modeling (Cvetkovic et al. 1992, Kübert and Finkel 2006, Li et al. 2007, Li and Abriola 2009, Schwede and Cirpka 2010, Klammler et al. 2012, Chen et al. 2014, de Barros 2018).

Other studies included field data on which the uncertainties are estimated according to the method developed in their corresponding research (Cai et al. 2011, Troldborg et al. 2010, 2012, Beland-Pelletier et al. 2011). Compared to pure numerical studies, field-oriented studies are not able to validate the accuracy of the mass discharge calculation because the original mass discharge released by the contaminant source is never known a priori. As mentioned by Béland-Pelltier et al. (2011): "it is impossible with any field approaches to measure 'the true value' of mass discharge across a control plane". The only option to validate a mass discharge measurement approach on field experiment is to simulate a dissolved contaminant plume with a controlled injection of common hydrogeological tracers in an aquifer. Such tracers present no harm for the environment and are generally well accepted by regulations agencies.

In this study, a fluorescent dye tracer was injected in an alluvial aquifer at a constant flow rate in order to create a steady state solute plume. The injection was performed in a monitoring well located upgradient from a pumping well where a constant pumping rate was applied. Mass discharge measurements were performed at three control planes located between the injection well and the pumping well. The FVPDM was used to accurately measure the groundwater fluxes at each monitoring well of the control planes while solute concentrations were measured by classical groundwater samplings. These groundwater samplings were performed when the solute plume was assumed steady state. The objective of the present study is to test the control plane approach for the calculation of a plume mass discharge in a heterogeneous alluvial aquifer, under controlled groundwater flow and solute transport conditions and for an existing setup of monitoring wells.

After the description of the experimental setup, the results of FVPDM experiments are presented for selected monitoring well and solute mass discharge is calculated for each of the three control panel. The comparison of the calculated solute mass discharges at the injection well, at the control plane and at the pumping well is discussed as initial data for further use in a more complete numerical model.

4.2.2. Materials and methods

This study took place on the experimental test site of Hermalle-sous-Argenteau. The environmental characteristics of this site are described in detail in section 3.3.2.

4.2.2.1. Controlled steady state solute plume

The objective of the tracer injection was to create a controlled steady state solute plume in the alluvial aquifer where radially converging flow conditions were induced by pumping (Figure 62).

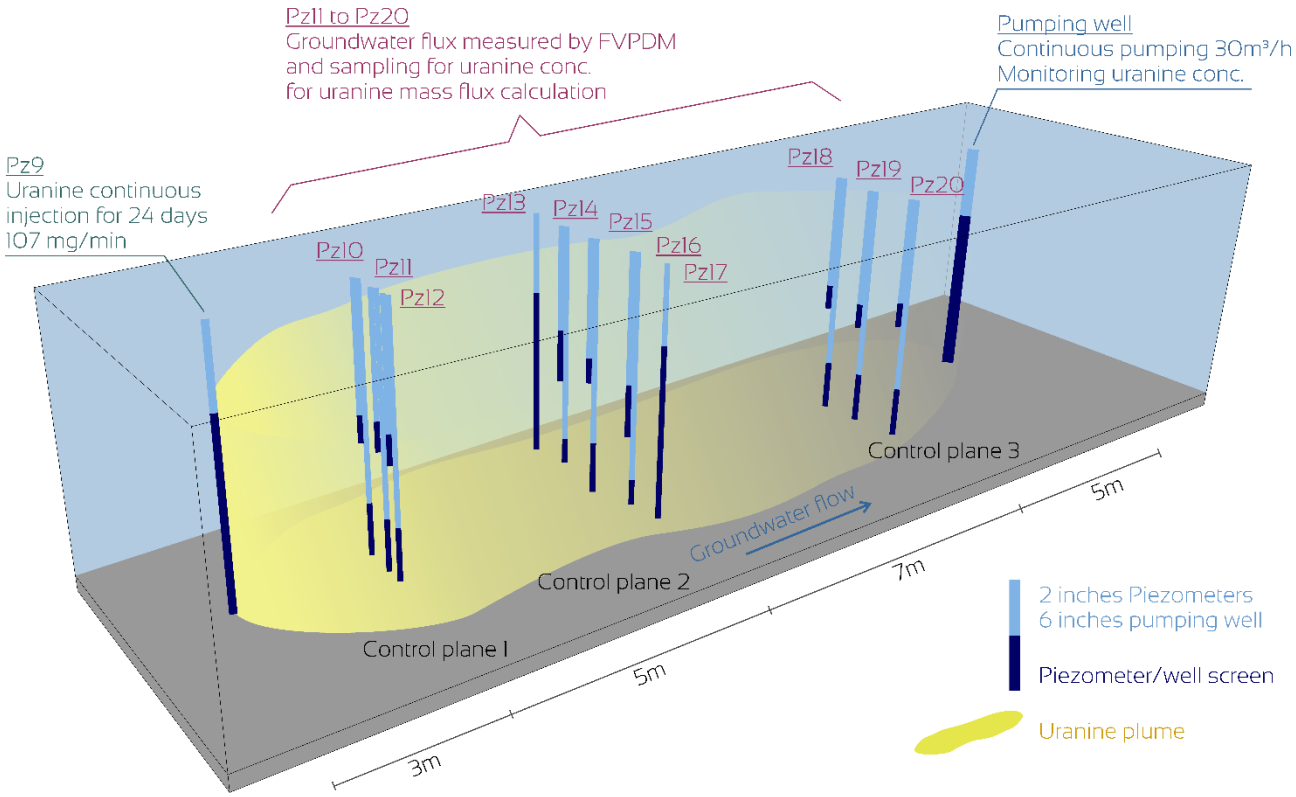

Figure 62: Experimental setup used to create a steady state solute plume of Uranine in the aquifer. Uranine is constantly injected at Pz9 during 24 days at 107 mg/min. Flow in the aquifer is forced by a pumping at 30.6 m³/h at the pumping well located 20m from Pz9. Groundwater fluxes and Uranine concentration are measured at each monitoring well*s of the three intermediate control planes in order to calculate Uranine mass fluxes and mass discharges.*

A fluorescent dye tracer, Uranine (CAS no. 518-47-8), was injected in Pz9 at a constant flow rate of 42.6 mL/min and at a concentration of 2500 ppm during 24 days. During this injection, the water column in Pz9 was continuously mixed using a Grundfos MP1 submersible pump in order to vertically homogenize tracer concentrations and to insure a uniform distribution of the 107 mg/min tracer mass discharge on the whole thickness of the aquifer. At the pumping well, located 20 m downgradient from the injection well, a constant

pumping flow rate of 30.6 m³/h was applied with a Grundfos SP30-3 submersible pump and constantly monitored with a Magflux 7200 electromagnetic flow meter, and the Uranine concentrations were measured every minute using a Schnegg GGUN FL30 fluorometer. It was hence possible to calculate a mass discharge balance between the Uranine injected at Pz9 and the Uranine recovered at the Pumping Well. When the Uranine concentrations stabilized at the Pumping well, the Uranine plume and the associated Uranine mass fluxes in the aquifer were assumed to be steady state.

4.2.2.2. Uranine mass flux measurement

Once the Uranine plume was stabilized and considered steady state in the aquifer, Uranine mass fluxes were calculated for each monitoring well from measurements of groundwater fluxes and Uranine concentrations. The monitoring wells available at the site are aligned and form three control planes that intersect the Uranine dissolved plume at a distance of 3, 8 and 15 meters from the injection well Pz9 (Figure 62).

Uranine concentration is measured on groundwater samples collected 24 days after the start of the Uranine injection. Monitoring well sampling procedure included a traditional dynamic pumping with a purge of three time the water volume comprised in the internal tubing and in the filter pack. The samples were analyzed in the laboratory on a spectrofluorometer.

Groundwater fluxes were measured at each monitoring well using the basic configuration of the FVPDM (section 2.5). As the FVPDM also require the use of a tracer to measure groundwater flux, Amino-G Acid was chosen for its absorption and emission UV wavelength of 355 and 445 nm respectively, which are significantly separated from the Uranine used to create the solute plume (495 and 520 nm). This limits the possible interference between the two fluorescent dyes for their quantification using an optical method. A centrifugal surface pump was used to mix the water column within the tested monitoring wells at a flow rate of 12 L/min. A Watson-Marlow Qdos60 was used to inject Amino-G Acid (CAS n°86-65-7) as a fluorescent dye tracer for the FVPDM experiments. Amino-G acid concentrations were monitored with a Schnegg GGUN FL30 fluorometer. The complete experimental data of tracer injection flow rate and concentration for each monitoring well tested by FVPDM are gathered in Table 12. The FVPDM experiments were interpreted using the analytical solution developed by Brouyère et al (2008) for steady state groundwater flow (section 2.3). The flow distortion coefficient (a_w) induced by the well constriction was calculated using the Drost formula (Equation 8) based on the hydraulic conductivity and on the radius of the filter pack and of the well screen. a_w is given in Table 13 for each tested monitoring well.

Table 12: Geometric configurations of the monitoring wells of the three control planes and experimental setup used for FVPDM experiments.

Piezometer	Control plane	Groundwater level [m below surface]	Top filter depth [m below surface]	Bottom filter depth [m below surface]	Q_{inj} [mL/min]	C_{inj} [ppb]	T_{inj} [h]
Pz10_shallow	1	3.34	4.8	5.8	79.9	5000	55.32
Pz10_deep		3.32	8	10	372	5000	1.08
Pz11_shallow		3.32	4.7	5.7	23	1000	4.35
Pz11_deep		3.33	8.1	10.1	550	5000	0.98
Pz12_shallow		3.24	4.9	5.9	23	1000	6.97
Pz12_deep		3.29	8.1	10.1	414	5000	1.08
Pz13	2	3.28	3.1	9.6	460	4970	1.20
Pz14_shallow		3.21	4	6	43.2	750	2.67
Pz14_deep		3.18	8.3	9.3	450	5000	1.05
Pz15_shallow		3.18	4.5	5.5	75	5000	41.15
Pz15_deep		3.17	7.8	9.8	500	5000	1.07
Pz16_shallow		3.13	4.9	6.9	46.2	1000	4.00
Pz16_deep		3.16	8.5	9.5	500	4970	1.25
Pz17		3.15	2.9	9.4	246	500	1.17
Pz18_shallow	3	3.25	4.6	5.6	112	5000	39.43
Pz18_deep		3.24	8	10	600	3488	1.10
Pz19_shallow		3.18	4.7	5.7	70	3488	54.67
Pz19_deep		3.18	7.7	9.7	500	4651	1.30
Pz20_shallow		3.2	4.2	5.2	100	5000	39.43
Pz20_deep		3.19	7.8	9.8	500	5000	0.98

4.2.2.3. Uranine mass discharge calculation

The groundwater fluxes and Uranine concentration measured at every monitoring well were multiplied to give Uranine mass fluxes that were further integrated on a flow surface representative of the corresponding flow section of the control plane (Equation 1 and Equation 2).

The flow surfaces were firstly assumed to be rectangles centered on each monitoring well screen and limited laterally at half the distance between each monitoring wells and vertically at the top and bottom of the aquifer (Figure 66). The mass discharges calculated for each representative surface flow were added to obtain a total Uranine mass discharge for each control plane which can be compared to the injected Uranine mass discharge.

In a second step, the groundwater fluxes and Uranine concentration were continuously interpolated on the surface of each control plane on a regular grid of 5 cm cell size (Figure 67). The small number of data available on each control plane prevented the use of complex statistical interpolation methods. Among the more adequate deterministic methods, the Inverse Distance Weight method was chosen and used with a power coefficient of 2 and a variable search radius including 10 measurements points, in order to smooth the interpolated values into a realistic spatial distribution. The initial data points used for the interpolation consisted of the grid cells corresponding to each monitoring well screen.

4.2.3. Results

4.2.3.1. Uranine mass discharge recovered at the pumping well

The evolution of Uranine concentration at the pumping well is shown in Figure 63. After 10 days, the Uranine concentration seemed stabilized at the pumping well, implying that the Uranine plume had reached a steady state. From this moment, Uranine concentrations in the water pumped form the recovery well remained stable, oscillating around a median value of 184±15 ppb. Using the applied pumping rate of 30.58 m^3/h, it was possible to calculate Uranine mass discharge at the pumping well of 94 mg/min which represents 88% of the Uranine mass discharge injected at Pz9 (107 mg/min). The difference between the injected and retrieved Uranine mass discharge can be due to degradation of Uranine in the aquifer, to a retardation of the Uranine as a consequence of sorption or immobile water, to inaccuracy of Uranine concentration measurements at the pumping well or a combination of these factors.

The variation of Uranine concentration with time after 10 days can be due either to small variation of groundwater flow in the alluvial aquifer that can dilute more or less the dye tracer or to variations in the Uranine mass discharge injected at Pz9. This later reason is supported by the necessary frequent refills of the Uranine injection tank using limited equipment available in the field which could have induced some variations of Uranine concentration around the theoretically dimensioned 2500 ppm.

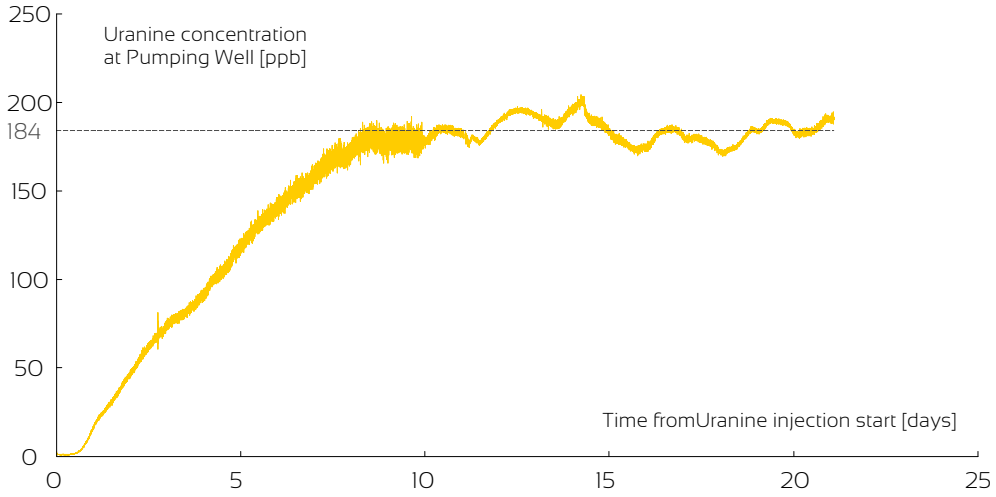

Figure 63: Evolution of Uranine concentration at the pumping well. After 10 days, the Uranine concentration stabilized at a value of 184 ppb, giving an Uranine mass discharge of 94 mg/min corresponding to 88% of the Uranine mass discharge injected at Pz9.

4.2.3.2. Groundwater flux

The results of the FVPDM experiments undertaken in the 20 monitoring wells of the three control planes are given in Table 13. Figure 64 and Figure 65 show examples of results obtained in Pz20_deep and Pz20_shallow respectively. The groundwater fluxes measured in the deeper part of the aquifer vary between 6.83×10^{-5} and 7.85×10^{-4} m/s (or 5.9 to 67.9 m/d). The highest fluxes are measured closer to the pumping well, which is expected in such radial converging flow conditions. The groundwater fluxes measured in the monitoring wells of the upper part of the aquifer vary between 1.11×10^{-5} and 4.75×10^{-5} m/s (1 to 4.1 m/d), 10 times lower in average than those measured in the deepest part of the aquifer. These results are consistent with the results obtained previously at the site for identical pumping conditions (section 3.3.4).

While being relatively identical for the three deeper monitoring wells of the first control plane (CP1), groundwater fluxes significantly varied laterally in second and third control plane (CP2 and CP3). In CP2 the measured groundwater fluxes tended to increases towards Pz13, to the left of the control plane from 4 to 47 m/d. Inversely, in CP3 the groundwater fluxes increased towards Pz20, to the right of the control plane from 24 to 68 m/d. This may indicate the presence of sedimentary structures that are likely to deviate the Uranine plume in from straight to a curvy path within the alluvial aquifer.

The groundwater discharge calculated for control plane increased from 7.5 m^3/h at CP1 to 12.4 m^3/h at CP2 and to 21.3 m^3/h at CP3 which is consistent with the pumping rate of 30.6 m^3/h applied at the pumping well.

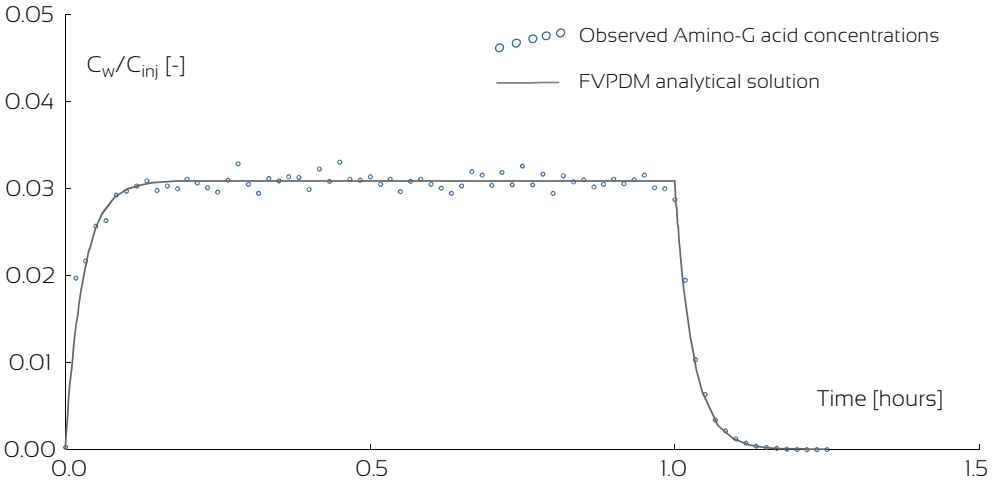

Figure 64: Tracer concentration at Pz20_deep during the FVPDM experiment. The interpretation using the FVPDM analytical solution allowed to calculate a groundwater flux of in the aquifer 67.86 m/d.

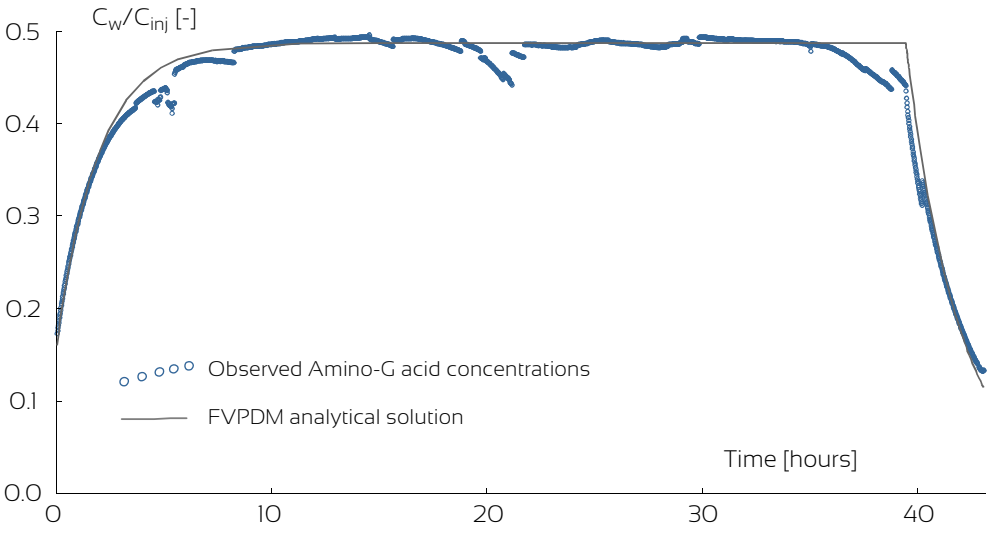

Figure 65: Tracer concentration at Pz20_shallow during the FVPDM experiment. The interpretation using the FVPDM analytical solution allowed to calculate a groundwater flux of in the aquifer 2.67 m/d.

Table 13: Results of the groundwater flux measurements, of the Uranine concentration measurement and of the Uranine mass discharge calculation at the three control planes.

Monitoring well	Control plane	Apparent groundwater flux (q_{app}) [m/s]	α_w [-]	Groundwater flux in the aquifer (q_D) [m/s]	Base window [m below surface]	Top window [m below surface]	Width window [m]	Flow area [m^2]	Total water discharge per control plane [m^3/h]	Uranine conc. [ppb]	Uranine mass flux [$mg/min/m^2$]	Uranine mass discharge [mg/min]	Total mass discharge per control plane [mg/min]
Pz10_shallow	1	6.21×10^{-5}	3.115	1.99×10^{-5}	6.9	3.2	0.637	2.484	7.53	6762.35	8.09	19.06	**70.39**
Pz10_deep		1.25×10^{-3}	3.412	3.66×10^{-4}	10	6.9	0.637	1.975		0.56	0.01	0.02	
Pz11_shallow		1.30×10^{-4}	3.115	4.16×10^{-5}	6.9	3.2	0.531	2.071		7509.15	18.75	36.84	
Pz11_deep		1.41×10^{-3}	3.412	4.13×10^{-4}	10	6.9	0.531	1.646		0.25	0.01	0.01	
Pz12_shallow		6.65×10^{-5}	3.115	2.14×10^{-5}	7	3.2	0.425	1.701		6955.55	8.91	14.40	
Pz12_deep		1.40×10^{-3}	3.412	4.10×10^{-4}	10	7	0.425	1.276		1.25	0.03	0.04	
Pz13	2	1.62×10^{-3}	2.968	5.46×10^{-4}	10	3.2	1.086	7.602	12.37	14.86	0.49	1.80	**54.93**
Pz14_shallow		1.48×10^{-4}	3.115	4.75×10^{-5}	7.15	3.2	1.039	4.313		2828.78	8.06	33.08	
Pz14_deep		3.97×10^{-4}	3.412	1.16×10^{-4}	10	7.15	1.039	2.962		2.31	0.02	0.05	
Pz15_shallow		5.34×10^{-5}	3.115	1.71×10^{-5}	6.65	3.2	1.036	3.783		2427.70	2.50	8.93	
Pz15_deep		3.62×10^{-4}	3.412	1.06×10^{-4}	10	6.65	1.036	3.472		0.15	0.00	0.01	
Pz16_shallow		3.46×10^{-5}	3.115	1.11×10^{-5}	7.7	3.2	1.034	4.859		3350.90	2.23	10.38	
Pz16_deep		2.33×10^{-4}	3.412	6.83×10^{-5}	10	7.7	1.034	2.378		0.15	0.00	0.01	
Pz17		1.43×10^{-4}	2.968	4.82×10^{-5}	10	3.2	0.928	6.499		67.56	0.20	0.96	
Pz18_shallow	3	5.09×10^{-5}	3.115	1.63×10^{-5}	6.8	3.2	1.230	4.674	21.29	75.20	0.07	0.33	**24.19**
Pz18_deep		9.60×10^{-4}	3.412	2.81×10^{-4}	10	6.8	1.230	3.936		4.40	0.07	0.29	
Pz19_shallow		5.69×10^{-5}	3.115	1.83×10^{-5}	6.7	3.2	1.116	4.130		1302.25	1.43	5.58	
Pz19_deep		1.67×10^{-3}	3.412	4.89×10^{-4}	10	6.7	1.116	3.684		7.90	0.23	0.85	
Pz20_shallow		9.62×10^{-5}	3.115	3.09×10^{-5}	6.5	3.2	1.003	3.509		2778.75	5.15	17.04	
Pz20_deep		2.68×10^{-3}	3.412	7.85×10^{-4}	10	6.5	1.003	3.509		0.60	0.03	0.10	

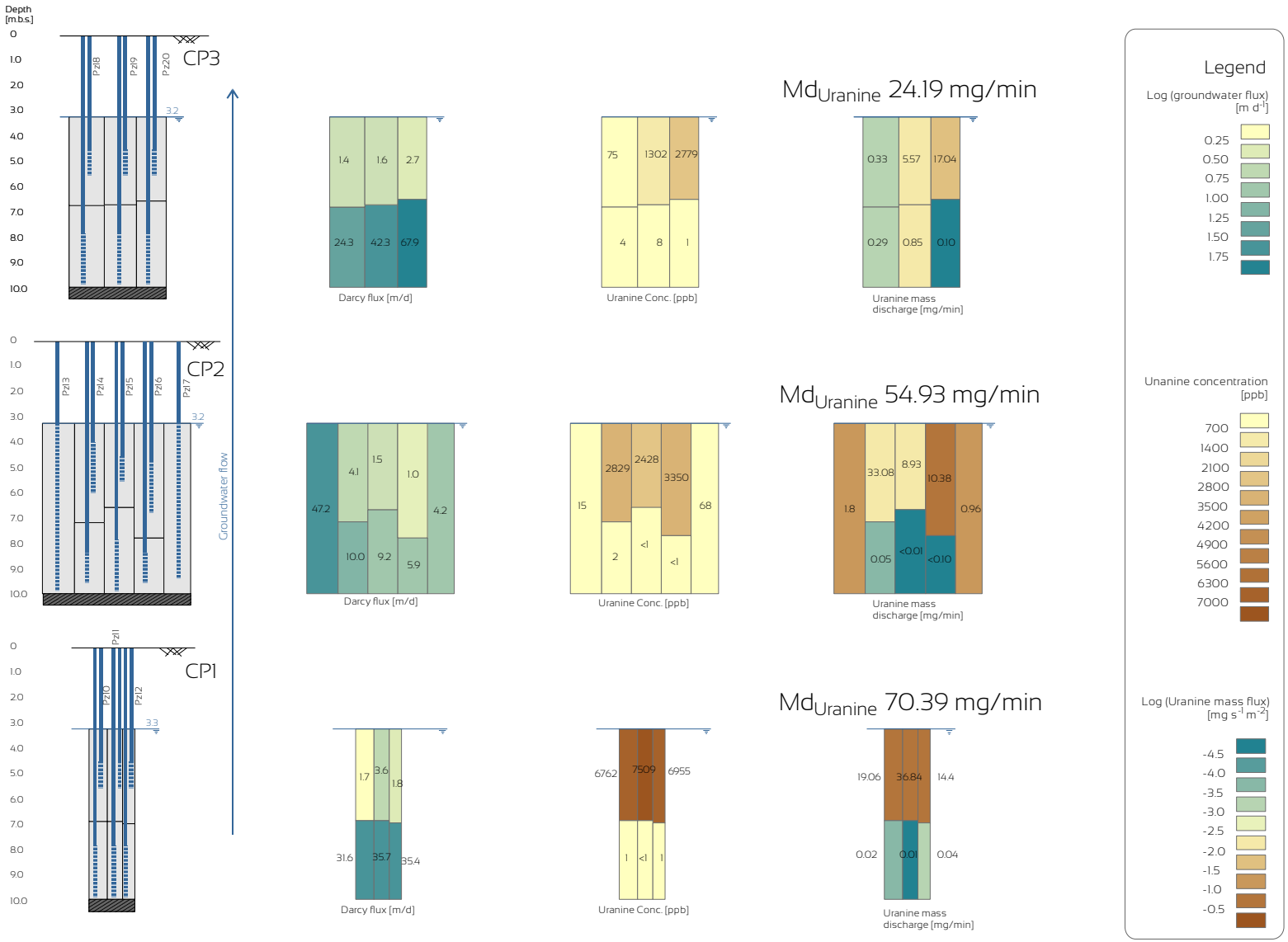

Figure 66: Results of groundwater flux and Uranine concentration measurements, and mass discharge calculations on the three control planes. The mass discharge recovery rates for control plane 1, 2 and 3 are 69, 56 and 24% respectively of the injected Uranine mass discharge. The highest mass discharges are always in the shallow part of the aquifer were the Uranine concentrations are higher despite lower groundwater fluxes.

4.2.3.3. Uranine concentration

Uranine concentrations measured in the 20 monitoring wells of the three control planes are gathered in Table 13. Uranine concentrations measured in the monitoring wells screened in the lower part of the aquifer were comprised between 0.2 and 7.9 ppb and in the monitoring wells screened in the upper part of the aquifer between 75.2 and 7509.2 ppb. Despite being sometimes low, the Uranine concentrations measured at deeper monitoring wells remained above the detection limit of the spectrofluorometer.

The highest Uranine concentrations were measured at CP1, closer to the injection monitoring well. Despite using a mixing pump at the injection well (Pz9) to homogenize the tracer injection on the whole thickness of the aquifer, only 1 ppb of Uranine was found in the monitoring wells screened in the lower part of the aquifer. Two factors can explain this observation. Primarily, the groundwater flux in the lower part of CP1 was 10 to 50 times higher than in the upper part and induced a higher dilution of the Uranine injected at Pz9 in the lower part of the aquifer. Secondly, a vertical structure was expected to be present in the area between Pz9 and the first control plane and could deviate the Uranine plume towards the upper part of the aquifer (Klepikova et al. 2016, Hoffman 2018 personal communication).

The same vertical heterogeneity is observed for Uranine concentrations at CP2. Results obtained at Pz13 and Pz17 must be considered carefully since these two monitoring well located at the ends of CP2 are screened on the whole thickness of the aquifer. Uranine concentrations measured on water samples retrieved by pumping did not correspond to a mean Uranine concentration over the vertical axis of the screen. They rather represented the different contributions of each layer of the aquifer in terms of groundwater flow rate and are consequently more influenced by the low concentrations coming from the more productive lower part of the aquifer.

At CP3, Uranine concentrations measured at the lower part of the aquifer at CP3 are higher than those measured in the other control planes. This can be due to the pump that is installed at the bottom of the pumping well and that creates a vertical hydraulic gradient directed downwards, thereby deviating the Uranine plume towards the deeper part of the aquifer at that location. Uranine concentrations showed an increasing from Pz18_shallow to Pz20_shallow. The Uranine plume seems to be deported towards Pz20_shallow and thereby not fully encompassed by the control plane.

4.2.3.4. Uranine mass discharge

Despite showing 10 to 20 times lower groundwater fluxes than those observed in depth, the upper part of the aquifer showed Uranine concentration three orders of magnitude higher than the lower part. Hence, 99% of the Uranine mass discharge measured at CP1 passed through the upper part of the aquifer. The highest Uranine mass discharge was calculated at Pz11_shallow which occupies a central position in the control plane. The total

mass discharge calculated at CP1 was 70.39 mg/min which represent 66% of the Uranine mass discharge injected at Pz9.

Calculated Uranine mass discharge showed the same spatial repartition at CP2 with the majority of the Uranine mass discharge passing through the upper part of the aquifer and the total Uranine mass discharge of 54.93 mg/min which represent 51% of the Uranine mass discharge injected at Pz9. This poor mass discharge balance could most probably be explained by an underestimated Uranine mass flux calculated at Pz13 and Pz17. At these two fully screened monitoring wells, groundwater flux and Uranine concentrations measurement are more representative by the low Uranine flux of the lower part of the aquifer. Another explanation can be that the CP2 is not wide enough to fully encompass the Uranine plume.

With significant measured Uranine concentrations measured, calculated Uranine mass discharges are slightly higher at the bottom of the aquifer at CP3 than at the CP1 and CP2 but are never more than 1 mg/min. The total Uranine mass discharge calculated at CP3 is 24.19 mg/min, only 23% of the Uranine mass discharge injected at Pz9. Even if the lateral spreading of the Uranine plume should be reduced close to the pumping well due to the radial converging flow, CP3 seem to be not wide enough to capture the whole Uranine plume, leading to an underestimated Uranine mass discharge.

4.2.4. General discussion

The error on the mass discharge calculated at each of the three control planes are 34, 49 and 77% for CP1, CP2 and CP3 respectively. These values are very similar to values from all the previous field studies on the subject that varies between 19 to 74% (Troldborg et al. 2012). Only Cain et al. (2011) quantified an error of less than 10% but with a control plane with (1) had a very high density of measurement points and (2) in a quite homogeneous aquifer. Despite being relatively low considering the limited spatial representativity of the available control planes, discrepancies between injected Uranine mass discharge and the Uranine mass discharge calculated need to be discussed.

First, the three available control planes have a limited width that certainly does not encompass the entire Uranine plume, leading to an under estimation of the Uranine mass discharge. The monitoring wells located at the ends of the control planes still show significant Uranine concentrations. This specifically for CP3 where the highest Uranine concentration is found on the right hand side monitoring well. A significant mass discharge is probably passing to the right of the third control plane.

Second, the spatial resolution of the control plane seems inappropriate relatively to the spatial heterogeneity of the aquifer. Kübert and Finkel (2006) insisted on the fact that the vertical and horizontal resolution of the control plane must be dimensioned according to the vertical and horizontal degree of heterogeneity of the aquifer. On the present experimental test site, the horizontal resolution of the control plane is reasonable but the vertical

resolution is relatively poor with respect to the high vertical heterogeneity of the alluvial aquifer. Uranine mass discharge calculated on these control plane of inadequate spatial resolution is thereby prone to low accuracy.

Third, the simple rectangular surface flow considered representative for each monitoring well of the control plane might not be relevant. A recent model of the Hermalle-sous-Argenteau alluvial aquifer carried out to better explain a heat and solute tracer test (Wildemeersch et al. 2014) only succeeded to represent the observed data when considering a smooth vertical variation of the hydraulic properties between the upper part and the lower part of the aquifer (Klepikova et al. 2016, Hoffmann, personal communication). Based on these observations, Inverse Distance Weight interpolation was tested on the three control planes (Figure 67). Uranine mass discharge calculated based on the interpolated values of groundwater flux and Uranine concentration are 90.1, 75.4 and 36.5 mg/min for CP1, CP2 and CP3 respectively, which represent a decreasing of 11 to 21% of the error on the mass discharge relative to the injected Uranine mass discharge.

Despite delivering less discrepancies between injected and measured Uranine mass discharges, these last results must be considered with care. Such interpolation can induce zones of combined significant groundwater flux and Uranine concentrations, potentially leading to artificially high Uranine mass fluxes. In CP1 the high groundwater fluxes measured at the bottom of the aquifer propagated upward while high Uranine concentrations measured in the shallow monitoring wells propagated downwards. This created a zone of high Uranine mass flux in the central part of CP1. Furthermore, CP1 might be located to close to the plume source to apply such smoothing methods. As mentioned by Troldborg et al. (2010, 2012) control planes located at a certain distance from the source (> 100 m) may allow for more accurate mass discharge calculation because spatial concentration distribution can be smoothed by local hydrodynamic dispersion leading to a smaller spatial variability of the contaminant mass flux. When the control plane is located closer to the source of solute, higher concentration gradients are likely to be observed leading to higher errors in case of low spatial resolution control planes. Smooth interpolation may be better suited for Uranine mass discharge at CP3, located further from the plume source.

Despite the potentially inadequate spatial resolution of the control plane, the Uranine mass discharge calculation gave results consistent with the Uranine mass discharge at the injection well and at the pumping well. The errors must be put in perspective with the general uncertainties of common hydrogeological measurement techniques such as pumping test or point to point tracer test (Suthersan et al. 2016). These results demonstrated that even with limited resources for the implementation of control planes, decent solute mass discharge results can be obtained.

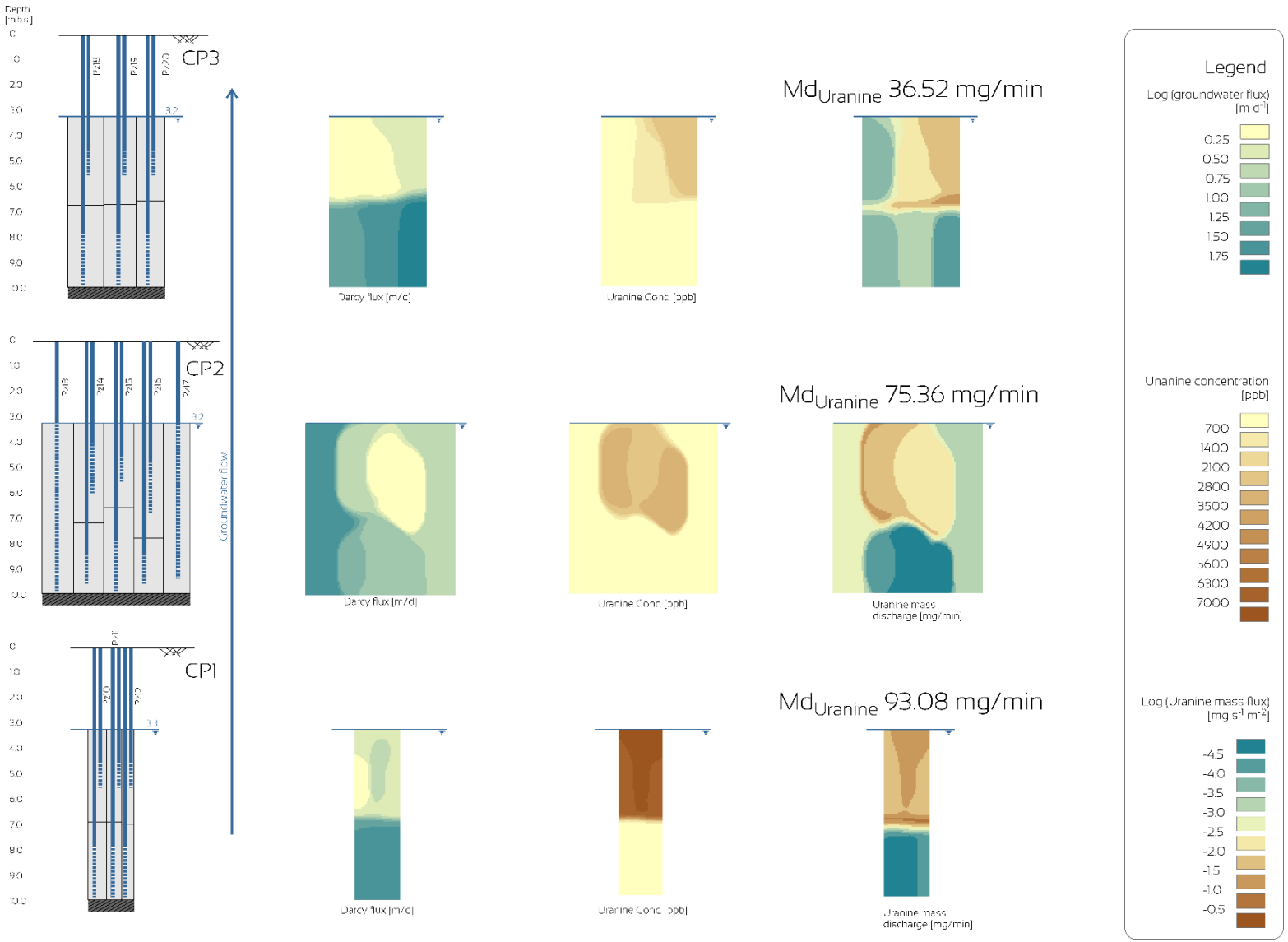

Figure 67: Interpolation of measured groundwater flux and Uranine concentration by Inverse Distance Weight on the surface of the control plane. Such interpolation can induce zones of combined significant groundwater flux and Uranine concentrations, potentially leading to artificially high Uranine mass fluxes as in CP1. Uranine mass discharge calculated with interpolated values showed less discrepancies with the injected Uranine mass discharge than the simpler rectangular interpolation schema.

As mentioned in section 1.4.3, numerous geostatistical methods exist to estimate the uncertainties on mass discharge calculations based on control plane and legitimate the mass discharge results. Nevertheless, applying joint geostatistical simulations (Li et al. 2007) or Bayesian geostatistical simulations (Troldborg et al. 2010), may not be relevant on the present limited dataset. These methods are described as suitable for relatively homogeneous aquifers and for control plane wide enough to capture the whole lateral extend of the solute plume. In this case, the high variance of the natural logarithm of the hydraulic conductivity of this site is 2.01 and lies in the upper limit of applicability of these methods (Troldborg et al. 2012). A better option would be to consider Monte Carlo simulations (Kübert and Finkel 2006) based on an existing model of the site of Hermalle-sous-Argenteau (Klepikova et al. 2016). Groundwater and solute mass flux results obtained in this study constitute an ideal basis for modelling applications. Such a modelling study can highlight the benefit of groundwater and solute mass flux measurements for model calibration.

4.2.5. Conclusion

This study relates the first solute mass discharge measurement at a series of control planes in a heterogeneous alluvial aquifer where a solute was injected at a controlled mass discharge. Results showed a high vertical variation of groundwater fluxes and solute concentrations in the alluvial aquifer. Despite based on a sampling array of monitoring wells that was not ideal regarding the spatial heterogeneity of the aquifer, solute mass discharge calculated at the 3 control planes were consistent with the solute mass discharge injected upgradient in the aquifer. It the present case wider control planes should have been installed to fully encompass the solute plume. Furthermore, a denser vertical distribution of measurement points is necessary to better characterize the solute plume vertically. The type of spatial interpolation of data form the multi-level well array of a control plane can have a significant impact on the calculated mass discharge value and the interpolation method should be chosen adequately.

This study showed the interest of the FVPDM for the measurement of solute mass discharge in aquifers. It also illustrated the importance of accurate and precise groundwater flux measurements that are too often disregarded when calculating mass discharge.

Further integration of these mass flux and mass discharge results into a numerical model is planned and will allow for the estimation of the uncertainties and for the illustration of the relevance of groundwater flux, contaminant mass flux and mass discharge measurements for model calibration.

4.3. Innovative contaminant mass flux monitoring in an aquifer influenced by tidal effects.

This section is based on the following publication:

Jamin, P., Cosme, F., Briers, P., Orban, P., De Greene, K. & S. Brouyère (2019). Monitoring of contaminant mass fluxes in an aquifer subject to tidal cycles. Submitted to Groundwater Monitoring and Remediation.

4.3.1. Introduction

Rivers and coasts remain convenient locations for industrial activities and large manufacturing plants due to access to transport, infrastructure and proximity to major urban centers. Nearby surface water courses, however, typically act as regional groundwater discharge zones, resulting in the discharge of contaminants generated by these activities, with potential risks for aquatic ecology residing in surface water and underlying benthic sediments, where biota is known to be very sensitive (Chen and Pinder 2011).

Exposure to contamination of these aquatic receptors is dependent upon the load of contaminant they might receive, namely contaminant mass discharge. Mass discharge depends simultaneously on the concentration in contaminants and on the extent of submarine groundwater discharge. This groundwater discharge occurs when the time averaged tidally influenced groundwater elevation is higher than the corresponding sea level elevation at the discharge point (Burnett et al 2006). Characterization of such groundwater flow systems can be challenging, especially in coastal environment where tidal fluctuations result in transient groundwater flow towards these receptors. This can also be further complicated by the high spatial heterogeneity of subsurface deposits enhanced by anthropogenic influence such as mixing of natural sediments and backfill materials, presence of subsurface built structures such as sheet pile walls or even occurrence of other sources of contaminant discharge (Keery et al. 2007, Rønde et al. 2017).

Quantification of contaminant discharge from groundwater to surface water should not be based solely on measured concentrations in groundwater and on averaged groundwater fluxes. Transient groundwater flow conditions strongly influence contaminant behavior by dilution, increasing solubility or degradation and subsequently their concentration at observation points (Trezzi et al. 2016, Bianchin et al. 2010, Robinson et al. 2009, Ensign et al. 2008, Brovelli et al. 2007, La Licata et al. 2007, Taniguchi 2002, Moore 1999, Squillace 1996). Mass flux estimates can substantially be improved, if groundwater fluxes are measured locally and explicitly considered instead of simple calculation of Darcy' law based on local hydraulic conductivity and gradient (Milosevic et al. 2012, Rein et al. 2009). Smart complementary methods allowing groundwater discharge quantification can be used but the key point in such transient environment it to dispose of high frequency observations enabling a fine characterization of the transient nature of groundwater flow conditions (Hatch et al. 2006, Kalbus et al. 2006, Ellis et al. 2007, Hyun et al. 2011, Dujardin et al. 2014).

These considerations allow to conclude that there is a need to address the risk posed by groundwater contaminations in coastal ecosystems using contaminant mass flux calculations (Li et al 2004). In such transient groundwater flow conditions, these calculations must be based on direct continuous groundwater flux measurements in order to capture the time variability of these transient flows. Conventional direct measurement of groundwater fluxes such as Point Dilution Method (Drost et al., 1968) are unable to quantify groundwater fluxes in transient flow conditions. Passive Flux Meters (Hatfield et al., 2004) provide averaged groundwater fluxes over the field deployment time. Other in-well techniques, including the Colloidal Borescope (Kearl et al. 1997), Acoustic Doppler Flowmeter (Wilson et al., 2001) and In-Well PVP (Osorno et al. 2018) require several hours of measurements to deliver acceptable results, a time frame not compatible with rapidly changing groundwater flow conditions.

The Finite Volume Point Dilution Method (FVPDM) (Brouyère et al. 2008) is better suited to monitor changes in groundwater flow as it can perform a direct continuous measurement of transient groundwater fluxes (Jamin and Brouyère 2018). The FVPDM was tested successfully in porous and fractured media (Brouyère et al. 2008, Goderniaux et al. 2010, Jamin et al. 2015), and showed high resolution and accuracy. Recently, Jamin and Brouyère (2018) developed the interpretation framework needed for monitoring groundwater fluxes over time using the FVPDM and demonstrated the ability of the method to monitoring highly transient groundwater fluxes.

The aim of this research is to validate the FVPDM as an innovative technique for monitoring tidal influenced transient groundwater fluxes and to demonstrate the high potential of the technique for flux-based characterization of contaminated aquifers. The methodology includes the use of the FVPDM for the monitoring of transient groundwater fluxes at 6 monitoring wells located in the coastal aquifer of concern. Groundwater samples were collected simultaneously to the groundwater flux measurements in order to quantify contaminant concentrations and further calculate contaminant mass fluxes. After a brief description of the environmental context of the contaminated site and of the existing conceptual site model, the methodology of continuous monitoring of contaminant mass fluxes is described. The significant benefits resulting from the use of the FVPDM and from such mass flux monitoring approaches are presented in the light of the results of the investigations. Groundwater flux monitoring with the FVPDM enabled a significant refinement of the conceptual site model, which highlights the great interest of the method for contaminated aquifers characterization.

4.3.2. Site description

4.3.2.1. Environmental setting

The investigated site is located on the south bank of an estuary and has been historically occupied by a metal processing facility. The activities have resulted in point like sources of groundwater contamination which are potentially confounded by more diffuse sources of contamination. The river consists of an inverse estuary where evaporation significantly exceeds the inflow of fresh water and has a semi-diurnal tidal cycle with two high and two low tides per day. A typical maximum daily tidal range is on the order of 2.5 m with a mean low tide of approximately -1.3 m above mean see level (ASL) and a mean high tide of approximately +1.2m ASL. Extreme spring tidal range can reach 3.44 m. The geology is reported to be composed only by Quaternary sediments. The base of the sequence is constituted of a thick (80 m+) clay layer that is overlain by a Holocene aged estuarine/coastal and aeolian clays, silts and sands layer of 6.5 m thick. The base clay is considered to be a regional aquiclude. The main natural groundwater flow occurs in the silty and sandy layers and discharges naturally into the river.

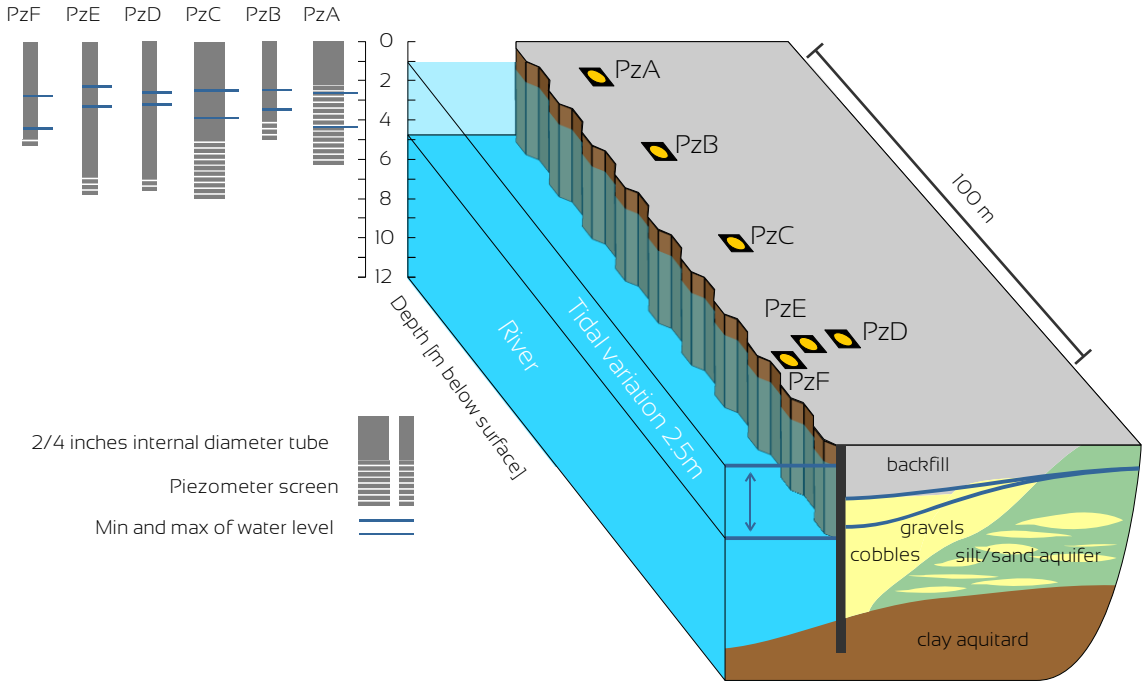

Figure 68: Cross section of the west side of the site in the area where a sheet pile wall separates the land from the river to create a wharf. The aquifer is made of silts, sands, slags and gravels, and is hydraulically connected to the river where tidal variations of 2.5 m occurs. The 6 tested monitoring wells are screened at different depth in the aquifer.

The area of interest for this study is the western border of the site, along the river, in the zone where a sheet pile wall (SPW) was installed to create a wharf (Figure 68). This wharf and the adjoining plant area are underlain by a hard stand and is therefore relatively flat with an elevation of approximately +3.5 m ASL. Upon construction of the SPW, materials of both anthropogenic and natural origins were used as backfills for the wharf basement, mostly river gravels and cobbles. The groundwater table in this zone is commonly found between 2.5 and 4.5 m below the surface. The gravels and cobbles unit underneath the wharf is the focus of the present study.

4.3.2.2. Existing conceptual site model

Piezometric maps at site scale based on measurements collected during low tide periods in 2012, 2013 and 2014 indicate that, in the area of the SPW, groundwater flows from East to West (Figure 69a). The gravels and cobbles composing the wharf backfill are considered to act as preferential flow path with groundwater flowing from South to North along the SPW, towards its northern end. According to the preliminary conceptual site model (CSM), the SPW is assumed to act as a low permeability barrier. However, the preliminary CSM mentions the presence of conduits, flaps and drains in the SPW for storm water evacuation, which have the potential to interact with the groundwater flow system in the area. Piezometric head data also indicate that tidal effects propagate with the wharf backfill along the SPW. However, the available data before this research do not allow to confirm if the transfer of pressure fully propagates along the SPW from North to South (hypothesis: the SPW is impervious) or, at least for some part, across the SPW (hypothesis: SPW not fully impervious).

The key contaminants of interest detected in groundwater **a**re manganese, cadmium, lead and zinc. Manganese and cadmium concentration data indicate an apparent decrease in concentration along the main groundwater flow direction along the wharf area from South to North. Five hypotheses were formulated to assist in understanding the decrease in manganese and cadmium concentrations along the groundwater flow path (Figure 69). (1) The plume has progressively migrated from South to North but has not reached the northern end of the sheet pile wall yet. (2) Progressive mixing occurs between the south-north oriented impacted groundwater plume and less contaminated groundwater coming from the East. This progressive mixing with lateral groundwater flow supports the decrease of concentration along the groundwater flow path. If this is the case, a progressive increase in groundwater fluxes should be observed from south to north (Figure 69b). (3) Tidal mixing effects contribute to mix episodically manganese and cadmium concentrations at the north edge of the plume. If tidal mixing is occurring, a more complex evolution of groundwater fluxes should be observed, with time-varying groundwater fluxes related to tides and inversion of groundwater flow direction at the northern edge of the SPW. During flow inversions, groundwater fluxes should be maximum at low tide, null at mid tide and high at high tide (Figure 69c). (4) A transfer of contaminant occurs through more permeable parts of the SPW (Figure 69d). (5) A combination of the above-mentioned hypotheses.

Based on this conceptual model, the present study was designed to contribute to answer to the three following questions. What are the magnitudes of groundwater fluxes? How do groundwater fluxes respond to changes in piezometric levels in relation with tidal effects? What are the mass fluxes of manganese, cadmium, lead and zinc in groundwater and the influence of tidal effects on the fate of these contaminants in groundwater in the area of the sheet pile wall?

To answer to these questions, single-well FVPDM tracer experiments (Brouyère et al. 2008) were undertaken to monitor the groundwater fluxes continuously during several tides cycles and to take samples simultaneously to quantify contaminant concentrations as a basis to estimate contaminant mass fluxes in the groundwater.

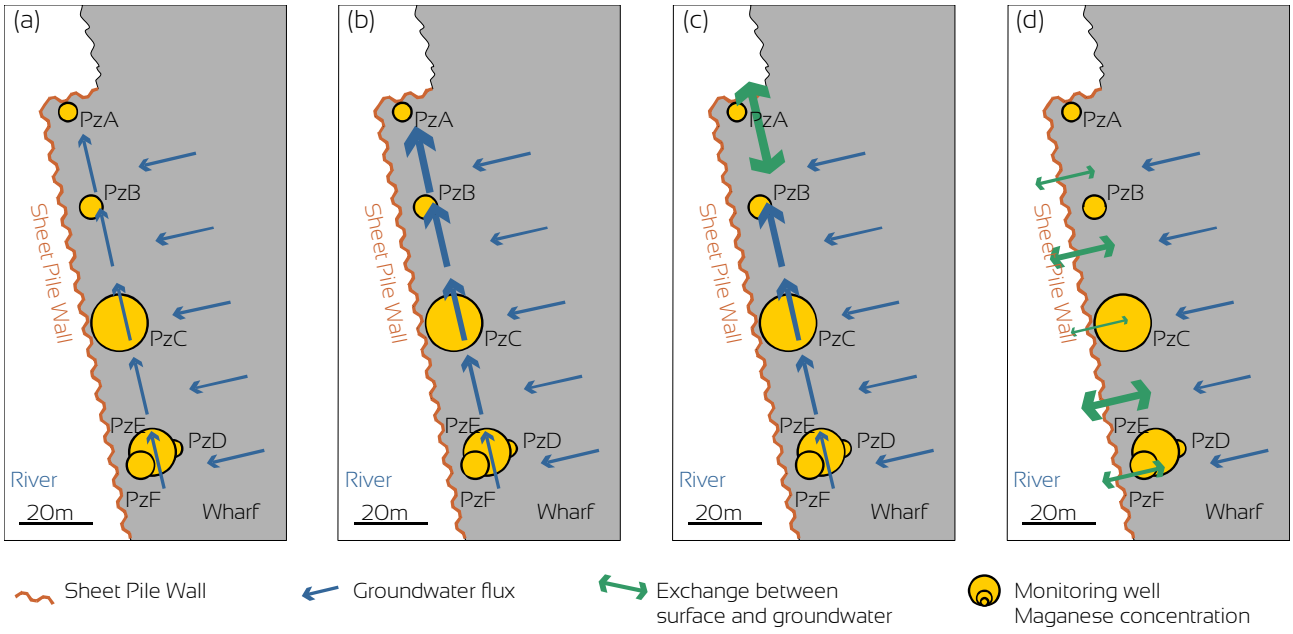

Figure 69: (a) Based on piezometric data, groundwater flows from East to West towards the SPW where it directs to the northern edge and probably discharges to the river. The decrease of manganese concentrations from PzC to PzA can be explained by 5 different hypotheses. (a) The plume has progressively migrated from South to North but has not reached yet the northern end of the sheet pile wall. (b) Progressive mixing occurs between groundwater plume and less contaminated groundwater coming laterally from the East. In this case, a progressive increase in groundwater fluxes should be observed from south to north. (c) Tidal mixing effects contribute to dilute episodically manganese concentrations at the north edge of the plume. If tidal mixing is occurring, time-varying groundwater fluxes during the tides in the river and inversion of groundwater flow direction at the northern edge of the SPW should be observed. (d) A transfer of contaminant occurs through more permeable parts of the SPW. A combination of these above-mentioned hypotheses can also be considered.

4.3.3. Materials and methods

4.3.3.1. Experimental setup

The general FVPDM setup used for this series of field experiments was as follows (Figure 70):

1. A mixing pump and circulation loop to ensure homogeneous tracer concentration in the tested well. The pump was a centrifugal surface pump with an approximate flow rate of 10 L/min.

2. A peristaltic pump used to inject the tracer inside the circulation loop at a precise and constant low flow rate ranging from 20 mL/min to 400 mL/min, from one monitoring well to another.

3. A field fluorometer (Schnegg GGUN FL30 fluorometer coupled to a Tetraedre TRMC-5 data logger) for direct, continuous and simultaneous measurements of fluorescent dye tracer, temperature and turbidity. The fluorometer was placed in line in the circulation loop and the tracer was Uranine (CAS n° 518-47-8).

4. A valve placed on the circulation loop, allowing to take groundwater samples for further chemical analysis of metal concentrations (Mn, Cd, Pb, Zn).

5. A pressure probe (Schlumberger CTD Diver) placed in the monitoring well to monitor changes in piezometric levels and electric conductivity during the FVPDM experiment. An identical probe was installed in the river and recorded the changes in river levels due to tidal cycles during the whole duration of the field campaign.

During an FVPDM experiment undertaken to monitor transient state groundwater flow, each variation of the tracer concentration in the tested well can be interpreted as resulting from a change in groundwater flux in the aquifer. When groundwater flow increases in the aquifer, tracer dilution in the well increases, and the measured concentration decreases. Conversely, when groundwater flow decreases in the aquifer, tracer dilution in the well decreases, and the measured concentration increases (Jamin and Brouyère 2018).

Laboratory experiments were conducted previously to the field campaign, in order to verify the influence of the physical and chemical composition of groundwater in the aquifer on the measurements of dye tracer with fluorometers (Magal et al. 2008). Salinity, temperature and concentration of metals in the proportions observed in groundwater from the site are unlikely to influence the measurement of Uranine concentrations.

To quantify groundwater fluxes, a total of 9 FVPDM were undertaken on the 6 monitoring wells of the wharf (Pz A to F), along the SPW to obtain a transect of groundwater fluxes along the inferred pathway towards the river. Tested wells are listed in Figure 68. Setup details for each experiment are given in Table 14.

Table 14: Experimental setup and data of the FVPDM experiments performed at the site.

Monitoring well	#	Duration [hours]	Q_{inj} [L/min]	Q_{mix} [L/min]	C_{inj} [ppb]	Nb of collected samples
PzA	1	51.17	0.14	9.00	232	5
PzA	2	45.08	0.05	6.00	500	11
PzB	1	36.50	0.11	7.00	502	7
PzC	1	21.80	0.15	11.00	466	4
PzC	2	16.83	0.40	5.00	1000	7
PzD	1	24.17	0.02	6.00	258	8
PzE	1	48.08	0.16	4.00	251	12
PzF	1	45.58	0.15	4.00	247	11
PzF	2	24.08	0.02	3.00	258	9

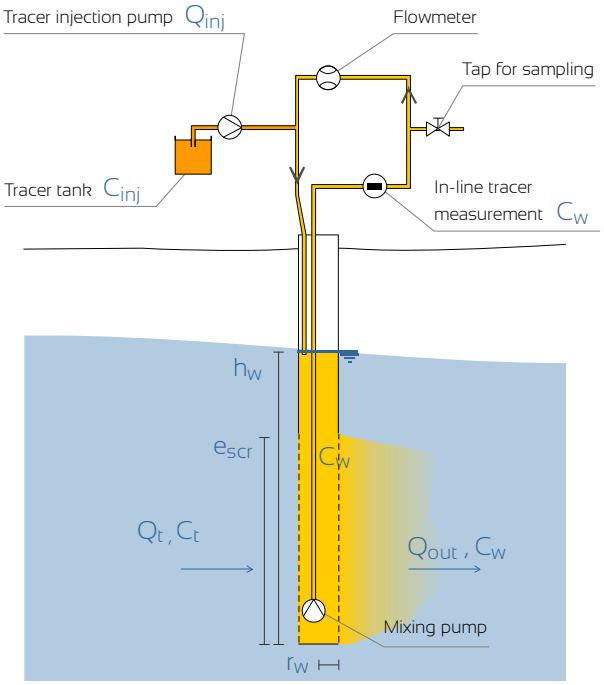

Figure 70: The FVPDM experimental setup comprises two pumps, a pump for injecting the tracer within the tested well at a controlled low flow rate and a pump used to ensure a good mixing of the tracer concentration in the well. In the present study, the fluorescent dye tracer concentration was measured using a field fluorometer placed inline on a circulation loop. A tap placed on the loop was used to retrieve groundwater samples for contaminant concentrations analysis.

4.3.3.2. Interpretation of the results

The interpretation of each FVPDM test was carried out in three parts. First, the experimental data and measurements were gathered to form continuous time series. Occasional gaps in the time series were filled by linear interpolation to obtain a more systematic dataset with a time step of 1 minute. All the time series were plotted to visualize the time evolutions of all parameters and to perform a visual check for potential inconsistencies. In a second step, a comprehensive interpretation of the FVPDM test was performed under transient groundwater flow conditions using the transient FVPDM solution (Jamin and Brouyère 2018) to deliver a value of groundwater flux at each measurement time step. Interpretation results were displayed graphically along with the evolution of tracer concentration in the tested well, groundwater and river level at the time of the experiment. Finally, contaminant mass fluxes were calculated for times where a groundwater sample was collected and multiplied by the measured groundwater flux at the corresponding time (IRTC 2010). Estimated mass fluxes are summarized and presented as median values for each tested well. No mass discharge calculation could be performed by the integration of these mass flux results on representative cross-sectional flow area because of the uneven distribution of monitoring wells along the contaminant plume and of the strong variability of both contaminant concentration and groundwater fluxes in the subsurface.

4.3.4. Results and discussion

4.3.4.1. Groundwater fluxes

The result of the monitoring of transient groundwater fluxes by the FVPDM is shown in Figure 71 for PzC and in Figure 72 for the PzE. For the sake of clarity, only these two FVPDM are described in detail. The results of groundwater flow monitoring are summarized in Figure 73.

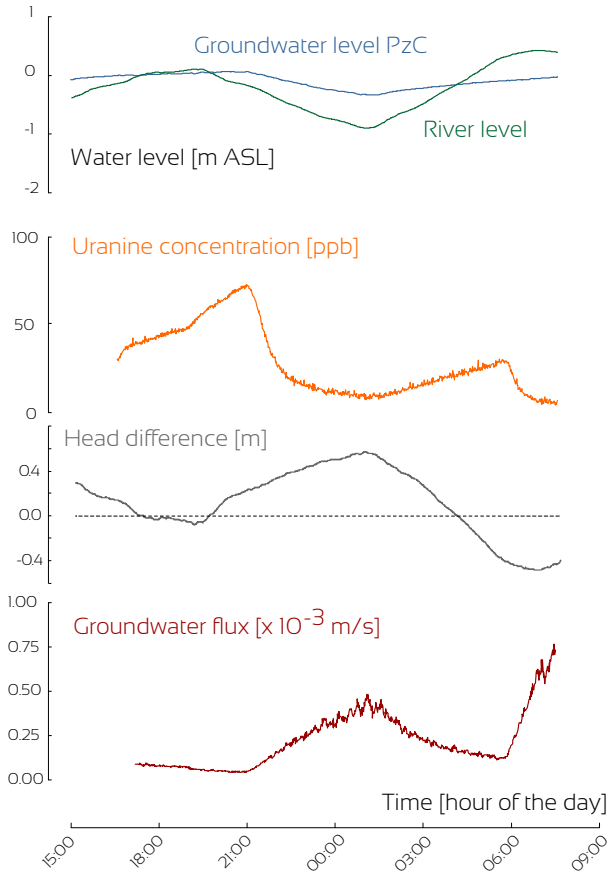

Figure 71: Groundwater fluxes calculated at PzC ranged from 4×10^{-5} to 7.5×10^{-4} m/s with a median value of 1.8×10^{-4} m/s. The head difference corresponds to difference between the piezometric head in the monitoring well and the water level in the river.

Estimated groundwater fluxes at PzC ranges from 4×10^{-5} to 7.5×10^{-4} m/s with a median value of 1.8×10-^{4} m/s. The maximum groundwater fluxes obtained during this test coincides with the maximum hydraulic gradients, regardless of the variations in the river level. A second FVPDM experiment was carried out in the same monitoring well a few days after, during a neap tide period. This second experiment lasted for 16 hours and recorded groundwater fluxes up to 2.88×10^{-3} m/s which was the highest flux measured at the site. That emphasized the importance of spring and neap tide on groundwater fluxes.

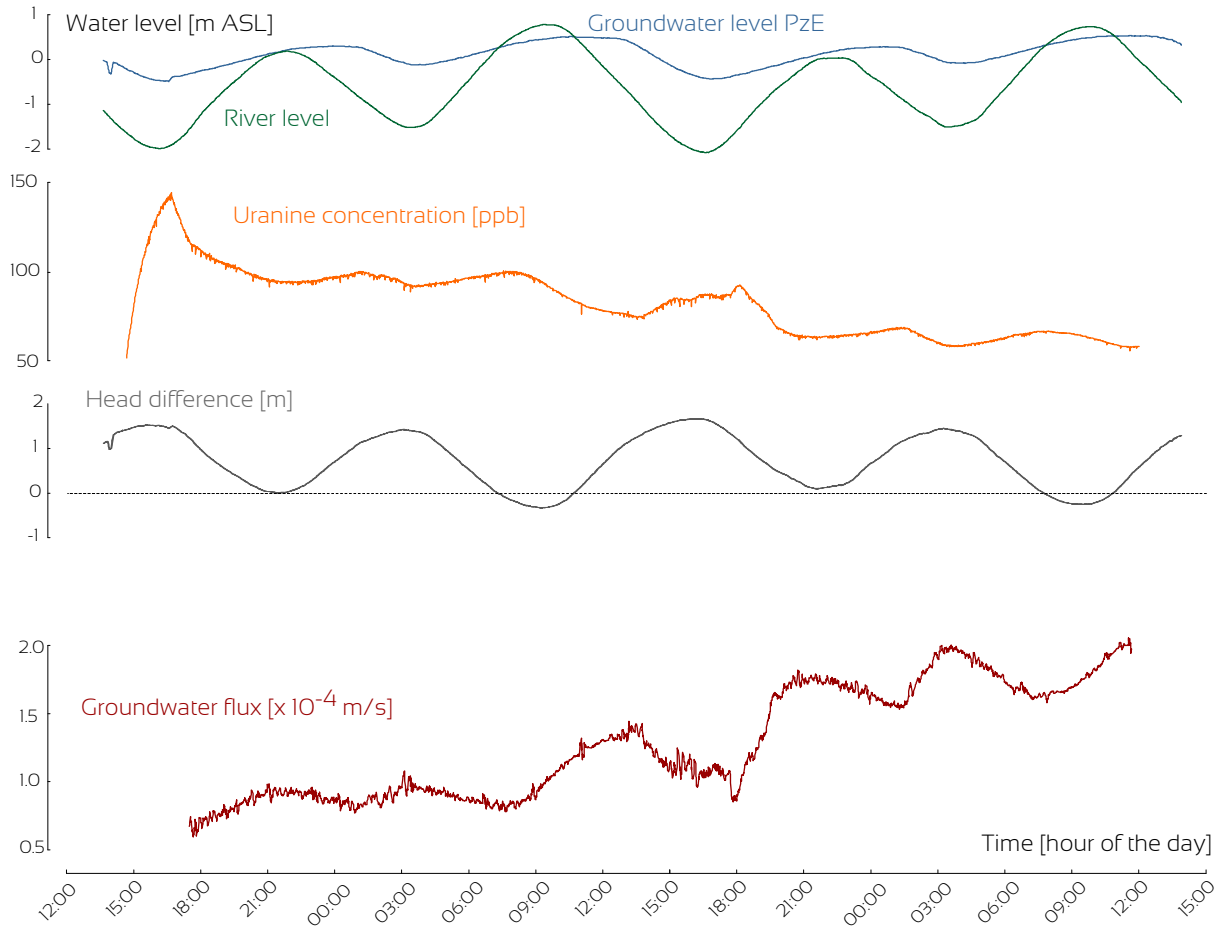

Figure 72: Groundwater fluxes calculated at PzE range from 0.6×10^{-4} to 2.1×10^{-4} m/s with a mean value of 1.1×10^{-4} m/s. The head difference corresponds to difference between the piezometric head in the monitoring well and the water level in the river.

Groundwater flux calculated from the FVPDM undertaken at PzE range from 0.6×10^{-4} to 2.1×10^{-4} m/s with a median value of 1.1×10^{-4} m/s. The relationship between the groundwater flux at PzE and the hydraulic gradient between the well and the river seems somehow cyclic. Maximal groundwater fluxes seemed to coincide with periods when the head difference between the river and the piezometric level in the well is larger. Moreover, the river level remained lower than the piezometric level at PzE during two high tide cycles of the FVPDM experiment. During that period, the groundwater flux could be particularly high due the fact that the hydraulic gradient between the river and the piezometric water level at PzE was not inverted at high tide. The gradient was hence oriented towards the river during 2 tide cycles and potentially lead to higher groundwater fluxes.

Complete results of all groundwater fluxes measured in all the monitoring wells are summarized in Figure 73 and Table 2. The mean groundwater flux measured at all the tested wells is on the order of 10^{-4} m/s, except for well PzD where groundwater fluxes are significantly lower, with a median value of 2.5×10^{-6} m/s. The maximum groundwater flux (2.9×10^{-3} m/s) was measured at well PzC low tide in the river. The range of groundwater flux

variations between high and low tide is quite limited to ± 0.5 10^{-4} m/s at most wells (PzB, PzE, PzF). For wells PzA and PzC, groundwater fluxes can vary by an order of magnitude. Those two wells are the more sensitive to changes in river levels, supporting the hypothesis that they have a preferential connection with the river in comparison with the other wells. At PzD, groundwater fluxes remained consistently low and did not show much variations with time.

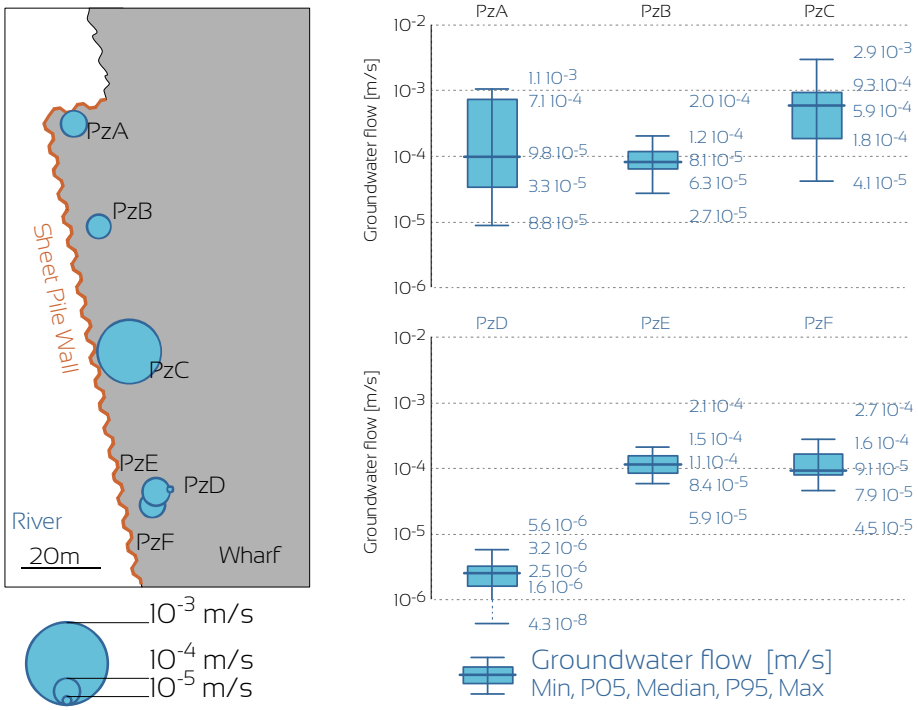

Figure 73 : Median groundwater fluxes measured at all the tested wells is in the order of 10^{-4} m/s. The overall lowest groundwater flux value was measured at PzD at a median value of 2.5×10^{-6} m/s and the highest flux at PzC at a median value of 5.9×10^{-4} m/s.

4.3.4.2. Concentrations of heavy metals in groundwater

Manganese, cadmium, lead and zinc are the four contaminants of interest. PzC and PzE usually showed the higher concentrations in these metal species (Figure 74).

At PzC, concentrations range from 11.6 to 16.44 mg/L for manganese, from 32.2 to 43.6 mg/L for cadmium, from 0.3 to 6.5 mg/L for lead and from 51 to 77.1 mg/L for zinc. The minimum and maximum concentrations are not observed simultaneously (i.e. in the same groundwater sample) for the four analyzed metals in PzC. The concentrations do not seem to vary according to tides.

At PzE, concentrations range from 7.5 to 13.59 mg/L for manganese, from 0.65 to 22.56 mg/L for cadmium, from 0.1 to 0.6 mg/L for lead and from 2.8 to 38.43 mg/L for zinc. The lowest concentrations of these four metals were found in the first groundwater sample taken at the beginning of the experiment and the highest concentration is found simultaneously in the same groundwater sample taken approximately 24 hours after the beginning of the experiment. Once again, the concentrations do not seem to vary according to tides.

Maximum concentrations measured at each monitoring well are mapped in Figure 74. They are systematically observed at PzC and, to a lesser extent, at PzE. PzB and PzD show the lowest concentrations and PzA and PzE always show intermediate concentrations. There is no evident influence of tide events on the concentrations of metals monitored in the aquifer.

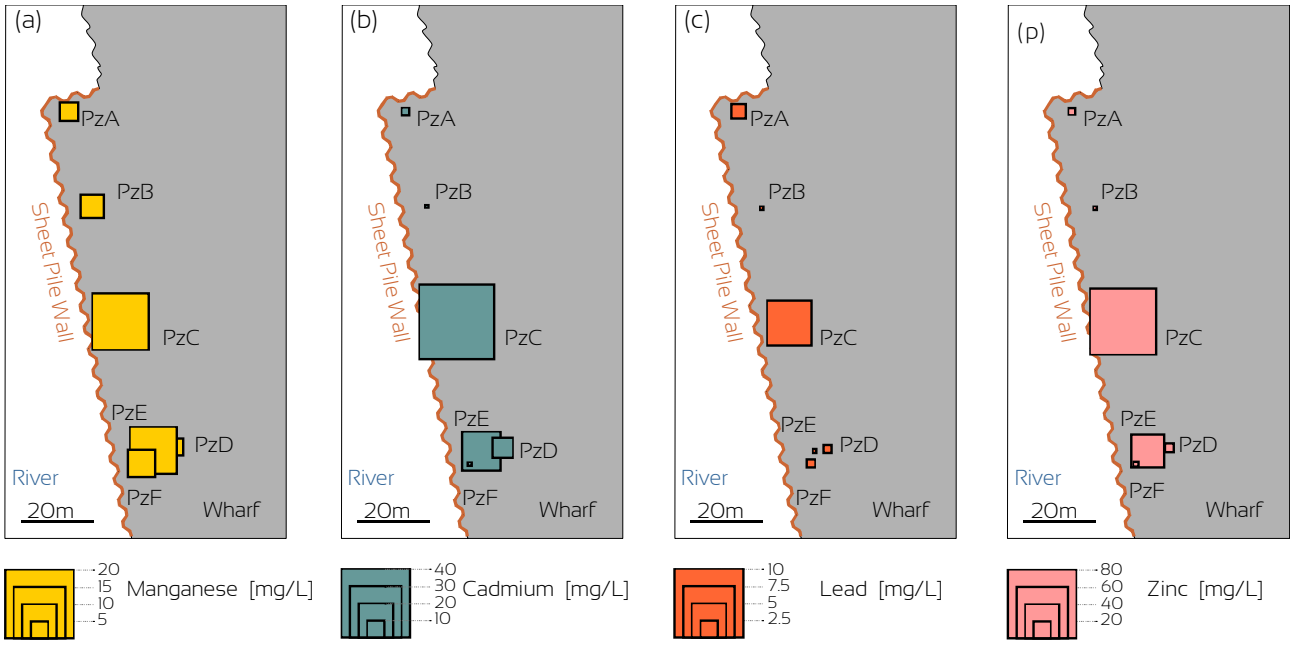

Figure 74: Results of the chemical analysis of metals in groundwater samples taken during the FVPDM tests. The size of the symbols represents the maximum concentration in manganese, cadmium, lead and zinc in groundwater. PzB and PzF generally show the lowest concentrations and PzC shows the highest metal concentration.

4.3.4.3. Contaminant mass fluxes

Combination of groundwater fluxes and metal concentrations were used to estimate mass fluxes of metals (in gram per day per square meters). Due to higher groundwater flux and higher metal concentration, monitoring well PzC shows the highest contaminant mass flux of the tested wells. The estimated mean solute mass flux ranged from 1 to 2401 g/day/m² in cadmium, from 2.3 to 770 g/day/m² in manganese, from 0.5 to 85.9 g/day/m² and from 2.2 to 4343 g/day/m² in zinc (Table 15). Lower mass fluxes were estimated at monitoring wells PzB and

PzD (Figure 75). These results are only representative of the conditions in close vicinity of the tested well and cannot be extrapolated to a representative flow area to estimate mass discharge for the broad contaminated area.

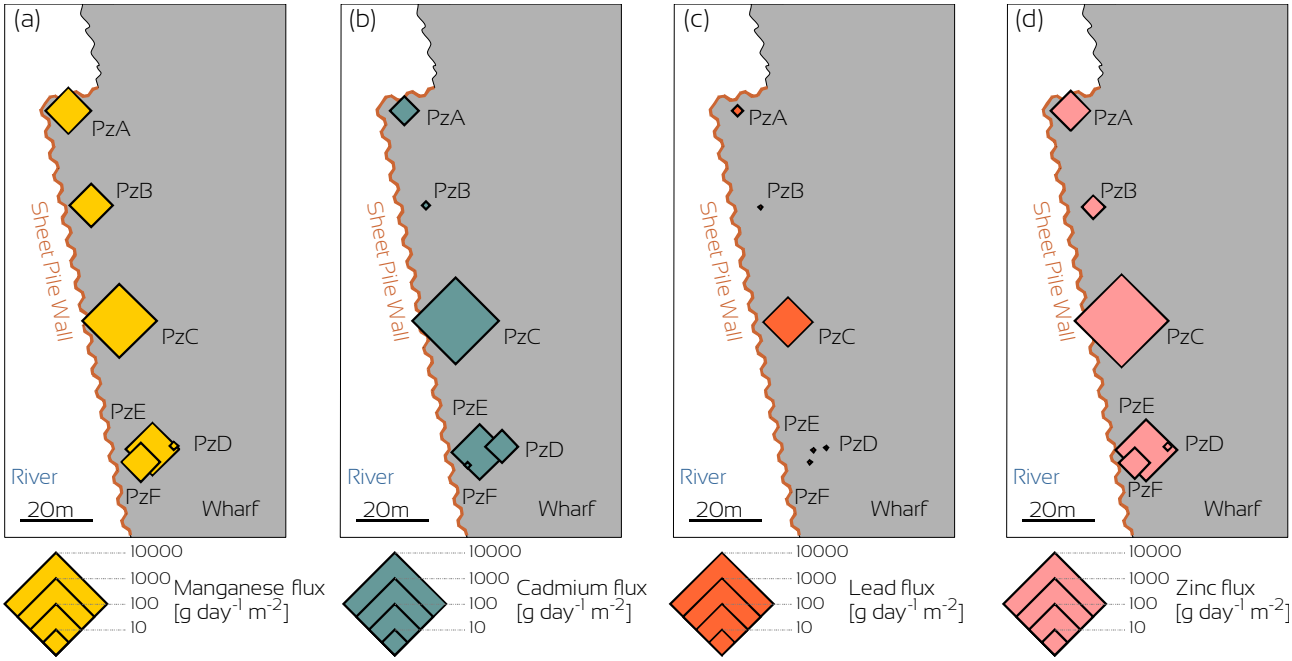

Figure 75: Median mass fluxes of manganese, cadmium, lead and zinc obtained by combining groundwater fluxes and metals concentrations measured during the FVPDM experiments. PzC gathers 93% of total manganese, cadmium and zinc mass flux and 75% of lead mass flux measured among the tested monitoring wells.

Table 15: Summary of the results of median value obtained for groundwater fluxes and mass flux in manganese, cadmium, lead and zinc.

Monitoring well	Median of measured groundwater flux [m/s]	Maximum groundwater flux during	Median of calculated Mn mass flux [g/day/m^2]	Median of calculated Cd mass flux [g/day/m^2]	Median of calculated Pb mass flux [g/day/m^2]	Median of calculated Zn mass flux [g/day/m^2]
PzA	9.8×10^{-5}	Low river level	63.0	13.4	2.7	35.4
PzB	8.1×10^{-5}	Low river level	49.1	2.1	0.7	8.3
PzC	5.9×10^{-4}	Low river level	770.1	2401.2	85.9	4343.7
PzD	2.5×10^{-6}	No correlation	2.3	0.7	0.5	2.2
PzE	1.1×10^{-4}	No correlation	114.7	148.6	0.7	251.7
PzF	9.1×10^{-5}	No correlation	32.9	19.2	1.2	16.5

4.3.5. Discussion

4.3.5.1. Benefits of continuous groundwater flux monitoring by FVPDM

Quantitatively, groundwater fluxes are found to be more important than expected. Using hydraulic conductivity (derived from slug test data) and hydraulic gradient data, the initial estimate of groundwater flux was 10^{-6} m/s. Based on the FVPDM measurements, the estimated median groundwater flux is on the order of 10^{-4} m/s, which means two orders of magnitude higher, with a maximum of 3×10^{-3} m/s at PzC during a low tide event. This emphasizes the necessity of direct in-situ groundwater flux measurements, especially in coastal aquifers affected by transient groundwater flow conditions.

Tide influence on groundwater flux variations are not as marked as expected. The two monitoring wells showing the largest range of variations are PzA and PzC, with maximal groundwater flux almost synchronous with low tides. Monitoring well PzE shows more complex variations of groundwater fluxes, with maximal values observed at high and low tides, with a slight time lag. For the other monitoring wells, variations of groundwater fluxes do not seem correlated with tide variations observed in the river. Even in the wells that exhibited the most significant groundwater fluxes variations (PzA, PzC), no clear evidence of an inversion of the groundwater flow direction was observed that would have resulted from river water infiltration in the wharf backfill. If it had been the case, the groundwater fluxes should have decrease to almost zero which has never been observed by the FVPDM experiments. This is certainly due to combined effect of strong groundwater discharge from inland and of the flaps present in the sheet pile wall preventing sea water intrusion in the aquifer when closed at high tide.

The nature of the tide also plays and important role on groundwater fluxes. Comparison between the two FVPDM performed at PzA revealed than groundwater fluxes may be 10 times lower during small amplitude tides (neap tides) than during high amplitude tides (spring tides). Unfortunately, PzA and PzC could not be tested during high amplitude tides due to restricted access to the wharf at these moments. FVPDM measurements in such a period could have revealed higher groundwater fluxes than those measured.

4.3.5.2. Benefits of contaminant mass fluxes compared to concentrations measurements

Metal concentrations measured in the groundwater vary between tested wells by more than 3 orders of magnitude. This supports the heterogeneous nature of the aquifer and the variability in groundwater flow conditions including groundwater flowing from inland. The highest concentrations are observed in PzC while contamination in the vicinity of well PzD seems limited. Variations with time of pollutant concentrations do not show any clear correlation with tidal events.

At monitoring wells PzA, PzE and PzF, the contaminant mass flux is around 10 to 100 g d^{-1} m^{-2}, while it is around 1 g d^{-1} m^{-2} at PzB and PzD. The maximum cadmium and zinc mass flux measured at PzC is on the order of 2 to 4 kg d^{-1} m^{-2}. Although the concentrations in cadmium and zinc measured at PzC are double those measured at PzE, the median cadmium and zinc mass fluxes calculated at PzC are more than 15 times higher at PzE. In general, the mean manganese, cadmium and zinc mass fluxes estimated at PzC are 7 to 3500 times higher than at other monitoring wells due to a combination of significant contaminant concentrations and high groundwater fluxes.

Spatial variability of calculated solute mass fluxes allows to suggest that contaminant transfer within the aquifer should be considered as localized channel flows, at least in the area of the monitoring well PzC. Among the zones of the wharf where contaminant mass fluxes were measured, the zone around PzC is the zone that contributes more to the risk for the river. Further investigations and risk reduction measures must focus on this zone for the threat it represents for the river.

4.3.5.3. Update of the conceptual site model

Based on the present results of the groundwater flux monitoring by FVPDM and of contaminants mass fluxes calculation, a revised CSM can be proposed. According to the previous CSM that considers the SPW as impervious, groundwater fluxes and contaminant mass fluxes should increase from South to North. There is no evidence of a regular increasing of the groundwater fluxes and of the contaminant mass fluxes from South to North.

Spatial distribution in groundwater fluxes along the wharf and groundwater flow dynamics supports the hypothesis of a groundwater flow system controlled by groundwater flow coming from inland rather by tidal changes. Furthermore, it can be considered that the SPW is not completely impervious and that direct discharge of contaminant mass fluxes from the aquifer into the river can occur through specific points of the sheet pile wall. The very high contaminant mass flux calculated at monitoring well PzC could thereby discharge directly into the River. This hypothesis is supported by field observations during which bubbling is observed in the river at low tide along with the measurement of higher metal concentration in the surface water in the zone of the PzC. Finally, spatial variability of solute mass fluxes suggests that contaminant transfer within the aquifer should be considered as localized channel flows, at least in the area of the monitoring well PzC.

4.3.6. Conclusions

This study constitutes the first real case application of the FVPDM to monitor natural transient groundwater fluxes at a contaminated site. With the same experimental setup and adjustment of the experiment parameters, the method was able to capture variable groundwater fluxes on a range of 4 order of magnitude, from 10-7 to 10-3 m/s, with a variation cycle between the highest and the lowest measure values of approximately 12 hours. This constitutes also the first practical application of the FVPDM as the basis for contaminant mass fluxes measurements.

The use of the FVPDM as the basis of contaminant mass flux measurement allowed to refine and improve significantly the conceptual site model. The strong spatial variability in the measured groundwater and contaminant fluxes supports the hypothesis of a pervious sheet pile wall and the direct discharge of contaminant from the aquifer into the river through specific points of the sheet pile wall. The relevance of contaminant mass flux measurements in addition to concentrations measurements for contaminated aquifers characterization is here emphasized. Among the tested monitoring wells contaminant concentrations varied only by an order of magnitude. However, contaminant mass fluxes that are more directly related to the risk assessment of the contamination varied by more than 3 orders of magnitude. Such valuable results allowed to focus further characterization and risk mitigation efforts on specific zones of the aquifer in order to significantly reduce the risk for the river ecosystems.

The general conclusion of this study is that the Finite Volume Point Dilution Method is a robust method for monitoring rapidly changing groundwater fluxes. FVPDM is an innovative technique that can be used as a reliable basis for contaminant mass fluxes measurements and monitoring even under highly transient conditions. Finally, this study proves once more the value of undertaking mass flux measurements for characterization of contaminated sites, risk assessment and design of risk mitigation measures.

General conclusion and perspectives

Synthesis of the main research outcomes

The general objective of the present study was to evaluate the potential of the Finite Volume Dilution Method for measurements of groundwater fluxes. A significant number of FVPDM experiments were performed under a very wide range of operational conditions.

FVPDM was applied in four different countries across the globe: Belgium, France, Canada and Australia. Hydrogeological conditions varied from relatively homogeneous and porous to very heterogeneous fractured aquifers. Tested aquifers were made of alluvial plain gravels, glacial sands, recent backfill materials or fractured granites. FVPDM experiments were undertaken at lab scale to validate the method to full field scale applications in various environments: urban and industrial areas up to harsh and remote natural territories. The application of the FVPDM ranged thus from pure fundamental research purposes to consultant-type field measurements and monitoring of groundwater fluxes, proving thereby the economic potential of the method. Finally, the FVPDM was successfully applied for point-type measurements of groundwater fluxes in steady state flow conditions but also for monitoring during several days of groundwater fluxes in transient flow conditions with variation time scales ranging from minutes to days.

Climatic conditions in which the technique was applied varied from cold environment with less than -5°C to warmer conditions up to 35°C. The used methodology comprised simple experimental setup to more advance configurations including the use of devices limiting vertically the zone of investigation. These devices were made of on-purpose hand-built supple joins to complex systems of double inflatable packers. From an operational point of view, a wide variety of pumps were tested whether for injecting the tracer or for mixing the water column in the well. Electromagnetic dosing pumps, syringe pumps, peristaltic pumps, surface impeller pumps, bladder pumps or submersible centrifugal pumps, all were evaluated and approved for specific FVPDM applications. The FVPDM was applied in monitoring wells of minimum 1.5 inches of internal diameter to 4 inches wells and in screened to uncased wells. The depth of the tested monitoring wells ranged from 0.5m up to 80 m. The shortest FVPDM

experiment performed during this research lasted for 20 minutes while the longest monitoring was carried out during more than 5 days.

Quantitatively, groundwater fluxes measured during this research ranged from 3.7×10^{-3} m/d to $3.3\times10^{+3}$ m/d, which is 6 orders of magnitude. However, measuring groundwater fluxes lower than 0.1 m/d using the FVPDM technique may be challenging because of the time required for the tracer concentrations to stabilize in the well. This does not constitute a limitation of the FVPDM technique from a physical or technical point of view, but only from an operational point of view. On the other hand, there is no theoretical maximum groundwater flux that could not be measured by the FVPDM. The uncertainties on the Darcy flux measured by the FVPDM came from ±41% in cases of very short experiments that were not ran long enough to reach the stabilized tracer concentration to ±1% for ideal field experiments. The best uncertainty value of 0.18% was achieved for a FVPDM experiment carried out in strictly controlled laboratory conditions. The accuracy of the FVPDM was also quantified during laboratory experiments. The difference between the actual water flux and the water flux measured by the FVPDM was as low as 0.15%. In general, the accuracy of the FVPDM can be claimed of ±5% for both steady state and transient groundwater fluxes measurements. The method was also demonstrated to be very sensitive to very small changes in groundwater fluxes even on periods as short as 5 minutes.

Conclusions

All the mathematical, laboratory and field developments and applications undertaken during this PhD allow to conclude that the Finite Volume Point Dilution Method is a reliable method for measurements of groundwater fluxes. The method provides precise and accurate results for measurements of groundwater flux in both steady and transient state flow conditions. It can be used for fast point type measurements up to long term continuous monitoring. The great strength of the FVPDM comparing existing groundwater fluxes measurement methods is its ability to monitor rapidly changing groundwater fluxes due to a fine sensitivity. The method also dispose of a wide range of application in terms of minimum and maximum measured groundwater fluxes.

From an operational point of view, the FVPDM was proven to be very robust and versatile. The different experimental setups used during this PhD for measuring groundwater fluxes in specific environments such as at precisely located fractures in large open boreholes, in deep and small diameter monitoring wells or in more common shallow wells demonstrated the on the broad spectrum of field conditions in which the method can be applied.

Finally, from a more general perspective, this research demonstrated the importance and the huge benefits of having direct and reliable in situ measurements of groundwater fluxes for any kind of hydrogeological studies. This research also proves once more the value of undertaking mass flux measurements for characterization of contaminated sites, risk assessment and design of risk mitigation measures.

Perspectives

Even if this research fully validated and extensively developed the FVPDM method for the measurement and the monitoring of steady state and variable groundwater fluxes, many perspectives of development and applications can still be considered. They can be relative to technical developments, methodological improvements or innovative applications.

One of the first technical advance that one can consider is a better integration of the experimental setup. Up to now, the FVPDM experiments have been performed using generic pumps, hoses and connections that were assembled directly in the field. A better integrated system can be imagined where all the pumps, connections, measurement devices and data logger are gathered in a compact and mobile box rapidly installed in the field. The only required field manipulation would thus be the connection of the circulation loop and of the tracer tank by means of quick coupling connections before pressing the start button. Such an integrated system will not only allow to save time in the field but it will also decrease the risk of leaky connections that can happen when all the pumps, pipes and junctions have to be assembled in the field. From the perspective of a monitoring of groundwater fluxes, a key development would concern the management of data resulting from the test. The data logger of the integrated system could be connected to the cellular network and thereby deliver real-time data and groundwater flux results. This connection would also allow a distant management of the experiment and instantaneous notifications in case of mechanical failure and measured values exceeding predefined thresholds.

This integrated conception of the FVPDM experimental setup can be pushed further when miniaturization techniques are considered. One of the major drawbacks of the system is the amount and the size of the needed equipment. This will prevent the installation of an FVPDM experiment for long term monitoring in monitoring well that are not secured against vandalism, degradation or theft. If the FVPDM experiment was integrated into an in-well equipment, the complete system could be discreetly hidden inside the tested well. The design of the in-well probe will be limited by the available diameter of the tested monitoring well. Two sizes of probe could be designed, one for 2 inches wells the other for 4 inches' wells. The challenge would then be to incorporate in this limited volume, the tracer injection pump, the device used to measure the tracer concentration, a device to stir the water column and homogenize the tracer concentrations, the data logger and the tracer reservoir itself. Power supply such as an integrated battery can only be considered if the power consumption of the device is low. Otherwise an external power source should be used. In the conception of this probe a reflection on the integration of packers must be undertaken.

In the context of characterization and monitoring of contaminated aquifers, a strategic development would be to couple, to the FVPDM experimental setup, a measurement of specific contaminants or other solute species. By doing this, the coupled system would allow the direct measurement and monitoring of solute fluxes in aquifers. This coupling can be done by connecting an autonomous water sampler connected on the circulation loop or by inserting, in-line the circulation loop, a specific probe for the measurement of chemical species aqueous

concentration. Such a device would thereby be the first system able to perform a direct monitoring of transient solute fluxes in aquifers.

The potential applications of the FVPDM have already be demonstrated in previous sections. Whether for strict research purposes to more applied consulting jobs, the present work illustrated the relevance of the FVPDM. Aside from the direct measurement of groundwater fluxes for hydrogeological characterization or in support of contaminant mass fluxes measurement, the FVPDM can also be used as a prevention technique. For example, the current protection of drinking water abstraction wells is performed by analyzing the water withdrawn at the pumping well. If one could have a system that allows for the real-time measurements of solute or contaminant fluxes in aquifers, such system could be installed in monitoring wells located upgradient at a certain distance of the abstraction well and send alerts in case of a threatening contaminant flux. This will allocate a certain response time to take actions and protect the abstraction well. Such a probe can also be used for the monitoring of contaminated aquifer, whether to evaluate the potential stability of the plume and the compliance with defined thresholds or to quantify the efficiency of remediation techniques in real time and avoid the further spreading of contaminant.

Finally, one of the major perspectives based on these research outcomes must be to continue encouraging contaminant flux-based management approaches of polluted aquifers.

References

Alberti, L., Lombi, S., & Zanini, A. (2011). Identifying sources of chlorinated aliphatic hydrocarbons in a residential area in Italy using the integral pumping test method. Hydrogeology Journal, 19(6), 1253–1267. http://doi.org/10.1007/s10040-011-0742-1

Alden, A. S., & Munster, C. L. (1997). Field Test of the In Situ Permeable Ground Water Flow Sensor. Groundwater Monitoring & Remediation, 17(4), 81–88. http://doi.org/10.1111/j.1745-6592.1997.tb01267.x

Allard, M. & Lemay M (2012). Nunavik and Nunatsiavut: from science to policy: an integrated regional impact study (IRIS) of climate change and modernization. ArcticNet, Quebec City, QC, 303 pp

Anaya-Romero, M., Marañón, T., Cabrera, F., Madejón, E., Madejón P., Murillo, J.M., Vrinceanu, N.O., Siebielec, G. & Geisse V. (2016). Soil Threats in Europe: Status, methods, drivers and effects on ecosystem services – Chapter 8: Soil contamination. JRC Techncial Reports, 13p. Available at https://esdac.jrc.ec.europa.eu/content/soil-threats-europe-status-methods-drivers-and-effects-ecosystem-services

Annable, M. D. (2008). Mass flux as a remedial performance metric at NAPL contaminated sites. Methods and Techniques for Cleaning-up Contaminated Sites, 177–186. http://doi.org/10.1016/j.arth.2016.06.010

Annable, M. D., Hatfield, K., Cho, J., Klammler, H., Parker, B. L., Cherry, J. A., & Rao, P. S. C. (2005). Field-scale evaluation of the passive flux meter for simultaneous measurement of groundwater and contaminant fluxes. Environmental Science and Technology, 39(18), 7194–7201. http://doi.org/10.1021/es050074g

API, American Petroleum Institute. (2003). Answers to frequently asked questions about managing risk at LNAPL sites. API Soil and Groundwater Research Bulletin, (18), 24. Retrieved from http://www.api.org/environment-health-and-safety/clean-water/ground-water/bulletins

Ballard, S. (1996). The in situ permeable flow sensor a ground-water flow velocity meter. Ground Water. http://doi.org/10.1111/j.1745-6584.1996.tb01883.x

Ballard, S., Barker, G. T., & Nichols, R. L. (1996). A test of the in situ permeable flow sensor at Savannah River, SC. Ground Water. http://doi.org/10.1111/j.1745-6584.1996.tb02019.x

Baptiste, N., & Chapuis, R. P. (2015). What maximum permeability can be measured with a monitoring well? Engineering Geology, 184, 111–118. http://doi.org/10.1016/j.enggeo.2014.11.006

Barbaro, J. R., & Neupane, P. P. (2006). Use of plume mapping data to estimate chlorinated solvent mass loss. Ground Water Monitoring and Remediation, 26(4), 115–127. http://doi.org/10.1111/j.1745-6592.2006.00117.x

Basu, N. B., Rao, P. S. C., Poyer, I. C., Annable, M. D., & Hatfield, K. (2006). Flux-based assessment at a manufacturing site contaminated with trichloroethylene. Journal of Contaminant Hydrology, 86(1–2), 105–127. http://doi.org/10.1016/j.jconhyd.2006.02.011

Batlle-Aguilar, J., Morasch, B., Hunkeler, D., Brouyère, S. (2014). Benzene dynamics and biodegradation in alluvial aquifers affected by river fluctuations. Groundwater, 52(3): 388-398. http://dx.doi.org/10.1111/gwat.12070

Bauer, S., Bayer-Raich, M., Holder, T., Kolesar, C., Müller, D., & Ptak, T. (2004). Quantification of groundwater contamination in an urban area using integral pumping tests. Journal of Contaminant Hydrology, 75(3–4), 183–213. http://doi.org/10.1016/j.jconhyd.2004.06.002

Bayer-Raich, M., Baumann, R., & Ptak, T. (2002). Estimation of contaminant mass flows in a multi-layered aquifer using pumping tests: numerical experiments at field-scale. Groundwater Quality: Natural and Enhanced Restoration of Groundwater Pollution, (275), 257–263.

Bayer-Raich, M., Credoz, A., Guimerà, J., Jordana, S., Sampietro, D., Font-Capó, J., … Grossemy, M. (2018). Estimates of Horizontal Groundwater Flow Velocities in Boreholes. Groundwater, 1–9. http://doi.org/10.1111/gwat.12820

Bayer-Raich, M., Jarsjö, J., Liedl, R., Ptak, T., & Teutsch, G. (2004). Average contaminant concentration and mass flow in aquifers from time-dependent pumping well data: Analytical framework. Water Resources Research, 40(8), 1–10. http://doi.org/10.1029/2004WR003095

Bayer-Raich, M., Jarsjö, J., Liedl, R., Ptak, T., & Teutsch, G. (2006). Integral pumping test analyses of linearly sorbed groundwater contaminants using multiple wells: Inferring mass flows and natural attenuation rates. Water Resources Research, 42(8), 1–10. http://doi.org/10.1029/2005WR004244

Bayless, E. R., Mandell, W. A., & Ursic, J. R. (2011). Accuracy of Flowmeters Measuring Horizontal Groundwater Flow in an Unconsolidated Aquifer Simulator. Ground Water Monitoring & Remediation, 31(2), 48–62. http://doi.org/10.1111/j.1745-6592.2010.01324.x

Beauheim, R. L. (2000). Evaluation of the colloidal borescope as a monitoring tool at the waste isolation pilot plant site. Sandia National Laboratories Report SAND2000-2162, 71 p.

Béland-Pelletier, C., Fraser, M., Barker, J., & Ptak, T. (2011). Estimating contaminant mass discharge: A field comparison of the multilevel point measurement and the integral pumping investigation approaches and their uncertainties. Journal of Contaminant Hydrology, 122(1–4), 63–75. http://doi.org/10.1016/j.jconhyd.2010.11.004

Bense, V. F., Kooi, H., Ferguson, G., & Read, T. (2012). Permafrost degradation as a control on hydrogeological regime shifts in a warming climate. Journal of Geophysical Research: Earth Surface, 117(3), 1–18. http://doi.org/10.1029/2011JF002143

Berg, S. J., & Gillham, R. W. (2010). Studies of water velocity in the capillary fringe: The point velocity probe. Ground Water, 48(1), 59–67. http://doi.org/10.1111/j.1745-6584.2009.00606.x

Bianchin, M., Smith, L., & Beckie, R. (2010). Quantifying hyporheic exchange in a tidal river using temperature time series. Water Resources Research, 46(7), 1–21. http://doi.org/10.1029/2009WR008365

Bockelmann, A., Ptak, T., & Teutsch, G. (2001). An analytical quantification of mass fluxes and natural attenuation rate constants at a former gasworks site. Journal of Contaminant Hydrology, 53(3–4), 429–453. http://doi.org/10.1016/S0169-7722(01)00177-2

Bockelmann, A., Zamfirescu, D., Ptak, T., Grathwohl, P., & Teutsch, G. (2003). Quantification of mass fluxes and natural attenuation rates at an industrial site with a limited monitoring network: A case study. Journal of Contaminant Hydrology, 60(1–2), 97–121. http://doi.org/10.1016/S0169-7722(02)00060-8

Bohling, G. C., Liu, G., Knobbe, S. J., Reboulet, E. C., Hyndman, D. W., Dietrich, P., & Butler, J. J. (2012). Geostatistical analysis of centimeter-scale hydraulic conductivity variations at the MADE site. Water Resources Research, 48(2), 1–15. http://doi.org/10.1029/2011WR010791

Brainerd, R. J., & Robbins, G. A. (2004). A tracer dilution method for fracture characterization in bedrock wells. Ground Water, 42(5), 774–780. http://doi.org/10.1111/j.1745-6584.2004.tb02731.x

Briggs, M. A., Walvoord, M. A., McKenzie, J. M., Voss, C. I., Day-Lewis, F. D., & Lane, J. W. (2014). New permafrost is forming around shrinking Arctic lakes, but will it last? Geophysical Research Letters, 41(5), 1585–1592. http://doi.org/10.1002/2014GL059251

Bright, J., Wang, F., & Close, M. (2002). Influence of the Amount of Available K Data on Uncertainty About Contaminant Transport Prediction. Ground Water, 40(5), 529–534. http://doi.org/10.1111/j.1745-6584.2002.tb02537.x

Britt, S. L., Parker, B. L., & Cherry, J. A. (2010). A downhole passive sampling system to avoid bias and error from groundwater sample handling. Environmental Science and Technology, 44(13), 4917–4923. http://doi.org/10.1021/es100828u

Brooks, M. C., Wood, A. L., Annable, M. D., Hatfield, K., Cho, J., Holbert, C., … Smith, R. E. (2008). Changes in contaminant mass discharge from DNAPL source mass depletion: Evaluation at two field sites. Journal of Contaminant Hydrology, 102(1–2), 140–153. http://doi.org/10.1016/j.jconhyd.2008.05.008

Brouyère, S. (2000). Etude et modélisation du transport et du piégeage des solutés en milieu souterrain variablement saturé. Evaluation des paramètres hydrodispersifs par la réalisation et l'interprétation d'essais de traçage in situ (in French). PhD Thesis, Université de Liège, Belgium, 572p. http://hdl.handle.net/2268/40804

Brouyère, S. (2003). Modeling tracer injection and well-aquifer interactions: A new mathematical and numerical approach. Water Resources Research, 39(3), 1070-1075.

Brouyère, S., Batlle-Aguilar, J., Goderniaux, P., & Dassargues, A. (2008). A new tracer technique for monitoring groundwater fluxes: the Finite Volume Point Dilution Method. Journal of Contaminant Hydrology, 95(3–4), 121–40. http://doi.org/10.1016/j.jconhyd.2007.09.001

Brouyère, S., Carabìn, G., & Dassargues, A. (2005). Influence of injection conditions on field tracer experiments. Ground Water, 43(3), 389–400. http://doi.org/10.1111/j.1745-6584.2005.0041.x

Brovelli, A., Mao, X., & Barry, D. A. (2007). Numerical modeling of tidal influence on density-dependent contaminant transport. Water Resources Research, 43(10), 1–15. http://doi.org/10.1029/2006WR005173

Brusseau, M. L., Carroll, K. C., Allen, T., Baker, J., Diguiseppi, W., Hatton, J., … Berkompas, J. (2011b). Impact of in situ chemical oxidation on contaminant mass discharge: Linking source-zone and plume-scale characterizations of remediation performance. Environmental Science and Technology, 45(12), 5352–5358. http://doi.org/10.1021/es200716s

Brusseau, M. L., Hatton, J., & Diguiseppi, W. (2011a). Assessing the impact of source-zone remediation efforts at the contaminant-plume scale through analysis of contaminant mass discharge. Journal of Contaminant Hydrology, 126(3–4), 130–139. http://doi.org/10.1016/j.jconhyd.2011.08.003

Burnett, W. C., Aggarwal, P. K., Aureli, A., Bokuniewicz, H., Cable, J. E., Charette, M. A., … Turner, J. V. (2006). Quantifying submarine groundwater discharge in the coastal zone via multiple methods. Science of the Total Environment, 367(2–3), 498–543. http://doi.org/10.1021/acsami.6b16505

Buteau, S., Fortier, R., & Allard, M. (2010). Permafrost Weakening as a Potential Impact of Climatic Warming. Journal of Cold Regions Engineering, 24(1), 1–18. http://doi.org/10.1061/(ASCE)0887-381X(2010)24:1(1)

Cai, Z., Wilson, R. D., Cardiff, M. A., & Kitanidis, P. K. (2011). Increasing Confidence in Mass Discharge Estimates Using Geostatistical Methods. Ground Water, 49(2), 197–208. http://doi.org/10.1111/j.1745-6584.2010.00709.x

Campbell, T. J., Hatfield, K., Klammler, H., Annable, M. D., & Rao, P. S. C. (2006). Magnitude and directional measures of water and Cr(VI) fluxes by passive flux meter. Environmental Science and Technology, 40(20), 6392–6397. http://doi.org/10.1021/es060268b

Chapman, S., Parker, B., Cherry, J., Munn, J., Malenica, A., Ingleton, R., … Piersol, J. (2015). Hybrid multilevel system for monitoring groundwater flow and agricultural impacts in fractured sedimentary bedrock. Groundwater Monitoring and Remediation, 35(1), 55–67. http://doi.org/10.1111/gwmr.12084

Chen, H., & Pinder, G. F. (2011). Investigation of Groundwater Contaminant Discharge into Tidally influenced Surface-water Bodies: Theoretical Analysis. Transport in Porous Media, 89(3), 289–306. http://doi.org/10.1007/s11242-011-9772-3

Chen, X., Brooks, M. C., & Wood, A. L. (2014). The uncertainty of mass discharge measurements using pumping methods under simplified conditions. Journal of Contaminant Hydrology, 156, 16–26. http://doi.org/10.1016/j.jconhyd.2013.09.006

Chiogna, G., Cirpka, O. A., Grathwohl, P., & Rolle, M. (2011). Transverse mixing of conservative and reactive tracers in porous media: Quantification through the concepts of flux-related and critical dilution indices. Water Resources Research, 47(2), 1–15. http://doi.org/10.1029/2010WR009608

Clemo, T. (2010). Coupled aquifer-borehole simulation. Ground Water, 48(1), 68–78. http://doi.org/10.1111/j.1745-6584.2009.00597.x

CRC CARE (2016). Flux-based groundwater assessment and management, CRC CARE Technical Report no. 37, CRC for Contamination Assessment and Remediation of the Environment, Adelaide, Australia, 103p. http://doi.org/10.13140/RG.2.2.26276.07042

Cvetkovic, V., Shapiro, A. M., & Dagan, G. (1992). A solute flux approach to transport in heterogeneous formations: 2. Uncertainty analysis. Water Resources Research, 28(5), 1377–1388. http://doi.org/10.1029/91WR03085

Dagenais, S., Molson, J., Lemieux, J-M., Fortier, R., & Therrien, R. (2017). Coupled cryo-hydrogeological modelling of permafrost degradation at Umiujaq, Quebec, Canada. GeoOttawa 2017, 12th Joint CGS/IAH-CNC Groundwater Conference, Ottawa, Canada, Oct. 1-4, 2017.

Dagenais, S., Molson, J., Lemieux, J-M., Fortier, R., & Therrien, R. (2019). Coupled cryo-hydrogeological modelling of permafrost degradation at Umiujaq, Nunavik, Canada. Hydrogeology Journal, submitted.

Darcy, H. (1856) Les fontaines publiques de la ville de Dijon. Exposition et application des principes à suivre et des formules à employer dans les questions de distribution d'eau (in French). Victor Dalmont Editeur, Paris, 647p.

Dassargues, A. (2019). Hydrogeology groundwater science and engineering. First Edition, CRC Press, ISBN 978-1-4987-4400-3, 471p.

de Barros, F. P. J. (2018). Evaluating the combined effects of source zone mass release rates and aquifer heterogeneity on solute discharge uncertainty. Advances in Water Resources, 117(April), 140–150. http://doi.org/10.1016/j.advwatres.2018.05.010

de Barros, F.P.J. & Nowak, W. (2010). On the link between contaminant source release conditions and plume prediction uncertainty. Journal of Contaminant Hydrology, 116(1–4), 24–34. http://doi.org/10.1016/j.jconhyd.2010.05.004

de Grandpré, I., Fortier, D., & Stephani, E. (2012). Degradation of permafrost beneath a road embankment enhanced by heat advected in groundwater. Canadian Journal of Earth Sciences, 49(8), 953–962. http://doi.org/10.1139/e2012-018

Dentz, M., Carrera, J. (2005). Effective solute transport in temporally fluctuating flow through heterogeneous media. Water Resources Research, 41, W08414, http://dx.doi.org/10.1029/2004WR003571.

Devlin, J. F. (2016). Sensitivity analyses of the theoretical equations used in point velocity probe (PVP) data interpretation. Journal of Contaminant Hydrology, 192, 140–145. http://doi.org/10.1016/j.jconhyd.2016.07.004

Devlin, J. F., & McElwee, C. D. (2007). Effects of measurement error on horizontal hydraulic gradient estimates. Ground Water, 45(1), 62–73. http://doi.org/10.1111/j.1745-6584.2006.00249.x

Devlin, J. F., McMaster, M., Katic, D., & Barker, J. F. (2002). Evaluating natural attenuation in a controlled field experiment by mass balances, flux fences and snapshots: a comparison of results. Groundwater Quality: Natural and Enhanced Restauration of Groundwater Pollution, (275), 245–250.

Devlin, J. F., Schillig, P. C., Bowen, I., Critchley, C. E., Rudolph, D. L., Thomson, N. R., … Roberts, J. A. (2012). Applications and implications of direct groundwater velocity measurement at the centimetre scale. Journal of Contaminant Hydrology, 127(1–4), 3–14. http://doi.org/10.1016/j.jconhyd.2011.06.007

Devlin, J. F., Tsoflias, G., McGlashan, M., & Schillig, P. (2009). An inexpensive multilevel array of sensors for direct ground water velocity measurement. Ground Water Monitoring and Remediation, 29(2), 73–77. http://doi.org/10.1111/j.1745-6592.2009.01233.x

Dietze, M., & Dietrich, P. (2011). A field comparison of BTEX mass flow rates based on integral pumping tests and point scale measurements. Journal of Contaminant Hydrology, 122(1–4), 1–15. http://doi.org/10.1016/j.jconhyd.2010.10.001

Difilippo, E. L., Carroll, K. C., & Brusseau, M. L. (2010). Impact of organic-liquid distribution and flow-field heterogeneity on reductions in mass flux. Journal of Contaminant Hydrology, 115(1–4), 14–25. http://doi.org/10.1016/j.jconhyd.2010.03.002

Dorn, C., Linde, N., Le Borgne, T., Bour, O., & Klepikova, M. (2012). Inferring transport characteristics in a fractured rock aquifer by combining single-hole ground-penetrating radar reflection monitoring and tracer test data. Water Resources Research, 48(11), W11521. http://doi.wiley.com/10.1029/2011WR011739

Drost, W., Klotz, D., Koch, A., Moser, H., Neumaier, F., & Rauert, W. (1968). Point dilution methods of investigating ground water flow by means of radioisotopes. Water Resources Research, 4(1), 125–146. http://doi.org/10.1029/WR004i001p00125

Dujardin, J., Anibas, C., Bronders, J., Jamin, P., Hamonts, K., Dejonghe, W., Brouyère, S., Batelaan, O. (2014). Combining flux estimation techniques to improve characterization of groundwater–surface-water interaction in the Zenne River, Belgium. Hydrogeology Journal, 22(7), 1657-1668. https://doi.org/10.1007/s10040-014-1159-4

Dupuit, J. (1863). Etudes théoriques et pratiques sur le mouvement des eaux dans les canaux découverts et àtravers les terrains perméables, Dunod, Paris, 303p.

EEA (2000). Management of contaminated sites in Western Europe. Topic report No 13/1999 European Environment Agency, Copenhagen. Available at https://www.eea.europa.eu/publications/Topic_report_No_131999

EEA (2014). Progress in management of contaminated sites. Soil datasets provided by Joint Research Centre (JRC), 52p. Available at https://www.eea.europa.eu/data-and-maps

EEA (2015). The European environment — State and outlook 2015. European Environment Agency, Copenhagen. Available at https://www.eea.europa.eu/soer

EEA (2017). Urban waste water treatment. Waterbase - Urban Waste Water Treatment EEA data and Water statistics provided by Eurostat, 31p. Available at https://www.eea.europa.eu/data-and-maps

EEA (2018). Use of fresh water resources. Data provided by EEA, Eurostat and JRC, 35p. Available at https://www.eea.europa.eu/data-and-maps

Einarson, M. (2017). Spatially Averaged, Flow-Weighted Concentrations - A More Relevant Regulatory Metric for Groundwater Cleanup. Groundwater Monitoring & Remediation, 37(4), 11–14. http://doi.org/10.1111/gwmr.12240

Einarson, M. D., & Mackay, D. M. (2001). Predicting Impacts of Groundwater Contamination. Environmental Science & Technology, 35(3), 66A–73A. http://doi.org/10.1021/es0122647

Elci, A., Molz, F. J., & Waldrop, W. R. (2001). Implications of Observed and Simulated Ambient Flow in Monitoring Wells. Groundwater, 39(6), 853–862. http://doi.org/10.1111/j.1745-6584.2001.tb02473.x

Ellis, P. A., Mackay, R., & Rivett, M. O. (2007). Quantifying urban river-aquifer fluid exchange processes: A multi-scale problem. Journal of Contaminant Hydrology, 91(1–2), 58–80. http://doi.org/10.1016/j.jconhyd.2006.08.014

Ensign, S. H., Piehler, M. F., & Doyle, M. W. (2008). Riparian zone denitrification affects nitrogen flux through a tidal freshwater river. Biogeochemistry, 91(2–3), 133–150. http://doi.org/10.1007/s10533-008-9265-9

Ernst & Young (2013), Evaluation of expenditure and jobs for addressing soil contamination in Member States, Final report to the European Commission, Directorate - General Environment. ENV.B.1/ETU/2011/0012, 442p.

Evans, S. G., & Ge, S. (2017). Contrasting hydrogeologic responses to warming in permafrost and seasonally frozen ground hillslopes. Geophysical Research Letters, 44(4), 1803–1813. http://doi.org/10.1002/2016GL072009

Falta, R. W. (2008). Methodology for comparing source and plume remediation alternatives. Ground Water, 46(2), 272–285. http://doi.org/10.1111/j.1745-6584.2007.00416.x

Fasbender, D., Peeters, L., Bogaert, P. and Dassargues, A. (2008). Bayesian data fusion applied to water table spatial mapping. Water Resources Research 44(12), W12422. http://dx.doi.org/10.1029/2008WR006921

Fortier, R, Lemieux, J.-M., Talbot-Poulin, M.-C., Banville, D.-R., Lévesque, R., Molson, J., & Therrien, R. (2014). Rapport de la phase IIIb du déploiement du réseau Immatsiak: Hydrogéologie d'un bassin versant dans une vallée près d'Umiujaq (in French) Technical report. Université Laval, Centre d'Etudes Nordiques, 275p.

Fortier, R., LeBlanc, A.M., & Yu, W. (2011). Impacts of permafrost degradation on a road embankment at Umiujaq in Nunavik (Quebec), Canada. Canadian Geotechnical Journal, 48(5), 720–740. http://doi.org/10.1139/t10-101

Fortier, R., Lemieux, J.-M., Molson, J., & Therrien, R. (2013). Rapport de la phase III du projet de déploiement du réseau Immatsiak: Campagne de forages pour l'installation de puits d'observation des eaux souterraines dans un petit bassin versant pergélisolé à Umiujaq (in French) Technical report. Université Laval, Centre d'Etudes Nordiques, 89p.

Fortier, R., Roy-Banville, D., Lévesque, R., Lemieux, J.-M., Molson, J., Therrien, R., & Ouellet, M. (2019). Development of a 3D cryohydrogeological model of a small watershed in a degrading permafrost environment in Umiujaq, Nunavik, Canada. Hydrogeology Journal, submitted.

Frampton, A., & Destouni, G. (2015). Impact of degrading permafrost on subsurface solute transport pathways and travel times. Water Resources Research, 51(9), 7680–7701. http://doi.org/10.1002/2014WR016689

Frampton, A., Painter, S. L., & Destouni, G. (2013). Permafrost degradation and subsurface-flow changes caused by surface warming trends. Hydrogeology Journal, 21(1), 271–280. http://doi.org/10.1007/s10040-012-0938-z

Ge, S., McKenzie, J., Voss, C., & Wu, Q. (2011). Exchange of groundwater and surface-water mediated by permafrost response to seasonal and long term air temperature variation. Geophysical Research Letters, 38(14), 1–6. http://doi.org/10.1029/2011GL047911

Ghorbani, A., Camerlynck, C., Florsch, N., Cosenza, P. and Revil, A. (2007). Bayesian inference of the Cole–Cole parameters from time- and frequency-domain induced polarization. Geophysical Prospecting, 55, 589–605. doi: 10.1111/j.1365-2478.2007.00627.x

Gibson, B., & Devlin, J. F. (2017). Laboratory validation of a point velocity probe for measuring horizontal flow from any direction. Journal of Contaminant Hydrology, 208(October 2017), 10–16. http://doi.org/10.1016/j.jconhyd.2017.10.005

Gleeson, T., Allen, D. M., & Ferguson, G. (2012). Teaching hydrogeology : a review of current practice. Hydrology and Earth System Sciences, 16, 2159–2168. http://doi.org/10.5194/hess-16-2159-2012

Goderniaux, P., Brouyère, S., Gutierrez, A., & Baran, N. (2010). Multi-tracer tests to evaluate the hydraulic setting of a complex aquifer system (Brévilles spring catchment, France). Hydrogeology Journal, 18(7), 1729–1740. http://doi.org/10.1007/s10040-010-0633-x

Goltz, M. N., Close, M. E., Yoon, H., Huang, J., Flintoft, M. J., Kim, S., & Enfield, C. (2009). Validation of two innovative methods to measure contaminant mass flux in groundwater. Journal of Contaminant Hydrology, 106(1–2), 51–61. http://doi.org/10.1016/j.jconhyd.2009.01.001

Goltz, M. N., Kim, S., Yoon, H., & Park, J. (2011). Review of groundwater contaminant mass flux measurement. Environmental Engineering Research, 16(4), 176–193. http://doi.org/10.4491/eer.2007.12.4.176

Government of Quebec (2019) Réseau de suivi des eaux souterraines du Quebec. Retrieved from http://www.environnement.gouv.qc.ca/eau/piezo/index.htm Cited 2 February 2019.

Grosse, G., Romanovsky, V., Jorgenson, T., Anthony, K. W., Brown, J., & Overduin, P. P. (2011). Vulnerability and feedbacks of permafrost to climate change. Eos, Transactions American Geophysical Union, 92(9), 73. http://doi.org/10.1029/2011EO090001

Guaraglia, D.O. & Pousa, J.L. (2014). Introduction to Modern Instrumentation: For Hydraulics and Environmental Sciences. Sciendo; Digital original edition, Kindle edition, ISBN 978-3110401714, 456p.

Guilbeault, M. A., Parker, B. L., & Cherry, J. A. (2005). Mass and Flux Distributions from DNAPL. Ground Water, 43(1), 70–86.

Guthrie, M. (1986). Use of a Geo Flowmeter for the Determination of Ground Water Flow Direction. Groundwater Monitoring & Remediation. http://doi.org/10.1111/j.1745-6592.1986.tb01244.x

Hadley, P.W. & Newell, C.J. (2012). MCLs, OoMs and Md: A groundwater remediation tipping point. Battelle Eighth International Conference on Remediation of Chlorinated and Recalcitrant Compounds, May 21-24, 2012, Monterey, California.

Hakoun, V., Mazzilli, N., Pistre, S., & Jourde, H. (2013). Teaching groundwater flow processes : connecting lecture to practical and field classes. Hydrological Sciences Journal, 17, 1975–1984. http://doi.org/10.5194/hess-17-1975-2013

Halevy, E., Moser, H., Zellhofer, O., & Zuber, A. (1967). Borehole dilution techniques a critical review. Isotope in Hydrology, I.A.E.A., Vienna. http://doi.org/10.1016/j.aqpro.2015.02.051

Hall, S. H. (1996). Practical single-well tracer methods for aquifer testing. In Workshop netbook, Tenth national outdoor action conference and exposition, National Groundwater Association, Colombus, Ohio, USA, 11p.

Hall, S. H., Luttrell, S. P., & Cronin, W. E. (1991). A Method for Estimating Effective Porosity and Ground-Water Velocity. Ground Water, 29(2), 171–174. http://doi.org/10.1111/j.1745-6584.1991.tb00506.x

Hatch, C. E., Fisher, A. T., Revenaugh, J. S., Constantz, J., & Ruehl, C. (2006). Quantifying surface water-groundwater interactions using time series analysis of streambed thermal records: Method development. Water Resources Research, 42(10), 1–14. http://doi.org/10.1029/2005WR004787

Hatfield, K., Annable, M., Cho, J., Rao, P. S. C., & Klammler, H. (2004). A direct passive method for measuring water and contaminant fluxes in porous media. Journal of Contaminant Hydrology, 75(3–4), 155–81. http://doi.org/10.1016/j.jconhyd.2004.06.005

Hatfield, K., Annable, M.D, Suzannah, K., Rao P.S.C., & Campbell, T. (2001). A new method for quantifying contaminant flux at hazardous waste sites. Proceedings of the Groundwater Quality 2001: Natural and Enhanced Restoration of Groundwater Pollution, Sheffield, U.K. June 2001, IAHS Publ. no. 275, 25-31.

Herold, M., Ptak, T., Bayer-Raich, M., Wendel, T., & Grathwohl, P. (2009). Integral quantification of contaminant mass flow rates in a contaminated aquifer: Conditioning of the numerical inversion of concentration-time series. Journal of Contaminant Hydrology, 106(1–2), 29–38. http://doi.org/10.1016/j.jconhyd.2008.12.006

Holder, T. H., Teutsch, G., Ptak, T., & Schwarz, R. (1998). A new approach for source zone characterization : the Neckar Valley study, IAHS Publication (International Association of Hydrological Sciences), (250), 49–55.

Huang, J., & Goltz, M.N., (2005). A three-dimensional analytical model to simulate groundwater flow during operation of recirculating wells. Journal of Hydrology. 314(1-4),67–77.

Hyun, Y., Kim, H., Lee, S. S., & Lee, K. K. (2011). Characterizing streambed water fluxes using temperature and head data on multiple spatial scales in Munsan stream, South Korea. Journal of Hydrology, 402(3–4), 377–387. http://doi.org/10.1016/j.jhydrol.2011.03.032

Ireson, A. M., van der Kamp, G., Ferguson, G., Nachshon, U., & Wheater, H. S. (2013). Hydrogeological processes in seasonally frozen northern latitudes: understanding, gaps and challenges. Hydrogeology Journal, 21(1), 53–66. http://doi.org/10.1007/s10040-012-0916-5

ITRC (2010). Use and measurement of mass flux and mass discharge. Interstate Technology and Regulatory Council, Integrated DNAPL Site Strategy Team, Technology Overview report, MASSFLUX-1., Washington, 154 p. Available at www.itrcweb.org.

James, S. C., Jepsen, R. A., Beauheim, R. L., Pedler, W. H., & Mandell, W. A. (2006). Simulations to verify horizontal flow measurements from a borehole flowmeter. Ground Water, 44(3), 394–405. http://doi.org/10.1111/j.1745-6584.2005.00140.x

Jamin, P., & Brouyère, S. (2018). Monitoring transient groundwater fluxes using the Finite Volume Point Dilution Method. Journal of Contaminant Hydrology, 218(July), 10–18. http://doi.org/10.1016/j.jconhyd.2018.07.005

Jamin, P., Dollé, F., Chisala, B., Orban, P., Popescu, I. C., Hérivaux, C., … Brouyère, S. (2012). A regional flux-based risk assessment approach for multiple contaminated sites on groundwater bodies. Journal of Contaminant Hydrology, 127(1–4), 65–75. http://doi.org/10.1016/j.jconhyd.2011.07.001

Jamin, P., Goderniaux, P., Bour, O., Le Borgne, T., Englert, A., Longuevergne, L., & Brouyère, S. (2015). Contribution of the finite volume point dilution method for measurement of groundwater fluxes in a fractured aquifer. Journal of Contaminant Hydrology, 182, 244–255. http://doi.org/10.1016/j.jconhyd.2015.09.002

Jarsjö, J., Bayer-Raich, M., & Ptak, T. (2005). Monitoring groundwater contamination and delineating source zones at industrial sites: Uncertainty analyses using integral pumping tests. Journal of Contaminant Hydrology, 79(3–4), 107–134. http://doi.org/10.1016/j.jconhyd.2005.05.011

Jiang, Y., Zhuang, Q., & O'Donnell, J. A. (2012). Modeling thermal dynamics of active layer soils and near-surface permafrost using a fully coupled water and heat transport model. Journal of Geophysical Research Atmospheres, 117(11), 1–15. http://doi.org/10.1029/2012JD017512

Kalbus, E., Reinstorf, F., & Schirmer, M. (2006). Measuring methods for groundwater – surface water interactions: a review. Hydrology and Earth System Sciences, 10(6), 873–887. http://doi.org/10.5194/hess-10-873-2006

Kalbus, E., Schmidt, C., Bayer-Raich, M., Leschik, S., Reinstorf, F., Balcke, G. U., & Schirmer, M. (2007). New methodology to investigate potential contaminant mass fluxes at the stream-aquifer interface by combining integral pumping tests and streambed temperatures. Environmental Pollution, 148(3), 808–816. http://doi.org/10.1016/j.envpol.2007.01.042

Kang, X., Shi, X., Deng, Y., Revil, A., Xu, H., & Wu, J. (2018). Coupled hydrogeophysical inversion of DNAPL source zone architecture and permeability fi eld in a 3D heterogeneous sandbox by assimilation time-lapse cross-borehole electrical resistivity data via ensemble Kalman fi ltering. Journal of Hydrology, 567(March), 149–164. http://doi.org/10.1016/j.jhydrol.2018.10.019

Kaufman, W.J. and Todd, D.K. (1962). Application of tritium tracer to canal seepage measurements. International Atomic Energy Agency, Tritium in the Physical and Biological Sciences 1, 83-94.

Kearl, P. M. (1997). Observations of particle movement in a monitoring well using the colloidal borescope. Journal of Hydrology, 200(January), 323–344. http://doi.org/10.1016/S0022-1694(97)00026-7

Kearl, P. M., & Roemer, K. (1998). Evaluation of Groundwater Flow Directions in a Heterogeneous Aquifer Using the Colloidal Borescope. Advances in Environmental Research, 2(1), 12–23.

Kearl, P. M., Korte, N. E., & Cronk, T. A. (1992). Suggested Modifications to Ground Water Sampling Procedures Based on Observations from the Colloidal Borescope. Groundwater Monitoring & Remediation, 12(2), 155–161. http://doi.org/10.1111/j.1745-6592.1992.tb00046.x

Kearl, P. M., Roemer, K., Rogoff, E. B., & Renn, R. M. (1998). Characterization of a fractured aquifer using the colloidal borescope. Advances in Environmental Research, 3(1), 49-57.

Keery, J., Binley, A., Crook, N., & Smith, J. W. N. (2007). Temporal and spatial variability of groundwater-surface water fluxes: Development and application of an analytical method using temperature time series. Journal of Hydrology, 336(1–2), 1–16. http://doi.org/10.1016/j.jhydrol.2006.12.003

Kempf, A., Divine, C. E., Leone, G., Holland, S., Mikac, J. (2013). Field Performance of Point Velocity Probes at a Tidally Influenced Site. Remediation, 23: 37–61. http://dx.doi.org/10.1002/rem.21337

Klammler, H., Hatfield, K., & Annable, M. D. (2007). Concepts for measuring horizontal groundwater flow directions using the passive flux meter. Advances in Water Resources, 30(4), 984–997. http://doi.org/10.1016/j.advwatres.2006.08.007

Klammler, H., Hatfield, K., Annable, M. D., Agyei, E., Parker, B. L., Cherry, J. A., & Rao, P. S. C. (2007). General analytical treatment of the flow field relevant to the interpretation of passive fluxmeter measurements. Water Resources Research, 43(4), 1–17. http://doi.org/10.1029/2005WR004718

Klammler, H., Hatfield, K., Luz, J., Annable, M., Newman, M., Cho, J., … Clark, C. (2012). Water and contaminant flux estimation from multi-layer passive flux meter measurements. WIT Transactions on Engineering Sciences, 74, 301–312. http://doi.org/10.2495/AFM120271

Klammler, H., Hatfield, K., Newman, M. A., Cho, J., Annable, M. D., Parker, B. L., … Perminova, I. (2016). A new device for characterizing fracture networks and measuring groundwater and contaminant fluxes in fractured rock aquifers. Water Resources Research, 52(7), 5400–5420. http://doi.org/10.1002/2015WR018389

Klepikova, M. V., Le Borgne, T., Bour, O., Gallagher, K., Hochreutener, R., & Lavenant, N. (2014). Passive temperature tomography experiments to characterize transmissivity and connectivity of preferential flow paths in fractured media. Journal of Hydrology, 512, 549–562. http://doi.org/10.1016/j.jhydrol.2014.03.018

Klepikova, M., Wildemeersch, S., Hermans, T., Jamin, P., Orban, P., Nguyen, F., Brouyère, S., Dassargues, A. (2016). Heat tracer test in an alluvial aquifer: Field experiment and inverse modelling, Journal of Hydrology, 540, 812-823. https://doi.org/10.1016/j.jhydrol.2016.06.066.

Klotz, D.; Moser, H.; Trimborn, P. (1979). Single borehole techniques present status and examples of recent applications. In Isotope in Hydrology, I.A.E.A., Neuherberg, 150–179.

Kübert, M., & Finkel, M. (2006). Contaminant mass discharge estimation in groundwater based on multi-level point measurements: A numerical evaluation of expected errors. Journal of Contaminant Hydrology, 84(1–2), 55–80. http://doi.org/10.1016/j.jconhyd.2005.12.003

Kurylyk, B. L., Hayashi, M., Quinton, W. L., McKenzie, J. M., & Voss, C. I. (2016). Influence of vertical and lateral heat transfer on permafrost thaw, peatland landscape transition, and groundwater flow. Water Resources Research, 52(2), 1286–1305. http://doi.org/10.1002/2015WR018057

La Licata, I., Langevin, C. D., & Dausman, A. M. (2007). Effect of tidal fluctuations on contaminant transfer to the ocean, (July), 334–342. http://doi.org/10.1016/j.scitotenv.2006.12.032

Labaky, W., Devlin, J. F., & Gillham, R. W. (2007). Probe for measuring groundwater velocity at the centimeter scale. Environmental Science and Technology, 41(24), 8453–8458. http://doi.org/10.1021/es0716047

Labaky, W., Devlin, J. F., & Gillham, R. W. (2010). Field comparison of the point velocity probe with other groundwater velocity measurement methods. Water Resources Research, 46(4), 1–9. http://doi.org/10.1029/2008WR007066

Lamontagne, S., Dighton, J., & Ullman, W. (2002). Estimation of groundwater velocity in riparian zones using point dilution tests. CSIRO Land and Water Technical Report 14/02, 17p.

Le Borgne, T., Bour, O., Paillet, F., and Caudal, J. P. (2006a). Assessment of preferential flow path connectivity and hydraulic properties at single-borehole and cross-borehole scales in a fractured aquifer. Journal of Hydrology, 328(1-2), 347-359. doi:10.1016/j.jhydrol.2005.12.029

Le Borgne, T., Bour, O., Riley, M. S., Gouze, P., Pezard, P. a., Belghoul, A., Lods, G., et al. (2007). Comparison of alternative methodologies for identifying and characterizing preferential flow paths in heterogeneous aquifers. Journal of Hydrology, 345(3-4), 134-148. doi:10.1016/j.jhydrol.2007.07.007

Le Borgne, T., Paillet, F., Bour, O., and Caudal, J.-P. (2006b). Cross-borehole flowmeter tests for transient heads in heterogeneous aquifers. Ground water, 44(3), 444-452. doi:10.1111/j.1745-6584.2005.00150.x

Lee, J., Rao, P. S. C., Poyer, I. C., Toole, R. M., Annable, M. D., & Hatfield, K. (2007). Oxyanion flux characterization using passive flux meters: Development and field testing of surfactant-modified granular activated carbon. Journal of Contaminant Hydrology, 92(3–4), 208–229. http://doi.org/10.1016/j.jconhyd.2006.12.002

Lemieux, J.-M., Fortier, R., Murray, R., Dagenais, S., Cochand, M., Delottier, H., Therrien, R., Pryet, A., & Parhizkar, M., (2019) Groundwater dynamics within a discontinuous permafrost watershed, Umiujaq, Nunavik, Canada. Hydrogeology Journal, submitted.

Lemieux, J.-M., Fortier, R., Talbot-Poulin, M.-C., Molson, J., Therrien, R., Ouellet, M., … Murray, R. (2016). Groundwater occurrence in cold environments: examples from Nunavik, Canada. Hydrogeology Journal, 24(6), 1497–1513. http://doi.org/10.1007/s10040-016-1411-1

Lengricht, J. & Graw K.U. (2002). Interaction of aquifer flow and observation wells detected by particle image velocimetry. Advances in Hydraulics and Water Engineering, 560-565. https://doi.org/10.1142/9789812776969_0102

Leschik, S., Bayer-Raich, M., Musolff, A., & Schirmer, M. (2011). Towards optimal sampling schedules for integral pumping tests. Journal of Contaminant Hydrology, 124(1–4), 25–34. http://doi.org/10.1016/j.jconhyd.2011.01.004

Levanon, E., Yechieli, Y., Gvirtzman, H., & Shalev, E. (2017). Tide-induced fluctuations of salinity and groundwater level in unconfined aquifers – Field measurements and numerical model. Journal of Hydrology, 551, 665–675. http://doi.org/10.1016/j.jhydrol.2016.12.045

Li, K. B., & Abriola, L. M. (2009). A multistage multicriteria spatial sampling strategy for estimating contaminant mass discharge and its uncertainty. Water Resources Research, 45(6), 1–15. http://doi.org/10.1029/2008WR007362

Li, K. B., Goovaerts, P., & Abriola, L. M. (2007). A geostatistical approach for quantification of contaminant mass discharge uncertainty using multilevel sampler measurements. Water Resources Research, 43(6), 1–14. http://doi.org/10.1029/2006WR005427

Li, L., Barry, D. A., Jeng, D.-S., & Prommer, H. (2004). Tidal dynamics of groundwater flow and contaminant transport in coastal aquifers. Coastal Aquifer Management: Monitoring, Modelling and Case Studies. http://doi.org/10.1111/sms.12468

Lubczynski, M.W., & Gurwin, J. (2005). Integration of various data sources for transient groundwater modeling with spatio-temporally variable fluxes—Sardon study case, Spain. Journal of Hydrology, 306 (1–4), 71-96. http://doi.org/10.1016/j.jhydrol.2004.08.038.

Lyon, S. W., & Destouni, G. (2010). Changes in Catchment-Scale Recession Flow Properties in Response to Permafrost Thawing in the Yukon River Basin. International Journal of Climatology, 30(14), 2138–2145. http://doi.org/10.1002/joc.1993

Ma, R., Zheng, C., Tonkin, M., & Zachara, J. M. (2011). Importance of considering intraborehole flow in solute transport modeling under highly dynamic flow conditions. Journal of Contaminant Hydrology, 123(1–2), 11–19. http://doi.org/10.1016/j.jconhyd.2010.12.001

Magal, E., Weisbrod, N., Yakirevich, A., & Yechieli, Y. (2008). The use of fluorescent dyes as tracers in highly saline groundwater. Journal of Hydrology, 358(1–2), 124–133. http://doi.org/10.1016/j.jhydrol.2008.05.035

Mahler, N., Sale, T., Smith, T., & Lyverse, M. (2012). Use of Single-Well Tracer Dilution Tests to Evaluate LNAPL Flux at Seven Field Sites. Ground Water, 50(6), 851–860. http://doi.org/10.1111/j.1745-6584.2011.00902.x

Maldaner, C. H., Quinn, P. M., Cherry, J. A., & Parker, B. L. (2018). Improving estimates of groundwater velocity in a fractured rock borehole using hydraulic and tracer dilution methods. Journal of Contaminant Hydrology, 214(August 2017), 75–86. http://doi.org/10.1016/j.jconhyd.2018.05.003

Malina, G., Krupanek, J., Grossmann, J., & Rijnaarts, H. (2006). Soil and Water Pollution Monitoring, Protection and Remediation, 69(January), 2011–2014. http://doi.org/10.1007/978-1-4020-4728-2.

Marchal, R., Pironț, L., Vandenheede, V, Brouyère, S. & Orban, P. (2018a). Principe de la méthodologie révisée de l'ESR pour le volet nappes. Délivrable 2 de la Convention pour l'amélioration de la méthodologie des

études simplifiées des risques (ESR) pour les eaux souterraines et à la réécriture du Guide de Référence pour l'Etude de Risques - partie C du Code Wallon de Bonne Pratique (AMER-N), 36p.

Marchal, R., Piront, L., Vandenheede, V, Brouyère, S. & Orban, P. (2018b). Nouvelle méthodologie, ses impacts et justifications. Délivrable 3 de la Convention pour l'amélioration de la méthodologie des études simplifiées des risques (ESR) pour les eaux souterraines et à la réécriture du Guide de Référence pour l'Etude de Risques - partie C du Code Wallon de Bonne Pratique (AMER-N), 29p.

Masciopinto, C., & Palmiotta, D. (2014). Estimation of water velocities in boreholes using a new passive flowmeter. Hydrological Sciences Journal, 59(9), 1738–1752. http://doi.org/10.1080/02626667.2014.888491

Masy, T., Caterina, D., Tromme, O., Lavigne, B., Thonart, P., Hiligsmann, S., & Nguyen, F. (2016). Electrical resistivity tomography to monitor enhanced biodegradation of hydrocarbons with Rhodococcus erythropolis T902. 1 at a pilot scale. Journal of Contaminant Hydrology, 184, 1–13. http://doi.org/http://dx.doi.org/10.1016/j.jconhyd.2015.11.001

McKenzie, J. M., & Voss, C. I. (2013). Permafrost thaw in a nested groundwater-flow system. Hydrogeology Journal, 21(1), 299–316. http://doi.org/10.1007/s10040-012-0942-3

Milosevic, N., Thomsen, N. I., Juhler, R. K., Albrechtsen, H. J., & Bjerg, P. L. (2012). Identification of discharge zones and quantification of contaminant mass discharges into a local stream from a landfill in a heterogeneous geologic setting. Journal of Hydrology, 446–447, 13–23. http://doi.org/10.1016/j.jhydrol.2012.04.012

Momii, K., Jinno, K., & Hirano, F. (1993). Laboratory studies on a new laser Doppler Velocimeter System for horizontal groundwater velocity measurements in a borehole. Water Resources Research, 29(2), 283–291. http://doi.org/10.1029/92WR01958

Moore, W. S. (1999). The subterranean estuary: A reaction zone of ground water and sea water. Marine Chemistry, 65(1–2), 111–125. http://doi.org/10.1016/S0304-4203(99)00014-6

Narbutovskih, S.M., McDonald, J.P., Schalla, R. & Sweeney, M.D. (2002). Application of the Colloidal Borescope to Determine a Complex Groundwater Flow Pattern. In Evaluation and Remediation of Low Permeability and Dual Porosity Environments, Sara M.N. & Everett L.G. Editors STP1415, 192p.

Newell, C. J., Farhat, S. K., Adamson, D. T., & Looney, B. B. (2011). Contaminant Plume Classification System Based on Mass Discharge. Ground Water, 49(6), 914–919. http://doi.org/10.1111/j.1745-6584.2010.00793.x

Nichols, E. M. (2010). In a State of (Mass) Flux. Ground Water Monitoring & Remediation, 24(3), 4–6. http://doi.org/10.1111/j.1745-6592.2004.tb01287.x

Nichols, E., & Roth, T. (2004). Flux Redux Using mass flux to improve cleanup decisions. LUSTLine Bulletin, 46, 6–9.

Novakowski, K. S., Lapcevic, P. A., Voralek, J. W., & Sudicky, E. A. (1998). A note on a method for measuring the transport properties of a formation using a single well. Water Resources Research, 34(5), 1351–1356. http://doi.org/10.1029/98WR00292

Novakowski, K. S., Lapcevic, P., Voralek, J., and Bickerton, G. (1995). Preliminary interpretation of tracer experiments conducted in a discrete rock fracture under conditions of natural flow. Geophysical Research Letters, 22(11), 1417-1420.

Novakowski, K. S., Bickerton, G., Lapcevic, P., Voralek, J., & Ross, N. (2006). Measurements of groundwater velocity in discrete rock fractures. Journal of Contaminant Hydrology, 82(1–2), 44–60. http://doi.org/10.1016/j.jconhyd.2005.09.001

O'Donnell, J. A., Aiken, G. R., Walvoord, M. A., & Butler, K. D. (2012). Dissolved organic matter composition of winter flow in the Yukon River basin: Implications of permafrost thaw and increased groundwater discharge. Global Biogeochemical Cycles, 26(4), 1–18. http://doi.org/10.1029/2012GB004341

Oglivi, N.A. 1958. An electrolytical method of determining the filtration velocity of underground waters. Bulletin of Science, Technology and Society 4: 1009–1012.

Osorno, T. 2016. Development and testing of an in- well point velocity PRO for preliminary site characterization. MSc thesis, Kansas University, 59p.

Osorno, T. C., Devlin, J. F., & Firdous, R. (2018). An In-Well Point Velocity Probe for the rapid determination of groundwater velocity at the centimeter-scale. Journal of Hydrology, 557(2018), 539–546. http://doi.org/10.1016/j.jhydrol.2017.12.033

Panagos, P., Van Liedekerke, M., Yigini, Y. & Montanarella, L. (2013). Contaminated Sites in Europe: Review of the Current Situation Based on Data Collected through a European Network. Journal of Environmental and Public Health. Vol. 2013, Article ID 158764, 11 p. dx.doi.org/10.1155/2013/158764

Parhizkar, M., Therrien, R., Molson, J., Lemieux, J.-M., Fortier, R., Talbot-Poulin, M.-C., Therrien, R., & Ouellet, M. (2017). An integrated surface-subsurface flow model of the thermo-hydrological behavior and effect of climate change in a cold-region watershed in northern Quebec, Canada. GeoOttawa 2017, 12th Joint CGS/IAH-CNC Groundwater Conference, Ottawa, Canada, Oct. 1-4, 2017.

Pérez, A.P. & Eugenio, N.R. (2018). Progress in the management contaminated sites in Europe - Status of local soil contamination in Europe. JRC Techncial Reports EUR 29124 EN, 193 p. Available at https://esdac.jrc.ec.europa.eu/public_path/shared_folder/doc_pub/EUR29124.pdf

Pitrak, M., Mares, S., and Kobr, M. (2007). A simple borehole dilution technique in measuring horizontal ground water flow. Ground Water, 45(1), 89–92.

Post, V. E. A., Banks, E., & Brunke, M. (2018). Groundwater flow in the transition zone between freshwater and saltwater: a field-based study and analysis of measurement errors. Hydrogeology Journal, 26(6), 1821–1838. http://doi.org/10.1007/s10040-018-1725-2

Prommer, H., Barry, D. A., & Davis, G. B. (2002). Modelling of physical and reactive processes during biodegradation of a hydrocarbon plume under transient groundwater flow conditions. Journal of Contaminant Hydrology, 59(1–2), 113–131. http://doi.org/10.1016/S0169-7722(02)00078-5

Ptak, T., Schwarz, R., Holder, T., & Teutsch, G. (2000). Ein neues integrales Verfahren zur Quantifizierung der Grundwasserimmission, Teil II: Numerische Lösung und Anwendung in Eppelheim. Grundwasser, 5(4), 176–183. http://doi.org/10.1007/s767-000-8369-4

Read, T., Bour, O., Bense, V., Le Borgne, T., Goderniaux, P., Klepikova, M. V., Hochreutener, R., Lavenant, N. and Boschero, V. (2013). Characterizing groundwater flow and heat transport in fractured rock using fiber-optic distributed temperature sensing. Geophysical Research Letters, 40(10), 2055–2059.

Rein, A., Bauer, S., Dietrich, P., & Beyer, C., (2009). Influence of temporally variable groundwater flow conditions on point measurements and contaminant mass flux estimations. Journal of Contaminant Hydrology, 108(3–4), 118–33. http://doi.org/10.1016/j.jconhyd.2009.06.005

Robinson, C., Brovelli, A., Barry, D. A., & Li, L. (2009). Tidal influence on BTEX biodegradation in sandy coastal aquifers. Advances in Water Resources, 32(1), 16–28. http://doi.org/10.1016/j.advwatres.2008.09.008

Rodhe, A. (2012). Physical models for classroom teaching in hydrology. Hydrology and Earth System Sciences, 16, 3075–3082. http://doi.org/10.5194/hess-16-3075-2012

Rolle, M., Eberhardt, C., Chiogna, G., Cirpka, O. A., Grathwohl, P., Enhancement of dilution and transverse mixing in porous media: Experiments and model-based interpretation. Journal of Contaminant Hydrology, 110, 130-142. http://doi.org/10.1016/j.jconhyd.2009.10.003

Romanovsky, V. E., Smith, S. L., & Christiansen, H. H. (2010). Permafrost thermal state in the polar northern hemisphere during the international polar year 2007-2009: A synthesis. Permafrost and Periglacial Processes, 21(2), 106–116. http://doi.org/10.1002/ppp.689

Rønde, V., McKnight, U. S., Sonne, A. T., Balbarini, N., Devlin, J. F., & Bjerg, P. L. (2017). Contaminant mass discharge to streams: Comparing direct groundwater velocity measurements and multi-level groundwater sampling with an in-stream approach. Journal of Contaminant Hydrology, 206(September), 43–54. http://doi.org/10.1016/j.jconhyd.2017.09.010

Rowland, J. C., Travis, B. J., & Wilson, C. J. (2011). The role of advective heat transport in talik development beneath lakes and ponds in discontinuous permafrost. Geophysical Research Letters, 38(17), 1–5. http://doi.org/10.1029/2011GL048497

Sale, T., Taylor, G. R., Iltis, G., and Lyverse, M. (2007). Measurement of LNAPL flow using single-well tracer dilution techniques. Ground Water, 45(5), 569–578. doi:10.1111/j.1745-6584.2007.00337.x

Schillig, P. C. (2012). VelProbePE: An automated spreadsheet program for interpreting point velocity probe breakthrough curves. Computers and Geosciences, 39, 161–170. http://doi.org/10.1016/j.cageo.2011.06.007

Schillig, P. C., Devlin, J. F., & Rudolph, D. (2016). Upscaling Point Velocity Measurements to Characterize a Glacial Outwash Aquifer. Groundwater, 54(3), 394–405. http://doi.org/10.1111/gwat.12357

Schillig, P. C., Devlin, J. F., Roberts, J. A., Tsoflias, G. P., & McGlashan, M. A. (2011). Transient Heterogeneity in an Aquifer Undergoing Bioremediation of Hydrocarbons. Ground Water, 49(2), 184–196. http://doi.org/10.1111/j.1745-6584.2010.00682.x

Schirmer, M., Dahmke, A., Dietrich, P., Dietze, M., Gödeke, S., Richnow, H. H., … Teutsch, G. (2006). Natural attenuation research at the contaminated megasite Zeitz. Journal of Hydrology, 328(3–4), 393–407. http://doi.org/10.1016/j.jhydrol.2005.12.019

Schwarz, R., Ptak, T., Holder, T., & Teutsch, G. (1998). Groundwater risk assessment at contaminated sites: a new investigation approach. IAHS Publication (International Association of Hydrological Sciences), (250), 68–71.

Schwede, R. L., & Cirpka, O. A. (2010). Stochastic evaluation of mass discharge from pointlike concentration measurements. Journal of Contaminant Hydrology, 111(1–4), 36–47. http://doi.org/10.1016/j.jconhyd.2009.10.011

Seidel, T., König, C., Schäfer, M., Ostermann, I., Biedert, T., & Hietel, D. (2014). Intuitive visualization of transient groundwater flow. Computers and Geosciences, 67, 173–179. http://doi.org/10.1016/j.cageo.2014.03.004

Sentenac, P., Hogson, T., Keenan, H., & Kulessa, B. (2015). Small scale monitoring of a bioremediation barrier using miniature electrical resistivity tomography. Journal of Applied Geophysics, 115, 24–31. http://doi.org/10.1016/j.jappgeo.2014.11.006

Silliman, S. E., & Mantz, G. (2000). The effect of measurement error on estimating the hydraulic gradient in three dimensions. Ground Water. http://doi.org/10.1111/j.1745-6584.2000.tb00208.x

Slater, A. G., & Lawrence, D. M. (2013). Diagnosing present and future permafrost from climate models. Journal of Climate, 26(15), 5608–5623. http://doi.org/10.1175/JCLI-D-12-00341.1

Smith, T., Sale, T., & Lyverse, M. (2012). Measurement of LNAPL Flux Using Single-Well Intermittent Mixing Tracer Dilution Tests. Ground Water, 50(6), 840–850. http://doi.org/10.1111/j.1745-6584.2012.00931.x

SPW (2017a). Etat des nappes d'eau souterraine de Wallonie (in French). Edition : Service public de Wallonie, DGO 3 (DGARNE), Belgique, D/2018/11802/06. Available at http://environnement.wallonie.be/de/eso/atlas/index.htm

SPW (2017b). Rapport sur l'état de l'environnement wallon (in French). Service Publique de Wallonie DGO3, SPW Editions, 368p. Available at http://etat.environnement.wallonie.be

Squillace, P.J. (1996) Observed and Simulated Movement of Bank- Storage Water. Groundwater, 34(1), 121-134. https://doi.org/10.1111/j.1745-6584.1996.tb01872.x

St. Jacques, J.M.S., & Sauchyn, D.J., (2009). Increasing winter baseflow and mean annual streamflow from possible permafrost thawing in the Northwest Territories, Canada. Geophysical Research Letters, 36(1), 1–6. http://doi.org/10.1029/2008GL035822

Sterrett, R.J. (2007). Groundwater and Wells 3rd Edition. Smyth Co Inc Publisher, 812p. ISBN-13: 978-0978779306

Sudicky, E. A. (1986). A natural gradient experiment on solute transport in a sand aquifer: Spatial variability of hydraulic conductivity and its role in the dispersion process. Water Resources Research, 22(13), 2069–2082. http://doi.org/10.1029/WR022i013p02069

Suthersan, S. S., Potter, S. T., Schnobrich, M. , Wahlberg, J. , Quinnan, J. , Welty, N. & Fewless, T. (2016). Rethinking Conceptual Site Models in Groundwater Remediation. Groundwater Monitoring and Remediation, 36, 22-30. http://doi.org/10.1111/gwmr.12192

Tait, N. G., Lerner, D. N., Smith, J. W. N., & Leharne, S. A. (2004). Prioritisation of abstraction boreholes at risk from chlorinated solvent contamination on the UK Permo-Triassic Sandstone aquifer using a GIS. Science of the Total Environment, 319(1–3), 77–98. http://doi.org/10.1016/S0048-9697(03)00438-8

Taniguchi, M. (2002). Tidal effects on submarine groundwater discharge into the ocean. Geophysical Research Letters, 29(12), 9–11. http://doi.org/10.1029/2002GL014987

Tarantola A. and Valette B. (1982). Inverse problems = quest for information. Journal of Geophysics, 50, 159-170.

Trezzi, G., Garcia-Orellana, J., Rodellas, V., Santos-Echeandia, J., Tovar-Sánchez, A., Garcia-Solsona, E., & Masqué, P. (2016). Submarine groundwater discharge: A significant source of dissolved trace metals to the North Western Mediterranean Sea. Marine Chemistry, 186, 90–100. http://doi.org/10.1016/j.marchem.2016.08.004

Troldborg M. (2010). Risk assessment models and uncertainty estimation of groundwater contamination from point sources. PhD thesis, Technical University of Denmark, Lyngby, Denmark, 108p.

Troldborg, M., Lemming, G., Binning, P. J., Tuxen, N., & Bjerg, P. L. (2008). Risk assessment and prioritisation of contaminated sites on the catchment scale. Journal of Contaminant Hydrology, 101(1–4), 14–28. http://doi.org/10.1016/j.jconhyd.2008.07.006

Troldborg, M., Nowak, W., Lange, I. V., Santos, M. C., Binning, P. J., & Bjerg, P. L. (2012). Application of Bayesian geostatistics for evaluation of mass discharge uncertainty at contaminated sites. Water Resources Research, 48(9), 1–19. http://doi.org/10.1029/2011WR011785

Troldborg, M., Nowak, W., Tuxen, N., Bjerg, P. L., Helmig, R., & Binning, P. J. (2010). Uncertainty evaluation of mass discharge estimates from a contaminated site using a fully Bayesian framework. Water Resources Research, 46(1), 1–19. http://doi.org/10.1029/2010WR009227

UNESCO (2018). The United Nations World Water Development Report 2018: Nature-based solutions for water. WWAP, UN-Water, Paris, 173p. Available at https://unesdoc.unesco.org/ark:/48223/pf0000261424

Verreydt, G., Annable, M. D., Kaskassian, S., Van Keer, I., Bronders, J., Diels, L., & Vanderauwera, P. (2013). Field demonstration and evaluation of the Passive Flux Meter on a CAH groundwater plume. Environmental Science and Pollution Research, 20(7), 4621–4634. http://doi.org/10.1007/s11356-012-1417-8

Verreydt, G., Bronders, J., Van Keer, I., Diels, L., & Vanderauwera, P. (2015). Groundwater Flow Field Distortion by Monitoring Wells and Passive Flux Meters. Groundwater, 53(6), 933–942. http://doi.org/10.1111/gwat.12290

Verreydt, G., Bronders, J., Van Keer, I., Diels, L., & Vanderauwera, P. (2010). Passive Samplers for Monitoring VOCs in Groundwater and the Prospects Related to Mass Flux Measurements. Ground Water Monitoring & Remediation, 30(2), 114–126. http://doi.org/10.1111/j.1745-6592.2010.01281.x

Verreydt, G., van Keer, I., Bronders, J., Diels, L., & Vanderauwera, P. (2012). Flux-based risk management strategy of groundwater pollutions: The CMF approach. Environmental Geochemistry and Health, 34(6), 725–736. http://doi.org/10.1007/s10653-012-9491-x

Walter, K., & Devlin, J. F. (2017). Application of 3D Printing to the Manufacturing of Groundwater Velocity Probes. Groundwater Monitoring and Remediation, 37(2), 71–77. http://doi.org/10.1111/gwmr.12210

Walvoord, M. A., & Striegl, R. G. (2007). Increased groundwater to stream discharge from permafrost thawing in the Yukon River basin: Potential impacts on lateral export of carbon and nitrogen. Geophysical Research Letters, 34(12). http://doi.org/10.1029/2007GL030216

West, L. J., and Odling, N. E. (2007). Characterization of a multilayer aquifer using open well dilution tests. Ground Water, 45(1), 74–84. doi:10.1111/j.1745-6584.2006.00262.x

Wildemeersch, S., Jamin, P., Orban, P., Hermans, T., Klepikova, M., Nguyen, F., … Dassargues, A. (2014). Coupling heat and chemical tracer experiments for estimating heat transfer parameters in shallow alluvial aquifers. Journal of Contaminant Hydrology, 169, 90–99. http://doi.org/10.1016/j.jconhyd.2014.08.001

Wilson, J. T., Mandell, W. A., Paillet, F. L., Bayless, E. R., Hanson, R. T., Kearl, P. M., … Pedler, W. H. (2001). Evaluation of Borehole Flowmeters Used to Measure Horizontal Ground-Water Flow in Limestones of Indiana, Kentucky, and Tennessee, 1999. Water Resources Investigations Report. United States Geological Survey, (4139), 144. http://doi.org/10.1016/S0016-2361(03)00174-1

Woodward, S. J. R., Wöhling, T., & Stenger, R. (2016). Uncertainty in the modelling of spatial and temporal patterns of shallow groundwater flow paths: The role of geological and hydrological site information. Journal of Hydrology, 534, 680–694. http://doi.org/10.1016/j.jhydrol.2016.01.045

Wright, N., Hayashi, M., & Quinton, W. L. (2009). Spatial and temporal variations in active layer thawing and their implication on runoff generation in peat-covered permafrost terrain. Water Resources Research, 45(5), 1–13. http://doi.org/10.1029/2008WR006880

Wu, Y. S., Lee, C. H., & Yu, J. L. (2008). Effects of hydraulic variables and well construction on horizontal borehole flowmeter measurements. Ground Water Monitoring and Remediation, 28(1), 65–74. http://doi.org/10.1111/j.1745-6592.2007.00184.x

Yang, J. H., Lee, K. K., & Clement, T. P. (2012). Impact of seasonal variations in hydrological stresses and spatial variations in geologic conditions on a TCE plume at an industrial complex in Wonju, Korea. Hydrological Processes, 26(3), 317–325. http://doi.org/10.1002/hyp.8236

Yoon, H. (2006). Validation of methods to measure mass flux of a groundwater contaminant. PhD thesis, Air Force Institute Of Technology, Wright-Patterson Air Force Base, Ohio, AFIT/GES/ENV/06M-08, 62p.

Zeru, A., & Schäfer, G. (2005). Analysis of groundwater contamination using concentration-time series recorded during an integral pumping test: Bias introduced by strong concentration gradients within the plume. Journal of Contaminant Hydrology, 81(1–4), 106–124. http://doi.org/10.1016/j.jconhyd.2005.08.005

Zha, Y., Yeh, T.-C. J., Mao, D., Yang, J. and Lu, W. (2014). Usefulness of flux measurements during hydraulic tomographic survey for mapping hydraulic conductivity distribution in a fractured medium. Advances in Water Resources, 71, 162-176.

Zhou, Y., & Cardiff, M. (2017). Oscillatory hydraulic testing as a strategy for NAPL source zone monitoring : Laboratory experiments. Journal of Contaminant Hydrology, 200, 24–34. http://doi.org/10.1016/j.jconhyd.2017.03.005

Zlotnik, V.A. and Zurbuchen, B.R. (2003). Field study of hydraulic conductivity in a heterogeneous aquifer: Comparison of single-borehole measurements using different instruments, Water Resources Research, 39 (4), WR001415, 12p.

Zosseder, K., Bender, S., & Wohnlich, S. (2009). Hydraulische Ursachen der zeitlichen Varianz von PAK-Konzentrationen in einem Kiesgrundwasserleiter. Grundwasser, 14(2), 97–111. http://doi.org/10.1007/s00767-009-0105-1